PhD THESIS

Defended at Aix-Marseille University
On 09 December 2022 by

Fatima HUSSEIN

Controlling the formation of organic nanostructures by supramolecular self-assembly and on-surface reactions

Discipline
Physique et Science de la Matière

Spécialité
Matière Condensée et Nanosciences

École doctorale
ED 352-Physique et Sciences de La Matière

Laboratoire/Partenaires de recherche
Institut Matériaux Microélectronique et
Nanosciences de Provence (IM2NP)

Composition of the jury

Xavier BOUJU CNRS	Reviewer
Nataliya KALASHNYK Lille University	Reviewer
Elena MAGNANO IOM-CNR	Examiner
Didier GIGMES CNRS	President of the jury
Luca GIOVANELLI Aix-Marseille University	Co-supervisor
Sylvain CLAIR CNRS	Supervisor

Institut Matériaux Microélectronique
Nanosciences de Provence

THÈSE DE DOCTORAT

Soutenue à Aix-Marseille Université
Le 09 Décembre 2022 par

Fatima HUSSEIN

Formation de nanostructures organiques contrôlées par auto-assemblages supramoleculaires et réactions sur surface

Discipline
Physique et Science de la Matière

Spécialité
Matière Condensée et Nanosciences

École doctorale
ED 352-Physique et Sciences de La Matière

Laboratoire/Partenaires de recherche
Institut Matériaux Microélectronique et
Nanosciences de Provence (IM2NP)

Composition du jury

Xavier BOUJU CNRS	Rapporteur
Nataliya KALASHNYK Université de Lille	Rapporteure
Elena MAGNANO IOM-CNR	Examinatrice
Didier GIGMES CNRS	Président du jury
Luca GIOVANELLI Aix-Marseille Université	Co-directeur de thèse
Sylvain CLAIR CNRS	Directeur de thèse

Institut Matériaux Microélectronique
Nanosciences de Provence

Affidavit

I, undersigned, Fatima Hussein, hereby declare that the work presented in this manuscript is my own work, carried out under the scientific direction of Sylvain Clair and the co-director Luca Giovanelli, in accordance with the principles of honesty, integrity and responsibility inherent to the research mission. The research work and the writing of this manuscript have been carried out in compliance with both the French national charter for Research Integrity and the Aix-Marseille University charter on the fight against plagiarism.

This work has not been submitted previously either in this country or in another country in the same or in a similar version to any other examination body.

Marseille, 07 october 2022.

List of Publications and Conferences

Scientific Publications

1. Giovanelli, L.; Pawlak, R.; **Hussein, F.**; MacLean, O.; Rosei, F.; Song, W.; Pigot, C.; Dumur, F.; Gigmes, D.; Ksari, Y.; Bondino, F.; Magnano, E.; Meyer, E.; Clair, S. On-Surface Synthesis of Unsaturated Hydrocarbon Chains through C−S Activation. **Chemistry A European Journal 2022**, 28 (47). DOI: 10.1002/chem.202200809.

2. **Hussein, F.**; Pigot, C.; Lairado, R. F.; Minissale, M.; Salomon, E.; Angot, T.; Dumur, F.; Nechab, M.; Gigmes, D.; Ksari, Y.; Clair, S.; Giovanelli, L. On-Surface homocoupling reactivity of a chiral bifunctional bromoindanone molecule on Cu(111). **New Journal of Chemistry 2022**, **46**, 22869-22876. DOI:1039/D2NJ04708J.

Contributions at National and International Conferences

1. "On-Surface Synthesis of Unsaturated Hydrocarbon Chains through C−S Activation" Giovanelli, L.; Pawlak, R.; Hussein, F.; MacLean, O.; Rosei, F.; Song, W.; Pigot, C.; Dumur, F.; Gigmes, D.; Ksari, Y.; Bondino, F.; Magnano, E.; Meyer, E.; Clair, S. European Conference on Surface Science (ECOSS 35), Luxembourg, August 29, 2022. **(Oral Presentation)**

2. "On-Surface Synthesis of Unsaturated Hydrocarbon Chains through C−S Activation" Giovanelli, L.; Pawlak, R.; Hussein, F.; MacLean, O.; Rosei, F.; Song, W.; Pigot, C.; Dumur, F.; Gigmes, D.; Ksari, Y.; Bondino, F.; Magnano, E.; Meyer, E.; Clair, S. Journée de l'IM2NP, France, Marseille, June 07, 2022. **Poster Prize Third Year of Thesis (Poster)**

3. "On-Surface Synthesis of Unsaturated Hydrocarbon Chains through C−S Activation" Giovanelli, L.; Pawlak, R.; Hussein, F.; MacLean, O.; Rosei, F.; Song, W.; Pigot, C.; Dumur, F.; Gigmes, D.; Ksari, Y.; Bondino, F.; Magnano, E.; Meyer, E.; Clair, S. Colloque Journées Thématiques inter-réseaux RTVide et RéMiSol: Assemblages Moléculaires : Quels défis technologiques ? (JT RTV RéMiSol), France, Paris, October 18, 2021. **(Poster)**

4. "On-Surface Synthesis of Unsaturated Hydrocarbon Chains through C−S Activation" Giovanelli, L.; Pawlak, R.; Hussein, F.; MacLean, O.; Rosei, F.; Song, W.; Pigot, C.; Dumur, F.; Gigmes, D.; Ksari, Y.; Bondino, F.; Magnano, E.; Meyer, E.; Clair, S. 12$^{\text{èm}}$ Meeting on NanoScience Advances, C'Nano meeting, France, Porquerolles, September 13, 2021. **(Poster)**

5. "On-Surface Synthesis of Unsaturated Hydrocarbon Chains through C−S Activation" Giovanelli, L.; Pawlak, R.; Hussein, F.; MacLean, O.; Rosei, F.; Song, W.; Pigot, C.; Dumur, F.; Gigmes, D.; Ksari, Y.; Bondino, F.; Magnano, E.; Meyer, E.; Clair, S. 17$^{\text{èm}}$ » Journées de la Matière Condensée (JMC 17), France, Rennes, August 24, 2021. **(Oral Presentation)**

Résumé

La formation contrôlée de nouveaux objets à l'échelle nanométrique représente un enjeu important pour le développement de nouveaux matériaux et de dispositifs électroniques. Dans ce contexte, l'objectif de cette thèse est de proposer de nouvelles stratégies pour contrôler la formation de nanostructures organiques sur des surfaces basées sur les concepts d'auto-assemblage supramoléculaire et de synthèse sur surface (*on-surface synthesis*) et d'étudier leurs propriétés. Tout d'abord, nous avons étudié par microscopie à effet tunnel (STM) en conditions ambiantes le contrôle de la taille des domaines formés à l'interface liquide-solide sur HOPG par une solution bimoléculaire d'acide trimésique (TMA) et d'acide benzoïque (BZA). Les résultats montrent que la formation des domaines est très sensible au rapport stœchiométrique entre les deux molécules et nécessite un réglage fin de ce dernier. Ensuite, nous avons étudié la polymérisation du 1,4-di(thiophen-2-yl)benzene (DTB) sur le Cu(111) sous ultra vide (UHV) par STM et par spectroscopie de photoélectrons (XPS), avec le soutien complémentaire de mesures de microscopie à force atomique non contact (nc-AFM) et d'une modélisation théorique basée sur la théorie de la fonctionnelle de la densité (DFT). Les résultats montrent la formation de chaînes hydrocarbonées non saturées interconnectées basée sur l'activation du C-S. Enfin, nous avons montré par STM et XPS sous UHV que l'utilisation du précurseur chiral bifonctionnel (*R*)-6-bromo-3-phenyl-2,3-dihydro-1*H*-inden-1-one (BrPhINDO) conduit à la formation de différentes structures liées de manière covalente sur le Cu(111) avec une inversion chirale induisant une racémisation partielle.

Mots clés : chimie supramoléculaire, synthèse en surface, interface liquide-solide, UHV, STM, XPS.

Abstract

The controlled formation of new objects at the nanoscale is an important challenge for the development of new materials and electronic devices. In this context, the objective of this thesis is to propose new strategies to control the formation of organic nanostructures on surfaces based on the concepts of supramolecular self-assembly and on-surface synthesis and investigate their properties. First, we studied by scanning tunneling microscopy (STM) at ambient conditions the control of the size of the domains formed at the liquid-solid interface on HOPG from a bimolecular solution of trimesic acid (TMA) and benzoic acid (BZA). The results show that the formation of the domains is very sensitive to the stoichiometry ratio between the two molecules and a fine-tuning of this latter is required. Then, we studied the polymerization of 1,4-di(thiophen-2-yl)benzene (DTB) on Cu(111) under ultra-high vacuum (UHV) by STM and photoelectron spectroscopy (XPS), supplemented by non-contact atomic force microscopy (nc-AFM) and theoretical modelling based on the density functional theory (DFT). The results show the formation of unsaturated hydrocarbon chains based on C-S activation. Finally, we demonstrated by STM and XPS under UHV that the use of the bifunctional chiral precursor (*R*)-6-bromo-3-phenyl-2,3-dihydro-1*H*-inden-1-one (BrPhINDO) leads to the formation of different covalently bonded structures on Cu(111) with chiral inversion inducing partial racemization.

Keywords: supramolecular chemistry, on-surface synthesis, liquid-solid interface UHV, STM, XPS.

Acknowledgments

First, I would like to express my sincere gratitude to my supervisors Mr. Sylvain CLAIR and Mr. Luca GIOVANELLI for providing me this opportunity to join their research group. I would like to thank them for their continuous supports, guidance and scientific discussions throughout my research and the writing of this thesis. Your humble behaviour and kind attitude pushed me to give my best to succeed in this project

I express my gratitude to all the collaborators which were enrolled in my work for their irreplaceable contributions and their help with a high degree of professionalism. I thank all my colleagues in the BACH beamline team at ELETTRA Synchrotron in Trieste, Italy, especially to Elena MAGNANO and Federica BONDINO. The experiments at the synchrotron were always made possible thanks to their scientific and technical support.

I also express my gratitude to Rémy PAWLAK and Ernst MEYER from the department of physics at Basel University (Switzerland) and to Oliver MACLEAN and Federico ROSEI from the Institut National de la Recherche Scientifique in Varennes, Québec (Canada). I also express my gratitude to Corentin PIGOT, Frédéric DUMUR, Malek NECHAB and Didier GIGMES from the ICR laboratory at Aix-Marseille university and to Eric SALOMON, Francisco ROMERO LAIRADO, Thierry ANGOT and Marco MINISSALE from the PIIM laboratory at Aix-Marseille university. Your contributions to my work helped me a lot to success in my research.

I am grateful to all the jury members for devoting their time and assessment to this thesis. My sincere gratitude goes to Mr. Xavier BOUJU and Mrs. Nataliya KALASHNYK for accepting to be reviewers of my manuscript, as well as Mr. Didier GIGMES and Elena MAGNANO for their agreeing to be the examiners of my thesis.

I thank all of my colleagues in the NANO group at the IM2NP laboratory for the lovely and friendly time they provided during the last three years.

Finally, I would like to say that this thesis could not be done without the support of my family and friends. A profound thanks to my parents, my brothers, and my sisters for their endless support, comprehension and love. Without you I would never achieve what I want to be.

Table des matières

Résumé étendu

Introduction

Depuis une trentaine d'années, l'étude de Feynman sur la création de domaines à l'échelle atomique pour la miniaturisation des machines a eu un impact significatif sur le début de la nanotechnologie et les nanosciences. Cette étude attire de plus en plus l'attention de la communauté scientifique, puisqu'elle permet de créer et de contrôler la formation de nouveaux nanomatériaux et nanocomposantes. Dans ce contexte, deux approches différentes existent : l'approche descendante connue sous le nom « Top-down » et l'approche ascendante, dite « Bottom-up ». La première approche consiste à contrôler la structure des objets à l'échelle nanométrique grâce aux outils macroscopiques. La lithographie est l'approche descendante la plus utilisée surtout dans les industries des semi-conducteurs et de la micro-électronique. La seconde consiste à produire des nanostructures ordonnées à partir d'un assemblage des molécules, aussi appelées blocs de construction, donnant lieu à des objets nanostructurés autoassemblées par des interactions non covalentes telles que les liaisons hydrogène ou halogène[1], [2]. Récemment, une nouvelle stratégie appelée « synthèse sur surface » est utilisée pour construire des nanostructures plus stables sur des surfaces. Ces dernières sont stabilisées par des liaisons covalentes telles que le couplage C-C[3]. L'objectif de cette thèse est d'élaborer de nouvelles stratégies pour la formation et le contrôle de nanostructures organiques sur surfaces, et d'étudier leurs propriétés. Dans ce contexte, différentes stratégies ont été proposées et appliquées dans ce travail. La première est basée sur l'introduction d'une molécule modulatrices (chapitre 3). La deuxième est d'explorer un nouveau type de chimie basé sur une réaction d'activation originale (chapitre 4). Et la dernière est d'étudier l'influence d'une bi-fonctionnalité et de l'asymétrie chirale du précurseur moléculaire (chapitre 5) sur les structures obtenues. Le chapitre 1 de ce manuscrit est consacré à une étude bibliographique sur les généralités des autoassemblages supramoléculaires et la synthèse sur surface, notamment sur les interactions mises en jeu, ainsi que sur les paramètres permettant d'influencer la morphologie des réseaux obtenus. Le chapitre 2 porte sur les principales techniques de caractérisation utilisées durant cette thèse.

Chapitre 1 : Formation de Nanoarchitectures par auto-assemblage supramoléculaire et réactions sur surface

L'auto-assemblage supramoléculaire en surface est un processus dans lequel des molécules, considérées comme des blocs de construction, sont déposées sur des surfaces solides pour s'y adsorber et former des structures organisées. Ces dernières sont obtenues via un équilibre entre les interactions molécule-molécule et les interactions molécule-substrat. Les interactions les plus fréquentes entre les molécules pour les processus d'auto-assemblage sont de nature non covalente (faible) tels que les interactions de van der Waals, les interactions $\pi - \pi$, les liaisons hydrogène, les liaisons halogènes et les interactions métal-organiques. Plusieurs exemples de ces interactions ont été étudiés pour stabiliser des auto-assemblages moléculaires sur les surfaces[4]–[8]. En outre, les interactions molécule-substrat ont un impact sur les auto-assemblages et donc le choix du substrat (nature atomique, symétrie et réactivité chimique) joue un rôle important pour l'ingénierie de ces structures[9].

Cependant, le désavantage de ce processus est que la stabilité thermique des domaines moléculaires obtenus en surface peut être faibles, ce qui réduit parfois les possibilités d'application. Une solution est l'utilisation de la nouvelle approche appelée « synthèse sur surface » basée sur des liaisons covalentes entre les molécules. Cette méthode permet de produire des réseaux plus stables que les réseaux auto-assemblés par des liaisons non-covalentes. Dans ce contexte, les réactions organiques les plus étudiées sur des surfaces en UHV sont le couplage Ullmann, le couplage de fonctions alcynes, la déshydrogénation aryle-aryle, la réaction de Diels-Alder, etc..[3] En effet, la chimie des structures obtenues par des d'auto-assemblages supramoléculaires ou par synthèse sur surface est influencée par une variété de paramètres. La prise en compte de la structure géométrique bien définie du substrat solide utilisé ainsi que celle du précurseur moléculaire, le taux de recouvrement sur la surface, le recuit thermique ou l'irradiation UV sont des paramètres importants qui peuvent affecter considérablement le chemin de réaction et la formation des produits finaux souhaités. Beaucoup de recherches ont été effectuées pour mieux comprendre les mécanismes régissant deux approches[9]–[14]. Les travaux de cette thèse présentés par la suite ont été réalisés dans le cadre de ce domaine d'études, sur une surface HOPG pour les auto-assemblages supramoléculaires et sur la surface métallique Cu(111) pour la synthèse sur surface.

Chapitre 2 : Techniques expérimentales

L'étude de l'auto-assemblage supramoléculaire et la synthèse sur surface pour différents systèmes a été réalisée en combinant différentes techniques expérimentales telles que la microscopie à effet tunnel (STM) et la microscopie à force atomique sans contact (nc-AFM), la spectroscopie de photoélectrons X (XPS) et la théorie de la fonctionnelle de densité (DFT). Toutes les mesures STM ont été réalisées dans notre groupe à l'IM2NP-Marseille soit à pression ambiante (chapitre 3) ou soit dans des conditions UHV (chapitre 4 et 5) avec les dispositifs expérimentaux présentées dans Figure R1. Dans le cadre de ma thèse, une partie des expériences XPS ont été effectuées à BACH, Synchrotron (Elettra) à Trieste afin d'analyser la chimie de la surface. Quelques autres expériences (nc-AFM, XPS) et mesures (DFT) ont été réalisées par nos collaborateurs afin de mieux analyser les résultats obtenus.
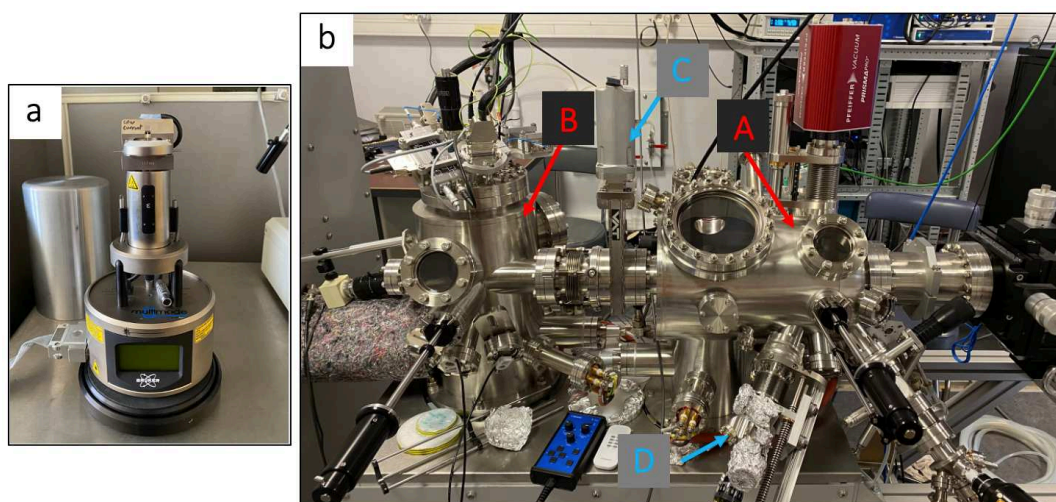
Figure R1. Dispositifs STM de notre groupe à l'IM2NP-Marseille fonctionnant à pression ambiante (a) et sous conditions UHV (b). (A) chambre de préparation des échantillons, (B) chambre d'analyse STM à basse température (9K), (C) vanne de séparation entre les chambres et (D) évaporateur des molécules.

Pour l'étude d'auto-assemblages supramoléculaires en conditions ambiantes, les molécules sont déposées à partir d'une solution liquide sur une surface de graphite fraîchement clivée tandis que pour la synthèse sur surface sous UHV, les molécules sont déposées par sublimation sur une surface métallique de Cu(111) nettoyée par bombardement avec des ions Ar$^+$ suivi par des recuits.

Chapitre 3 : Auto-assemblage d'une solution bimoléculaire d'acide trimésique et benzoïque sur HOPG

Ce chapitre étudie la formation des nanostructures par des processus d'autoassemblage bidimensionnel à partir d'une solution bimoléculaire en utilisant une nouvelle stratégie de contrôle précédemment proposée pour des systèmes tridimensionnels[15]. Elle est basée sur l'introduction de molécules modulatrices qui permet de contrôler la croissance des structures. Dans ce contexte, une solution bimoléculaire d'acide benzène 1,3,5-tricarboxylique (trimésique, TMA) et d'acide 4-(decyloxy)benzoïque (BZA), présentés dans la Fig.R2, a été déposée à l'interface liquide-solide sur HOPG et étudié par STM à température ambiante. TMA possède trois groupes carboxyliques conduisant à la formation d'un réseau 2D étendus[16] stabilisés par des liaisons hydrogènes tandis que BZA ne peut pas former qu'une seule liaison hydrogène à la frontière d'un domaine ce qui devrait limiter la taille des domaine dans le cas d'un mélange entre ces deux acides.
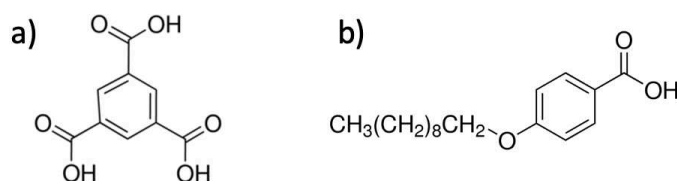
Figure R2. Schéma représentatif de (a) l'acide trimésique (TMA) et de (b) l'acide benzoïque (BZA).

Dans un premier temps, des solutions principales de chaque acide ont été préparées, l'une à partir des molécules TMA et l'autre à partir des molécules BZA. Puis à partir de ces solutions, les solutions bimoléculaires ont été préparées en variant le rapport stœchiométrique entre les deux acides. Ce rapport a été évalué par deux approximations basées sur la structure et la taille de domaine attendus. Ici la molécule plurifonctionnelle forme l'intérieur du domaine et la molécule monofonctionnelle forme la bordure du domaine. Dans la première approximation, par simplification la forme des molécules intérieures est considérée carrée tandis que dans la deuxième approximation on considère un réseau en nid d'abeille conforme au cas du système réel formé par TMA à l'intérieur du domaine. Les résultats obtenus par les deux approximations sont très similaires pour des tailles de domaine attendues comprises entre 0 et 15 nm. Donc, une solution bimoléculaire avec un rapport $\frac{n_{TMA}}{n_{BZA}} = 2.5$ a été préparée, permettant en principe des tailles de domaine de l'ordre de 10 nm x 10 nm aisément identifiables par STM. Le dépôt de 5μl de cette première solution sur la surface HOPG (Fig.R3a) montre la formation d'une

structure ordonnée avec un arrangement hexagonal des molécules. Les paramètres de la cellule unitaire (a = b = 17.5 ± 1 Å, γ = 60°) sont similaires à ceux de la littérature pour une structure formée seulement par des molécule TMA[16]. Le réseau est stabilisé par des liaisons hydrogènes entre les groupes carboxyles de TMA et un réseau en nid d'abeille, comme illustré dans le modèle de la Fig.R3d. Aucun auto-assemblage des molécules BZA ou d'une phase TMA-BZA mixte n'a été observé. Par conséquent, les molécules BZA ne s'adsorbent pas à la surface, donnant lieu à un réseau infini de TMA. Différentes solutions bimoléculaires ont été donc préparées et étudiées en diminuant le rapport stœchiométrique entre les deux acides afin de tenter d'observer une phase mixte.

Nous avons observé que pour toutes les solutions ayant un rapport $\frac{n_{TMA}}{n_{BZA}}$ supérieur à 10^{-1}, un réseau 2D avec un arrangement périodique constitué seulement des molécules TMA a été obtenu (Fig.R3a). Par contre, pour toutes les solutions ayant un rapport inférieur à 10^{-3}, différentes structures sont observées par les images STM (Fig.R3b). La structure dans ce cas est formée d'une disposition de rangées parallèles brillantes et sombres avec une distance entre deux rangées brillantes d'environ 2,7 à 3 nm (Fig.R3c). Ces régions brillantes peuvent être attribuées aux groupes phényles des molécules tandis que les régions sombres sont liées aux groupes alkyles. La structure cette fois est en accord avec les auto-assemblages de l'acide benzoïque déposés seules sur la surface HOPG[17]. Un modèle de la structure correspondante est illustré dans la Fig.R3e. Le réseau est stabilisé par des liaisons hydrogènes entre les groupes carboxyliques de BZA et aussi par des interactions de type van der Waals entre les chaînes alkyles.

Pour conclure, nous n'avons pas pu observer d'auto-assemblage entre les deux molécules TMA-BZA sur la surface HOPG par STM. En générale, la valeur théorique utilisée au départ pour préparer la solution bimoléculaire est correcte si toutes les molécules sont adsorbées sur la surface de manière stœchiométrique mais en réalité, l'équilibre entre les molécules en phase liquide et celles adsorbées à l'interface liquide-solide n'est pas équivalent pour les deux espèces moléculaires. Il est aussi possible que la formation des domaines soit très sensible au rapport stœchiométrique entre les molécules et nécessite un réglage fin de ce dernier.

$$\frac{n_{TMA}}{n_{BZA}}$$

$2.5 - 6.5 \times 10^{-1}$ $1 \times 10^{-3} - 6.1 \times 10^{-6}$
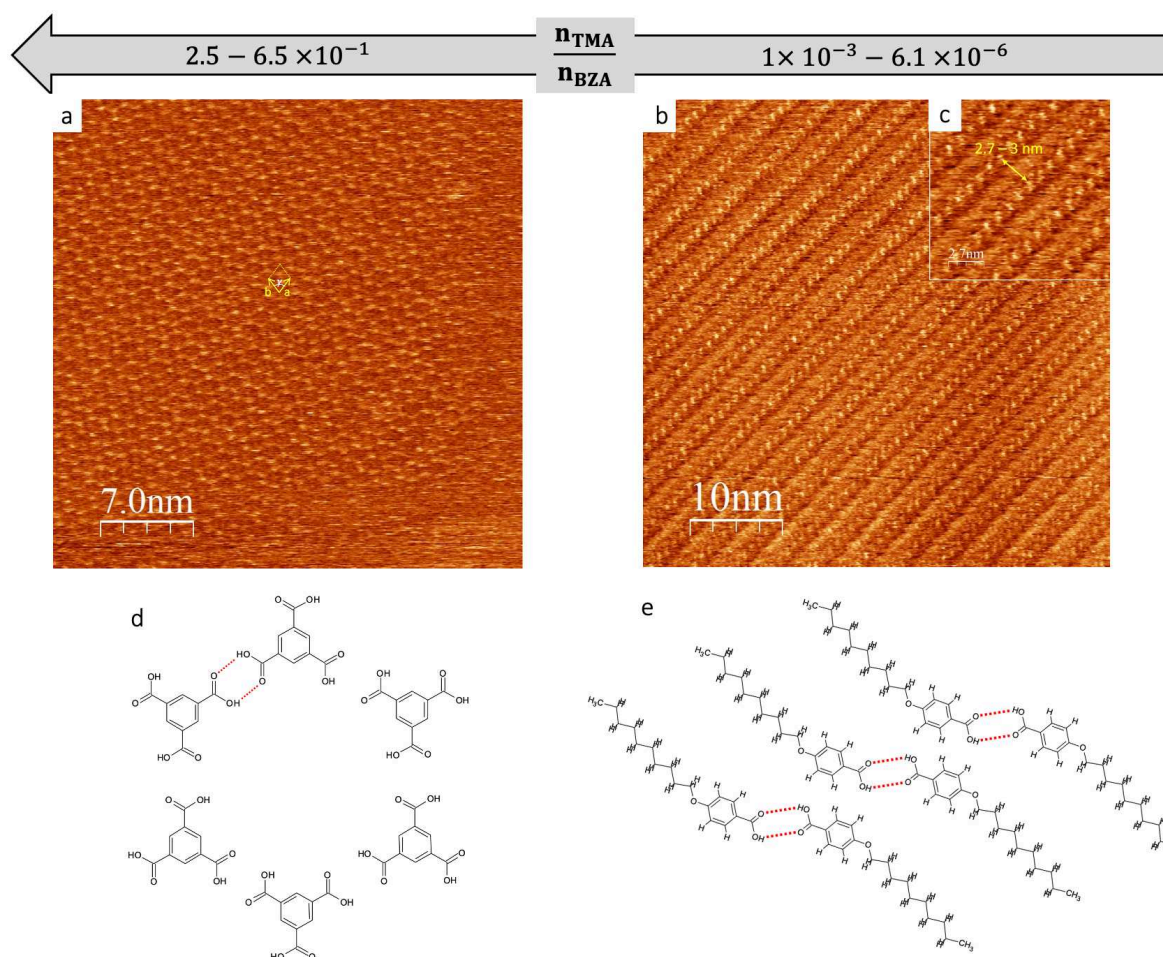
Figure R3. (a-c) Images STM des structures obtenues après dépôt à température ambiante d'une solution bimoléculaire de TMA et BZA sur la surface HOPG en fonction du rapport stœchiométrique $\frac{n_{TMA}}{n_{BZA}}$ entre les deux acides. (d-e). Le modèle structurel du réseau observé pour chaque image STM. Les liaisons hydrogènes sont illustrées par des lignes rouges pointillées. Paramètres STM : (a) $I = 1.2$ pA, $V = 368$ mV. (b) $I = 50$ pA, $V = 550$ mV.

Chapitre 4 : Formation des chaînes hydrocarbonées insaturés basée sur l'activation C-S par synthèse sur surface

Dans ce chapitre, nous étudions une réaction d'homo-couplage d'un précurseur à base de thiophène sur la surface de Cu(111) induite par l'approche de synthèse sur surface. Récemment, les dérivés du thiophène ont gagné beaucoup d'intérêt notamment car ils peuvent provoquer des réactions intra- ou intermoléculaires[18]. Ils sont utilisés pour former des couplages C-C par la méthode d'activation originale des liaisons C-S. Dans ce contexte, nous avons étudié le précurseur 1,4-di(thiophène-2-yl)benzène (DTB)[19] synthétisé par nos collaborateurs au

laboratoire ICR à Marseille. Il est constitué d'un cœur benzénique central et deux thiophènes liés avec lui par une simple liaison C-C, comme montre la figure R4a.

Dans un premier temps, un dépôt des molécules à température ambiante sur une surface de Cu(111) a été effectué. Une phase gazeuse 2D a été formée, empêchant l'acquisition des images STM. Le substrat est donc refroidi à 4.8K afin d'immobiliser les molécules et de permettre l'acquisition des images STM. Aucun autoassemblage à large échelle n'a été observé par STM (Fig.R4b), reflétant la faible interaction intermoléculaire entre ces précurseurs. La structure et l'intégrité des précurseurs ont été confirmées par des mesures nc-AFM avec une pointe fonctionnalisée en CO faite par nos collaborateurs à Basel (Fig.R4c) et aussi par des calculs DFT faits au Canada. Nous pouvons observer les unités de benzènes et de thiophènes qui s'adsorbent presque à plat sur la surface. De plus, différentes orientations d'adsorptions reliées à la position du soufre dans le cycle thiophène par rapport au cœur de la molécule ont été observées. Ensuite, un recuit du système à 150°C conduit à la formation de longues chaînes droites d'environ 20 nm qui sont alignées avec la direction de haute symétrique du substrat [1$\bar{2}$1] comme le montre l'image STM (Fig.R4d). Ces chaînes sont interconnectées aléatoirement et forment un réseau 2D réticulé étendu. Leurs structures ont été confirmées par des mesures nc-AFM (Fig.R4e) montrant que ces chaînes sont constituées des cycles benzéniques des molécules DTB interconnectées par différentes configurations de chaînes de type oligoacetylène. Le contraste homogène de ces chaînes confirme la configuration d'adsorption parfaitement plane et le détachement des atomes de soufres du polymère. Des mesures XPS ont été aussi effectuées au synchrotron Elettra à Trieste pour mieux comprendre la chimie du système. Le spectre des niveaux de cœur S2p pour le dépôt de DTB à température ambiante présente une composante principale à haute énergie de liaison avec une petite contribution décalée en énergie par rapport à la phase gazeuse et deux autres composantes mineures à basse énergie de liaison. La composante principale correspond à ce qui était observé pour d'autres dérivés de thiophènes[20] et les composantes peuvent être attribuées à différents sites d'adsorption. Le shift de -0.24 eV est lié à une diminution de taux de recouvrement sur la surface. Les deux composantes à basses énergies de liaisons peuvent être attribuées à des atomes de S détachés des molécules lors de l'ouverture des unités de thiophènes et liées à des atomes de Cu du substrat[21]. De plus, le spectre du C1s pour un tel dépôt présente un shift de -0.48 eV et un élargissement visible par rapport au C1s de la phase gazeuse, indiquant une interaction entre les atomes de C de la molécule et le substrat. Une partie de l'élargissement à basse énergie de liaison peut également être attribuée à la perte du S d'une petite fraction de molécules qui ont commencé à réagir.
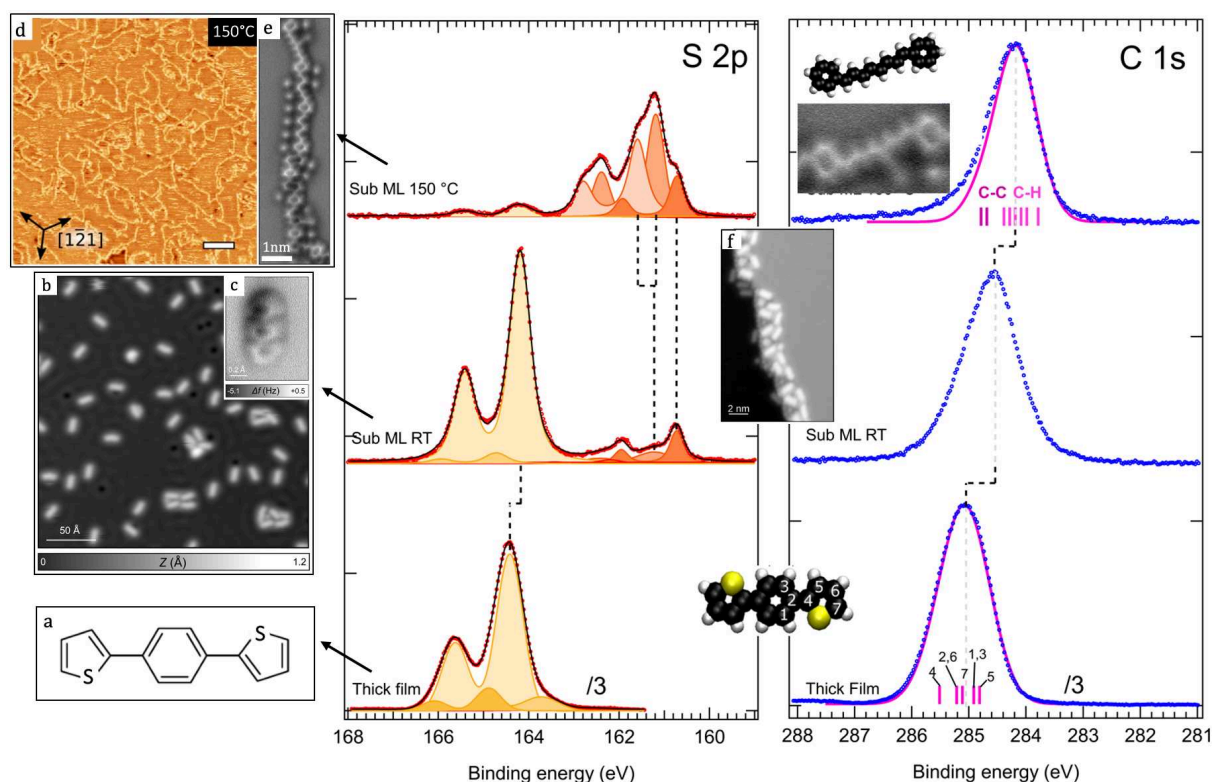
Figure R4. (Partie gauche) : (a) Structure du précurseur DTB. (b) Image STM acquise à 4.8K après dépôt de DTB sur Cu(111). (c) Image AFM haute résolution d'une seule molécule de DTB obtenue avec une pointe CO. (d) Image STM acquis à température ambiante après recuit l'échantillon à 150°C. (e) Image AFM haute résolution des chaînes polymères obtenues après recuit à 130°C. (f) Image STM acquise montrant les molécules en bords de marche. (Partie droite) : Mesures XPS des niveaux de cœur S2p et C1s pour DTB/Cu(111). Spectres inférieurs : couche épaisse déposé à température ambiante. Spectres supérieurs : dépôt d'une sous-monocouche à température ambiante et après recuit à 150°C. Les calculs DFT pour le C1s sont illustrés avec des lignes et tirets rose.

Après recuit à 150°C, presque la totalité du S2p se transforme en trois composantes à basse énergie de liaison. Les deux premières peuvent être liées à la formation de différentes structures de coordinations de S-Cu aux bords de marches[22] (Fig.R4f). Par contre, la composante à plus basse énergie de liaison correspond à la présence d'un soufre dans une coordination inférieur en forme d'atomes isolés à côtés des chaînes polymères (petits points brillants dans la Fig.R4e). En même temps que l'ouverture des unités de thiophène et le détachement du S, le spectre du C1s présente un shift vers les basses énergies de liaison. Son énergie et sa forme sont cohérentes avec d'autres spectres de dérivés de polymères 2D[23]. La nature des différentes composantes de C a été identifiée par des calculs DFT, montrant que des liaisons C-C sont présentes à haute énergie de liaison tandis que à basse énergies sont des liaisons C-H.

Ces résultats montrent que la réaction de polymérisation a eu lieu à 150°C. En fait, des mesures STM et AFM ont été effectué en recuisant à des températures plus basses, indiquant que la polymérisation commence en fait entre 80 et 100°C ou des chaînes pas très ordonnées et des unités de thiophène non réagi ont été observés. De plus, des mesures XPS en fonction de la température ont été réalisées, montrant que le rendement de la réaction d'activation C-S est très élevé et peut avoir lieu entre 50 et 120°C.

Dans une deuxième partie, une étude de la stabilité thermique des chaînes polymériques a été effectué en chauffant l'échantillon jusqu'à 500°C. La combinaison des mesures STM, AFM et XPS montre que des réactions de cyclisation se produisent à 300°C et à 500°C une réaction de graphitisation a lieu avec la formation de petits patches de graphène sur la surface. Des phénomènes similaires ont été observés dans d'autres études pour divers systèmes après recuit à haute température.

Pour conclure, après dépôt sur le Cu(111), un recuit à 120°C était suffisante pour activer la liaison C-S et la formation des chaînes de polymères hydrocarbonés insaturées organisées en un réseau réticulé et entièrement conjugué. La combinaison des différentes techniques d'analyse expérimentales a permis de mieux comprendre le mécanisme de la réaction. La figure R5 illustre le processus de formation des différents produits de réaction lors de la désulfurisation des unités de thiophène. Les chaines linéaires formées sont constituées de segments *cis*- et *trans*-oligoacetylène ainsi que d'unités pentalène. L'interconnexion entre les chaînes est obtenue lors d'un couplage entre le carbone terminal et le radical du carbone le plus proche de l'anneau de benzène.
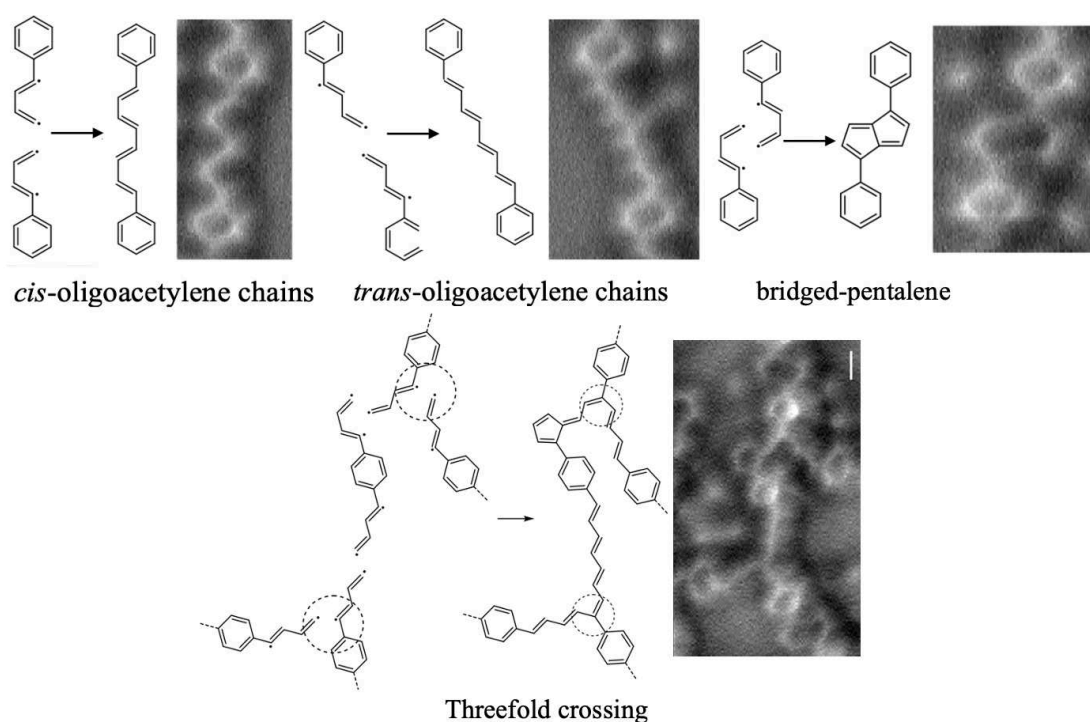
cis-oligoacetylene chains   *trans*-oligoacetylene chains   bridged-pentalene

Threefold crossing

Figure R5. Images AFM haute résolution des produits obtenus et les schémas de couplage correspondants.

Chapitre 5 : Réactivité d'homocouplage sur surface d'une molécule chirale bifonctionnelle de bromoindanone sur Cu(111)

Dans cette partie de thèse, une nouvelle stratégie a été proposée et appliquée pour contrôler la formation de nanostructures organiques en surface. Elle est basée sur le dépôt d'un précurseur bifonctionnel possédant une chiralité définie. En fait, plusieurs études ont montré qu'une telle stratégie de couplage séquentiel hiérarchique peut être appliquée pour améliorer le processus de croissance de la polymérisation en surface[3]. Dans ce contexte, le précurseur (*R*)-6-bromo-3-phenyl-2,3-dihydro-1*H*-inden-1-one (BrPhINDO) illustré dans la Fig.R6 a été étudié sur la surface de Cu(111). Il est constitué d'un coeur 1-indanone avec un atome de brome en position 6 et un groupe phényle sur un carbone asymétrique en position 3. Cette molécule chirale doit avoir une configuration d'adsorption préférentielle avec le corps de la molécule à plat et le groupement phényle hors du plan de la surface. Différents types de couplages intermoléculaires ont été observés dans la littérature pour des précurseurs avec des groupes fonctionnels similaires tels que la réaction d'Ullmann et la réaction de Knoevenagel. Pour caractériser les différents produits de réactions obtenus, une étude STM à basse température (LT-STM) suivi d'une étude XPS ont été effectuées.
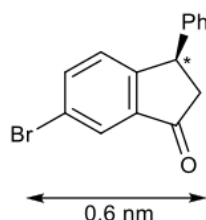
Figure R6. Structure moléculaire du *R*-stéréo-isomère étudié du précurseur chiral BrPhINDO.

Un premier dépôt d'une sous-monocouche de BrPhINDO à température ambiante sur le Cu(111) conduit à plusieurs structures différentes, rendant difficile de distinguer les interactions intermoléculaires en jeu. Un deuxième dépôt d'une monocouche a donc été effectué en maintenant le substrat à 100°C. Une phase beaucoup plus homogène a été obtenue (Fig.R7a) constituée de deux motifs d'arrangements supramoléculaires d'un bloc de construction commun. Le plus abondant est constitué des chaînes moléculaires (type-1, rectangle rose) d'environ 7-10 nm de longueur et 2,6 nm de largeur. Le moins abondant est présenté à la fin de ces chaînes ou entre elles, parfois fusionnée à l'intérieur. Ce sont des anneaux moléculaires composé de trois sous-unités, possédant une symétrie C3 (cercle vert) que nous nommons structure α par la suite. La taille du bloc de construction dans les deux arrangements est proche de celle d'une molécule de BrPhINDO. Par contre, le contraste des sous-unités observées n'est pas asymétrique, ce qui révèle que l'anneau de phényle peut être détaché de la molécule ou non apparent dans le contraste d'image à cause de son orientation particulière hors plan. Ensuite, des recuits à différentes températures ont été effectués pour activer les interactions intermoléculaires. À 200°C, le taux de recouvrement a diminué de plus de 50% à cause d'une désorption importante, donnant lieu à une diffusion des molécules sur la surface ce qui facilite le couplage intermoléculaire. Ici, un autre type de chaînes allongées a été observé (type2, rectangle blanc) avec des structures isolées bien définies appelées γ et possédant une symétrie C2 (rectangle bleu). En augmentant la température de recuit jusqu'à 300°C et 400°C (Fig.R7c-d), les chaînes de type 2 évoluent en structures plus longues et interconnectées avec plus d'abondance des structures isolées γ. La taille de ces chaînes partiellement réticulées d'environ 8-24 nm de longueur et 1-3 nm de largeur est cohérente avec les tailles typiques pour des chaînes polymériques covalente de systèmes similaires. Deux autres structures isolées ont été identifiées, une possédant une symétrie C3 appelée β (triangle rouge) et l'autre avec une symétrie C3 en forme hexagonale appelée δ (hexagone jaune).
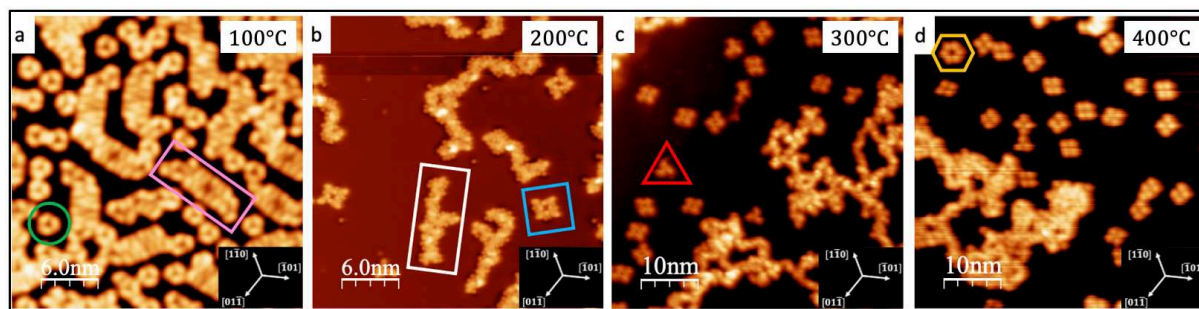
Figure R7. Images STM acquises à basse température (9K) après dépôt de *R*-BrPhINDO sur une surface de Cu(111) chaude (T$_{Cu}$=100°C)(a) et après recuit à 200°C (b) à 300°C (c) et à 400°C (d). Les cadres en couleurs correspondent aux différentes structures observées : rectangle rose pour les chaînes de type-1, le cercle vert pour la structure α, le rectangle blanc pour les chaînes de type-2, le rectangle bleu pour la structure γ, le triangle rouge pour la structure β et l'hexagone jaune pour la structure δ.

On remarque que toutes les structures présentent une chiralité définie pour des températures de recuits supérieures à 100°C. En se basant sur les résultats STM et la réactivité attendue du précurseur, des modèles structuraux ont été proposées. La figure R8 montre les différents produits obtenus en fonction de la température de recuit et les modèles correspondant à chacun. Les structures α sont stabilisées par des liaisons hydrogène entre trois monomères. Par contre, les β qui ont une tendance à disparaitre à des températures de recuit plus élevées sont formées par trois dimères couplés par réaction d'Ullmann et reliés entre eux par des liaisons hydrogène. L'abondance des deux autres structures γ et δ augmente en fonction de la température. Elles peuvent être formées par des sous-unités de base où deux dimères couplés par une réaction d'Ullmann sont reliés entre eux par une réaction de Knoevenagel. Des liaisons hydrogène entre deux ou trois sous-unités peuvent alors se produire pour former les structures γ et δ, respectivement.

Pour mieux comprendre les mécanismes réactionnels en surface, des mesures XPS pour les niveaux de cœur C1s, O1s et Br3p ont été effectuées par nos collaborateurs au laboratoire PIIM à Marseille pour une monocouche déposée sur le Cu(111) à température ambiante et recuite à différentes températures. Les résultats sur le Br 3p confirment la débromation des molécules lors de l'adsorption sur la surface avec le Br qui reste adsorbé jusqu'à 500°C, comme observés dans d'autres études qui donnent lieu à des interactions intermoléculaires de type d'Ullmann. Le rapport stœchiométrique entre les atomes de C et les atomes de Br après dépôt ainsi qu'après recuit à 100°C donne une valeur de 14 proche du rapport C:Br d'une molécule intact (qui est 15) qui diminue après recuit à 200°C. Malheureusement, on ne peut pas conclure que le groupe phényle a été détaché de la molécule à une telle température et on a le Br adsorbé sur la surface

Jusqu' à 500°C. Par contre, le spectre d'O1s diminue en fonction de la température ce qui est cohérent avec la progression de la réaction de Knoevenagel.
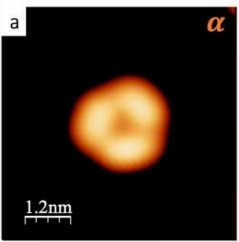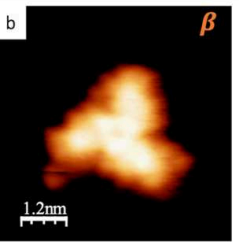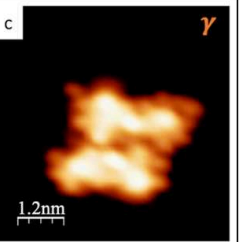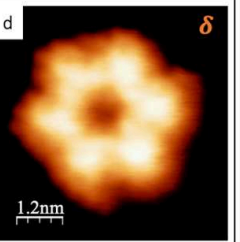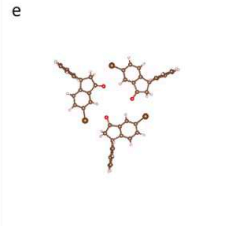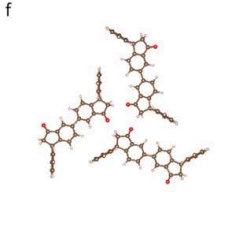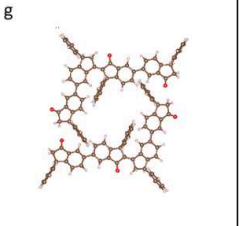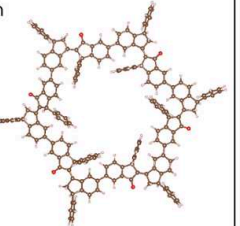

Figure R8. Les images STM (a-d) et les modèles correspondants (e-h) de toutes les structures isolées observées en fonction de leur plage de stabilité de température sur la surface de Cu(111).

De manière remarquable, toutes les structures présentent une prochiralité définie avec une distribution énantiomérique asymétrique due à l'apparition d'une inversion prochirale pour une fraction des précurseurs (racémisation partielle). Ce dernier est imputé à une perte de phényle ou à une inversion de chiralité lors de l'adsorption. Pour vérifier cette asymétrie chirale, l'autre énantiomère de la même molécule (S-BrPhINDO) a été déposé sur le Cu(111) et étudié dans des conditions similaires. Les résultats montrent aussi deux prochiralités de toutes les structures (β, γ, δ) avec une distribution de prochiralité inversé, confirmant ainsi l'inversion partielle qui se produit sur la surface.

Conclusion

Ce mémoire est consacré à contrôler des nouvelles stratégies pour développer et caractériser des nanostructures organiques sur des surfaces formées par autoassemblage supramoléculaire et par synthèse sur surface. D'abord, nous avons montré que l'introduction d'une molécule modulatrice peut être une bonne approche pour contrôler la taille des domaines auto-assemblés sur la surface d'un système bimoléculaire aromatique possédant différents groupes fonctionnels. De plus, nous avons montré que la formation des domaines peut être très sensible au rapport stœchiométrique entre les molécules utilisées ce qui nécessite un réglage fin de ce rapport. Ensuite, nous avons exploré un nouveau type de chimie basée sur une activation originale, l'activation C-S, permettant la création des nouveaux types de réactifs à partir d'un

précurseur à base de thiophène. Enfin, nous avons montré que l'ajout d'une bifonctionnalité particulière ainsi que d'une asymétrie au précurseur moléculaire peuvent influencer sur la chiralité de ce précurseur et sur la formation des nanostructures organiques en surface.

Références

[1]   Vincenzo Balzani Prof., Alberto Credi Dr., Margherita Venturi Prof., "The Bottom-Up Approach to Molecular-Level Devices and Machines," Chemistry A European Journal, pp. 5524–5532, Dec. 16, 2002.

[2]   D. H. Gracias, J. Tien, T. L. Breen, C. Hsu, and G. M. Whitesides, "Forming Electrical Networks in Three Dimensions by Self-Assembly," *Science*, vol. 289, no. 5482, pp. 1170–1172, Aug. 2000, doi: 10.1126/science.289.5482.1170.

[3]   S. Clair and D. G. de Oteyza, "Controlling a Chemical Coupling Reaction on a Surface: Tools and Strategies for On-Surface Synthesis," *Chem. Rev.*, vol. 119, no. 7, pp. 4717–4776, Apr. 2019, doi: 10.1021/acs.chemrev.8b00601.

[4]   K. Tahara *et al.*, "Two-Dimensional Porous Molecular Networks of Dehydrobenzo[12]annulene Derivatives via Alkyl Chain Interdigitation," *J. Am. Chem. Soc.*, vol. 128, no. 51, pp. 16613–16625, Dec. 2006, doi: 10.1021/ja0655441.

[5]   C. Janiak, "A critical account on π–π stacking in metal complexes with aromatic nitrogen-containing ligands †," *J. Chem. Soc., Dalton Trans.*, no. 21, pp. 3885–3896, 2000, doi: 10.1039/b003010o.

[6]   J. V. Barth *et al.*, "Building Supramolecular Nanostructures at Surfaces by Hydrogen Bonding," *Angew. Chem. Int. Ed.*, vol. 39, no. 7, pp. 1230–1234, Apr. 2000, doi: 10.1002/(SICI)1521-3773(20000403)39:7<1230::AID-ANIE1230>3.0.CO;2-I.

[7]   T. T. T. Bui, S. Dahaoui, C. Lecomte, G. R. Desiraju, and E. Espinosa, "The Nature of Halogen···Halogen Interactions: A Model Derived from Experimental Charge-Density Analysis," *Angew. Chem.*, vol. 121, no. 21, pp. 3896–3899, May 2009, doi: 10.1002/ange.200805739.

[8]   A. Dmitriev, H. Spillmann, N. Lin, J. V. Barth, and K. Kern, "Modular Assembly of Two-Dimensional Metal–Organic Coordination Networks at a Metal Surface," *Angew. Chem.*, vol. 115, no. 23, pp. 2774–2777, Jun. 2003, doi: 10.1002/ange.200250610.

[9]   M. S. Baviloliaei and L. Diekhöner, "Molecular self-assembly at nanometer scale modulated surfaces: trimesic acid on Ag(111), Cu(111) and Ag/Cu(111)," *Phys. Chem. Chem. Phys.*, vol. 16, no. 23, pp. 11265–11269, 2014, doi: 10.1039/C4CP01429D.

[10]   Takashi Yokoyama, Shiyoshi Yokoyama, Toshiya Kamikado, Yoshishige Okuno & Shinro Mashiko, "Selective assembly on a surface of supramolecular aggregates with controlled size and shape," Nature, pp. 619–621, Oct. 11, 2001.

[11]   M. Stöhr, M. Wahl, C. H. Galka, T. Riehm, T. A. Jung, and L. H. Gade, "Controlling Molecular

Assembly in Two Dimensions: The Concentration Dependence of Thermally Induced 2D Aggregation of Molecules on a Metal Surface," *Angew. Chem. Int. Ed.*, vol. 44, no. 45, pp. 7394–7398, Nov. 2005, doi: 10.1002/anie.200502316.

[12]   L. Grill, M. Dyer, L. Lafferentz, M. Persson, M. V. Peters, and S. Hecht, "Nano-architectures by covalent assembly of molecular building blocks," *Nature Nanotech*, vol. 2, no. 11, pp. 687–691, Nov. 2007, doi: 10.1038/nnano.2007.346.

[13]   F. Palmino, C. Loppacher, and F. Chérioux, "Photochemistry Highlights on On-Surface Synthesis," *ChemPhysChem*, vol. 20, no. 18, pp. 2271–2280, Sep. 2019, doi: 10.1002/cphc.201900312.

[14]   Q. Shen *et al.*, "Self-assembled two-dimensional nanoporous molecular arrays and photoinduced polymerization of 4-bromo-4′-hydroxybiphenyl on Ag(111)," *The Journal of Chemical Physics*, vol. 142, no. 10, p. 101902, Mar. 2015, doi: 10.1063/1.4906116.

[15]   T. Tsuruoka, S. Furukawa, Y. Takashima, K. Yoshida, S. Isoda, and S. Kitagawa, "Nanoporous Nanorods Fabricated by Coordination Modulation and Oriented Attachment Growth," *Angew. Chem. Int. Ed.*, vol. 48, no. 26, pp. 4739–4743, Jun. 2009, doi: 10.1002/anie.200901177.

[16]   Stefan Griessl, Markus Lackinger, Michael Edelwirth, Michael Hietschold, Wolfgang M. Heckl, "Self-Assembled Two-Dimensional Molecular Host-Guest Architectures From Trimesic Acid," Single Molecules, pp. 25–31, Mar. 11, 2002.

[17]   K. S. Mali, K. Lava, K. Binnemans, and S. De Feyter, "Hydrogen Bonding Versus van der Waals Interactions: Competitive Influence of Noncovalent Interactions on 2D Self-Assembly at the Liquid-Solid Interface," *Chem. Eur. J.*, vol. 16, no. 48, pp. 14447–14458, Dec. 2010, doi: 10.1002/chem.201001653.

[18]   L. E. Dinca *et al.*, "Tailoring the Reaction Path in the On-Surface Chemistry of Thienoacenes," *J. Phys. Chem. C*, vol. 119, no. 39, pp. 22432–22438, Oct. 2015, doi: 10.1021/acs.jpcc.5b05418.

[19]   L. Giovanelli *et al.*, "On-Surface Synthesis of Unsaturated Hydrocarbon Chains through C−S Activation," *Chemistry A European J*, vol. 28, no. 47, Aug. 2022, doi: 10.1002/chem.202200809.

[20]   T. Zhang *et al.*, "Lone-Pair Delocalization Effects within Electron Donor Molecules: The Case of Triphenylamine and Its Thiophene-Analog," *J. Phys. Chem. C*, vol. 122, no. 31, pp. 17706–17717, Aug. 2018, doi: 10.1021/acs.jpcc.8b06475.

[21]   R. Gutzler *et al.*, "Ullmann-type coupling of brominated tetrathienoanthracene on copper and silver," *Nanoscale*, vol. 6, no. 5, pp. 2660–2668, 2014, doi: 10.1039/C3NR05710K.

[22]   E. Wahlström, I. Ekvall, H. Olin, S.-Å. Lindgren, and L. Walldén, "Observation of ordered structures for S/Cu(111) at low temperature and coverage," *Phys. Rev. B*, vol. 60, no. 15, pp. 10699–10702, Oct. 1999, doi: 10.1103/PhysRevB.60.10699.

[23]   Shiyong Wang, Qiang Sun, Oliver Gröning, Roland Widmer, Carlo A. Pignedoli, Liangliang Cai, Xin Yu, Bingkai Yuan, Can Li, Huanxin Ju, Junfa Zhu, Pascal Ruffieux, Roman Fasel & Wei Xu, "On-surface synthesis and characterization of individual polyacetylene chains," Nature Chemistry View all journals Search Login, pp. 11, pages 924-930 (2019), Sep. 02, 2019.

General introduction

''There's Plenty of Room at the Bottom: An Invitation to Enter a New Field of Physics'' was the title of a famous lecture given by Richard P. Feynman at the annual American Physical Society meeting at Caltech in 1959[1]. In this conference, Feynman established the inception of the field based on his vision of atomic scale for computer and machine miniaturization, where a vast quantity of information could be stored and encoded into small spaces. He had a significant impact on the beginning of nanotechnology and nanoscience, aiming at the creation of new nanomaterials and nanocomponents by the study and manipulation of matter and particles on the nanometer scale. As fundamental building blocks for the creation of nanoscale devices, molecules are studied and employed in the development of molecular electronics[2]. The size of devices has gradually decreased to a few tens of nanometers, and now, it has physical and technological limitations. In this issue, lots of nanodevice research were performed in order to explore the miniaturization down to the nanoscale. In this context, two different approaches have been explored.

The first is known as the ''top-down'' approach, and it consists of starting with bulk material before removing some of them to engineer nanostructures. The photolithography is the most used top-down approach, which consists of exposing a wafer to light through a patterning mask. This technique is particularly used in the semiconductor and electronics industries.

The second approach is called the ''bottom-up'' approach. It studies the creation of ordered nanostructures by assembling together elementary molecules, designed as building blocks, resulting in self-organized supramolecular growth or so-called self-assembled nanostructures[3]. The latter are directly influenced by the molecular structure and the function which are programmed during the synthesis of molecules. They have a size between a few angstroms to several nanometers and can have different sizes and natures, for example organic molecules or metal atoms. In 1987, the Nobel prize in chemistry was awarded to Jean-Marie Lehn, Donald Cram, and Charles Pedersen for their development and use of ''molecules with structure-specific interactions of high selectivity''[4] in order to build 3D organic nanostructures based on self-assembly.
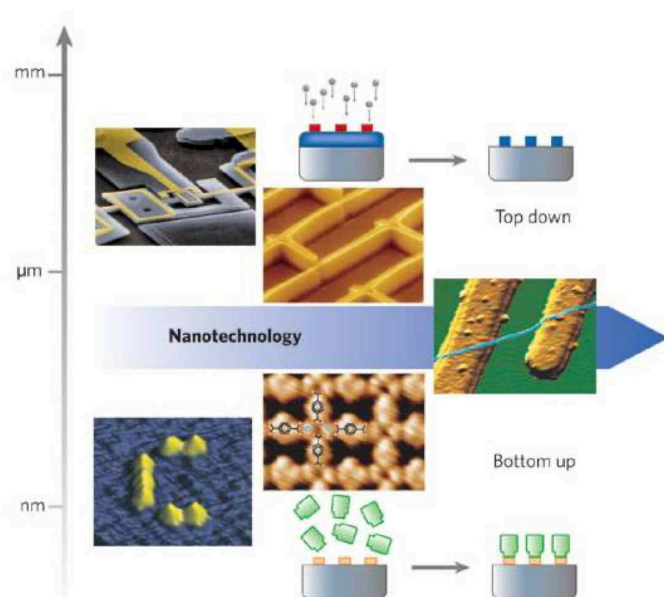
Figure 1. Illustration of top-down and bottom-up approaches. Reproduced from [5].

The concept of supramolecular self-assembly was further developed in a solid state on a surface that served as a supporting template for the molecular building blocks[6]. Once adsorbed on the surface, these building blocks form self-assembled nanostructures that rely on molecule-surface interaction and non-covalent intermolecular interactions such as hydrogen or halogen bonds. The formation of nanostructures on surfaces involves a mechanism that strongly depends on kinematic and thermodynamic conditions[5]. Recently, a novel strategy called "on-surface synthesis" is used to build more stable molecular nanostructures on surfaces stabilized by covalent bonds. The most studied covalent bond is the C-C coupling. Controlling and tuning the formation of organic nanostructures by C-C bonds was developed as a technique for the synthesis of polymer nanoarchitectures with specific novel functions. This was elucidated by Fasel and Mullen by synthesizing graphene nanoribbons (GNRs) with atomic precision on the surface[7], [8].

The development of scanning probe microscopy such as scanning tunneling microscopy (STM) and atomic force microscopy (AFM), allows a direct visualization of the molecular structures adsorbed on solid surfaces with atomic resolution. STM and AFM images illustrate the self-assembled structure, reflecting the interaction between molecule-molecule and molecule-substrate. Both noncovalent interactions and covalent bonds play an important role in the assembly process. STM and AFM techniques can be applied in a variety of environmental conditions such as organic solvents, ultra-high vacuum (UHV), and gases. Our group has two STM setups working one under ambient conditions and the other under UHV conditions.

The objective of this thesis was to engineer and control new strategies for the formation of organic nanostructures on surfaces and investigate their properties. For this, we proposed a new approach to control the formation process of nanostructures by the introduction of modulator molecules. We explored a new chemistry type based on an original activation reaction. We also studied the influence of the particular function and symmetry of the molecular precursor. In this context, self-assembled nanostructures stabilized by hydrogen bonds interactions are engineered and characterized in order to control the size of domains formed on the surface (Chapter 3). Another approach consisting of engineering covalent nanostructures by on-surface synthesis is investigated for two different molecular precursors in order to drive an original activation, the C-S activation, reaction allows access to new type of reagents (Chapter 4) and study the influence of the chirality of a bifunctional precursor (Chapter 5). All STM results presented in this manuscript were performed in our group at IM2NP, Marseille. We also did different Synchrotron experiments at ELETTRA, Trieste. The measurements were supplemented by non-contact AFM, X-ray photoelectron spectroscopy (XPS), and by density functional theory (DFT) calculations performed by our collaborators.

References

[1]   Vincenzo Balzani Prof., Alberto Credi Dr., Margherita Venturi Prof., "The Bottom-Up Approach to Molecular-Level Devices and Machines," Chemistry A European Journal, pp. 5524–5532, Dec. 16, 2002.

[2]   B. Xu and N. J. Tao, "Measurement of Single-Molecule Resistance by Repeated Formation of Molecular Junctions," *Science*, vol. 301, no. 5637, pp. 1221–1223, Aug. 2003, doi: 10.1126/science.1087481.

[3]   D. H. Gracias, J. Tien, T. L. Breen, C. Hsu, and G. M. Whitesides, "Forming Electrical Networks in Three Dimensions by Self-Assembly," *Science*, vol. 289, no. 5482, pp. 1170–1172, Aug. 2000, doi: 10.1126/science.289.5482.1170.

[4]   J.-M. Lehn, "Towards Complex Matter: Supramolecular Chemistry and Self-organization," *Eur. Rev.*, vol. 17, no. 2, pp. 263–280, May 2009, doi: 10.1017/S1062798709000805.

[5]   J. V. Barth, G. Costantini, and K. Kern, "Engineering atomic and molecular nanostructures at surfaces," *Nature*, vol. 437, no. 7059, pp. 671–679, Sep. 2005, doi: 10.1038/nature04166.

[6]   J. V. Barth, "Molecular Architectonic on Metal Surfaces," *Annu. Rev. Phys. Chem.*, vol. 58, no. 1, pp. 375–407, May 2007, doi: 10.1146/annurev.physchem.56.092503.141259.

[7]   P. Ruffieux *et al.*, "On-surface synthesis of graphene nanoribbons with zigzag edge topology," *Nature*, vol. 531, no. 7595, pp. 489–492, Mar. 2016, doi: 10.1038/nature17151.

[8]   J. Cai *et al.*, "Atomically precise bottom-up fabrication of graphene nanoribbons," *Nature*, vol. 466, no. 7305, pp. 470–473, Jul. 2010, doi: 10.1038/nature09211.

Chapter 1: Molecular nanoarchitectures based on self-assembly and on-surface reactions

This chapter provides an overview of the state-of-the-art concerning the fundamental concepts of supramolecular self-assembly and on-surface reactions based respectively on noncovalent and covalent intermolecular interactions on well-defined surfaces. The different factors and parameters supporting the control and the manipulation of reactions at the molecular scale are discussed. Some examples depicted from the literature based on scanning tunneling microscopy (STM), atomic force microscopy (AFM) and X-ray photoelectron spectroscopy (XPS) are also illustrated. This chapter is divided into four main sections that deal with the organic nanostructures formed by supramolecular self-assembly in the first two sections and by on-surface reactions in the last two sections.

1.1 Supramolecular self-assembly processes driven by noncovalent interactions

The supramolecular self-assembly on solid surfaces formed by noncovalent intermolecular interaction refers to a process in which molecules, considered as nanosized building blocks, form organized structures. This process has an important meaning in supramolecular chemistry and the nanotechnology field[1]–[3]. The term ''self'' refers to the spontaneousness of this process that does not require any guidance. The self-assembly process is the result of a complex balance between molecule-molecule interactions and molecule-substrate interactions. The noncovalent interactions used as the driving forces for molecular system engineering can be divided into different groups, such as van der Waals interactions, $\pi - \pi$ stacking, hydrogen bonds, halogen bonds, and metal-organic interactions. Table 1.1 briefly summarizes the corresponding energy, the interaction distance, and some nanoarchitecture examples for each type of noncovalent interaction.

In fact, not only the molecule-molecule but also the molecule-surface interactions play a crucial role in the molecular self-assembly process. The choice of the atomic nature of the substrate, its symmetry and its chemical reactivity is of prime importance for supramolecular structure engineering. Also, the adsorption energy of the molecules on the surface should be strong enough to prevent molecules desorption, but not too strong since the molecules have to diffuse freely to interact together

Noncovalent interactions	Energy (eV)	Interaction distance (nm)	References
van der Waals	E $\approx$ 0.02 − 0.1	< 1	[4]–[7]
Interaction $\pi - \pi$	E $\approx$ 0.1	0.33 − 0.38	[8]–[10]
Hydrogen bond	E $\approx$ 0.05 − 0.7	0.15 − 0.35	[11]–[14]
Halogen bond	E $\approx$ 0.05 − 1.86	0.26 − 0.36	[15], [16]
Metal-organic	E $\approx$ 0.5 − 2	0.15 − 0.25	[17]–[19]

Table 1.1. Classification of noncovalent interactions in the self-assembly process for molecules on surfaces, with corresponding energies and typical interaction distances.

1.1.1 Van der Waals interactions

Van der Waals forces (vdW) are attractive interactions between atoms or molecules, named by the Dutch scientist *Johannes Diderik van der Waals*. They are induced by the polarization fluctuations between atoms, which can be perfectly described in quantum dynamics. These fluctuations give a non-symmetric shape to the electron clouds around the atomic cores. Furthermore, van der Waals interactions are quite weak, non-selective and non-directive interactions (Table 1.1). Compared to other intermolecular interactions, vdW is the weakest type of interaction but at the same time, it is the most frequent non-covalent interaction in nature. Many examples of these interactions have been reported to stabilize self-assemblies[4]–[7]. Particularly, using organic molecular building blocks with lateral alkyl or alkoxy chains allows for the formation of two-dimensional self-assemblies by vdW interactions[20] and at the liquid-graphite interface[21], it is commonly used to direct the molecular assembly.

Numerous researches on the influence of van der Waals interactions on self-assembled nanostructures are performed in ambient conditions by STM at the liquid/solid interface. For example, the deposition of the bisDBAs molecule at the 1,2,4-trichlorobenzene (TCB)/HOPG interface[4] is illustrated in Fig.1.1. The STM image in Fig.1.1b shows the self-assembled structure. It is a Kagomé network formed of bright rhombic features and striped dark features between them. The bright features can be attributed to the π-electron-conjugated cores and the striped features to alkyl chains of molecules. A structural model based on the interactions between the interdigitation of alkyl chains between molecules was proposed (Fig.1.1c). The driving force for these chain arrangements is van der Waals interactions. Furthermore, the alkyl chains are aligned along the symmetry axes of the substrate. This means that the interaction between alkyl chains and the surface contributes to the creation of this dense network.
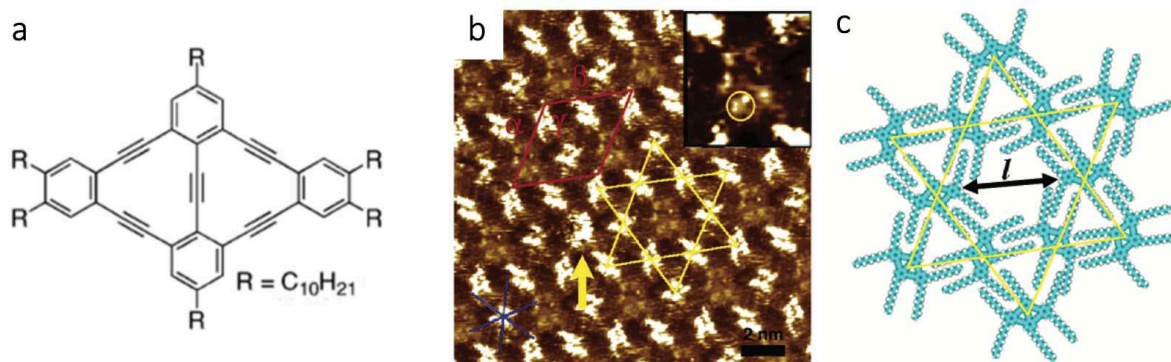
Figure 1.1. (a) Structure of the decadehydrotetrabenzo[12]annuleno[12]annulene (bisDBAs) molecule. (b) STM image of bisDBA molecule physisorbed at the (TCB)/HOPG interface. The Kagomé network is illustrated in yellow. The inset of (b) represents the expansion of the central void of the Kagomé structure with the position of some bright spots of TCB molecules (yellow circle). The yellow arrow indicates a trapped bis-annulene molecule in the central void of the Kagomé structure. Cell parameters (1 molecule per unit cell): $\alpha = 5$ nm, $\beta = 4.9$ nm, $\gamma = 120°$. (c) Molecular model of the Kagomé network of (b). Figures taken from [4].

1.1.2 Interaction π − π

π − π interactions describe the forces between neighboring aromatic groups with well-defined geometries. These interactions are dedicated to the attraction and repulsion interactions between molecules that possess π-electron systems. Depending on the relative orientation of the aromatic rings, three different conformations, illustrated in Fig.1.2, were identified for the π − π interaction. The face-to-face orientation of aromatic rings (Fig.1.2a), the T-shaped conformation (Fig.1.2b) where the plane of an aromatic ring is perpendicular to the plane of another ring, and the parallel displaced conformation (Fig.1.2c) where two aromatic rings are parallel with an offset between them. For a benzene dimer, it was shown that the T-shaped and parallel displaced orientations are more stable than the face-to-face π-stacking[10]. The application of π − π interactions has triggered a lot of interest in self-assembly in solutions and on surfaces[22].
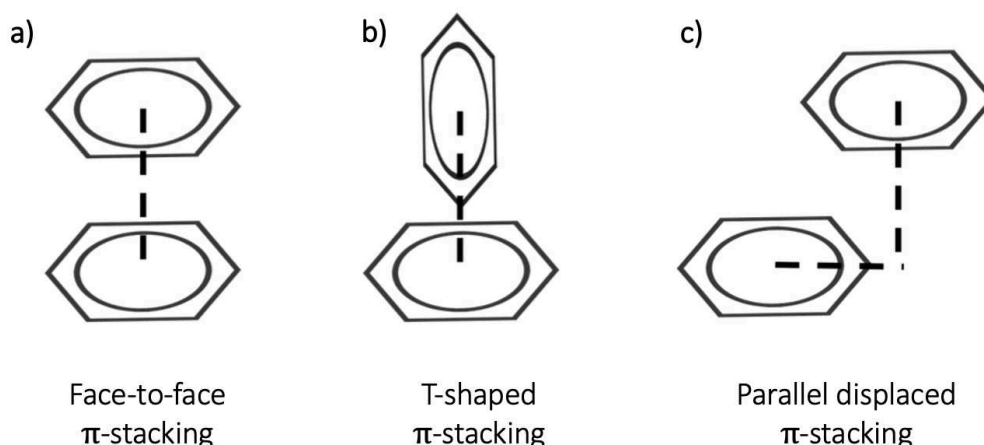
Figure 1.2. The aromatic rings conformations of π − π interactions: (a) Face-to-face stacking, (b) T-shaped π-stacking, and (c) Parallel displaced π-stacking. Image reproduced from[23].

Most molecular blocks built with π-conjugated segments are stabilized by π − π type interactions. On Cu(111) surface, distinctive discrete ring-shaped supramolecular structures were observed by Jethwa et al.[24] with the 1,5-triazole molecule (Fig.1.3a). This molecule is composed of a triazole ring (three-nitrogen atoms moiety) linked by a biphenyl group on one side and by a phenanthrene group on the other. Two distinct conformers, labeled as P and M, exist and can result from the steric hindrance between the phenanthrene and biphenyl groups. The STM image in Fig.1.3c shows the assembly of the 1,5-triazole molecules into ring-shaped structures, called "supramolecular corrals". In their study, they suggested that the observed corral-ring-shaped nanostructures in Fig.1.3 are produced through π − π interaction.

Figure 1.3. (a) Chemical structure of 1,5-triazole molecule. (b) The two conformers of 1,5-triazole result from the steric hindrance between phenanthrene and biphenyl groups: P- and M-conformer. (c) STM images showing the two confined conformers P and M of the ring-shaped nanostructures of 1,5-triazole molecule deposited on the Cu(111) surface. (d) Close-up on the 16-monomer ring structure formed by the P-conformer. Figures are taken from[24].
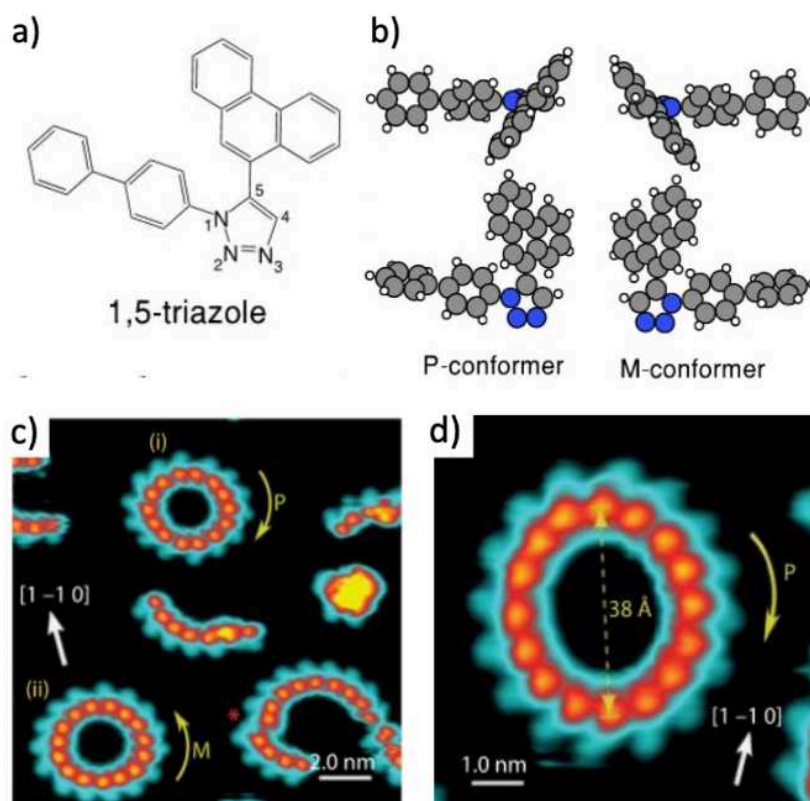
1.1.3 Hydrogen bond

The hydrogen bond is an attractive interaction between the hydrogen atom of a molecule or a molecular fragment and an atom or a group of atoms in a different (or the same) molecule. It can be defined schematically as $X - H \cdots A$ interaction formed between a strongly polar group $X^{\delta-} - H^{\delta+}$ (X = O, N) and a proton acceptor group $A^{\delta-}$ (A = O, N, S, etc.). Frequently, the hydrogen bond can be determined by its characteristics based on particular interaction geometries. The distance between the $X \cdots A$ moieties for $X - H \cdots A$ interaction is limited to 2.7 to 3.2 Å. In addition, the positive directionality preference characteristics as well as the angular cutoff are two other geometric criteria for hydrogen bonds. Contrary to vdW interactions, H-bonds are stronger, highly directive and the geometry of the arrangement is constrained since it can only be formed between two active sites in a specific direction.

Until now, numerous 2D organic self-assemblies stabilized by hydrogen bonds were studied on metal surfaces[25]. An example of molecular self-assembly built through hydrogen bonds is

given by Beton et al.[12], for the perylene-carboxylic di-imide (PTDCI) molecules and the 1,3,5-triazine-2,4,6-triamine (melamine) molecules deposited on Ag/Si(111)-$\sqrt{3} \times \sqrt{3}$ $R30°$ surface. The STM image shows that the co-adsorption of PTCDI and melamine molecules leads to the formation of an open honeycomb network (Fig.1.4b). The straight edges and the vertices of each hexagon correspond to the PTDCI and melamine molecules, respectively. A structural model was proposed in Fig.1.4c, which shows that the honeycomb structure is stabilized through $N - H \cdots O$ and $N - H \cdots N$ hydrogen bonds between the two molecules (PTCDI-melamine junction, Fig.1.4a).
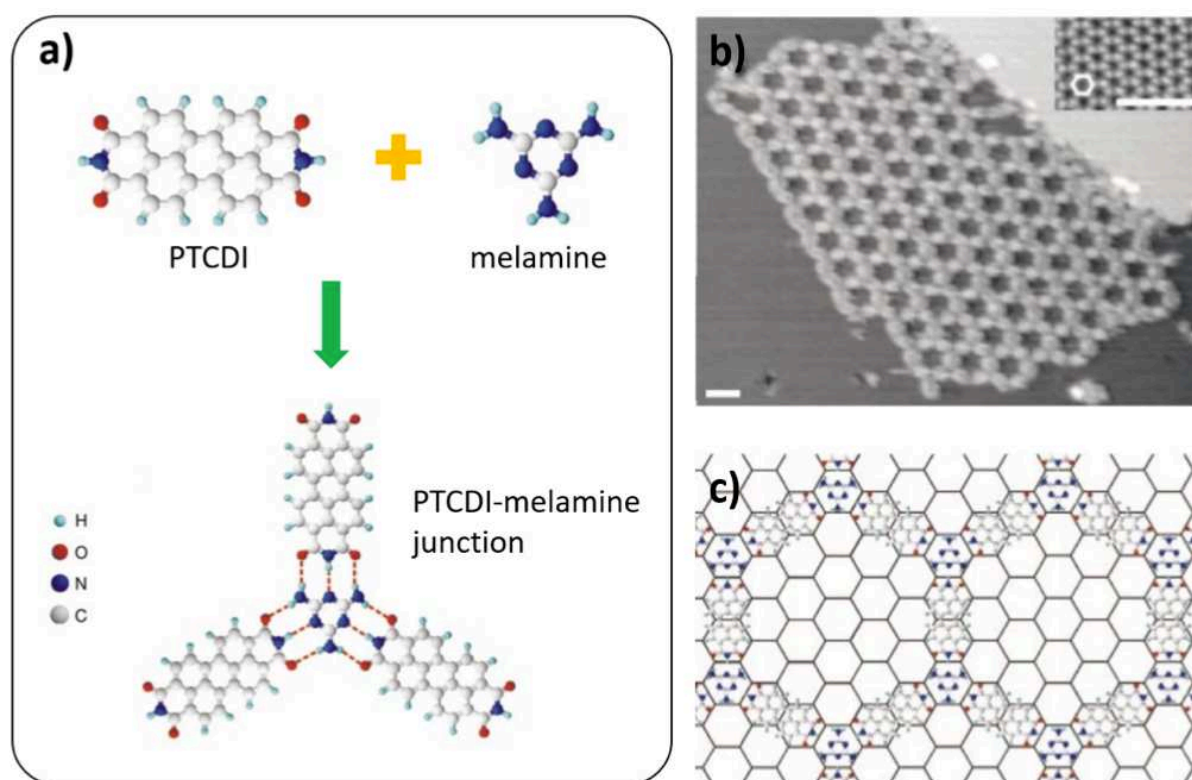
Figure 1.4. (a) Chemical structure of the perylene-carboxylic di-imide (PTDCI) molecules, the 1,3,5-triazine-2,4,6-triamine (melamine) molecules, and the PTCDI-melamine junction. The dotted lines between the molecules represent the hydrogen bonds. (b) STM image of PTCDI and melamine molecules on Ag/Si(111)-$\sqrt{3} \times \sqrt{3}$ $R30°$ surface (scale bar 3 nm). (c) The corresponding structural model of the structure observed in (b). Figures adapted from [12].

In addition, Bisti et al.[26] investigated the hydrogen bond effect of the croconic acid molecules by XPS core levels (Figure 1.5). They observed a modification in the O1s core level spectra between the gas phase (black line, A) and the condensed phase (orange line, B) related to the hydrogen bond formation. The gas phase spectrum shows the presence of two main components (1, 2) plus a satellite (S1) and two minor components coming from CO_2 (green)

and H_2O (blue) contaminants. The low (1) and the high (2) binding energy (BE) components are arising from the two different chemical environments of the oxygen atoms in the hydroxyl (O1 and O2) and carbonyl (O3, O4 and O5) groups (the component S1 corresponds to the related shake-up of the carbonyl groups). As detailed in Chapter 2 (section 2.1.2), this chemical shift can be explained by the different valence charges around the O atoms: the 1s BE of O in the carbonyl group is lower because the bond length is shorter and the electron charge around O atoms is more important than that in the hydroxyl group.
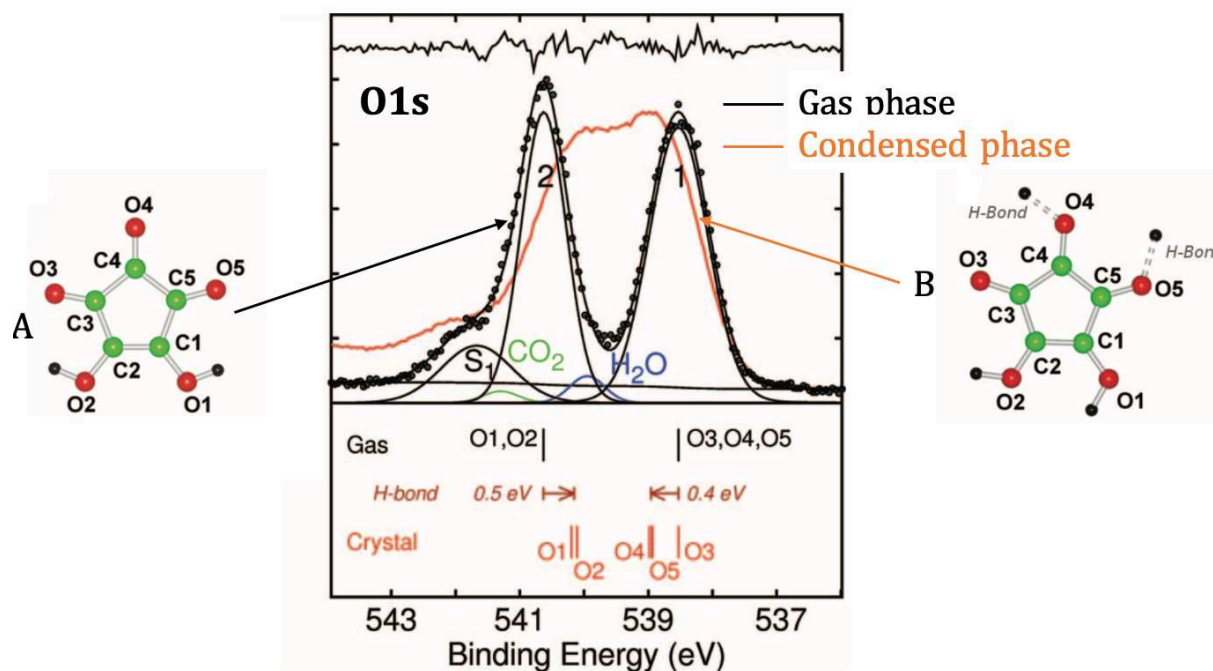
Figure 1.5. (Left, Right) Molecular structure of two croconic acid corresponding to the molecules in gas phase (A) and in a crystal phase (B). In B, H-bonds are illustrated by dashed lines. Figures adapted from [26].

In the condensed phase, the energy separation between the C=O and C-O-H components reduces sensibly. This is interpreted as coming from the formation of hydrogen bonds between the carbonyl and hydroxyl groups of neighboring molecules: the oxygen donors (hydroxyl groups) shift toward low BE while the acceptors (carbonyl groups) experience a high BE shift (bottom panel in Fig.1.5). The formation of hydrogen bonds lead to a modification in the charge density around the oxygen atoms. In the case of the acceptors carbonyl groups, the O loses part of its negative charge in favor of a bonding interaction with the H atoms while, for donor hydroxyl groups, the negative charge around O increases leading to a lowering of their BE.

1.1.4 Halogen bond

As mentioned above, the building of many supramolecular networks can be based on weak interactions such as van der Waals, $\pi - \pi$ stacking, and hydrogen bonds. In addition, the application of halogen bonds interactions has received a lot of interest due to their ability to generate systems with high stability. By definition, halogen bond (XB) is an attractive interaction that can be described as $R - X \cdots Y$ between the halogen bond donor $R - X$ in one molecular entity and the halogen bond acceptor Y in another (or the same) molecular entity. X is a halogen atom and R is a group covalently bound to X. Halogen bonds possess numerous similarities with the hydrogen bond, wherein the halogen atoms work as electrophiles.

Figure 1.6 illustrates the process of the halogen bond formation that originates from the non-spherical charge distribution around the halogen atom. A widely established theory to understand this type of interaction is the σ-hole model (Fig.1.6b). On the surface of X (F, Cl, Br, I) atoms, the electrostatic potential is negative around the bond axis in the orthogonal direction of $R - X$, while it is positive in its center (σ-hole). The ability of the halogen bond donor is related to the XB strength and it increases with halogen atom polarizability in the following order: $I > Br > Cl > F$. A particular type of halogen bond is the halogen-halogen $R - X \cdots X - R$ interaction. According to the geometry feature, Bui et al.[15] discovered and investigated two different types of interactions: type 1 and 2 in Fig.1.6c and d. The type-1 interaction is a van der Waals interaction type in which the angles θ_1 and θ_2 between two $R - X$ groups are identical. In this type, *trans* and *cis* geometry can be presented (Fig.1.6c). Type-2 is an attractive interaction between the electron-deficient area and the electron-rich area of X, where $\theta_1 = 180°$ and $\theta_2 = 90°$ (Fig.1.6d). According to the International Union of Pure and Applied Chemistry (IUPAC), only the type-2 is considered a true halogen-halogen bond.

Recently, various examples of halogenated structures have been realized at the liquid-graphite interfaces[27], [28] and on metallic surfaces[29], [30]. Molecular building blocks with bromine or iodine substituents are typically used to create halogenated nanostructures due to their significant XB donor ability.
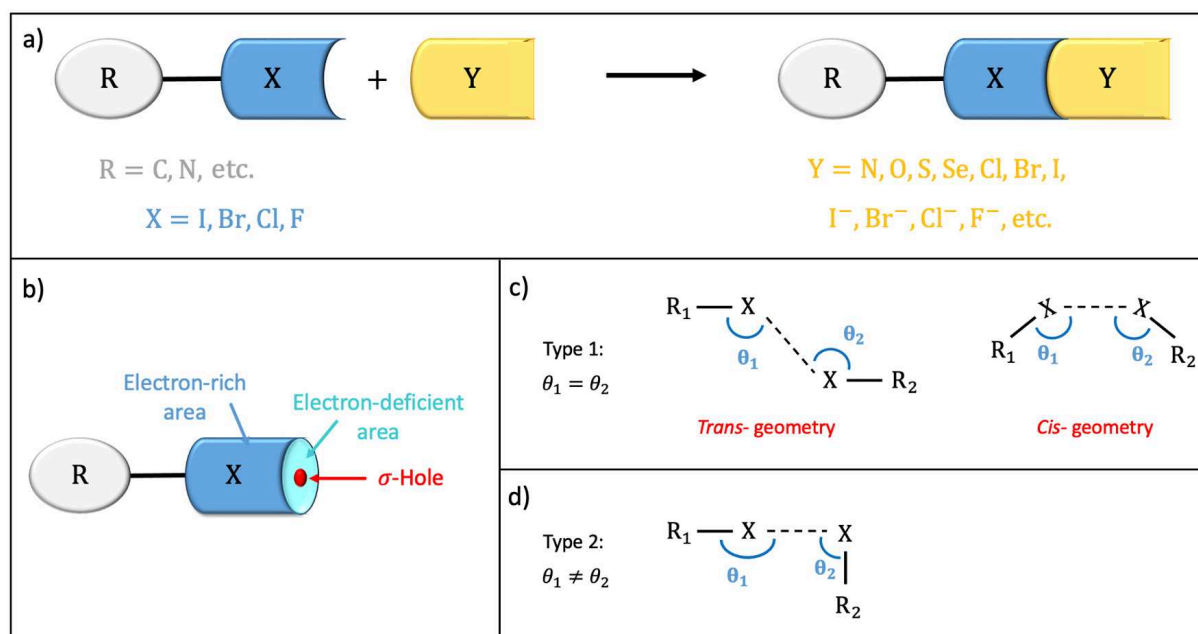
Figure 1.6. (a) Representative schematic of halogen bonds interaction. (b) Scheme of the anisotropic electron density dispersion around halogen atoms covalently bonded. (c, d) Type 1 (c) and type 2 (d) of halogen-halogen interactions. Adapted from [15],[31].

For instance, Kawai et al.[30] studied the self-assembly of the fully fluoro-substituted phenyleneethynylene (BPEPE-F18, Fig.1.7a) molecules on the Ag(111) surface. Despite being the poorest XB donor, fluorine can be used for mediating XB structures. The high-resolution AFM image in Fig.1.7b shows the appearance of the four benzene rings of BPEPE-F18 molecule with the same contrast. Also, highly directional $C - F \cdots F$ bonds were discovered and represented as white dashed lines in Fig.1.7c. By combining experimental and calculation studies, the directional $C - F \cdots F$ bonding is considered halogen-halogen bonding since the electrostatic potential on F is anisotropically distributed.

Figure 1.7. (a) Structure of the fully fluoro-substituted phenyleneethynylene (BPEPE-F18) molecule. (b) A High-resolution AFM image was taken at 4.8K showing BPEPE-F18 self-assembly on Ag(111). (c) Close-up image of the white square area in (b) with superimposed molecules. Figures are taken from [30].

1.1.5 Metal-organic interactions

Metal-organic interactions, also known as metal-ligand bonds, are ion-dipole interactions between organic moieties (or ligand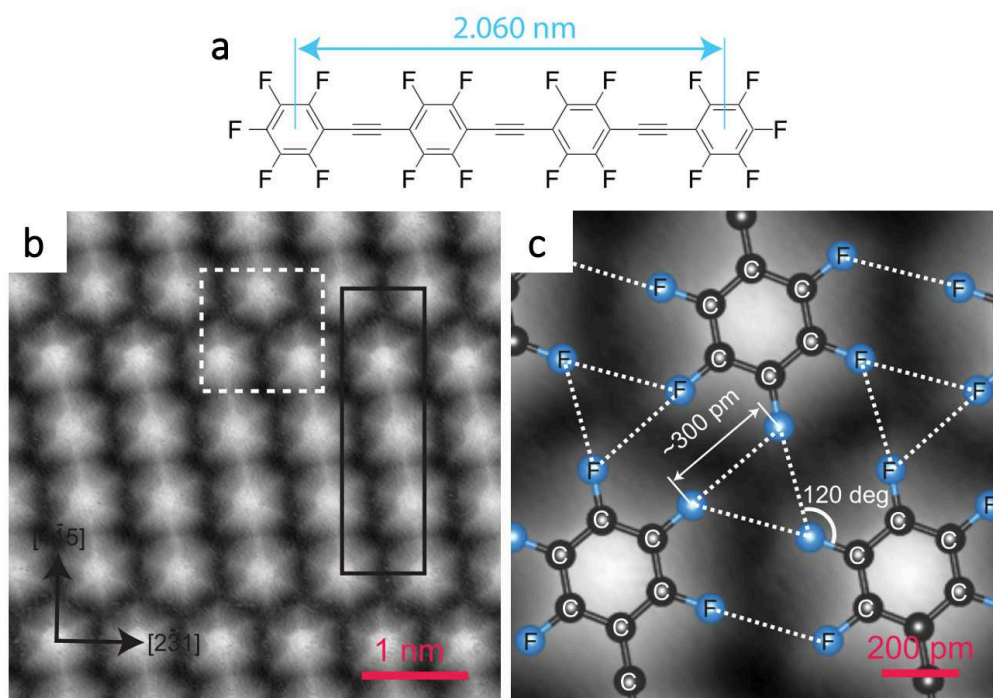s) and metallic centers. Typically, these interactions are stronger than hydrogen bonds (Table 1.1) and have also a selective and directive character[32]. For these reasons, metal-organic interactions are very interesting for the generation of supramolecular networks. They have been reported in one, two, and three dimensions[33]–[35]. Metal-organic interactions have been extensively studied in solution but they also represent an interesting topic for on-surface structures. The combination of a metal center (Cu, Fe, Co, Mn, etc.) and a functional group (carboxyl, hydroxyl, thiol, carbonitrile, etc.) leads to the creation of various coordination networks[17], [36]–[39]. The geometry of such arrangements is often determined by the organic moieties' properties (geometry, steric crowding, chemical function) and the electronic properties of the metal centers. Today, two approaches have been established to create such nanoarchitectures on solid surfaces: the co-adsorption of molecules with extrinsic metal centers, and the deposition of molecules directly on metal surfaces such as Cu, Au, Ag where the coordination is obtained through the intrinsic metal adatoms on the surface. For instance, after the deposition of the NC-Ph$_5$-CN molecules (Fig.1.8a) on Cu(111) surface held

at 250K, an extended honeycomb lattice was observed by Pivetta et al.[40]. This network is stabilized by the threefold interaction between CN groups and Cu adatoms, which is commensurate to the surface lattice (Fig.1.8c).
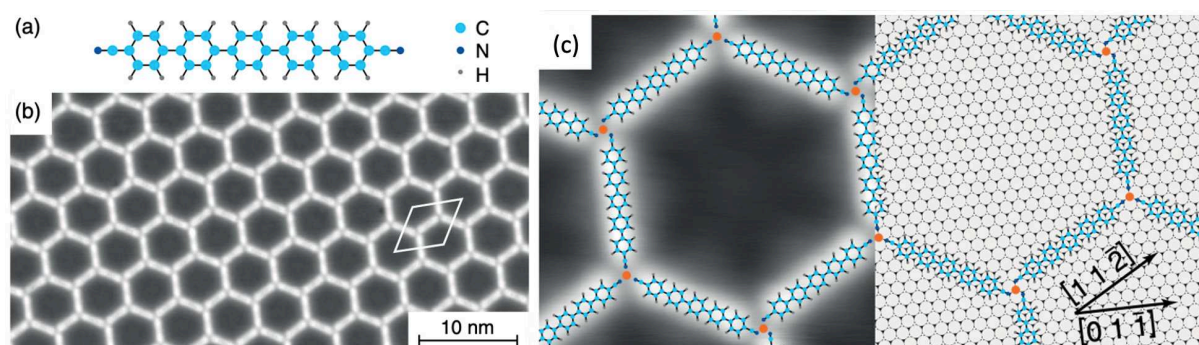

Figure 1.8. (a) Structure of the NC-Ph$_5$-CN molecule: Light blue, gray and cyan colors correspond to carbon, hydrogen, and Nitrogen atoms, respectively. (b) STM image showing the structure on Cu(111) surface covered by (NC-Ph$_5$-CN)$_3$Cu$_2$ honeycomb lattice ($V_t = -0.6$ V, $I_t = 20$ pA). (c) Close-up view of image (b) superposed with the corresponding model ($V_t = -0.02$ V, $I_t = 20$ pA). Figure taken from [40].

In addition, Di Giovannantonio et al.[41] studied the formation of the polymeric network created by Ullmann coupling of 1,4-dibromobenzene (dBB) on Cu(110) surface (Figure 1.9). The STM image shows the ordered structure observed at room temperature and the atomic resolution of the substrate (Fig.1.9b). The corresponding DFT model is given in (Fig.1.9c). Organometallic chains are formed at RT, corresponding to Ph-CuBr-Ph and showing that the halogen atoms are a critical stabilizing element for the formation of an intermediate structure in the Ullmann reaction. Fig.1.9d represents the C 1s core level for dBB deposited at different temperatures. Here again, the core level shift can be ascribed to the oxidation state of the C atoms within the different structures. For the thick film (4ML), the main component (red) at high BE corresponds to the C2 atoms in the pristine molecule. A small contribution (brown) is present at higher BE originating from the oxidized C1 atoms bound to Br. For 1ML at RT, three components are observed. The low BE component (1) is assigned to the reduced C1 atoms bound to Cu. The two other components (2 and 3) can be related to the remaining C atoms of the benzene rings (C2). The C-metal bond disappears after annealing at 500K. Only two components are then observed: component 4 is due to the C-H bond (C2) and component 5 to the C-C (C1).
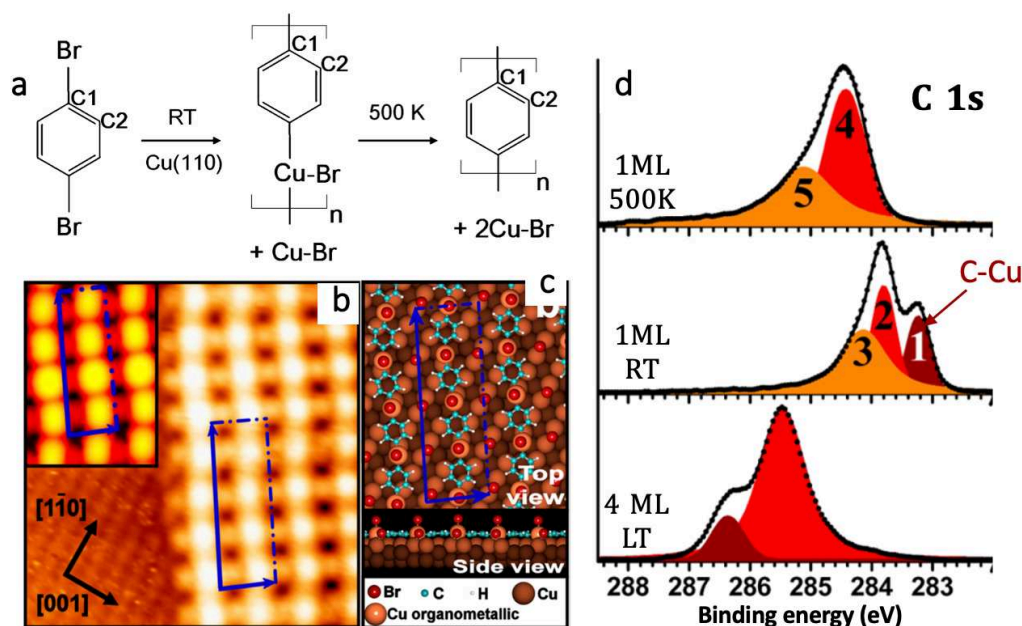
Figure 1.9. (a) Representative schematic of the intermediate formation of organometallic compounds in the Ullmann coupling reaction of 1,4-dibromobenzene on Cu(110). (b) 5.5nm × 5.5nm STM image of a submonolayer of dBB deposited on Cu(110) at RT. The lower left part showing the copper substrate with atomic resolution. The STM simulation of the structure is shown in the inset (2.1nm × 2.9nm). (c) Top and side views of DFT-optimized geometry. The blue vectors correspond to the unit cell. (d) C 1s core level spectra for dBB on Cu(110) for a thick film (4 ML) and for a monolayer deposition at different temperatures. Figures taken from [41].

1.1.6 Stereochemistry in adsorption systems

The stereochemistry is a branch of chemistry that studies the relative spatial arrangement in molecules[42]. An important part of this research area is the family of chiral molecules that cannot be superimposed on their mirror image by translation or rotation as shown in Fig.1.10a. The most frequent type of chiral molecule has a point chirality at a tetrahedral single atom. This atom is typically a carbon atom linked to four different groups and it represents the stereogenic (asymmetric) center of the molecule. These molecules can appear in two non-superimposable mirror forms, known as "*enantiomers*". Another type of molecule, called achiral, possess an inversion symmetry or mirror plane (Fig.1.10b). An intermediate case called "prochiral" molecules can also occur (Fig.1.10d). It corresponds to the molecules that are achiral in the gas phase, but upon adsorption they become chiral[43], [44]. Furthermore, the probability to form two enantiomers on the surface is the same. Thus, the adsorption of prochiral molecules leads always to the formation of a racemic mixture.
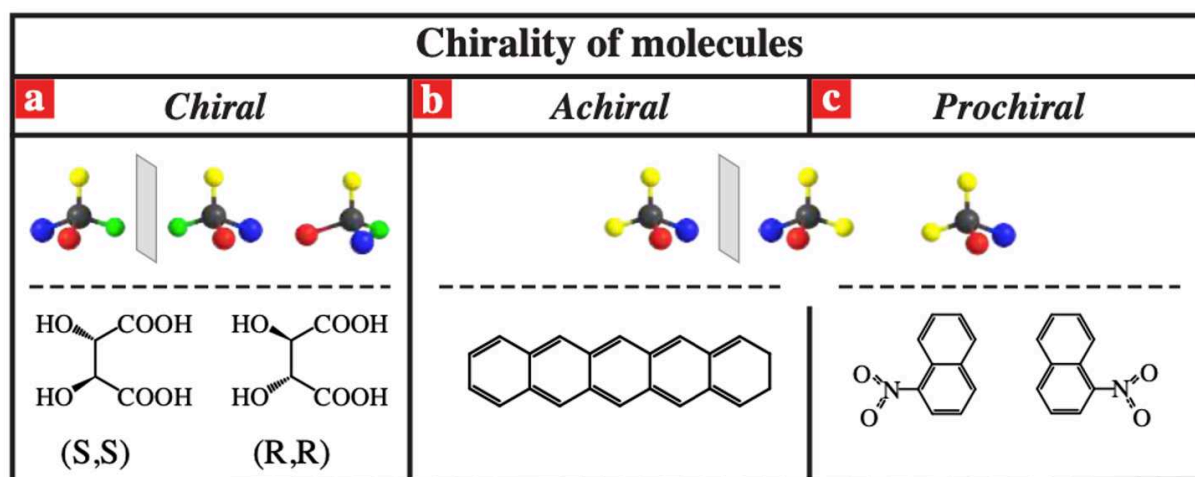
Figure 1.10. Representative schematic of molecule chiralities with the corresponding example. (a) Chiral molecules: tartaric acid. (b) Achiral molecules: pentacene. (c) Prochiral molecules: naphtho [2, 3-a] pyrene. Figure adapted from [45].

In recent years, surface chirality has received a lot of interest in experimental work[46], [47]. The chirality on surfaces can be induced by the adsorption of chiral molecules[48], [49]. It can also come from achiral molecules due to their chiral ordering on the substrate[44], [50]. Moreover, the substrate crystallography could have an impact on the chirality of the molecular structure at the surface[51]. In chapter 5 of this thesis, the chirality of organic nanostructure formed by on-surface reactions of a chiral molecular precursor, the (R)-6-bromo-3-phenyl-2,3-dihydro-1H-inden-1-one (BrPhINDO) molecule, deposited on Cu(111) surface will be discussed.

1.2 Parameters governing supramolecular self-assembly on surfaces

1.2.1 The molecular design

The intermolecular interactions can be modified by changing the molecular substituents used. This modification can result in important changes in the supramolecular organization. For example, Yokoyama et al.[52] studied four different molecules based on tertiarybutylphenyl porphyrin on Au(111) surface as illustrated in Fig.1.11. The first one is the H_2-TBPP molecule (Fig.1.11a) composed of a porphyrin core and four di-tertiarybutylphenyl (tBP) substituents. At low coverage, single isolated H_2-TBPP molecules are observed at the elbow of the Au(111) surface reconstruction (Fig.1.11e). The second one is the CTBPP molecule (Fig.1.11b) obtained by changing the tBP substituent of the H_2-TBPP molecule with a cyanophenyl substituent. CTBPP molecules self-assembled into triangular clusters on Au(111) surface at low coverage,

as shown in Fig.1.11f. According to DFT calculations (Fig.1.11j), these triangular clusters are formed by three CTBPP molecules coupled together through hydrogen bonds between the cyanophenyl substituents. The two other molecules are the *cis*- and *trans*-BCTBPP molecules obtained by replacing a second tBP group in the H$_2$-TBPP molecule with a cyanophenyl substituent (Fig.1.11c, d, respectively). The *cis*-BCTBPP molecules form supramolecular tetramer structures, Fig.1.11g. The *trans*-BCTBPP molecules are organized in linear chains stabilized by hydrogen bonds between the cyanophenyl substituents (Fig.1.11h). The anti-parallel cyanophenyl substituents in the observed structure are coupled to one another through $C - H \cdots N - C$ hydrogen bonds. This is confirmed by DFT calculations illustrated in Fig.1.11l.
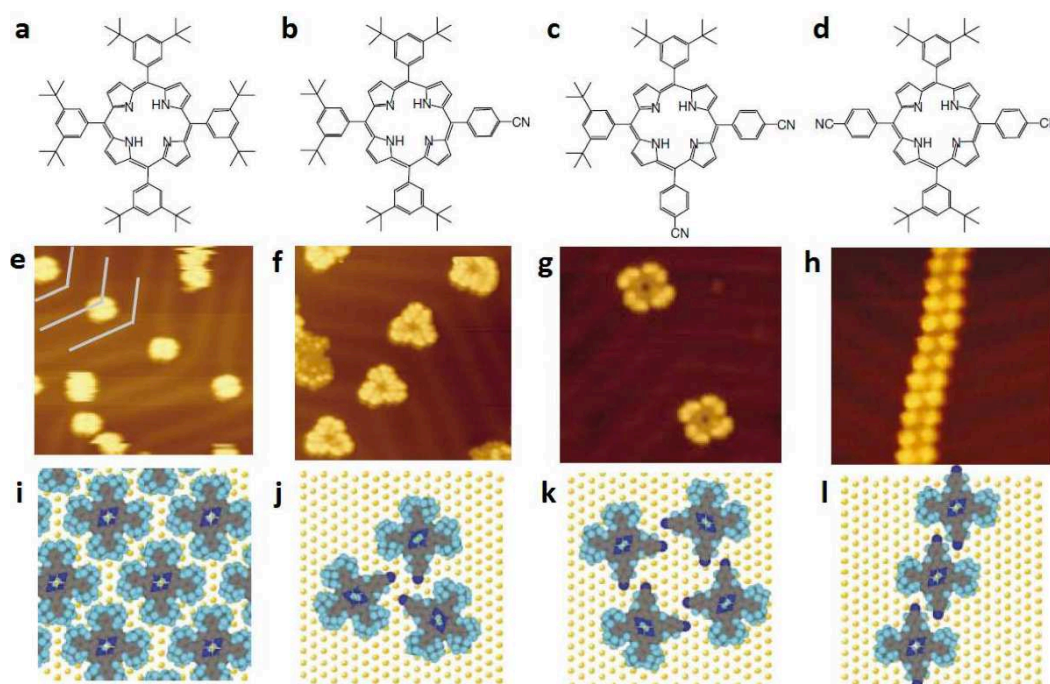
Figure 1.11. (a-d) Chemical structures of H$_2$-TBPP (a), CTBPP (b), *cis*-BCTBPP (d), and *trans*-BCTBPP (d). (e-h) 20 nm $\times$ 20 nm STM images at 63K on Au(111) surface and (i-l) the corresponding molecular models for H$_2$-TBPP (e, i), CTBPP (f, j), *cis*-BCTBPP (g, k), and for *trans*-BCTBPP (h, l). Figures adapted from [52].

1.2.2 Precursor coverage

The supramolecular self-assembly can be influenced by the precursor coverage. This amount is defined as the ratio between the area of the surface covered by molecules to the total area of the sample surface. It is expressed in terms of monolayer (ML), where 1ML corresponds to a surface that is fully covered by molecules in a defined phase. Depending on the surface coverage, different phases of self-assembled structures can be formed. For example, M. Stöhr

et al.[53] reported three different molecular organizations depending on the coverage of 4,9-diaminopherylene-quinone-3,10-diimine (DPDI) on Cu(111) surface (Fig.1.12). At a surface coverage between 0.1 and 0.7 ML, DPDI molecules self-assemble into a 2D honeycomb network with a DPDI molecule on each side of the hexagons. By increasing the surface coverage up to 0.85 ML, a 0D trimeric phase of DPDI molecule is formed, where three DPDI molecules are assembled into a triangle.
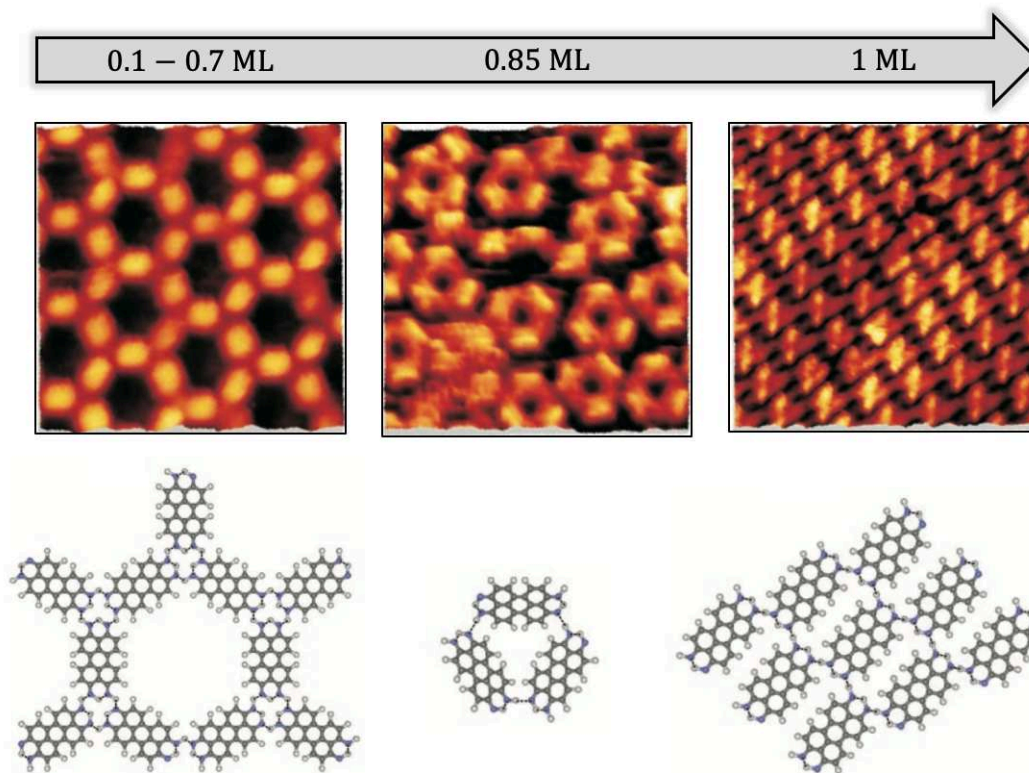
Figure 1.12. $9\,nm \times 9\,nm$ STM images and the corresponding chemical structures for different surface coverage of the DPDI molecules on Cu(111) surface. All the polymeric islands were obtained after annealing the sample at 300°C. Adapted from [53].

Finally, at higher surface coverage of 1 ML, molecular chains of DPDI molecules are created and leading to the formation of a closely-packed network. Therefore, the surface coverage is an important parameter for the control of supramolecular self-assembly of DPDI. For a low surface coverage, porous networks can be obtained, while a high surface coverage facilitates the formation of compact structures.

1.2.3 The substrate

Another parameter that can drastically affect the supramolecular self-assembly is the substrate used. For example, the Cu(111) surface has a strong reactivity and can be used to

create preferential adsorption sites. The deposition of anthraquinone molecules[54] on Cu(111) surface leads to the formation of a porous hexagonal network which is not observed on surfaces with less reactivity. Moreover, Diekhöner et al.[55] deposited the trimesic acid (TMA) molecules on three different substrates and observed them with STM. On Ag(111), TMA molecules self-assemble into a honeycomb phase, as shown in Fig.1.13a. After annealing of the substrate at 420K, a close-packed phase is formed, presented in Fig.1.13b. On Cu(111) surface (Fig.1.13c, d), TMA molecules have always a triangular form and thus, are still lying flat on the surface. The STM image shows a honeycomb structure with the same periodicity and bonding distance as on Ag(111).
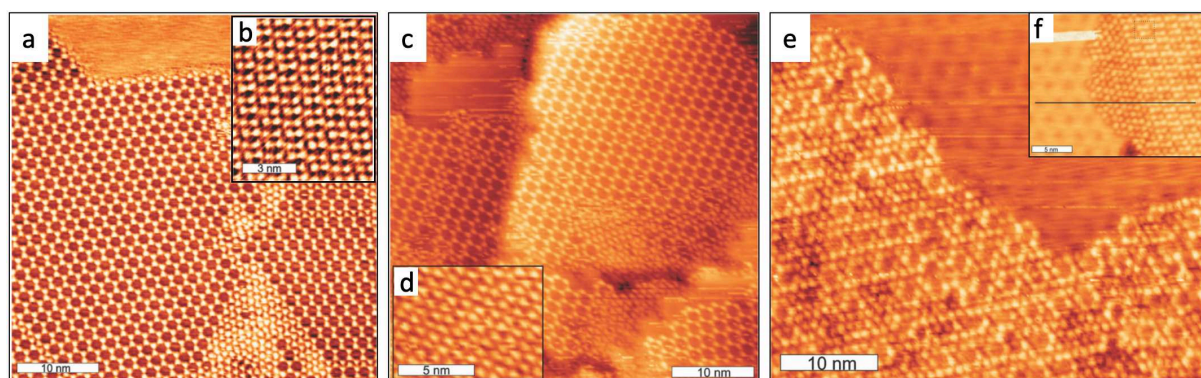
Figure 1.13. STM images of TMA molecules on (a, b) Ag(111), on (c, d) Cu(111), and on (e, f) Ag/Cu(111) surfaces: (a) honeycomb structure after deposition at room temperature. (b) Close-packed phase after annealing at 420K. (c) Honeycomb and close-packed phases after deposition of 0.7 ML at RT. (d) Close-up image of the "High-density" structure. (e) Intermixed structure at RT of sub-monolayer of TMA and (f) the structure after annealing at 350K.Reproduced from [55].

However, on some regions of the surface (around 20%), closer packed structures are also observed (Fig.1.13d), different from that observed on the Ag surface after annealing. The third substrate was the Ag (1 ML) evaporated on Cu(111) surface. TMA molecules form a combined phase consisting of a standard honeycomb structure with a TMA molecule in the center of each hexagonal pore and some patches with closer packed TMA molecules. After annealing the sample to 350K, a well-ordered close-packed phase is formed (Fig.1.13f). This phase with two pair-up TMA molecules was also observed locally on Ag(111) surface.

Another interesting factor that can strongly tune the molecular self-assembly process is the surface reconstruction. According to Böhringer et al.[56], the formation of self-assembled organic nitronaphthalene nanoclusters was facilitated by the Au(111) $(22 \times \sqrt{3})$ surface reconstruction.

F. Silly et al.[57] provide another example of the formation of organic self-assembly via surface reconstruction. Figure 1.14 illustrates their results for the PTCDI-melamine thin film grown on Au(111) surface. After deposition of PTCDI and melamine on Au(111) surface followed by subsequent annealing at 80°C for 15 hours, a supramolecular architecture is formed (Fig.1.14a). This network consists of the alternation of double rows of hexagons and single rows of parallelograms. Each hexagon is composed of 6 PTCDI and 6 Melamine molecules, while each parallelogram is composed of 4 PTCDI and 6 Melamine molecules (Fig.1.14b). The molecular architectures are both stabilized by two H ⋯ O and one H ⋯ N hydrogen bonds between PTCDI and melamine molecules. The separation between two adjacent parallelogram rows is 6.3 nm, matching the periodicity of the herringbone reconstruction along the $[1\bar{1}0]$ direction. In contrast, PTCDI and Melamine molecules form a honeycomb structure composed only of hexagons on other substrates such as Ag/Si(111) surface[12], as described in paragraph 1.1.3 above. This example demonstrates the influence of the surface reconstruction of Au(111) to tailor the PTCDI-Melamine self-assembly in order to match the $[1\bar{1}0]$ direction periodicity of the surface reconstruction.
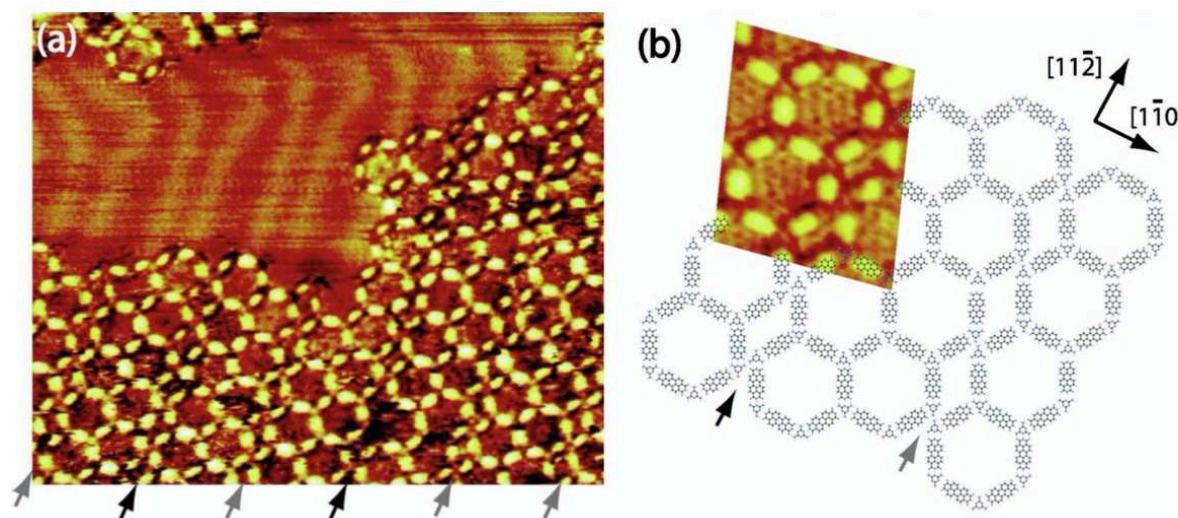

Figure 1.14. (a) Room temperature STM image of the PTCDI-melamine supramolecular network (hexagons and parallelograms) formed on Au(111) substrate. (b) the corresponding molecular model of the PTCDI-melamine nanoarchitecture with a high-resolution STM image superimposed. The gray and black rows correspond to the two different types of parallelograms. Taken from [57].

1.3   On-surface synthesis of covalently bonded nanostructures

The bottom-up fabrication of molecular nanostructures directly on the surface by covalent bond formation is also called the on-surface synthesis approach. Recently, it has gained an enormous research interest since it represents a successful method to produce functional nanostructures, 1D molecular wires, nanoribbons, and 2D networks on surfaces[58], [59]. However, although on-surface synthesis stabilized by covalent bond produces more stable networks than self-assembled networks stabilized by non-covalent intermolecular interactions, it is still difficult to create highly ordered nanoarchitectures since the diffusion control of each reaction component on surfaces is not easy. Several organic reactions that allow the creation of ordered and extended networks have been reported on surfaces in UHV such as Ullmann coupling, terminal alkyne coupling, aryl-aryl dehydrogenation, Diels-Alder reaction, etc., which are known processes in solution chemistry[60]. Table 1.2 summarizes the frequent examples of this reaction type and their chemical reaction schemes as well as the corresponding references. In contrast to solution reactions, the molecules are confined in two-dimensional space, which reduces their degrees of freedom while they diffuse on the underlying substrate. The achievement of such reactions (Table 1.2) is sometimes complicated in the solution phase because the molecules are barely or not soluble in typical solvents. Moreover, due to the catalytic activities of the surface and UHV environment, some reactive substances and intermediates, which are not allowed in the classical approach, can be stabilized and new unexpected reactions might occur. In this concept, further considerations are required for successful on-surface synthesis reactions. The three crucial factors are resumed in the following points:

i.   The choice of the surface (materials type or crystallographic orientation, etc.) through the control of molecular diffusion. Also, surfaces should play a catalytic role and exhibit chemical reactivity with the deposited molecular units.

ii.   The rational design of molecular building blocks, particularly functional groups which are designed to initiate covalent bonding with consideration of the molecule-molecule and molecule-substrate interactions.

iii. Response to external stimuli such as thermal annealing, UV irradiation, electron injection, etc.

The chemistry of on-surface reactions is influenced by a variety of parameters, making it difficult to consider all cases in detail. Therefore, the second section will focus on the importance of different stimuli to achieve a successful on-surface synthesis reaction such as heat treatment, UV irradiation, and tip-induced reactions.
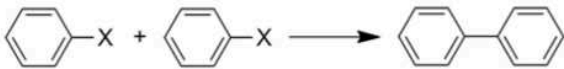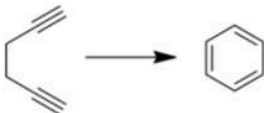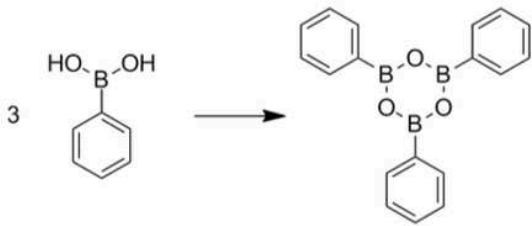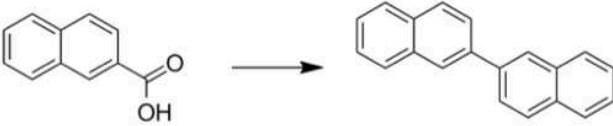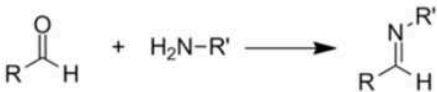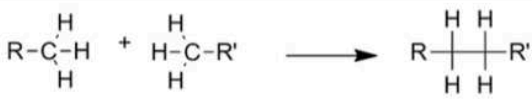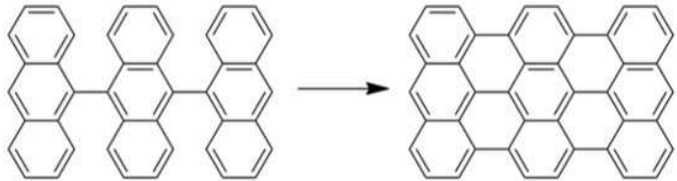
Reaction type	Scheme of chemical reaction	Ref.
Ullmann coupling		[61],[62]
Alkyne coupling	R—≡—H + H—≡—R ⟶ R—≡—≡—R	[63],[64]
Bergman reaction		[65],[66]
Boronic acid condensation		[67]-[69]
Decarboxylation reaction		[70]
Diels-Alder reaction		[71]
Dealkylation of ethers	R-O-R ⟶ R-OH + HO-R	[72]
Schiff-base reaction		[73]-[75]
Wurtz coupling	R–X + X–R ⟶ R–R	[76]
Alkane polymerization		[77]
Aryl-aryl dehydrogenation		[59],[78]

Table 1.2. Categories of on-surface reactions with the corresponding chemical reactions schemes and the corresponding references.

1.4 Influence of external parameters on the formation of organic nanoarchitectures by on-surface synthesis

1.4.1 Thermal annealing

Since 2007, the thermal annealing is considered the most adapted approach in on-surface synthesis after the successful work of Grill et al.[62]. Here, the temperature can be precisely controlled by using different technologies such as cryocoolers, heaters, thermocouples, pyrometers, etc. In fact, this approach is more efficient for large-area synthesis since the samples are totally heated, and it prevents a spatial control of the reaction on the surface. In addition, the polymerization of nanostructures induced by thermal control is a good way to produce covalently bonded nanostructures on surfaces[62], [77], [79]. This technique can produce sequential on-surface processes such as activation of molecules with distinct inequivalent reaction sites. For instance, Fasel et al.[59] used thermal annealing to generate atomically precise graphene nanoribbons (GNRs). They developed a new two-step approach by Ullmann-type coupling and cyclodehydrogenation. Here, the 10,10'-dibromo-9,9'-bianthryl molecules (DBBA, Fig.1.15a) were firstly deposited on the Au(111) surface. The first thermal annealing at 473K facilitated the debromination of DBBA precursors to create dehalogenated intermediates coupled to one another by C-C bonding. They diffuse on the surface, leading to the formation of non-planar linear polymers (Fig.1.15b). The STM image and simulations show the adjacent anthracene units which are tilted in the opposite direction from the metal surface. Then, further annealing of the sample at 673K allows the formation of armchair graphene nanoribbons (AGNR) where the intramolecular cyclodehydrogenation of the non-planar previously formed polymer took place. Figure 1.15 illustrates the whole chemical process. This example, like many others in the literature, demonstrate how thermal annealing can influence the possibility of some specific reaction pathways, thus providing new ways to produce functional products.
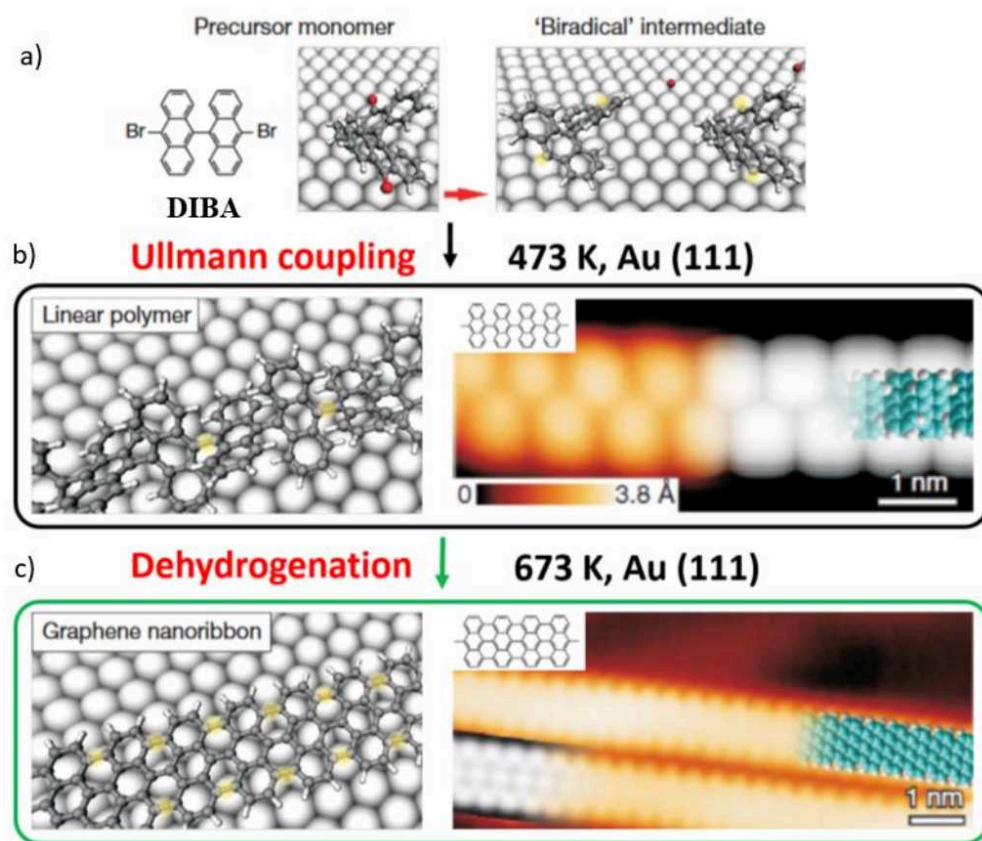
Figure 1.15. (a) Chemical structure (left) and the dehalogenation process (right) of the 10,10'-dibromo-9,9'-bianthryl precursor. (b) STM image (right panel) and the corresponding model (left panel) of the non-planar linear polymers formed by covalent bonding (Ullmann coupling) between the dehalogenated intermediates obtained after annealing the sample at 473K. (c) STM image (right panel) and the corresponding model (left panel) of GNRs formed by cyclodehydrogenation of the linear polymer after subsequent annealing at 673K. Figures adapted from [59].

1.4.2 UV irradiation

Another way to activate on-surface reactions is by UV irradiation. This approach has many advantages as:

i.   The required chemical reactive group is selectively excited according to the wavelength and light radiation polarization.

ii. High spatial resolution up to the limit of light diffraction (a few hundred nm), providing a better localization of the reaction than thermal annealing.

iii. Activation of the molecular systems from a distance without using chemicals since UV is a non-invasive source of energy.

The excitation of molecular adsorbates on surfaces in UHV as well as in air conditions can be performed through two different processes: adsorbate-excitation (ADS) and hot electron attachment (HEA)[80]. In the ADS photochemistry mechanism, a direct light-excitation of an electron from the HOMO towards its LUMO state is taking place by the adsorption of an incident photon into one molecular adsorbate, as presented in Fig.1.16a. Therefore, the role of the substrate is only limited to a slight modification of the HOMO-LUMO gap of the used molecule which is related to the molecular orbitals and surface hybridization. Thus, this process could take place on various underlying surfaces such as metals, semi-conductor, or bulk insulator surfaces.
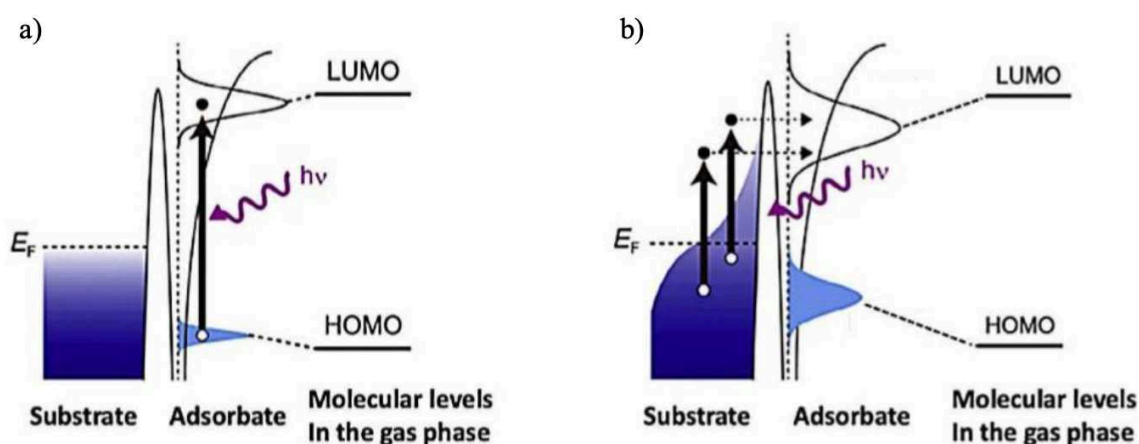
Figure 1.16. Schematic of photochemical reaction mechanisms for a molecule adsorbed on a surface: a) ADS process: Intramolecular excitation of one electron from the HOMO state to the LUMO state arising from light-absorption. B) HEA process: based on the attachment of one photoexcited hot electron of the substrate to the LUMO state of adsorbates. Black and white spots represent electrons and holes, respectively. Images adapted from [80].

The second mechanism is the hot electron attachment (HEA) where one photoexcited hot electron of the surface attaches to the LUMO state of the adsorbed molecule, leading to the formation of a transient anionic state (Fig.1.16b). HEA process requires primarily metal surfaces due to their optical properties allowing the creation of hot electrons upon light absorption. The two processes are distinctive by the wave-length required for electron excitation to occur: the ADS frequently needs a wavelength shorter than 300 nm, while HEA requires a higher wavelength.

An example of this technique is the deposition of 4-bromo-4'-hydroxy-biphenyl (BHBP) molecule on Ag(111) surface investigated by Chen et al.[81]. The BHBP molecule is composed of two benzene rings ended with a hydroxyl group on one side and with a bromine group on the other side (Fig.1.17a). An extended ordered square-like architecture was observed after the deposition, as shown in the STM image of Fig.1.17b. Each side of the square has a rod shape that can be attributed to an intact BHBP molecule. In STM images, the bromine group appears brighter than the hydroxyl group due to the higher electronic density of states. This is confirmed by the simulated STM image in Fig.1.17c. The use of four BHBP molecules allows the formation of four halogen bonds between the C-Br groups and four hydrogen bonds between the hydroxyl groups. This is in accordance with the bright protrusions and the dim depression of the squared structure in the STM image, respectively. After that, the entire surface was irradiated by UV laser for 10 minutes, leading to the transformation of the squared-like structure into a hexagonal porous network (Fig.1.17d). The size of each side of the hexagons is shorter than the intact BHBP molecule. Moreover, the bright and dark protrusions disappeared. In this way, each side of the hexagon was ascribed to a biphenyl biradical molecule stabilized by the substrate Ag atoms. In this study, Chen et al. declaimed that the UV irradiation induced the occurrence of C-Br and C-OH cleavage. By further annealing of the sample at room temperature, linear polymers with hundreds of nanometers in length were formed (Fig.1.17g). These polymers are poly-*p*-phenylene chains formed of the biphenyl radicals connected to one another by C-C coupling. The experiment without UV irradiation failed to produce biradical structures or polymers which highlights the crucial role of UV irradiation for the C-OH and C-Br cleavage at low temperatures.
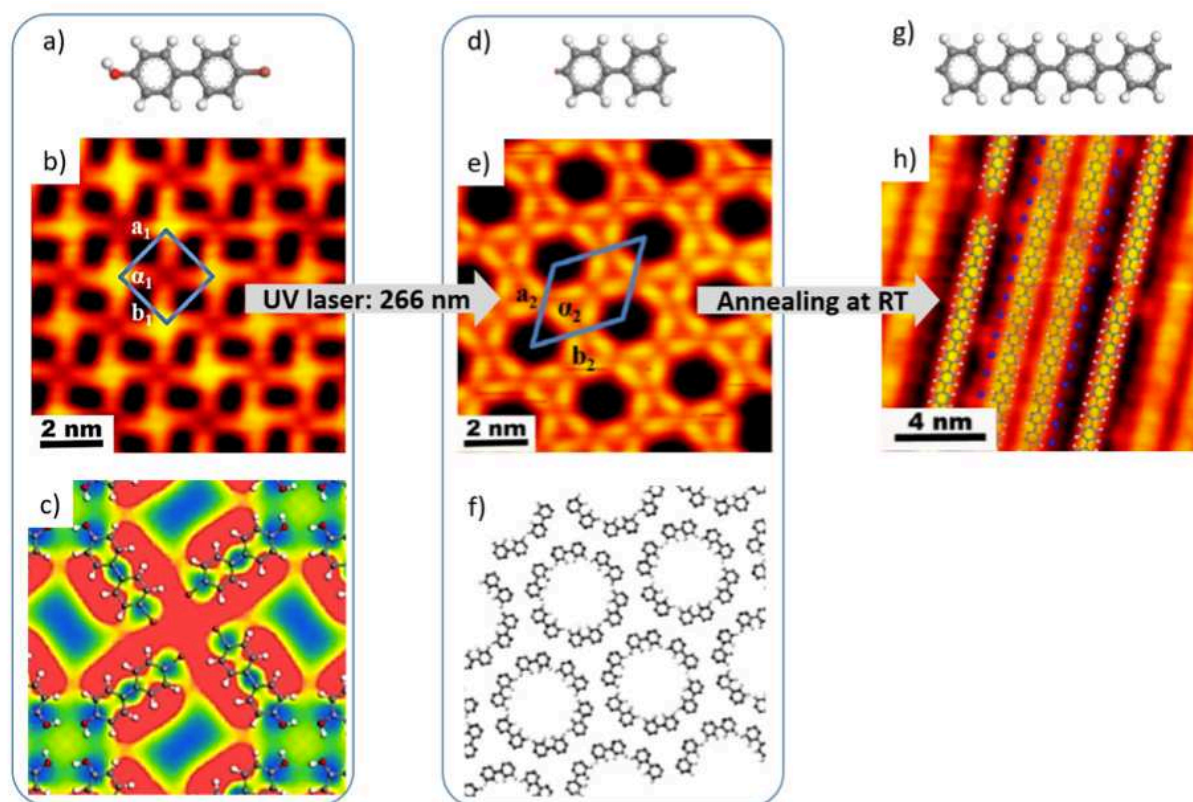
Figure 1.17. Block 1) Before UV irradiation: (a) Molecular structure of the 4-bromo-4'-hydroxy-biphenyl (BHBP) molecule. Carbon, hydrogen, bromine, and oxygen atoms are shown as grey, white, ochre, and red atoms, respectively. (b) STM image measured at 77K of BHBP molecules self-assembled on Ag(111) surface. (c) STM simulations of the square-like structure observed in (b). Block 2) After 10 min UV irradiation at 80K (wavelength 266 nm): (d) molecular structure of the generated biphenyl biradicals. (e) STM image of the hexagonal nanopores and (f) the corresponding molecular model. Block 3) After 1h annealing of the sample at RT: (g) Molecular structure showing the C-C coupling between biradicals. (h) High-resolution STM image of linear polymers superimposed with the molecular model. Figure adapted from [81].

1.4.3 Tip induced reaction

The tunneling current and the bias voltage are important parameters to obtain a high-resolution STM image and they can be used to conduct a chemical reaction in the case of an inelastic tunneling process. The sharp tip of STM acts as an electron emitter and can be an excellent candidate to activate tip-induced on-surface reactions in addition to the thermal annealing and light external stimuli. Depending on the polarity of the bias voltage applied between the tip and the sample, the tunneling current can flow from the tip into empty electron states above the Fermi level (E_F) of the sample or, otherwise, from the sample into empty states

of the tip. In addition to their electronic structures, molecules also have a mechanical degree of freedom (translation, rotation, and vibration), that can be excited via an inelastic tunneling process (IET) by the tunneling electrons. While IET process, tunneling current and bias voltage could be utilized to conduct a chemical reaction by using tunneling electrons or electric field between the tip and the sample. It is realized by locating the STM tip at the proximity of the surface. Thus, the tunneling electrons energy leads to a various excitation (Fig.1.18).
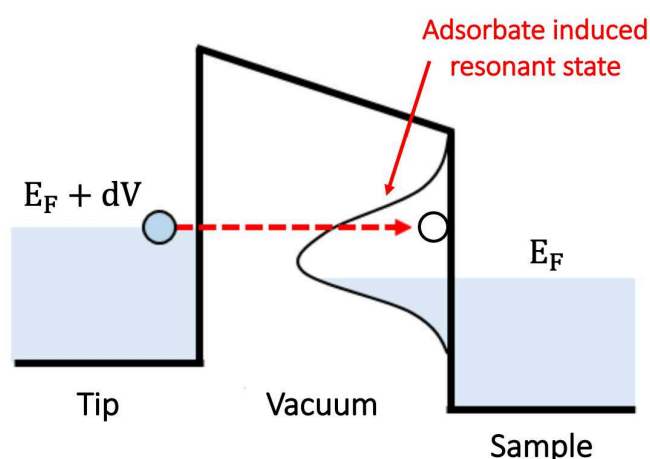
Figure 1.18. Schematic representative of electron injection in an inelastic-electron tunneling (IET) process. Figure reproduced from [82].

Therefore, the advantage of this technique is the possibility to control the initialization of the reaction with atomic resolution and monitor the reactants and products at the precise moment. For example in 2000, Hla et al.[82] successfully realized the Ullmann coupling reaction of iodobenzene molecules on Cu(111) surface using STM tip in manipulation. The adsorption process of two intact iodobenzene molecules at Cu(111) step edge is shown in Fig.1.19. In the first manipulation, electrons have been injected by positioning the STM tip at a fixed height above the molecule and applying a bias voltage of 1.5 V. Two protrusions are formed as a result of the iodine-carbon bond cleavage (Fig.1.19b, c). They correspond to the iodine atom (smaller protrusion) and the phenyl molecule (larger protrusion) after the cleavage. Then, a lateral manipulation was performed to space the iodine atom and the phenyl molecule (Fig.1.19d). The iodine atom in the middle of two phenyls was moved out of this domain, leaving the reaction path (Fig.1.19e). A final manipulation was performed to bring the two phenyls close to each other by C-C coupling (Fig.1.19f).
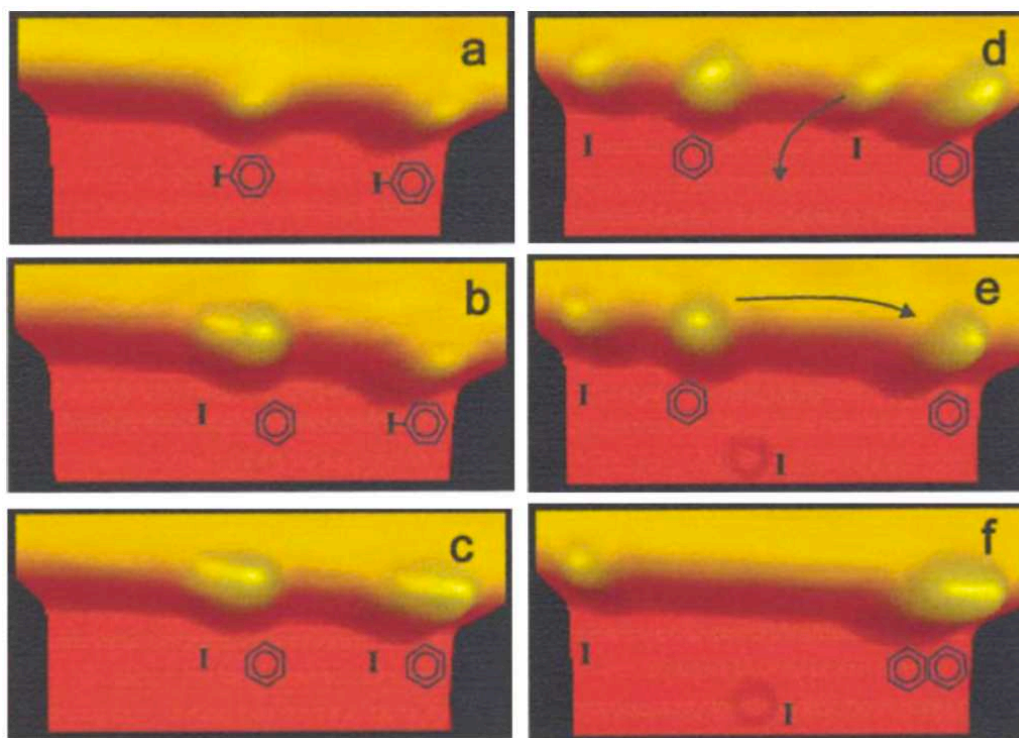
Figure 1.19. STM images showing the different steps of the tip-induced Ullmann coupling reaction. (a) Adsorption of two iodobenzene molecules at the step edge of Cu(111) substrate. (b, c) Abstraction of the two iodine from molecules by a voltage pulse. (d) Separation of iodine atoms from phenyl radicals by lateral manipulation. (e, f) The two phenyls are brought close to each other after leaving the iodine atom of the reaction path. Figures adapted from [82].

This technique is not only a molecular-scale technique but it is also adapted to create large polymers. For example, the control of a two-dimensional polymer on a metallic surface using tip manipulation was demonstrated by our group[83]. The deposition of a boronic acid precursor (BDBA) on an Ag(100) surface leads to the formation of 2D supramolecular networks. Then, the molecular domain was locally perturbed thanks to the use of the STM tip in order to initiate a dehydration reaction. The latter propagated slowly until the H-bonded phase disappeared completely and an extended nanoporous covalent network was formed. The evolution of the reaction is illustrated in Fig.1.20.
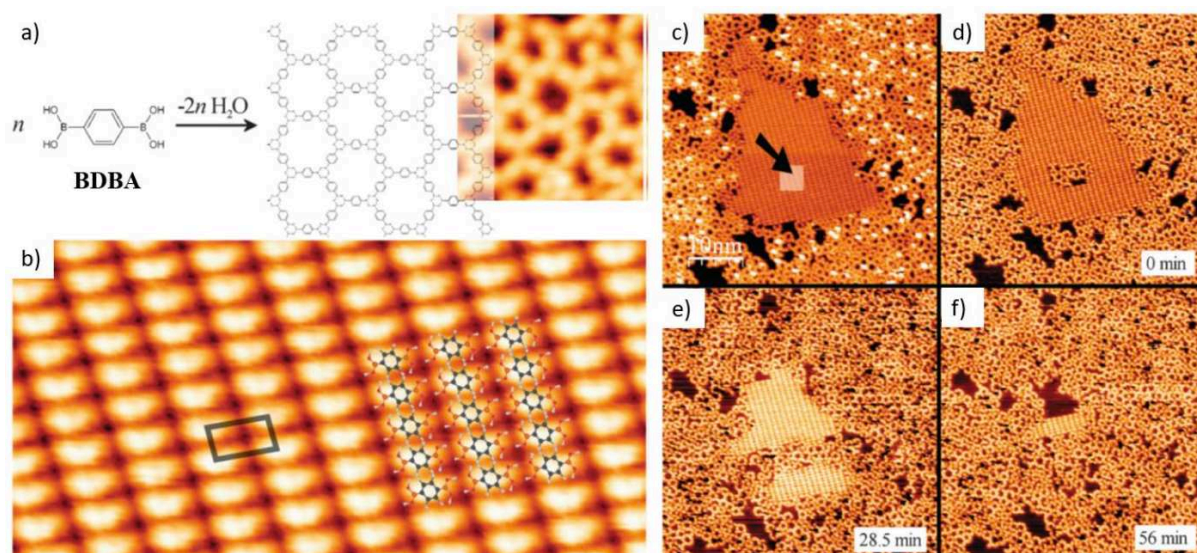
Figure 1.20. (a) Schematic representation of the 1,4-benzenediboronic acid (BDBA) tip-induced polymerization on Ag (100) surface (left panel) and STM image of the real polymer network (right panel). (b) $10 \times 5 \ nm^2$ STM image of BDBA hydrogen-bonded phase with a superimposed model. (c) A small area (white rectangle) is scanned after bringing the STM tip very close to the H-bonded layer. (d) The polymerization is immediately initiated and (e, f) propagates progressively until the H-bonded phase has completely disappeared. Figures from [83].

1.5   Outline of the thesis

In the past two decades, surface-supported supramolecular self-assembly and on-surface reactions have emerged as promising strategies to grow functional molecular building blocks with atomic precision, with potential applications in the nanotechnology field. As presented in this chapter, a lot of works has been invested to enrich the toolbox of supramolecular self-assembly and on-surface synthesis as well as to obtain a better knowledge of the chemical reaction mechanisms on the surfaces. Nevertheless, further contributions are required both to increase our knowledge and experience in the field and to apply that knowledge in practical and beneficial applications in future. In this context, the work of this thesis was carried out.

In this thesis, the presented results involve the preparation of supramolecular self-assembly on the carbon-based surface HOPG as well as the on-surface synthesis on the noble Cu(111) metallic surface. Various techniques are used for surface characterization such as Scanning tunneling microscopy at ambient conditions (room-temperature STM) and under ultra-high vacuum conditions (low-temperature STM), X-ray photoemission spectroscopy (XPS), atomic force microscopy (AFM), and density functional theory (DFT). The combined study of all these

techniques enables the disclosure of the potential mechanisms. Therefore, the thesis manuscript is organized as follows:

Chapter 2 represents the experimental techniques and set-up used during my PhD and gives a brief presentation of the different types of substrates, sample preparations, and a description of the UHV LT-STM experimental set-up of our group at IM2NP. The results obtained in this thesis are presented in Chapter 3, Chapter 4, and Chapter 5.

Chapter 3 focuses on the control of the size of the domains formed by the self-assembly process by non-covalent bonds between two organic molecules on the HOPG substrate. The experimental results are performed under ambient conditions and monitored by STM.

Chapter 4 investigates the drive of the homocoupling reaction using the on-surface synthesis approach of a new dithiophenyl-functionalized precursor on Cu(111) surface. Thermal annealing leads to the activation of the C-S reaction and the formation of fully conjugated reticulated networks formed with interconnected unsaturated hydrocarbon chains.

Chapter 5 concentrates on the study of the adsorption of a chiral molecule on the Cu(111) surface and the various low-dimensional structures formed by different types of intermolecular reactions. We demonstrate that adsorption-induced chiral inversion leads to partial racemization.

The thesis is finalized by a general conclusion in which we summarize all the results and open the door for further perspectives.

References of chapter 1

[1]   H. W. Roesky and M. Andruh, "The interplay of coordinative, hydrogen bonding and π–π stacking interactions in sustaining supramolecular solid-state architectures.," *Coord. Chem. Rev.*, vol. 236, no. 1–2, pp. 91–119, Jan. 2003, doi: 10.1016/S0010-8545(02)00218-7.

[2]   S. De Feyter and F. C. De Schryver, "Two-dimensional supramolecular self-assembly probed by scanning tunneling microscopy," *Chem. Soc. Rev.*, vol. 32, no. 3, pp. 139–150, Apr. 2003, doi: 10.1039/b206566p.

[3]   J. V. Barth, G. Costantini, and K. Kern, "Engineering atomic and molecular nanostructures at surfaces," in *Nanoscience and Technology*, Co-Published with Macmillan Publishers Ltd, UK, 2009, pp. 67–75. doi: 10.1142/9789814287005_0008.

[4]   K. Tahara *et al.*, "Two-Dimensional Porous Molecular Networks of Dehydrobenzo[12]annulene Derivatives via Alkyl Chain Interdigitation," *J. Am. Chem. Soc.*, vol. 128, no. 51, pp. 16613–16625, Dec. 2006, doi: 10.1021/ja0655441.

[5]   M. Abel, A. Dmitriev, R. Fasel, N. Lin, J. V. Barth, and K. Kern, "Scanning tunneling microscopy and x-ray photoelectron diffraction investigation of C 60 films on Cu(100)," *Phys. Rev. B*, vol. 67, no. 24, p. 245407, Jun. 2003, doi: 10.1103/PhysRevB.67.245407.

[6]   B. Calmettes, S. Nagarajan, A. Gourdon, M. Abel, L. Porte, and R. Coratger, "Bicomponent Supramolecular Packing in Flexible Phthalocyanine Networks," *Angew. Chem. Int. Ed.*, vol. 47, no. 37, pp. 6994–6998, Sep. 2008, doi: 10.1002/anie.200802628.

[7]   L. Gao *et al.*, "Understanding and controlling the weakly interacting interface in perylene ∕ Ag (110)," *Phys. Rev. B*, vol. 73, no. 7, p. 075424, Feb. 2006, doi: 10.1103/PhysRevB.73.075424.

[8]   C. Janiak, "A critical account on π–π stacking in metal complexes with aromatic nitrogen-containing ligands †," *J. Chem. Soc. Dalton Trans.*, no. 21, pp. 3885–3896, 2000, doi: 10.1039/b003010o.

[9]   Christian G. Claessens, J. Fraser Stoddart, "π–π INTERACTIONS IN SELF-ASSEMBLY," Journal of Physical Organic Chemistry, pp. 254–272, 1997.

[10]   C. A. Hunter and J. K. M. Sanders, "The nature of .pi.-.pi. interactions," *J. Am. Chem. Soc.*, vol. 112, no. 14, pp. 5525–5534, Jul. 1990, doi: 10.1021/ja00170a016.

[11]   Johannes V. Barth Priv.-Doz. Dr., Jens Weckesser, Chengzhi Cai Dr., Peter Günter Prof. Dr., Lukas Bürgi Dr., Olivier Jeandupeux Dr., Klaus Kern Prof. Dr, "Building Supramolecular Nanostructures at Surfaces by Hydrogen Bonding," Angewandte International Edition Chemie, pp. 1230–1234, Apr. 04, 2000.

[12]   J. A. Theobald, N. S. Oxtoby, M. A. Phillips, N. R. Champness, and P. H. Beton, "Controlling molecular deposition and layer structure with supramolecular surface assemblies," *Nature*, vol. 424, no. 6952, pp. 1029–1031, Aug. 2003, doi: 10.1038/nature01915.

[13]   G. R. Desiraju, "The C−H···O Hydrogen Bond: Structural Implications and Supramolecular Design," *Acc. Chem. Res.*, vol. 29, no. 9, pp. 441–449, Sep. 1996, doi: 10.1021/ar950135n.

[14]   Thomas Steiner Dr., "The Hydrogen Bond in the Solid State," Angewandte International Edition

Chemie, pp. 48–76, Jan. 04, 2002.

[15]   T. T. T. Bui, S. Dahaoui, C. Lecomte, G. R. Desiraju, and E. Espinosa, "The Nature of Halogen⋯Halogen Interactions: A Model Derived from Experimental Charge-Density Analysis," *Angew. Chem.*, vol. 121, no. 21, pp. 3896–3899, May 2009, doi: 10.1002/ange.200805739.

[16]   G. Cavallo *et al.*, "The Halogen Bond," *Chem. Rev.*, vol. 116, no. 4, pp. 2478–2601, Feb. 2016, doi: 10.1021/acs.chemrev.5b00484.

[17]   A. Dmitriev, H. Spillmann, N. Lin, J. V. Barth, and K. Kern, "Modular Assembly of Two-Dimensional Metal–Organic Coordination Networks at a Metal Surface," *Angew. Chem.*, vol. 115, no. 23, pp. 2774–2777, Jun. 2003, doi: 10.1002/ange.200250610.

[18]   W. Wang, X. Shi, S. Wang, M. A. Van Hove, and N. Lin, "Single-Molecule Resolution of an Organometallic Intermediate in a Surface-Supported Ullmann Coupling Reaction," *J. Am. Chem. Soc.*, vol. 133, no. 34, pp. 13264–13267, Aug. 2011, doi: 10.1021/ja204956b.

[19]   José I. Urgel, David Écija, Guoqing Lyu, Ran Zhang, Carlos-Andres Palma, Willi Auwärter, Nian Lin & Johannes V. Barth, "Quasicrystallinity expressed in two-dimensional coordination networks," nature chemistry, May 16, 2016.

[20]   C. Peng *et al.*, "Structural Evolutions of the Self-Assembled *N* -Decyldecanamide on Au(111)," *J. Phys. Chem. C*, vol. 122, no. 39, pp. 22538–22543, Oct. 2018, doi: 10.1021/acs.jpcc.8b06517.

[21]   K. S. Mali and S. De Feyter, "Principles of molecular assemblies leading to molecular nanostructures," *Philos. Trans. R. Soc. Math. Phys. Eng. Sci.*, vol. 371, no. 2000, p. 20120304, Oct. 2013, doi: 10.1098/rsta.2012.0304.

[22]   E. Geagea, J. Jeannoutot, L. Morgenthaler, S. Lamare, F. Palmino, and F. Chérioux, "On-Surface Synthesis of Ligands to Elaborate Coordination Polymers on an Au(111) Surface," *Nanomaterials*, vol. 11, no. 8, p. 2102, Aug. 2021, doi: 10.3390/nano11082102.

[23]   W.-R. Zhuang *et al.*, "Applications of π-π stacking interactions in the design of drug-delivery systems," *J. Controlled Release*, vol. 294, pp. 311–326, Jan. 2019, doi: 10.1016/j.jconrel.2018.12.014.

[24]   S. J. Jethwa *et al.*, "Supramolecular Corrals on Surfaces Resulting from Aromatic Interactions of Nonplanar Triazoles," *ACS Nano*, vol. 11, no. 8, pp. 8302–8310, Aug. 2017, doi: 10.1021/acsnano.7b03484.

[25]   L. Xing, Z. Peng, W. Li, and K. Wu, "On Controllability and Applicability of Surface Molecular Self-Assemblies," *Acc. Chem. Res.*, vol. 52, no. 4, pp. 1048–1058, Apr. 2019, doi: 10.1021/acs.accounts.9b00002.

[26]   F. Bisti *et al.*, "The electronic structure of gas phase croconic acid compared to the condensed phase: More insight into the hydrogen bond interaction," *J. Chem. Phys.*, vol. 138, no. 1, p. 014308, Jan. 2013, doi: 10.1063/1.4773059.

[27]   F. Silly, "Selecting Two-Dimensional Halogen–Halogen Bonded Self-Assembled 1,3,5-Tris(4-iodophenyl)benzene Porous Nanoarchitectures at the Solid–Liquid Interface," *J. Phys. Chem. C*, vol. 117, no. 39, pp. 20244–20249, Oct. 2013, doi: 10.1021/jp4057626.

[28]   R. Gutzler *et al.*, "Halogen bonds in 2D supramolecular self-assembly of organic

semiconductors," *Nanoscale*, vol. 4, no. 19, p. 5965, 2012, doi: 10.1039/c2nr31648j.

[29]   K. J. Shi, X. Zhang, C. H. Shu, D. Y. Li, X. Y. Wu, and P. N. Liu, "Ullmann coupling reaction of aryl chlorides on Au(111) using dosed Cu as a catalyst and the programmed growth of 2D covalent organic frameworks," *Chem. Commun.*, vol. 52, no. 56, pp. 8726–8729, 2016, doi: 10.1039/C6CC03137D.

[30]   S. Kawai *et al.*, "Extended Halogen Bonding between Fully Fluorinated Aromatic Molecules," *ACS Nano*, vol. 9, no. 3, pp. 2574–2583, Mar. 2015, doi: 10.1021/nn505876n.

[31]   M Haukka, P Hirva, K Rissanen, *Dihalogens as Halogen Bond Donors*. 2016.

[32]   J. V. Barth, "Molecular Architectonic on Metal Surfaces," *Annu. Rev. Phys. Chem.*, vol. 58, no. 1, pp. 375–407, May 2007, doi: 10.1146/annurev.physchem.56.092503.141259.

[33]   Bradley J. Holliday, Chad A. Mirkin Prof., "Strategies for the Construction of Supramolecular Compounds through Coordination Chemistry," Angewandte International Edition Chemie, Jun. 01, 2001.

[34]   M. Ruben, J. Rojo, F. J. Romero-Salguero, L. H. Uppadine, and J.-M. Lehn, "Grid-Type Metal Ion Architectures: Functional Metallosupramolecular Arrays," *Angew. Chem. Int. Ed.*, vol. 43, no. 28, pp. 3644–3662, Jul. 2004, doi: 10.1002/anie.200300636.

[35]   Alexander Semenov, Joachim P. Spatz, Martin Möller, Jean-Marie Lehn, Bernd Sell, Dieter Schubert, Christian H. Weidl, Ulrich S. Schubert, "Controlled Arrangement of Supramolecular Metal Coordination Arrays on Surfaces," Angewandte International Edition Chemie, pp. 2547–2550, Sep. 03, 1999.

[36]   G. Pawin *et al.*, "A Surface Coordination Network Based on Substrate-Derived Metal Adatoms with Local Charge Excess," *Angew. Chem.*, vol. 120, no. 44, pp. 8570–8573, Oct. 2008, doi: 10.1002/ange.200802543.

[37]   U. Schlickum *et al.*, "Metal−Organic Honeycomb Nanomeshes with Tunable Cavity Size," *Nano Lett.*, vol. 7, no. 12, pp. 3813–3817, Dec. 2007, doi: 10.1021/nl072466m.

[38]   N. Lin, A. Dmitriev, J. Weckesser, J. V. Barth, and K. Kern, "Real-Time Single-Molecule Imaging of the Formation and Dynamics of Coordination Compounds," *Angew. Chem. Int. Ed.*, vol. 41, no. 24, pp. 4779–4783, Dec. 2002, doi: 10.1002/anie.200290046.

[39]   A. Langner, S. L. Tait, N. Lin, R. Chandrasekar, M. Ruben, and K. Kern, "Ordering and Stabilization of Metal-Organic Coordination Chains by Hierarchical Assembly through Hydrogen Bonding at a Surface," *Angew. Chem. Int. Ed.*, vol. 47, no. 46, pp. 8835–8838, Nov. 2008, doi: 10.1002/anie.200803124.

[40]   M. Pivetta, G. E. Pacchioni, U. Schlickum, J. V. Barth, and H. Brune, "Formation of Fe Cluster Superlattice in a Metal-Organic Quantum-Box Network," *Phys. Rev. Lett.*, vol. 110, no. 8, p. 086102, Feb. 2013, doi: 10.1103/PhysRevLett.110.086102.

[41]   M. Di Giovannantonio *et al.*, "Insight into Organometallic Intermediate and Its Evolution to Covalent Bonding in Surface-Confined Ullmann Polymerization," *ACS Nano*, vol. 7, no. 9, pp. 8190–8198, Sep. 2013, doi: 10.1021/nn4035684.

[42]   K.-H. Ernst, "Stereochemical Recognition of Helicenes on Metal Surfaces," *Acc. Chem. Res.*, vol. 49, no. 6, pp. 1182–1190, Jun. 2016, doi: 10.1021/acs.accounts.6b00110.

[43]   C. B. France and B. A. Parkinson, "Naphtho[2,3- *a*]pyrene Forms Chiral Domains on Au(111)," *J. Am. Chem. Soc.*, vol. 125, no. 42, pp. 12712–12713, Oct. 2003, doi: 10.1021/ja037056o.

[44]   F. Vidal, E. Delvigne, S. Stepanow, N. Lin, J. V. Barth, and K. Kern, "Chiral Phase Transition in Two-Dimensional Supramolecular Assemblies of Prochiral Molecules," *J. Am. Chem. Soc.*, vol. 127, no. 28, pp. 10101–10106, Jul. 2005, doi: 10.1021/ja0525049.

[45]   Nataliya Kalashnyk, "Self-assembly of organic molecules on metals and thin insulating films: Hydrogen-bonded systems, chiral induction and peptide aggregation," University of Aarhus, Denmark, 2009.

[46]   S. M. Barlow and R. Raval, "Complex organic molecules at metal surfaces: bonding, organisation and chirality," *Surf. Sci. Rep.*, vol. 50, no. 6–8, pp. 201–341, Aug. 2003, doi: 10.1016/S0167-5729(03)00015-3.

[47]   K.-H. Ernst, "Supramolecular Surface Chirality," in *Supramolecular Chirality*, vol. 265, M. Crego-Calama and D. N. Reinhoudt, Eds. Berlin/Heidelberg: Springer-Verlag, 2006, pp. 209–252. doi: 10.1007/128_036.

[48]   M.. Ortega Lorenzo, C. J. Baddeley, C. Muryn & R. Raval, "Extended surface chirality from supramolecular assemblies of adsorbed chiral molecules," Nature, pp. 376–379, 2000.

[49]   S. M. Barlow *et al.*, "Supramolecular Assembly of Strongly Chemisorbed Size- and Shape-Defined Chiral Clusters: *S* - and *R* -Alanine on Cu(110)," *Langmuir*, vol. 20, no. 17, pp. 7171–7176, Aug. 2004, doi: 10.1021/la049391b.

[50]   C. B. France and B. A. Parkinson, "Naphtho[2,3- *a*]pyrene Forms Chiral Domains on Au(111)," *J. Am. Chem. Soc.*, vol. 125, no. 42, pp. 12712–12713, Oct. 2003, doi: 10.1021/ja037056o.

[51]   S. W. Im *et al.*, "Chiral Surface and Geometry of Metal Nanocrystals," *Adv. Mater.*, vol. 32, no. 41, p. 1905758, Oct. 2020, doi: 10.1002/adma.201905758.

[52]   Takashi Yokoyama, Shiyoshi Yokoyama, Toshiya Kamikado, Yoshishige Okuno & Shinro Mashiko, "Selective assembly on a surface of supramolecular aggregates with controlled size and shape," Nature, pp. 619–621, Oct. 11, 2001.

[53]   M. Stöhr, M. Wahl, C. H. Galka, T. Riehm, T. A. Jung, and L. H. Gade, "Controlling Molecular Assembly in Two Dimensions: The Concentration Dependence of Thermally Induced 2D Aggregation of Molecules on a Metal Surface," *Angew. Chem. Int. Ed.*, vol. 44, no. 45, pp. 7394–7398, Nov. 2005, doi: 10.1002/anie.200502316.

[54]   G. Pawin, K. L. Wong, K.-Y. Kwon, and L. Bartels, "A Homomolecular Porous Network at a Cu(111) Surface," *Science*, vol. 313, no. 5789, pp. 961–962, Aug. 2006, doi: 10.1126/science.1129309.

[55]   M. S. Baviloliaei and L. Diekhöner, "Molecular self-assembly at nanometer scale modulated surfaces: trimesic acid on Ag(111), Cu(111) and Ag/Cu(111)," *Phys Chem Chem Phys*, vol. 16, no. 23, pp. 11265–11269, 2014, doi: 10.1039/C4CP01429D.

[56]   M. Böhringer *et al.*, "Two-Dimensional Self-Assembly of Supramolecular Clusters and

Chains," *Phys. Rev. Lett.*, vol. 83, no. 2, pp. 324–327, Jul. 1999, doi: 10.1103/PhysRevLett.83.324.

[57]   F. Silly, A. Q. Shaw, G. A. D. Briggs, and M. R. Castell, "Epitaxial ordering of a perylenetetracarboxylic diimide-melamine supramolecular network driven by the Au(111)-(22×3) reconstruction," *Appl. Phys. Lett.*, vol. 92, no. 2, p. 023102, Jan. 2008, doi: 10.1063/1.2830828.

[58]   S. Clair and D. G. de Oteyza, "Controlling a Chemical Coupling Reaction on a Surface: Tools and Strategies for On-Surface Synthesis," *Chem. Rev.*, vol. 119, no. 7, pp. 4717–4776, Apr. 2019, doi: 10.1021/acs.chemrev.8b00601.

[59]   J. Cai *et al.*, "Atomically precise bottom-up fabrication of graphene nanoribbons," *Nature*, vol. 466, no. 7305, pp. 470–473, Jul. 2010, doi: 10.1038/nature09211.

[60]   Q. Shen, H.-Y. Gao, and H. Fuchs, "Frontiers of on-surface synthesis: From principles to applications," *Nano Today*, vol. 13, pp. 77–96, Apr. 2017, doi: 10.1016/j.nantod.2017.02.007.

[61]   L. Lafferentz, F. Ample, H. Yu, S. Hecht, C. Joachim, and L. Grill, "Conductance of a Single Conjugated Polymer as a Continuous Function of Its Length," *Science*, vol. 323, no. 5918, pp. 1193–1197, Feb. 2009, doi: 10.1126/science.1168255.

[62]   L. Grill, M. Dyer, L. Lafferentz, M. Persson, M. V. Peters, and S. Hecht, "Nano-architectures by covalent assembly of molecular building blocks," *Nat. Nanotechnol.*, vol. 2, no. 11, pp. 687–691, Nov. 2007, doi: 10.1038/nnano.2007.346.

[63]   H.-Y. Gao, H. Wagner, D. Zhong, J.-H. Franke, A. Studer, and H. Fuchs, "Glaser Coupling at Metal Surfaces," *Angew. Chem. Int. Ed.*, vol. 52, no. 14, pp. 4024–4028, Apr. 2013, doi: 10.1002/anie.201208597.

[64]   B. Cirera *et al.*, "Synthesis of Extended Graphdiyne Wires by Vicinal Surface Templating," *Nano Lett.*, vol. 14, no. 4, pp. 1891–1897, Apr. 2014, doi: 10.1021/nl4046747.

[65]   D. G. de Oteyza *et al.*, "Direct Imaging of Covalent Bond Structure in Single-Molecule Chemical Reactions," *Science*, vol. 340, no. 6139, pp. 1434–1437, Jun. 2013, doi: 10.1126/science.1238187.

[66]   Q. Sun *et al.*, "On-Surface Formation of One-Dimensional Polyphenylene through Bergman Cyclization," *J. Am. Chem. Soc.*, vol. 135, no. 23, pp. 8448–8451, Jun. 2013, doi: 10.1021/ja404039t.

[67]   N. A. A. Zwaneveld *et al.*, "Organized Formation of 2D Extended Covalent Organic Frameworks at Surfaces," *J. Am. Chem. Soc.*, vol. 130, no. 21, pp. 6678–6679, May 2008, doi: 10.1021/ja800906f.

[68]   J. F. Dienstmaier *et al.*, "Isoreticular Two-Dimensional Covalent Organic Frameworks Synthesized by On-Surface Condensation of Diboronic Acids," *ACS Nano*, vol. 6, no. 8, pp. 7234–7242, Aug. 2012, doi: 10.1021/nn302363d.

[69]   C.-Z. Guan, D. Wang, and L.-J. Wan, "Construction and repair of highly ordered 2D covalent networks by chemical equilibrium regulation," *Chem. Commun.*, vol. 48, no. 24, p. 2943, 2012, doi: 10.1039/c2cc16892h.

[70]   H.-Y. Gao *et al.*, "Decarboxylative Polymerization of 2,6-Naphthalenedicarboxylic Acid at Surfaces," *J. Am. Chem. Soc.*, vol. 136, no. 27, pp. 9658–9663, Jul. 2014, doi: 10.1021/ja5033875.

[71]   Albert C. Aragonès, Naomi L. Haworth, Nadim Darwish, Simone Ciampi, Nathaniel J. Bloomfield, Gordon G. Wallace, Ismael Diez-Perez & Michelle L. Coote, "Electrostatic catalysis of a Diels–Alder reaction," Nature, pp. 88–91, Mar. 02, 2016.

[72]   B. Yang *et al.*, "Catalytic Dealkylation of Ethers to Alcohols on Metal Surfaces," *Angew. Chem.*, vol. 128, no. 34, pp. 10035–10039, Aug. 2016, doi: 10.1002/ange.201602414.

[73]   Z. Gong *et al.*, "Structural Variation in Surface-Supported Synthesis by Adjusting the Stoichiometric Ratio of the Reactants," *ACS Nano*, vol. 10, no. 4, pp. 4228–4235, Apr. 2016, doi: 10.1021/acsnano.5b07601.

[74]   S. Weigelt *et al.*, "Surface Synthesis of 2D Branched Polymer Nanostructures," *Angew. Chem. Int. Ed.*, vol. 47, no. 23, pp. 4406–4410, May 2008, doi: 10.1002/anie.200705079.

[75]   S. Weigelt *et al.*, "Covalent Interlinking of an Aldehyde and an Amine on a Au(111) Surface in Ultrahigh Vacuum," *Angew. Chem. Int. Ed.*, vol. 46, no. 48, pp. 9227–9230, Dec. 2007, doi: 10.1002/anie.200702859.

[76]   Q. Sun, L. Cai, Y. Ding, H. Ma, C. Yuan, and W. Xu, "Single-molecule insight into Wurtz reactions on metal surfaces," *Phys. Chem. Chem. Phys.*, vol. 18, no. 4, pp. 2730–2735, 2016, doi: 10.1039/C5CP06459G.

[77]   D. Zhong *et al.*, "Linear Alkane Polymerization on a Gold Surface," *Science*, vol. 334, no. 6053, pp. 213–216, Oct. 2011, doi: 10.1126/science.1211836.

[78]   Q. Sun, C. Zhang, H. Kong, Q. Tan, and W. Xu, "On-surface aryl–aryl coupling via selective C–H activation," *Chem Commun*, vol. 50, no. 80, pp. 11825–11828, Aug. 2014, doi: 10.1039/C4CC05482B.

[79]   L. Lafferentz, V. Eberhardt, C. Dri, C. Africh, G. Comelli, F. Esch, S. Hecht & L. Grill, "Controlling on-surface polymerization by hierarchical and substrate-directed growth," nature chemistry, pp. 215–220, Jan. 15, 2012.

[80]   F. Palmino, C. Loppacher, and F. Chérioux, "Photochemistry Highlights on On-Surface Synthesis," *ChemPhysChem*, vol. 20, no. 18, pp. 2271–2280, Sep. 2019, doi: 10.1002/cphc.201900312.

[81]   Q. Shen *et al.*, "Self-assembled two-dimensional nanoporous molecular arrays and photoinduced polymerization of 4-bromo-4′-hydroxybiphenyl on Ag(111)," *J. Chem. Phys.*, vol. 142, no. 10, p. 101902, Mar. 2015, doi: 10.1063/1.4906116.

[82]   S.-W. Hla, L. Bartels, G. Meyer, and K.-H. Rieder, "Inducing All Steps of a Chemical Reaction with the Scanning Tunneling Microscope Tip: Towards Single Molecule Engineering," *Phys. Rev. Lett.*, vol. 85, no. 13, pp. 2777–2780, Sep. 2000, doi: 10.1103/PhysRevLett.85.2777.

[83]   S. Clair, O. Ourdjini, M. Abel, and L. Porte, "Tip- or electron beam-induced surface polymerization," *Chem. Commun.*, vol. 47, no. 28, p. 8028, 2011, doi: 10.1039/c1cc12065d

Chapter 2: Experimental techniques

During this thesis, we studied the supramolecular self-assembly and the on-surface reactions of several molecules deposited on solid substrates in different environmental conditions. The approach employed is to combine complementary experimental techniques: scanning probe microscopies such as scanning tunneling microscopy (STM) and non-contact atomic force microscopy (nc-AFM), x-ray photoelectron spectroscopy (XPS) and density functional theory (DFT). The samples were prepared and analyzed in different experimental setups. The first section in this chapter outlines the different analysis techniques used. The following section presents the importance of the ultrahigh vacuum system and how to obtain it. The next section presents the different substrates that were used and their preparation. Finally, the last section describes the experimental setups of our group at IM2NP, Marseille.

2.2   Analysis and characterization techniques

In this section I will present the characterization techniques used in this thesis. All STM measurements are made in our group at IM2NP, Marseille either at ambient pressure (chapter 3) or under UHV conditions (chapters 4 and 5). The surface chemical analysis was performed by XPS with synchrotron radiation by our team at BACH beamline, Elettra synchrotron, Trieste. Some experiments were performed by our colleagues: the molecular synthesis by C. Pigot, F. Dumur, M. Nechab and D. Gigmes from ICR at Aix-Marseille University and the nc-AFM measurements were performed by R. Pawlak and E. Meyer from the Department of Physics of the University of Basel. Finally, the DFT modelling was performed by O. Maclean and F. Rosei at "Institut National de la Recherche Scientifique" in Varennes, Québec, Canada, and some XPS measurements by E. Salomon, T. Angot and F. Romero-Lairado from PIIM at Aix-Marseille University. All results have been interpreted in the framework of this PhD thesis.

2.2.1 Scanning Tunneling Microscopy

One of the most significant problems in surface physics is determining the surface topography. Scanning tunneling microscopy (STM) plays a crucial role for the development of surface science by giving a direct, real-space, local probe technique with atomic resolution[1]. It is one of the essential instruments for surface characterization due to its ability to study the surface structure atom-by-atom, the electronic and the geometric structure[1], [2]. Furthermore, the STM technique has been used to study chemisorption[3], epitaxy[4], solid-liquid interfaces[5],

and biological molecules[6]. The STM was invented in 1980 by Gerd Binnig and Heinrich Rohrer at the IBM research laboratory in Switzerland[2]. In 1983, they obtained the first STM image of a silicon surface with atomic resolution by imaging at low temperature and under ultra-high vacuum (UHV) conditions[7]. In 1986, a Nobel Prize in Physics has been awarded for this instrument.

General principles

The principle of STM is illustrated in Figure 2.1. A metal tip placed at the bottom of a scanning unit (a piezo-tube scanner) is brought to the vicinity (<10 Å) of a conductive or semi-conductive surface. A bias voltage is applied between the tip and the sample, leading to an electric current (up to a few nanoamps) called the tunneling current. This latter is measured for each point of the scanning zone through amplification and conversion to a voltage by an I/V converter. The tunneling current depends exponentially on the tip-sample distance (explained later). This allows high resolution (≤ 0.01nm) in the z-direction to be achieved.
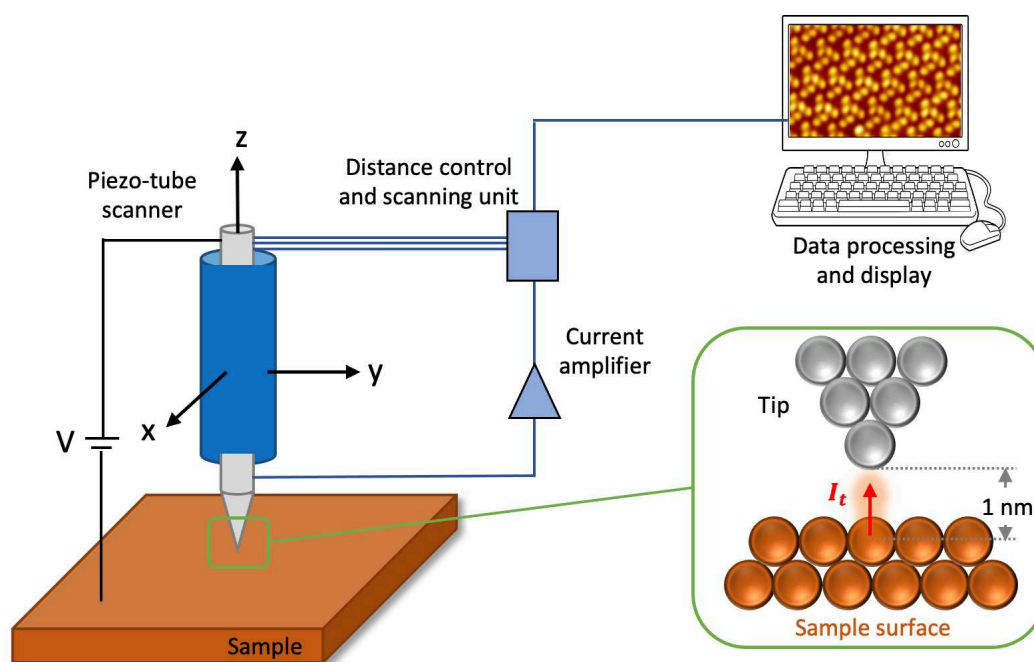

Figure 2.1. Schematic illustration of the principle of scanning tunneling microscope (STM). A bias voltage is applied between the metallic tip and the surface of the sample separated by a few angstroms. A tunneling current is measured between them and it is controlled by the piezo-tube scanner by adjusting the tip-sample distance. Figure reproduced from[8].

Tunneling Effect

The principle of STM is based on the quantum mechanical model of an electron tunneling through a one-dimensional barrier of width z assigned to the distance between the tip and the sample. The tunneling current is exponentially proportional to the tip-sample distance, as seen in this approximation expression:

$$I_t \propto e^{-kz\sqrt{U}}$$

Where k is a constant, z and U are the distance and the tunnel barrier height between the tip and the sample, respectively.

This exponential dependence on the distance z implies that only the surface atoms close to the tip atoms participate to the tunneling process. Thus, it is possible to determine their positions and rebuild the surface topography using STM.

Scanning modes

STM experiments can be performed in two different modes during the tip 2D scan: constant-current mode and constant-height mode, presented in Figure 2.2:
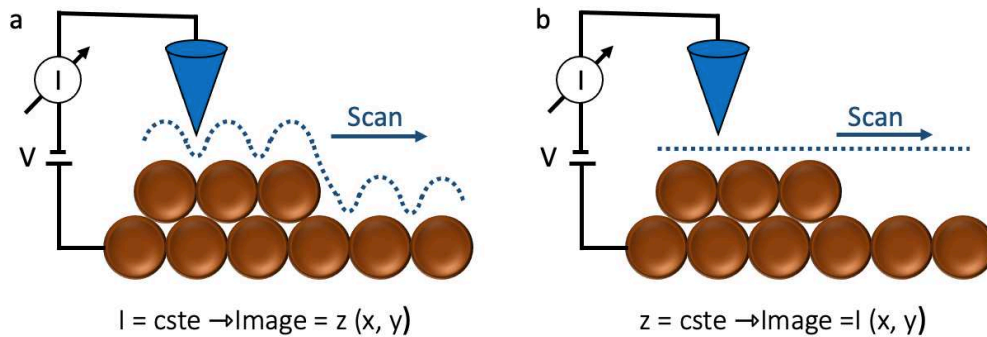
Figure 2.2. Schematic illustration of the two-imaging mode of STM: (a) constant-current and (b) constant-heigh.

- The Constant-current mode requires a complex setup adjusting the tip-sample distance at each measurement point by using a feedback loop that keeps the tunneling current constant while scanning. The surface topography in STM image is reconstructed from the set of measured data linked to the piezoelectric scanner tube motion in the z-direction.

- The Constant-height mode is rarely used but simpler than the constant-current mode since no feedback loop is required. In this mode, the tip-sample distance is maintained constant while the tunneling current is recorded. The surface topography is reconstructed using the data related to the tunneling current variation.

Theory

In STM experiment, the tip and the sample are separated by a vacuum gap (few Å). The expression of the tunneling current depends on the bias voltage applied between them. It could be expressed by considering the Pauli Exclusion Principle, which outlaws that two electrons cannot occupy the same quantum state. Two cases differing by the applied bias voltage are presented in Figure 2.3:

Figure 2.3. Energy diagrams of a tip(metal)-vacuum-sample(metal) tunneling junction at different bias voltages applied to the tip. Reproduced from[9].
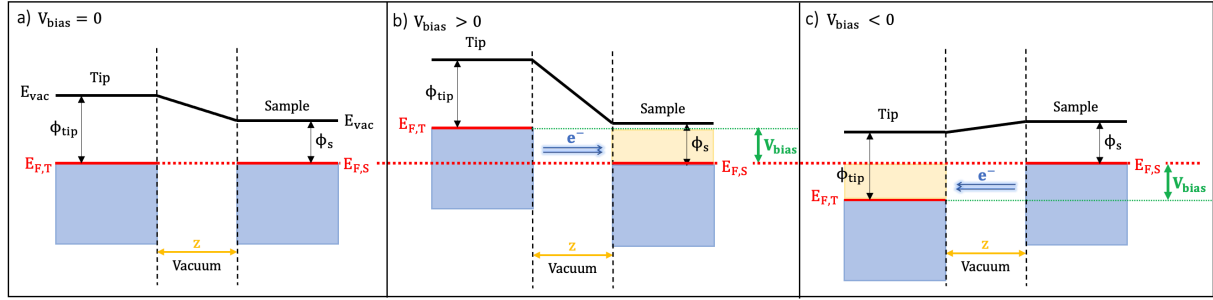
1. If $V_{bias} > 0$, the Fermi level of the sample shifts down by a quantity eV_{bias} with respect to the Fermi level of the tip. In this case, all electrons with energy between E_F and $E_F + eV_{bias}$ tunneling from the occupied states of the tip to the empty electronic states of the sample.

2. If $V_{bias} < 0$, the Fermi level of the sample shifts up with respect to the Fermi level of the tip by the same quantity eV_{bias}. In this case, the direction of electrons is inversed.

The tunneling between tip and surface is a complex problem, which has not been exactly solved until now. The most popular theoretical approach to calculate tunneling current is based on a time-dependent perturbation approach developed by Bardeen in 1961[10]. To calculate the tunneling current, further simplification was required. J. Tersoff and D.R. Hamann developed a simple model for the tunneling junction in 1983[11], [12]. The most important assumption for this model is the modelling of the STM tip as a spherical-tip with curvature radius R (Fig.2.4). This model, called the "Tersoff and Hamann model", solves the wave function equation only for an s-wave function. In this model, the tunneling current can be expressed as follows:

$$I_t \propto V_{bias} \rho_{tip} \rho_{sample}(r_0, E_F)$$

Where V_{bias} is the bias voltage applied between the tip and the sample, ρ_{tip}, ρ_{sample} the LDOS of the tip and the sample in the vicinity of the Fermi level, and r_0 the position of the tip
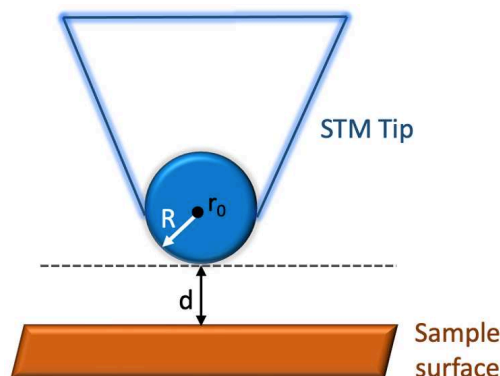
Figure 2.4. Schematic of the Tersoff and Hamann model. The tip is modeled by a sphere of radius R, center r_0, and tip-sample distance d.

This last expression shows that the tunneling current depends on both the local electronic density of states (LDOS) of the sample and of the tip.

The STM technique is considered also a powerful tool in spectroscopic measurements in which the current is acquired as a function of the tunneling voltage. This mode is more suitable for high-resolution analysis at low temperatures than STM at room temperature. During my thesis, I have only used the topography mode for sample characterization.

2.1.2 X-ray photoelectron spectroscopy (XPS)

General principles

The emission of electrons from molecules or solid upon absorption of light, also known as photoemission or photoelectron spectroscopy, is a complex phenomenon treated in many articles and books[13]. In the following a short introduction is given for the purposes of the present work.

When the photoelectrons come from core levels, photoemission is named X-ray photoelectron spectroscopy (XPS). XPS, is one of the most suitable methods dedicated for the chemical analysis of surfaces. It is based on the photoelectric effect[14]: when a photon of sufficient energy $h\nu$ strikes the surface of a solid of a given work function $e\phi$, electrons are emitted whose maximum kinetic energy is

$$E_k(\text{max}) = h\nu - e\phi$$

The electrons having this energy are those that are more loosely bound in the surface region. More generally, by analyzing the kinetic energy spectrum $I(E_k)$ of all the photoemitted electrons, one can access the binding energy E_b of the electrons in the vicinity of the surface, thus gaining detailed information on the surface chemical and electronic properties. The energy conservation upon photo-ionization gives:

$$E_k = h\nu - E_b - e\phi$$

The photon source to be employed depends on the energy range to be explored. For XPS, the core levels are probed which necessitates photon energies above 100 eV. These are produced by standard X-ray sources (single photon energy) or by tunable synchrotron radiation sources. The photoemission spectrum is measured by an electron energy analyzer. Electrons entering the analyzer are deviated by an electric field: only those within a certain energy range $E_k \pm \Delta E$ can reach the detector and contribute to the signal (see Fig.2.5).
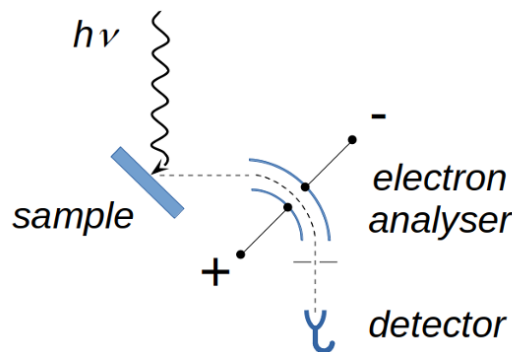
Figure 2.5. Outline of the photoemission experiment

Since it is measured by the analyzer, the correct expression between the electron kinetic and binding energy is given by

$$E_k = h\nu - E_b - e\phi_{sp}$$

where $e\phi_{sp}$ is the spectrometer work function. Generally, one can ignore it by referencing the binding energy spectra to the sample Fermi level.
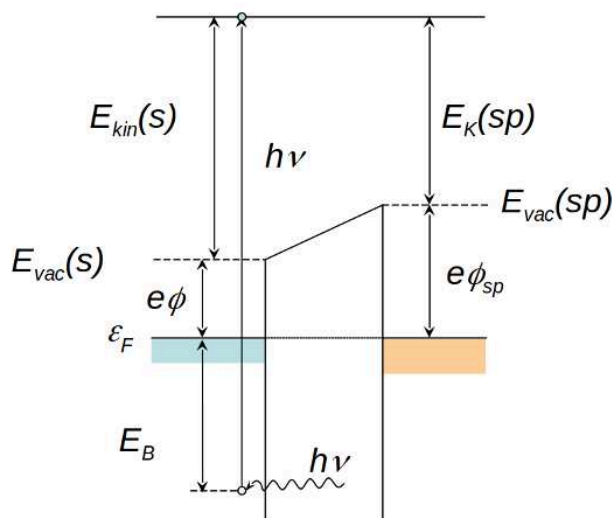
Figure 2.6. The sample (s) and the spectrometer (sp) have a common Fermi level (they are generally grounded) but a different work function. The photoelectron is excited by the impinging photon leaving behind a hole.

The resulting spectrum has the general form reported in Fig.2.7 where core level and valence band contributions are schematized. On the left hand side, low kinetic energy, secondary electrons having scattered inelastically, have just enough energy to cross the vacuum level to be detected. The electrons at $E_k = 0\ eV$ are then at $e\phi$ from states the Fermi level in the solid. At the highest E_k, electrons from the valence band and (as here, in case of metals) from the Fermi level are detected. In between, strong and sharp features reveal the presence of core levels.
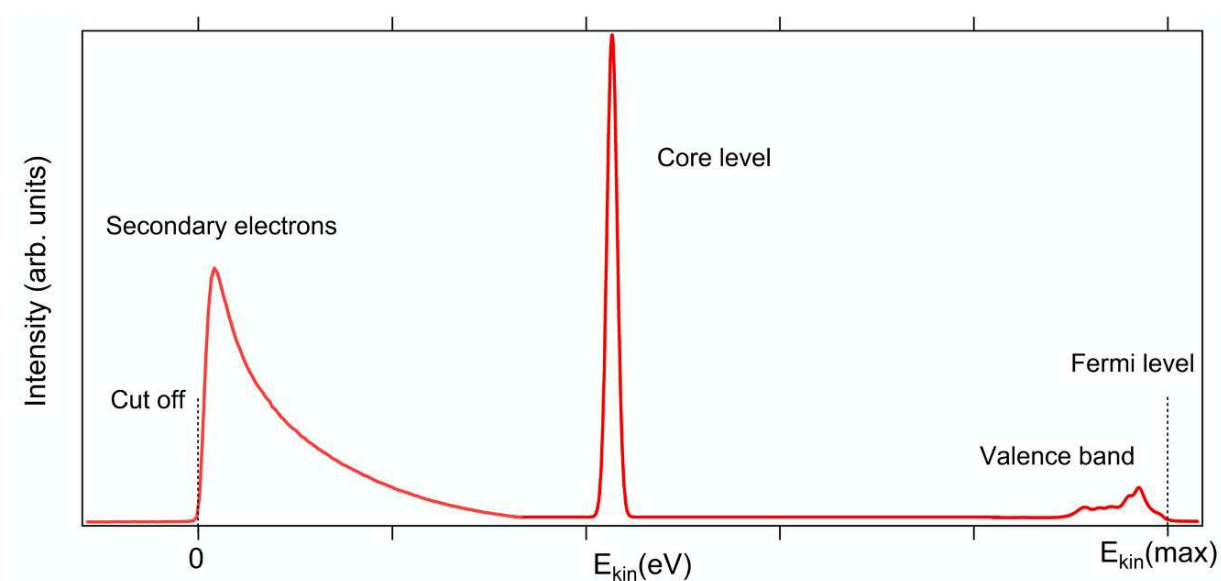
Figure 2.7. the typical shape of a XPS spectrum.

Surface analysis - qualitative

Each element of the periodic table (apart from hydrogen) possesses at least one core electron accessible through standard X-ray sources. Their binding energies E_b are characteristic of the element confering to XPS the power of measuring the chemical composition of the sample. Moreover, photoemitted electrons have moderate energies (100-1000 eV) which makes XPS a surface sensitive technique (see below). As an example, the wide energy range spectrum of an overlayer of di-chloro-carbazole organic molecules on Cu(111) is displayed in Fig.2.8. Several core level peaks are detected that originate from the overlayer and substrate atoms. At low BE the valence band is visible.
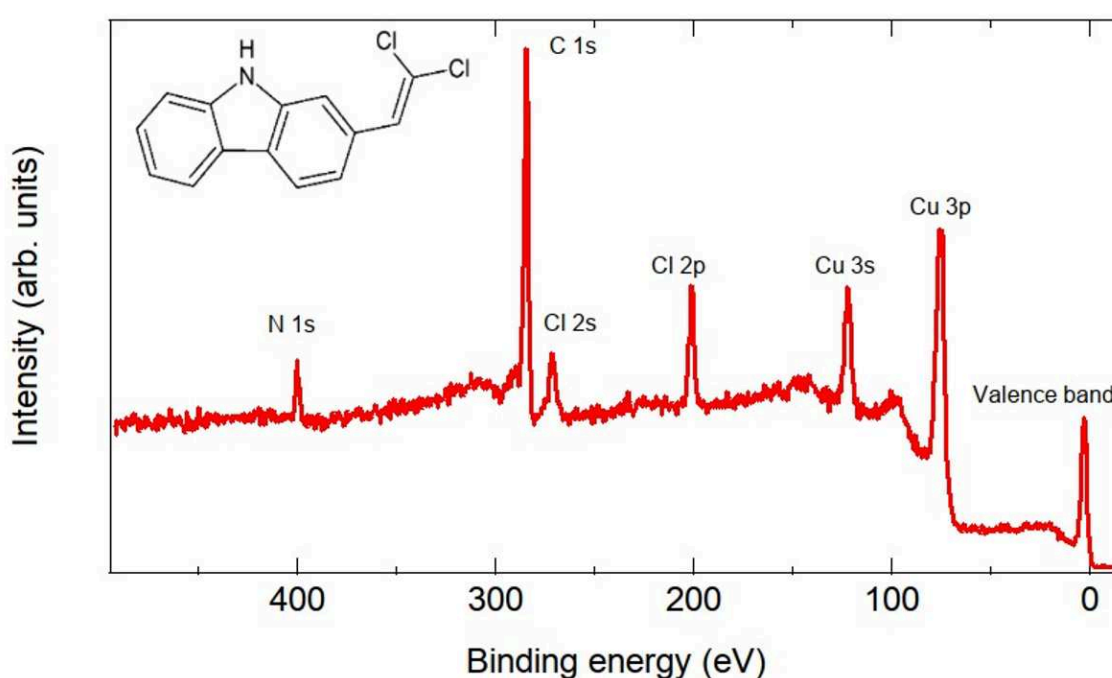
Figure 2.8. Wide energy scan of an overlayer of di-chloro-carbazole organic molecules on Cu(111) taken with 380 eV photon energy.

Surface analysis - quantitative

In an XPS spectrum, the intensity $I_{x,Cl}$ of each core level (CL) peak of a given element *x*, above the secondary electron background, is proportional to the number of atoms N_x present in the surface region and to the photoionization cross section for the given core level σ_x,cl (a tabulated value). For a given peak of intensity I_x one can then write:

$$N_x \sim {}^{I_x}\!/_{\sigma_x}$$

Several other factors influence the peak intensity but, if the near-surface region is homogeneous and if the kinetic energy of the peaks coming from different species are close enough (so that similar depths are probed), one can estimate the sample stoichiometry by the ratio of the core level intensities weighted by the corresponding cross sections:

$$N_x\!/_{N_y} \approx {}^{I_x}\!/_{I_y} * {}^{\sigma_y}\!/_{\sigma_x}$$

In the example of Fig. 2.8, one obtains ${}^{N_C}\!/_{N_N} = 13{,}9\ (14)$, ${}^{N_C}\!/_{N_{Cl}} = 6{,}3\ (7)$ and ${}^{N_N}\!/_{N_{Cl}} = 0{,}45\ (0{,}5)$ the number in parenthesis being the values expected from the nominal stoichiometry.

Surface analysis – chemical core level shift

One of the most powerful characteristics of XPS is to be sensitive to the oxidation state of a given chemical species. This feature is illustrated in Fig.2.9 where the high resolution C 1s spectrum of a lead-phthalocyanine (PbPc) is displayed. The carbon atoms within the molecule experience different chemical environments which results in three main peaks. The most intense one is due to the benzene rings and the second one to $C - N$. The carbon atoms of the C-N component experience a more oxidative environment with respect to the benzene atoms because N is more electronegative then C. As a consequence, its BE is increased. This phenomenon, known a chemical core-level shift, can be explained as follows. The valence electrons of an atom pass sometime between the core electrons and the nucleus, thus screening the nucleus and reducing the core level binding energy. When some charge is depleted from the valence electrons to form a bond with a neighboring atom, the binding energy of the core level is increased. This can also be seen in terms of the potential energy in a system composed of a positive charge (the nucleus) at the center of a negatively charged sphere (the valence charge). The potential energy experienced by core level electrons is modified by bonding with neighboring atoms. When the valence charge is depleted (oxidation) the total potential energy is lowered and the core level E_b increased.

A third, smaller peak is visible in the spectrum of PbPc at higher BE than the $C - N$ component. This peak is due to a final state effect. The creation of the core-hole can induce excitations within the molecule, namely between occupied π and unoccupied π^* states. If the C

1s photoelectron leaves the molecule in an excited state, its kinetic energy will be reduced to conserve the total energy. This can produce satellites at higher BE with respect to the original core level, also named shake-up structures.

In order to extract the above information, after having subtracted the secondary electron background, a deconvolution of the measured core level spectrum in different components is needed. Each core level component is modeled by a convolution of a Lorentzian (finite life time of the core level) and a gaussian (experimental resolution, thermal broadening, disorder,…). The resulting Voigt profile is used as a model for least square fitting of high resolution spectra. The intensity of each component (main component plus the corresponding shake-up) reflects the fraction of each chemically inequivalent site within a given atomic specie.
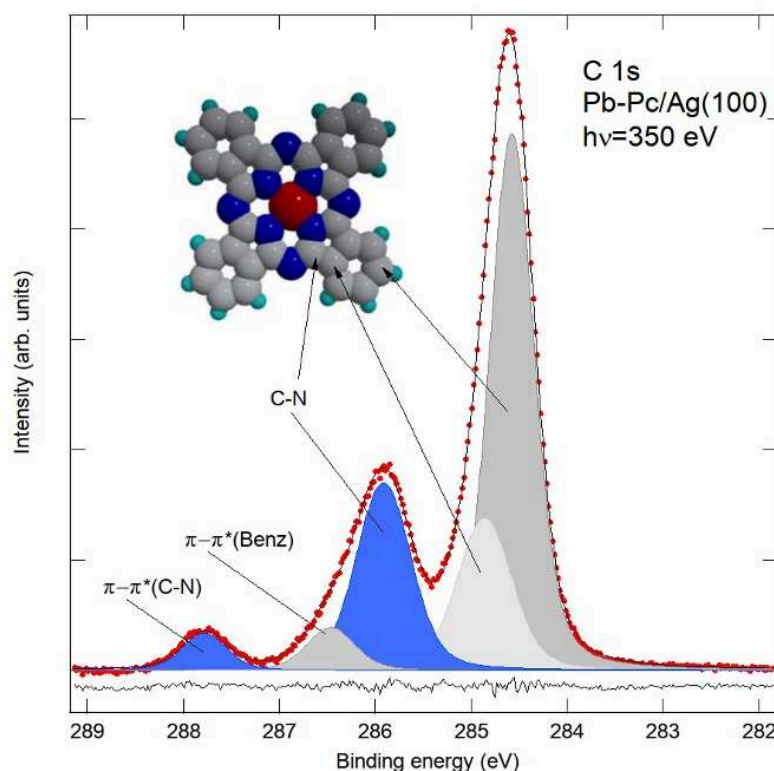
Figure 2.9. the high resolution XPS spectrum of a thick film of Pb-phthalocyanine (inset).

Surface sensitivity

The photoelectrons from the core level peaks (main line and satellites) and the valence band are called primary photoelectrons. At very low kinetic energy the XPS spectrum displays the intense, featureless peak of the secondary electrons resulting from the inelastic collisions of primary photoelectrons and the other electrons in the solid. The mean free path (λ), is the mean

distance traveled between two inelastic collisions. This value limits the depth of the sample that can be probed and it is described by the attenuation law as follows:

$$I = I_0 \left[\exp\left(\frac{-z}{\lambda(\theta)} \right) \right] \quad (2.23)$$

Where I is the intensity measured by the detector, I_0 is the intensity of the photoelectrons emitted from the surface atoms, $exp\left(\frac{-z}{\lambda(\theta)} \right)$ is the probability for the photoelectrons to be ejected from the sample, z is the probing depth, and θ is the angle between emission photoelectron direction and the normal of the surface (Fig.2.8).

The mean free path (λ) depends in a complex way on the chemical nature of the solid and the kinetic energy of the emitted photoelectrons. However, an approximation value of λ as a function of E_k can be determined from the universal curve of the inelastic mean free path of electrons (Fig.2.10).

Figure 2.10. The universal curve represents the evolution of the inelastic mean free path of electrons (IMFP) in a solid as a function of their kinetic energy[15].
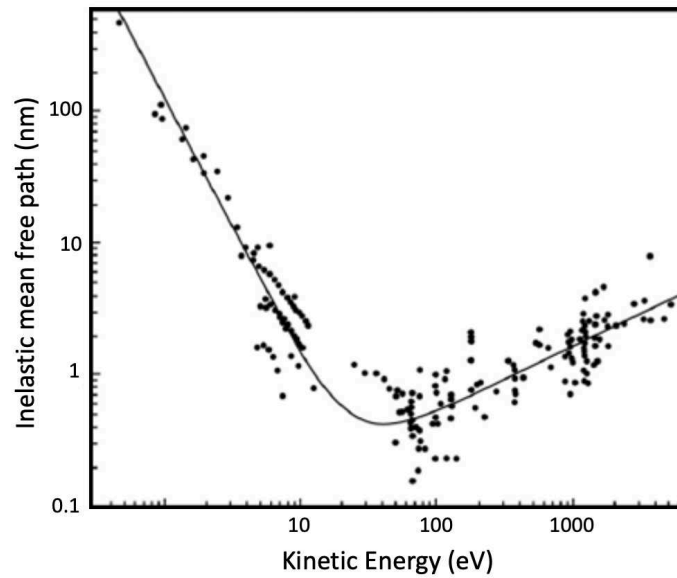
Using an excitation source with tunable photon energy allows to get a high surface sensitivity of the photoemission spectrum. For example, using a synchrotron radiation gives rise to a minimum IMFP observed for a photoelectron with kinetic energy around 50 eV.

2.2 Ultra-High Vacuum

A vacuum environment is described by the pressure of the residual gases which is usually below 10^{-4} mbar. Such pressure is required for experimental techniques using free particles (electrons or ions) in order to increase as much as possible their mean free path in the gas phase. The study of surfaces needs a clean environment since the experiment takes a long time for sample preparation and characterization. Therefore, ultra-high vacuum (UHV) conditions (P=$10^{-10} - 10^{-11}$ mbar) are required and not simply normal high-vacuum conditions (10^{-6} mbar) where a clean surface can be rapidly contaminated by the residual gas atmosphere[13].

The number of particles striking a surface of $1 cm^2$ per second is given by the kinetic gas theory:

$$\dot{n}_s = \frac{1}{4} N_g \bar{v}$$

Where N_g is the number of gas molecules per cm^3 and $\bar{v} = \sqrt{\frac{8 R T}{\pi M}}$ their mean thermal velocity. R the gas constant, T the absolute temperature and M the molecular weight.
Thus, $\dot{n}_s$ can be expressed as follows:

$$\dot{n}_s \approx 2.7 \times 10^{22} \frac{p}{\sqrt{MT}} \ (cm^{-2} s^{-1})$$

Where p is the gas pressure in mbar. For example, at a pressure of 10^{-6} mbar, the build-up of a monolayer of nitrogen with capacity of 3.10^{14} particles/cm^2, M=28 g/mol, and T=300K takes 1 second ($\dot{n}_s = 10^6 \cdot p$). Indeed, the time of coverage τ_c depends on the adsorption probability of the impinging molecules s:

$$\tau_c = \frac{1}{(\dot{n}_s \cdot s)} \approx \frac{10^{-6}}{s \cdot p}$$

This indicates that under UHV conditions (pressure of 10^{-10} mbar), the researcher has 1 hour to perform an experiment with an uncontaminated clean surface, which is usually enough time to carry out most experimental measurements. However, these UHV conditions are not so stringent in the work with "real" surfaces and an impurity layer is present. For this, it will be useful to use noble gas ion sputtering to remove atomic layers and do a chemical analysis.

The majority of UHV systems today are consisting of stainless steel parts connected together by flanges with copper metal seals. They also possess a borosilicate glass joined to stainless steel parts with a bakeable metal to glass seal. In order to reach UHV conditions in the apparatus, different type of pumps can be used with advantages and disadvantages for each of them. But all UHV pumps need another forevacuum system because they cannot be operated

at atmospheric pressure. Our UHV system is equipped of a turbomolecular type pump (TMP) with a primary pump, an ion pump and a titanium sublimation pump (TSP). The primary pump allows the obtention of a vacuum with a pressure of 10^{-2} mbar and then the turbomolecular pump provides the UHV pressure of $10^{-10} - 10^{-11}$ mbar. This pump can be turned off in the UHV regime to eliminate the vibrations induced by its rotation mechanism. In this case, the ion pump is used to keep the UHV conditions. After each sample preparation, the pressure generally rises in the chamber. Consequently, the titanium sublimation pump is used to recover the pressure.

2.3 Substrates

In this section, two different substrates used in this thesis will be presented. A brief description of their crystallographic structure and their preparation will be given.

2.3.2 HOPG

Highly Oriented Pyrolytic Graphite (HOPG) surface (Fig.2.11) was used as the substrate for the self-assembled molecular networks studied by STM at the liquid/solid interface (chapter 3). HOPG belongs to lamellar materials since its crystal structure is consisting of stacked two-dimensional graphene layers.
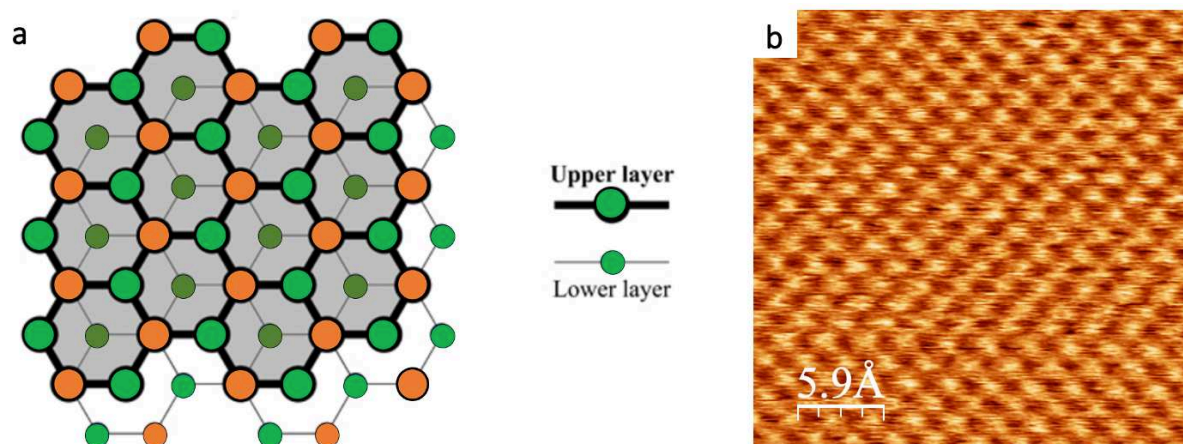
Figure 2.11. (a) Schematic representation of the atomic structure of HOPG. The distance between two layers is about 0.34 nm and is 0.14nm between two adjacent carbon atoms. (b) $3\,nm \times 3nm$ STM image of a HOPG substrate taken in ambient conditions.

In each layer, the carbon atoms form a honeycomb like network known as "graphene" with a distance of 0.14 nm between them. The distance between layers is about 0.34 nm. Thus, carbon atoms in a single plane of HOPG interact much more strongly than those in adjacent

planes. This is the reason why we can easily clean the surface of this material by a mechanical cleaving to produce an atomically clean surface. The principle consists of taking a piece of tape, press it onto the flat surface, and then pull it off.

2.3.3 Cu(111)

The on-surface synthesis studied in chapter 4 and 5 was performed on the Cu(111) surface. The copper crystal has a face-centered cubic (fcc) structure with a lattice constant of a = 0.361 nm as shown in Figure 2.12a. The face (111) of the copper as shown in Fig.2.12a is a hexagonal close packed (hcp) system with a distance of 0.255 nm between two neighbored Cu atoms[16]. Real copper surfaces possess some atoms able to move on the surface and called adatoms (dark brown in Fig.2.12b). Theses adatoms play a crucial role on the reaction mechanism that can be at play on the surface. In some cases, it is possible to observe intermediate reaction step in the reaction mechanism involving adatoms[17], [18]. Moreover, the reaction mechanism can also depend on the catalytic effect of the Cu(111) surface with the deposited precursors.
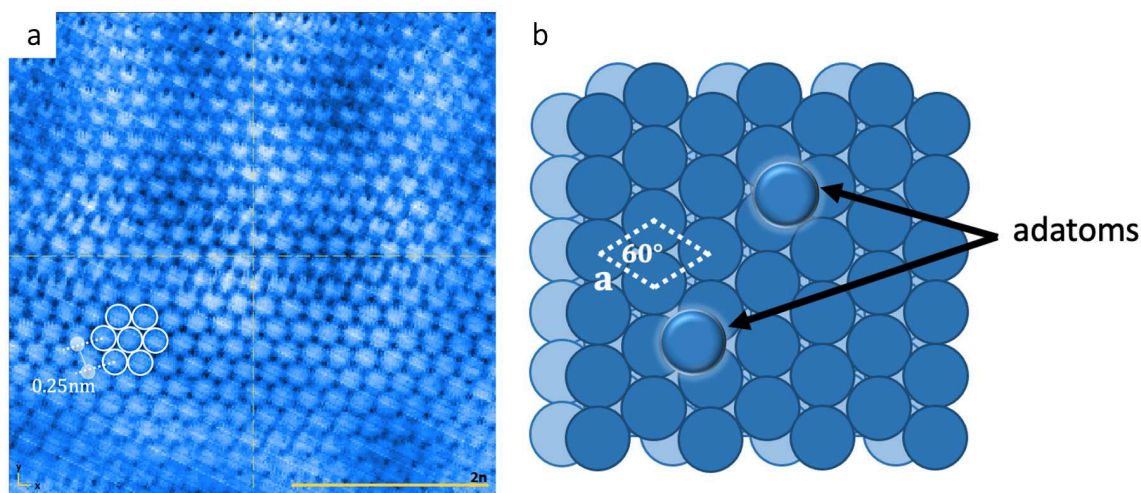
Figure 2.12. (a) High-resolution STM image of a clean Cu(111) surface. (b) Top view of the (111) surface shows a unit cell with constants lattice. The STM parameters are $0.1\,V, 50\,pA, T = 5K$.

2.3.4 Sample preparations

In this thesis, we studied molecule adsorption on a noble metal surface and on HOPG. Two investigations under different conditions were performed: the first at ambient conditions and the second under UHV conditions. For the first study, the molecules were deposited from a

solution on a freshly cleaved graphite surface. The preparation of the molecular solutions is detailed in chapter 3. For the second study, there are two phases for sample preparations: the preparation of the substrate and the molecular deposition. The Cu(111) surface was cleaned *in-situ* under UHV conditions by several cycles of sputtering and annealing. The sputtering is done with an Ar^+ ion source with an energy of one kilovolt. The annealing was then performed with a temperature of 550°C. Before molecules the deposition, the surface topography (atomically clean and flat) was verified by STM. Then, the molecular deposition is done by a controlled sublimation under UHV detailed in the next section. After deposition, the surface was analyzed by different UHV techniques.

2.4 Experimental setups

The STM experiments were performed in two different experimental setups. The first one is consisting of a Bruker multimode 8 STM with a Nanoscope 5 controller operating at ambient conditions (Figure 2.13a). A few μl of a molecular solution was studied at the liquid-solid HOPG interface by this microscopy giving an STM image of the surface topography as schematized in Fig. 2.13b. A detailed description of the preparation process and the results are presented in chapter 3.
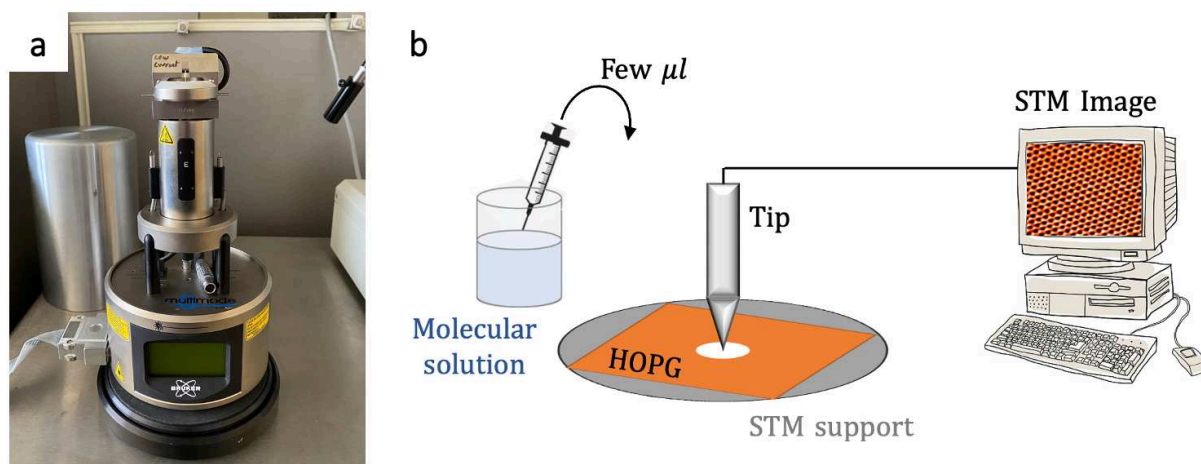

Figure 2.13. (a) Ambient conditions scanning tunneling microscopy (STM) device. (b) Representative schematic of the experimental process.

The second experimental setup is the new UHV system of our group at the IM2NP (Figure 2.15). It is composed of two chambers: a preparation chamber and a characterization chamber.

The preparation chamber is equipped of an ion Ar^+ sputter gun and a heating system for sample annealing. After each sputtering cycle, an annealing temperature of 550°C was employed to reconstruct the Cu(111) surface. The advantage of our system is the possibility of controlling and operating the cleaning cycles in a fully automatic way. Finally, we used a commercial evaporator system for molecule deposition (Kentax TCE-BSC, Figure 2.14)[19]. It possesses a three-cell evaporator designed for materials with a low sublimation temperature. The synthesized molecules are charged into one of the three crucibles in quartz (Figures 2.14b and c). Quartz is chosen due to its resistance to thermal shock and the fact that there are no interactions with molecules during the heating process. A cooling tank keeps the evaporator's head cold, protecting the diffusion of heat from one crucible to another, and a four holes shutter (Fig.2.14d) controls how each crucible is closed and opened. The temperature regulation (300K to 900K) is ensured through an electronic controller (Fig.2.14e).
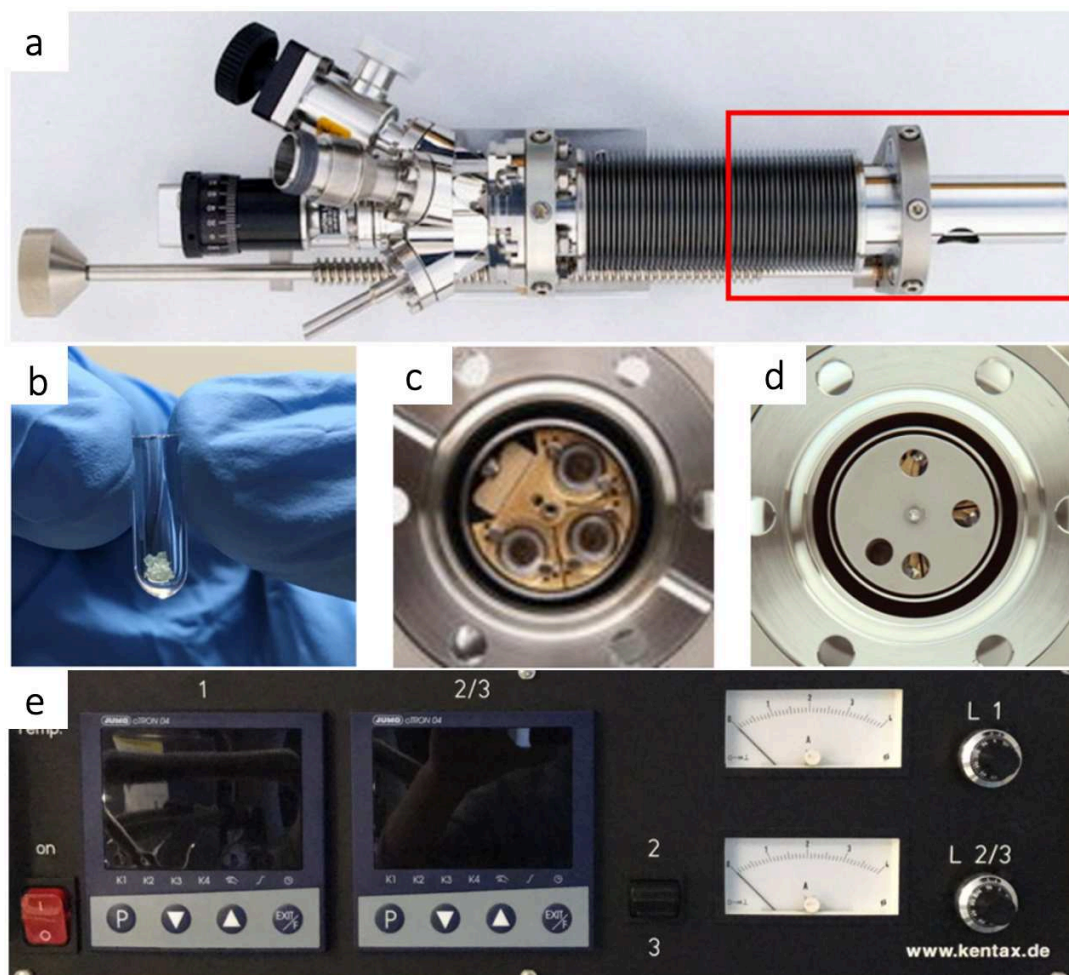
Figure 2.14. The UHV molecular evaporator Kentax TCE-BSC: a) Global view of the device. b) A molecule-filled crucible in quartz. c) the three crucibles in quartz mounted in the evaporator. d) Shutter for the control of the open and close of each crucible. e) electronic control unit. Adapted from[19]

The analysis chamber is consisting of a low-temperature STM (Scienta-Omicron Infinity LT-STM)[20]. This system is connected to a closed-cycle cryostat (cryogen-free) giving a very low temperature (T<10 K) for a long measurement time. A Nanonis MIMEA RC5 electronic controller is used for the voltage applied to the sample in STM experiments.
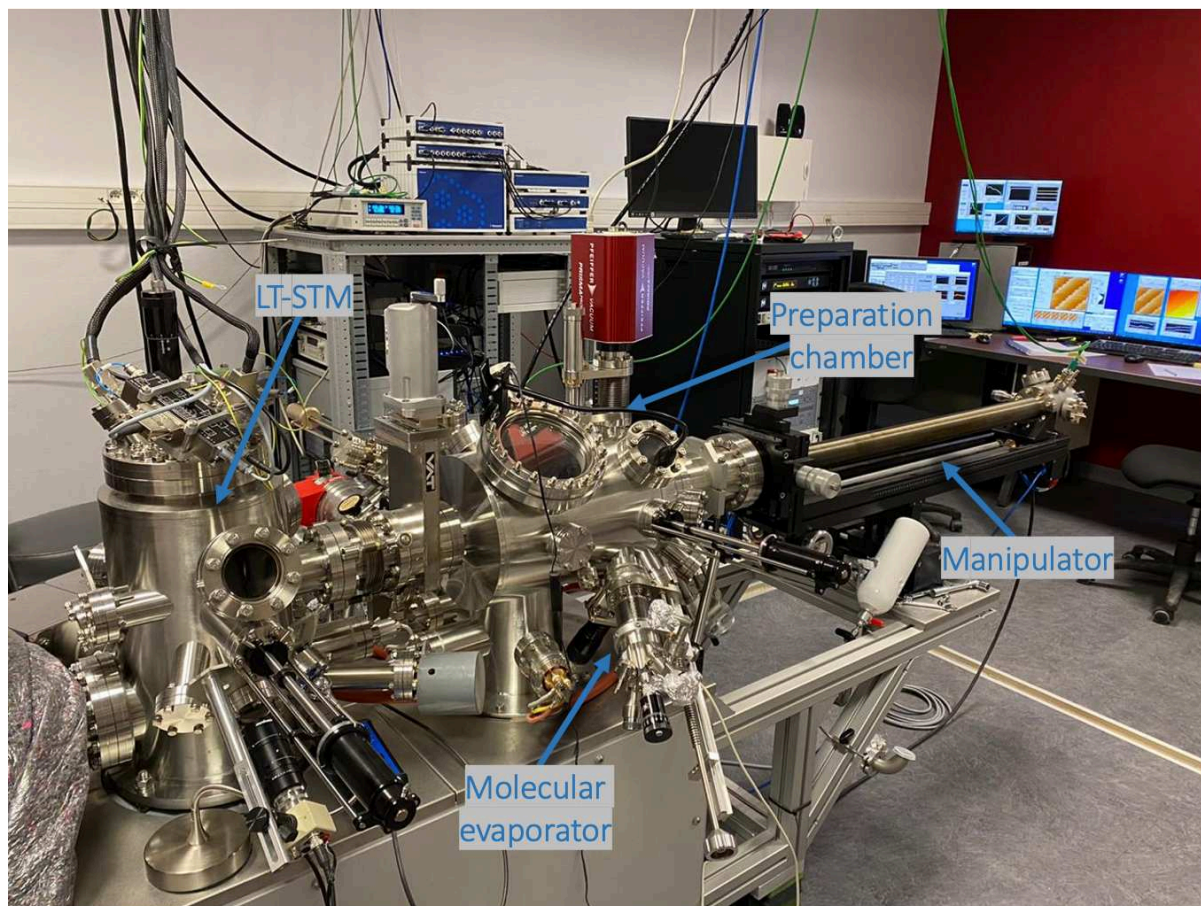
Figure 2.15. The new experimental setup of NANO group at IM2NP, Marseille.

The substrate is first mounted on a sample holder. Then, it is inserted into the UHV system through a load-lock chamber used to introduce the sample from ambient pressure without breaking the vacuum in all chambers, and without necessitating bake-up of the experimental system. The samples can be transferred between the different vacuum chambers with a manual transfer system.

References of chapter 2

[1]   J. V. Lauritsen, R. T. Vang, and F. Besenbacher, "From atom-resolved scanning tunneling microscopy (STM) studies to the design of new catalysts," *Catal. Today*, vol. 111, no. 1–2, pp. 34–43, Jan. 2006, doi: 10.1016/j.cattod.2005.10.015.

[2]   G. Binnig, H. Rohrer, Ch. Gerber, and E. Weibel, "Surface Studies by Scanning Tunneling Microscopy," *Phys. Rev. Lett.*, vol. 49, no. 1, pp. 57–61, Jul. 1982, doi: 10.1103/PhysRevLett.49.57.

[3]   Flemming Besenbacher, "Scanning tunnelling microscopy studies of metal surfaces," *Published under licence by IOP Publishing Ltd*, Progress in Physics, p. 1737, 1996.

[4]   R. Wolkow and Ph. Avouris, "Atom-resolved surface chemistry using scanning tunneling microscopy," *Phys. Rev. Lett.*, vol. 60, no. 11, pp. 1049–1052, Mar. 1988, doi: 10.1103/PhysRevLett.60.1049.

[5]   S. De Feyter and F. C. De Schryver, "Self-Assembly at the Liquid/Solid Interface: STM Reveals," *J. Phys. Chem. B*, vol. 109, no. 10, pp. 4290–4302, Mar. 2005, doi: 10.1021/jp045298k.

[6]   M. Amrein, A. Stasiak, H. Gross, E. Stoll, and G. Travaglini, "Scanning Tunneling Microscopy of recA-DNA Complexes Coated with a Conducting Film," *Science*, vol. 240, no. 4851, pp. 514–516, Apr. 1988, doi: 10.1126/science.3358130.

[7]   G. Binnig, H. Rohrer, F. Salvan, Ch. Gerber, and A. Baro, "Revisiting the 7×7 reconstruction of Si(111)," *Surf. Sci. Lett.*, vol. 157, no. 2–3, pp. L373–L378, Jul. 1985, doi: 10.1016/0167-2584(85)91088-6.

[8]   S. Woedtke, Inst. f. Exp. u. Ang. Phys. der CAU Kiel, 2002.

[9]   KONSTANTIN SIMONOV, "Effect of Substrate on Bottom- Up Fabrication and Electronic Properties of Graphene Nanoribbons," ACTA UNIVERSITATIS UPSALIENSIS UPPSALA, 2016.

[10]   J. Bardeen, "Tunnelling from a Many-Particle Point of View," *Phys. Rev. Lett.*, vol. 6, no. 2, pp. 57–59, Jan. 1961, doi: 10.1103/PhysRevLett.6.57.

[11]   J. Tersoff and D. R. Hamann, "Theory and Application for the Scanning Tunneling Microscope," *Phys. Rev. Lett.*, vol. 50, no. 25, pp. 1998–2001, Jun. 1983, doi: 10.1103/PhysRevLett.50.1998.

[12]   J. Tersoff and D. R. Hamann, "Theory of the scanning tunneling microscope," *Phys. Rev. B*, vol. 31, no. 2, pp. 805–813, Jan. 1985, doi: 10.1103/PhysRevB.31.805.

[13]   G. Ertl, J. Küppers, *Low Energy Electrons and Surface Chemistry*.

[14]   C. N. Berglund and W. E. Spicer, "Photoemission Studies of Copper and Silver: Theory," *Phys. Rev.*, vol. 136, no. 4A, pp. A1030–A1044, Nov. 1964, doi: 10.1103/PhysRev.136.A1030.

[15]   J.Rault, *Chemical and Electronic Structure of the Metal-Ferroelectric Interface as a Function of Ferroelectric Polarization*. Université Pierre et Marie Curie, 2013.

[16]   B. J. Albers *et al.*, "Combined low-temperature scanning tunneling/atomic force microscope for atomic resolution imaging and site-specific force spectroscopy," *Rev. Sci. Instrum.*, vol. 79, no. 3, p. 033704, Mar. 2008, doi: 10.1063/1.2842631.

[17]   D. Barton *et al.*, "Formation of Organometallic Intermediate States in On-Surface Ullmann

Couplings," *Chem. - Eur. J.*, vol. 23, no. 25, pp. 6190–6197, May 2017, doi: 10.1002/chem.201605802.

[18]   R. Gutzler *et al.*, "Ullmann-type coupling of brominated tetrathienoanthracene on copper and silver," *Nanoscale*, vol. 6, no. 5, pp. 2660–2668, 2014, doi: 10.1039/C3NR05710K.

[19]   "https://www.kentax.de/uhv-evaporator-tce-three-cell.html."

[20]   "https://scientaomicron.com/en/products-solutions/SPM/INFINITY-SPM-Lab/technology/LT%20STM/101."

Chapter 3: Self-assembly of a bimolecular solution of Trimesic and benzoic acid on HOPG

In this chapter, we report the two-dimensional self-assembly of a mixed solution of two aromatic acids that possess different alkyl and carboxyl groups. The liquid-solid interface on HOPG (Highly Oriented Pyrolytic Graphene) is investigated by room temperature scanning tunneling microscopy (RT-STM). The studied molecules are the benzene- 1,3,5-tricarboxylic acid (trimesic acid, TMA) and the 4-(decyloxy)benzoic acid (BZA) of the raw formula $C_9H_6O_6$ and $C_{19}H_{30}O_3$ respectively. They will be named in the rest of the manuscript by their acronyms TMA and BZA. These acids belong to the family of aromatic molecules with carboxyl functionalities, which are frequently studied on graphite surface.

3.1   Introduction

As described in chapter 1, self-assembly processes provide unique ways to obtain functional nanomaterials and extended molecular architectures stabilized by non-covalent bonds[1], [2] by using well-designed molecules as building blocks[3], [4]. Among the various self-assembled structures described in the literature, the supramolecular motifs based on hydrogen-bonding interactions are frequently observed due to their nature which is relatively strong, selective, and directional. For this type of bonding, the carboxyl functional group is a widely exploited synthon since it has the ability to form a double hydrogen bond motif. The role of H-bonds in the process of 2D crystallization is excellently illustrated by the behavior of benzene carboxylic acids, which can form diverse supramolecular networks[5]. The carboxylic acid functions in various acids such as trimesic acid (TMA), phthalic acid, isophthalic acid (ISA), terephthalic acid (TA) and benzoic acid (BA) can all act as hydrogen-bond donors and acceptors at the same time. It has been established that phthalic acid cannot form extended hydrogen-bonded arrays, whereas TA and ISA form dense monolayers in which the molecular self-assembly is dominated by hydrogen-bonding interactions[6]. On the other hand, the self-assembly of TMA[7]–[10] has been described as a prototype system for supramolecular self-assemblies that is formed in ultrahigh vacuum (UHV) conditions[7] and at the liquid-solid interface[11]. TMA has also proven to be a useful precursor for a variety of multicomponent surface architectures[8]–[10]. It is a planar carboxylic acid with three-fold symmetry comprising a phenyl ring and three identical carboxyl end groups at the 1,3,5-positions. For instance, the deposition of a TMA solution on HOPG surface under ambient conditions at room temperature leads to the formation

of two crystallographic structures[12]. M. Lackinger et al.[13] investigated the dependence of these observed structures on the solvent used. Figure 3.1a and b shows the two models of the two phases that can exist or coexist on the HOPG surface.
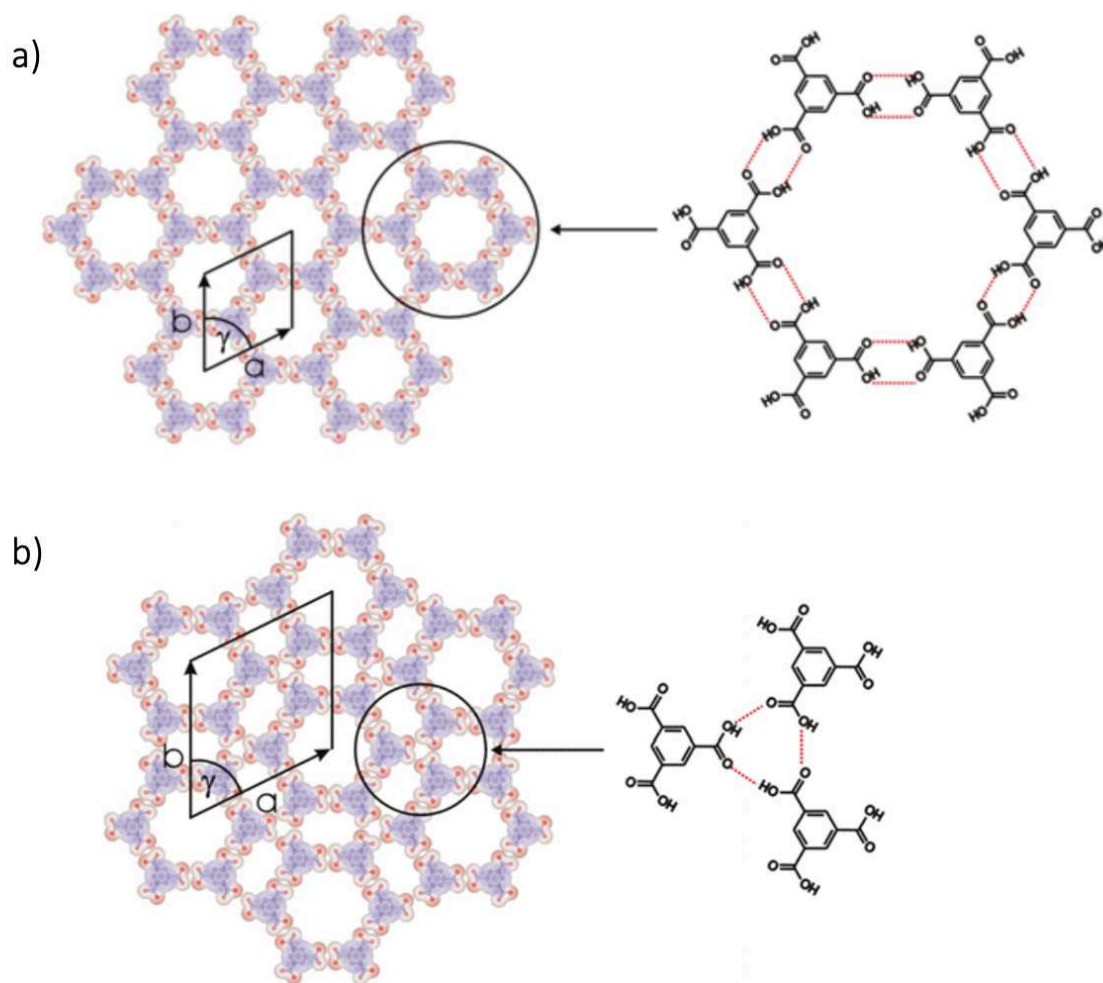
Figure 3.1. Schematic models of the different crystallographic structures found for TMA on HOPG surface. (a) The honeycomb structure (a = b = 1.7nm, $\gamma = 60°$, 2 molecules per unit cell). (b) The flower structure (a = b = 2.7nm, $\gamma = 60°$, 6 molecules per unit cell). Figure taken from [12].

Accordingly, TMA solubilized in fatty acids ($C_{n-1}H_{2n-1}COOH$) at the liquid-solid HOPG interface can self-assemble in different ways: for long chain length (n > 7) solvents like for octanoic and nonanoic acid, the honeycomb structure was found. For short chain length (n < 7) solvents like for butyric, pentanoic, and hexanoic acid, the flower structure was always found. Only for $n = 7$ (heptanoic acid), the two structures coexist on the surface. Figure 3.2 presents an overview showing this solvent dependence (middle panel) and the two corresponding STM images (a and b) of TMA monolayer dissolved in two different solvents at the HOPG interface.

Figure 3.2. (Middle panel) Overview showing the dependence of TMA structure formed at the interface on the solvent nature. (a, b) 15 nm × 15 nm STM images of the monolayer formed at the interface between HOPG and a saturated solution of TMA in heptanoic acid (a, honeycomb) and pentanoic acid (b, flower) solvents. Adapted from [13].

In the case of heptanoic acid, the two structures, "honeycomb" and "flower" structures, coexist (a and b respectively in Fig.3.2). They are formed both with a perfec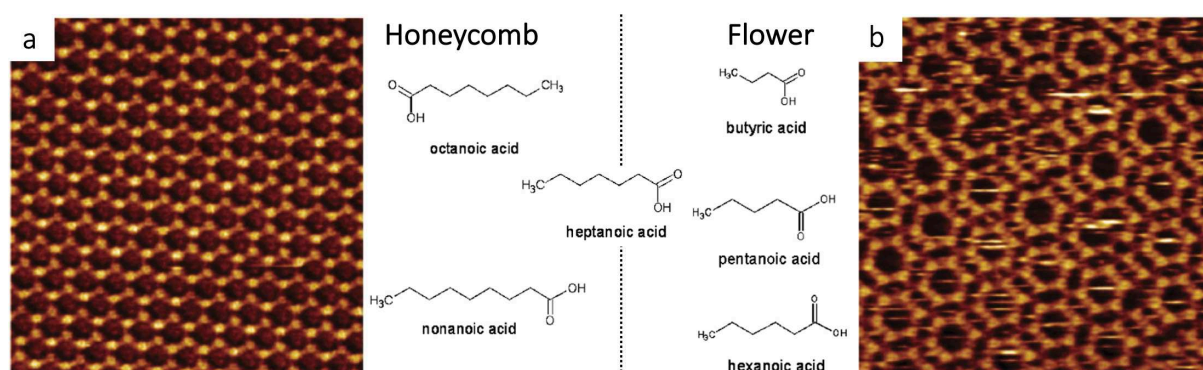t arrangement of hydrogen bonds between carboxyl groups and form sixfold rings. The main difference is that hydrogen bonds are formed between molecular pairs for the honeycomb structure, whereas for the flower structure, the hydrogen bonds occur also periodically between three carboxylic groups. All H-bonds (dotted red lines in fig.3.1) have a length of 2.92 ± 0.2Å for (a) and 2.96 ± 0.2Å for (b). In contrast to hydrogen bonds, van der Waals interactions between alkyl chains on the graphite surface can give to the molecular self-assembly an unconventional directionality. For instance, the adsorption of alkoxy-benzoic acids (BZA) molecule bearing an alkoxy chain on a graphite surface illustrates this type of interactions. The BZA is a carboxylic acid comprising a phenyl ring, a carboxyl group, and an alkoxy chain. In comparison with TA, ISA, and TMA molecules, the peculiarity of the 2D self-assembly of BZA is that one acid molecule can only form one hydrogen-bonding motif as shown in Figure 3.3.
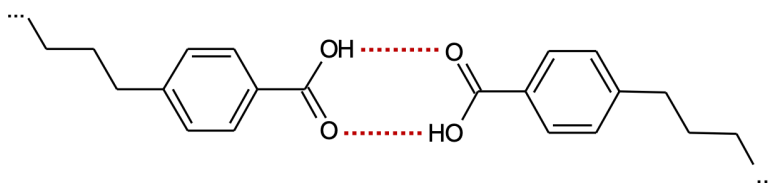

Figure 3.3. Schematic showing the hydrogen bonds (red dashed lines) formed between two alkoxy-benzoic acid (BZA) molecules.

De Feyter et al.[14] study the self-assembled structure of a benzoic acid derivative, the 4-alkoxybenzoic acids ($4 - OC_{20}BA$), at the liquid-solid HOPG interface. Figure 3.4 shows the

STM image of the $4 - OC_{20}BA$ monolayer physisorbed at the 1-phenyloctane/HOPG interface and the corresponding model. The STM image (Fig.3.4a) shows a stable monolayer that emerges with a lamellar structure (the width of each lamella is $\Delta L = 5.7 \pm 0.1$ nm) with two contrast regions. The bright region can be attributed to the aromatic core of the molecules according to their high electron density. While the darker contrast can be related to the alkoxy chains. The structure is formed by hydrogen bonds between the carboxyl groups of two molecules and van der Waals interaction between the alkyl chains as shown in the tentative model in Fig.3.4b and the schematic interactions in Fig.3.4c.
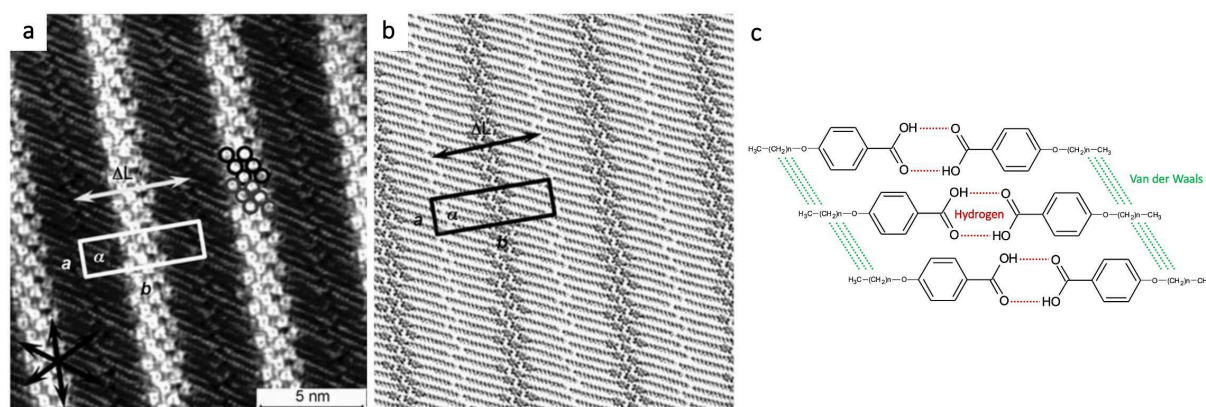
Figure 3.4. (a) High resolution STM image of 4-OC$_{20}$BA (BZA) molecule after deposition at the 1-phenyloctane/HOPG interface. The structure consisting of a lamellar feature with a width of $\Delta L = 5.7 \pm 0.1$ nm of each lamella. The unit cell parameters are $a = 1.79$nm, $b = 5.73$nm, $\alpha = 87.9°$. STM parameters: $I_t = 0.25$ nA, $V_{bias} = -0.78$V. (b) The corresponding model of the molecular structure observed in (a). (c) self-assembled structures formed by hydrogen bonding (red dashed lines) and van der Waals interactions (green dashed lines). Figure reproduced from [14].

The self-assembly of bimolecular systems are in general difficult to assess and have been less investigated[15]–[18], [10]. Nevertheless, interesting effects can be produced. In particular, it has been shown that the addition of a modulator molecule can induce an anisotropic crystal growth by taking advantage of competitive interactions[19]. The strategy is illustrated in Figure 3.5. Here, the growth of a supramolecular crystal from a multi-functional precursor is restricted on its surface by the interaction with a mono-functional modulator that prohibits the growth development. When modulators having the same chemical functionality as the organic linker are used, the coordination interaction between the metal ions and the organic linkers is hindered. This leads to the creation of a competitive environment that controls the rate of framework extension and the crystal growth.
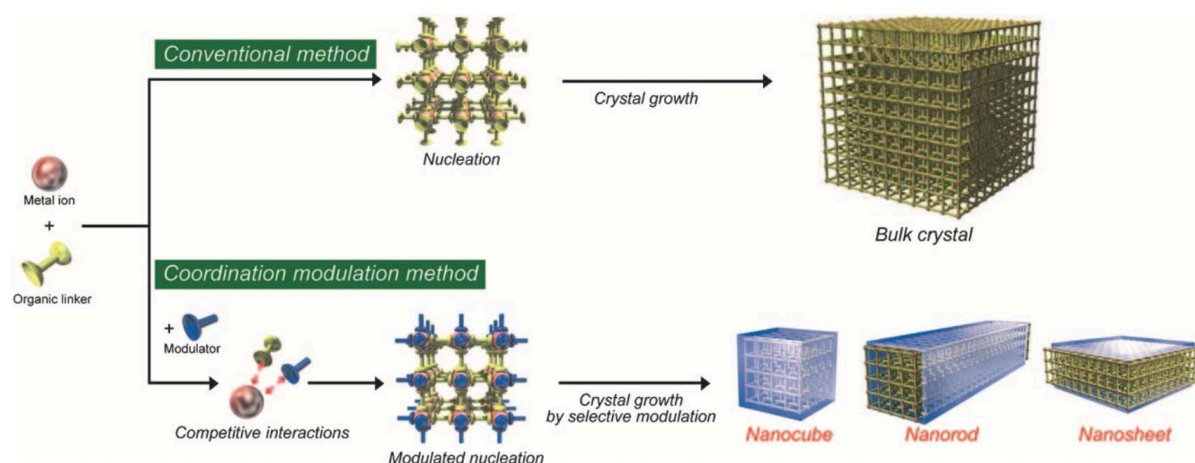
Figure 3.5. The coordination modulation strategy for the formation of porous coordination polymer (PCP) nanocrystals. Figure adapted from [19].

This strategy, initially proposed for three-dimensional systems, has been only once applied to an adsorbed system on a surface[20]. In this chapter we propose to extend this modulator strategy by investigating the 2D self-assembly of a bimolecular solution of the two acids, the trimesic acid (TMA) and benzoic acid (BZA), presented in Fig.3.6 and that possess different alkoxy and carboxyl substitutions at the liquid-HOPG interface. This bimolecular solution is expected to control the formation of 2D network on the surface due to the particular structure of the two acids.
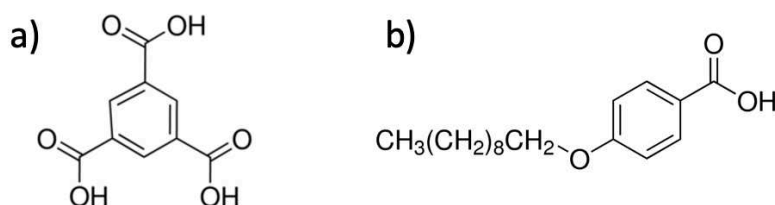
Figure 3.6. Schematic representative of (a) Benzene-1,3,5-tricarboxylic (TMA) acid and (b) 4-(Decyloxy)benzoic (BZA) acid.

Based on previous results reported in the literature for TMA and BZA as presented above, TMA possesses three carboxylic groups leading to the formation of complementary intermolecular hydrogen bonding and extended 2D domains, while the BZA molecule can be involved in only one intermolecular hydrogen bonding motif at the border of a domain. Thus, the use of a bimolecular solution of these two acids is expected to limit the domain size of the obtained structure, as illustrated schematically in the example structure in Fig.3.7 for a stoichiometric ratio of 1:1.
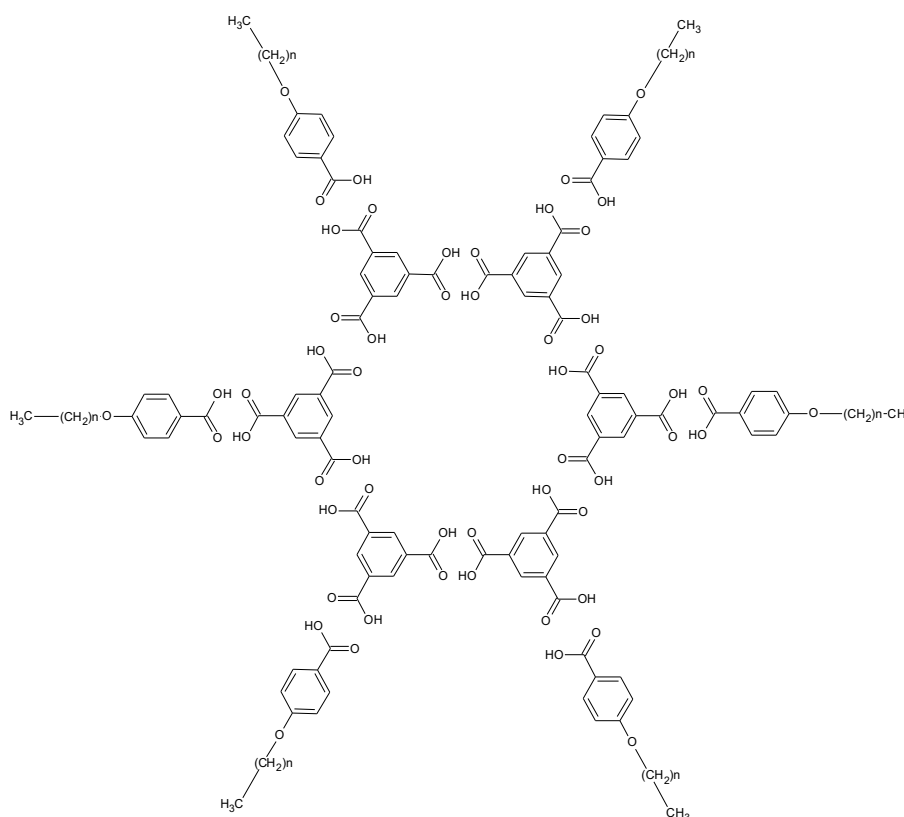
Figure 3.7. Molecular structure of the expected domain obtained from a bimolecular solution of TMA and BZA. For a stoichiometric ratio of 1:1, the domain is limited to six TMA coupled together by hydrogen bonding forming a hexagon and to six BZA molecules.

3.2 Self-assembly of TMA molecules on HOPG interface

First, we present the self-assembly of a monomolecular solution of TMA molecules on the HOPG surface. All STM measurements presented in this chapter were taken at room temperature. A main solution of TMA is prepared with a concentration of 1.2×10^{-2} mol/l by using the nonanoic acid as solvent. This solution is noted "TMA-High" solution (see section 3.4, Table 3.1). The STM image of the TMA layer organization after the deposition of 5µl of this prepared solution on the HOPG surface is presented in Fig.3.8. The network is built-up of a repetition of disjoint dots arranged in a hexagonal lattice. Two domains coexist on the surface noted A and B with two different orientations relative to the substrate and with an angle about 17° between them. The unit cell of the supramolecular network is hexagonal with a size of 17.5 ± 1 Å and an angle of 62°. It corresponds to that reported for the honeycomb network in the literature[13]. The unit cells includes then two molecules which are not individually resolved, only the network periodicity is visible in this image.

96
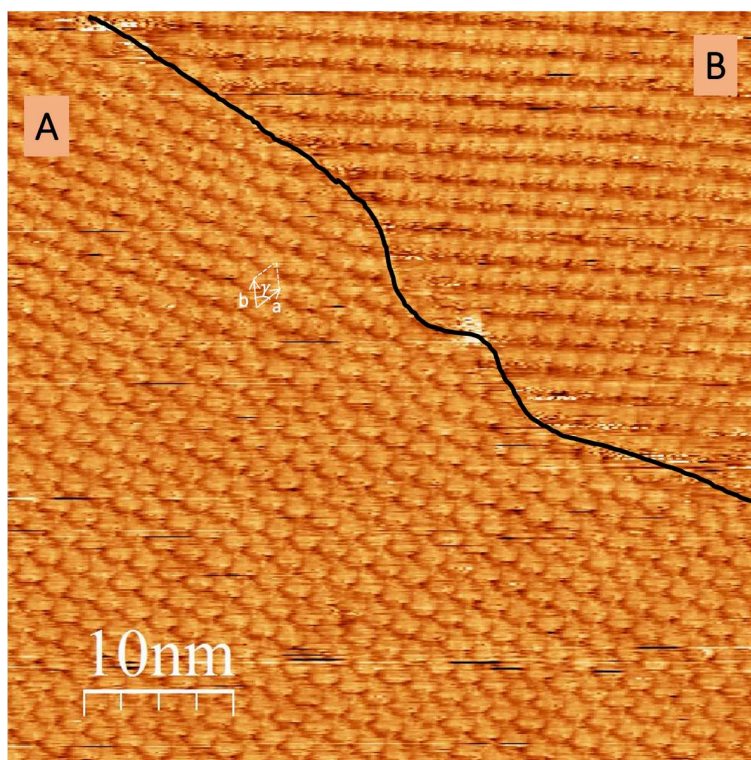
Figure 3.8. STM image of 2D supramolecular networks after deposition of TMA molecules on HOPG surface. Typical organization of a hydrogen-bonded honeycomb structure is observed. The individual molecules are not individually resolved, only the network periodicity is visible, with two molecules per unit cell. Two different domains coexist noted A and B. STM parameters: $I = 48$ pA, $V = 963$ mV.

3.3 Bimolecular solutions on HOPG

In this section, we describe the preparation procedure of the studied bimolecular solutions. The first step was the preparation of a main solution of each acid, one is prepared from TMA and the other from BZA molecules. Then, by varying the stoichiometry ratio between the two molecules, different bimolecular solutions were prepared from the main solutions. Therefore, we estimate first the stoichiometry ratio between the two acids, then we prepare the bimolecular solutions. Finally, the liquid-HOPG interface of each solution was studied by (RT-STM).

Estimation of the stoichiometry ratio

The expected obtained structure is formed with multi-functional molecules coupled together forming the interior (Int) of the domain. Moreover, these interior molecules are coupled with the mono-functional molecules that form the border (Ext) of the domain. The stoichiometry ratio between the two molecules was estimated as a function of the domain size (D) formed on

the surface by combining two different approximations. In the first approximation, the interior molecules were considered to have a squared shape and thus form a square domain (Fig.3.9). The intermolecular distance is set as "d". In this event, the number of interior molecules that formed the domain would be proportional to the area of the domain (here in square geometry $n_{Int} = (\frac{D}{d})^2$) while the number of the molecules on the border would be proportional to the perimeter ($n_{Ext} = 4 * D/d$). Therefore, the stoichiometry ratio between the two molecules is directly proportional to the size D of the domain: $^{n_{Int}}/_{n_{Ext}} = D/(4 * d)$.
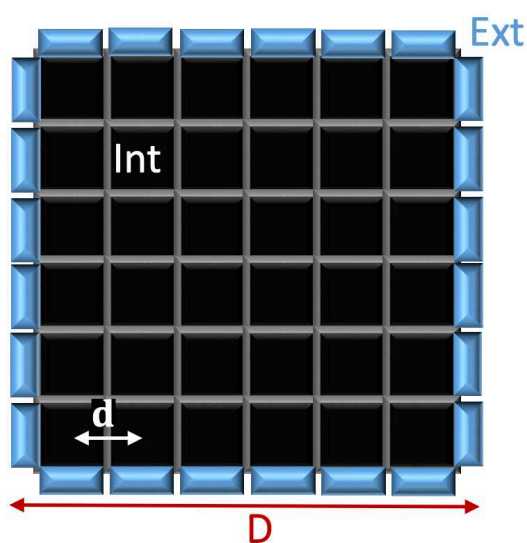
Figure 3.9. Representative schematic of the constrained domain formed by the two molecules on the surface by considering, in the first approximation, that the interior molecules have a square shape.

In the real case, the interior molecules are expected to be the TMA molecules and the BZA on the border of the domain. In the present approximation we consider that the virtual square molecules have the same intermolecular distance as TMA. As presented above, previous studies identified the TMA molecule to have a honeycomb structure with a unit cell size of a = 1.72 nm and an area of $a^2 \cdot \frac{\sqrt{3}}{2} \sim 2.56$ nm^2 (Fig.3.1) as the observed structure for molecules in nonanoic acid solvent. Thereover, TMA honeycomb structure is consisting of two molecules per unit cell. Thus, the average surface area of one TMA molecule is about ~ 1.28 nm^2. Moreover, the distance between two TMA molecules can be calculated as follow. The TMA network is formed of a hexagonal structure as illustrated below in Fig.3.10a,b. In the (OT_1T_2) triangle, the distance $OM = a/2$ with a = 1.72 nm the unit cell parameter and the angle $\widehat{MT_1O} = 60°$. Thus, $\tan 60° = \frac{a/2}{d_{TMA}/2}$ and the distance between two TMA molecule can be

written as $d_{TMA} = \frac{a}{\tan 60°} = \frac{a\sqrt{3}}{3} \cong 1\text{nm}$. In addition, in the definition of a regular hexagon, the diagonal size is equal $2 \times$ side size, i.e. $T_1T_4 = 2 \times d_{TMA}$ (this distance will be used in the second approximation).
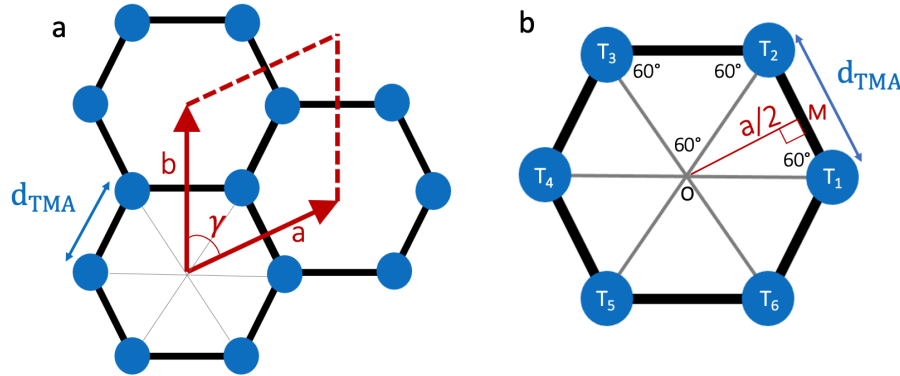
Figure 3.10. Representative schematic of the honeycomb structure formed by TMA molecules as observed in the literature. (a) three hexagons of TMA network showing the unit cell parameters $a = b = 1.7\text{nm}, \gamma = 60°$. TMA molecules are represented by blue circles. (b) Close-up of one hexagon showing the different distances and angles.

Hence, the stoichiometry ratio between the two molecules can be written as:

$$\frac{n_{TMA}}{n_{BZA}} = \frac{D}{4 \times d_{TMA}} \approx 0.25 \times D[\text{nm}]$$

Figure 3.11 represents this stoichiometry ratio $\left(\frac{n_{TMA}}{n_{BZA}}\right)$ as a function of the size of the domain (D) in nm.
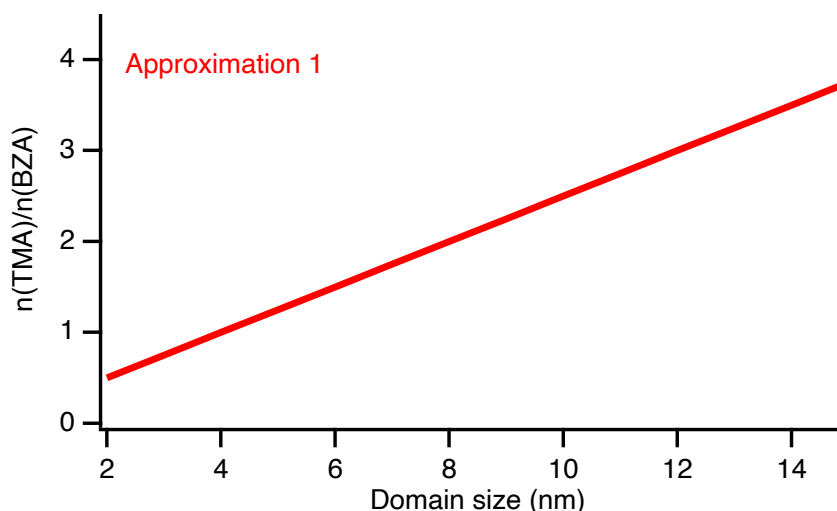
Figure 3.11. The stoichiometry ratio between the interior (TMA) and the border (BZA) molecules as a function of the domain size (D) in the framework of the first square shape approximation.

In the real system, TMA molecules are not square but triangular and the formed domains can exhibit various geometrical patterns. Thus, a second approximation is applied. Many domains can be a build-up from a similar molecular network and differ by their size and shape, i.e. number of TMA and BZA molecules inside each domain and their relative organization (Fig.3.10). In this approximation, we can consider the real honeycomb TMA network expected. We denote the TMA molecule as a blue triangle and BZA molecule as the black rectangle. The smallest domain that can be obtained here is composed of a sixfold ring of trimesic acid molecules (Fig.3.12, A) connected by hydrogen bonds with one benzoic acid molecule at each end of TMA (similar to the domain shown in Fig.3.7). Thus, in domain A we have 6 inside and 6 border molecules, $\frac{n_{TMA}}{n_{BZA}} = 1$, the size of this domain is $S(A) = 1 * \text{diagonal} = 2 * d_{TMA}$. In domain B, we have 2 fused rings surrounded by 8 border molecules, thus $\frac{n_{TMA}}{n_{BZA}} = 1.25$ and $S(B) = 2 * a = 2\sqrt{3} * d_{TMA}$. In domain C we have $\frac{n_{TMA}}{N_{bza}} = 1.44$ and $S(C) = 2 * S(A) + 1 *$ $d_{TMA} = 5 * d_{TMA}$. In this way, we can create specific (virtual) domains of increasing size and calculate for each of them the ratio $\frac{n_{TMA}}{N_{bza}}$ and the size D. Fig.3.11 shows some of the different domains that can be attained on the surface with the corresponding number of TMA and BZA molecules in each of them. In this second approximation, the reference size S(A) is defined as the width of the hexagon formed by one sixfold ring of TMA molecules.
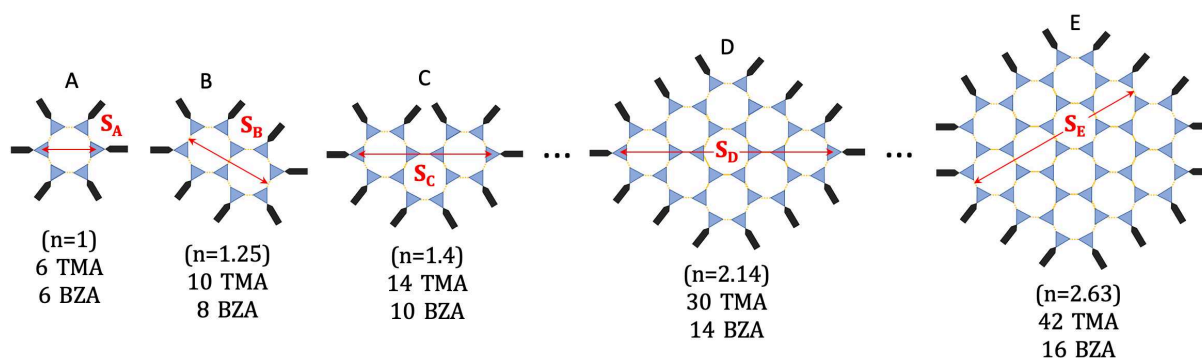
Figure 3.12. Schematic present a selection of built-up domains (A, B, C, ...) that can be formed on the surface with the corresponding number of molecules and the ratio n between the two molecules.

Therefore, the stoichiometry ratio between the two molecules $\left(\frac{n_{TMA}}{n_{BZA}}\right)$ is represented in Fig.3.13 as a function of the domain size (D) in nm.
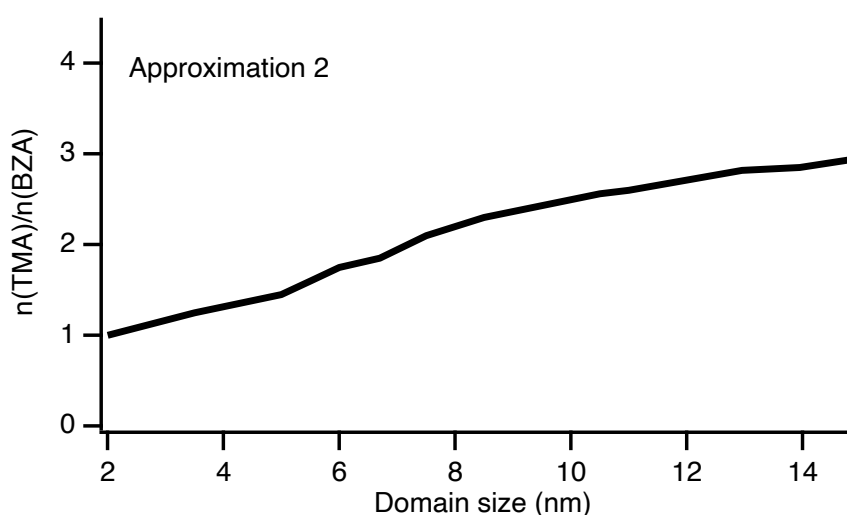
Figure 3.13. The stoichiometry ratio between TMA and BZA molecule in solution as a function of the domain size (in nm) corresponding to the second approximation.

The assessment of these two approximations yielded very similar results for domain sizes between 0 and 15 nm as shown in Fig.3.14. We can see here, that if we want to create domains of size 10 nm x 10 nm, that should be easily observed in STM images, a ratio of 2.5 can be expected.
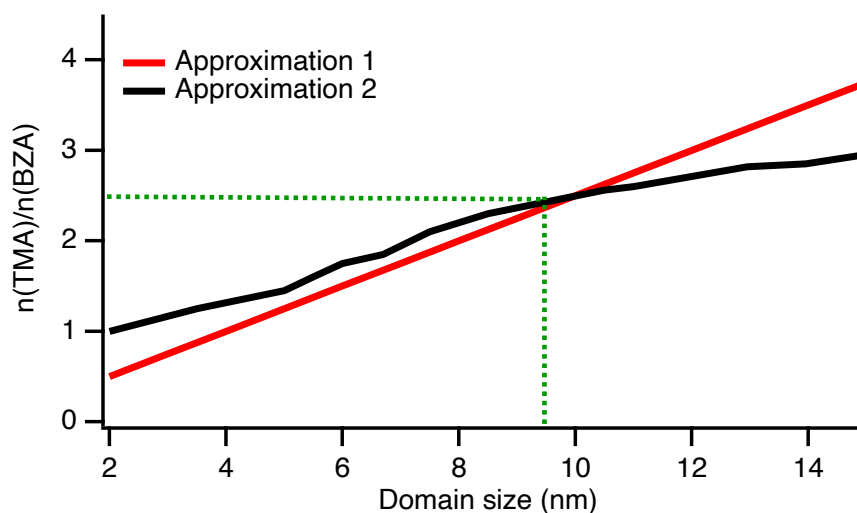
Figure 3.14. Comparison of the stoichiometry ratio between TMA and BZA molecules expected as a function of the network size (in nm) for the two different approximations.

3.4   Preparation of the solutions

In order to prepare a bimolecular solution with the estimated stoichiometry ratio $^{n_{TMA}}/_{n_{BZA}} \sim 2.5$, two base solutions were prepared with one molecular precursor each. First, two beakers were cleaned with alcohol under ultrasound for a few minutes. A few grams of TMA molecules and BZA molecules were added to each of the beakers containing nonanoic acid. The solutions noted TMA-X and BZA-X respectively were mixed and sonicated for 15 min. Finally, different solutions were prepared from these two base solutions by varying the stoichiometry ratio starting from 2.5 as estimated below. All parameters for the base solutions are presented in table 3.1.

	TMA-Low	TMA-High	BZA-Low	BZA-High
Mass (g)	0.00075	0.0078	0.00274	0.12345
Volume (ml)	7	3	3	9
Molecular mass (g/mol)	210	210	278	278
Concentration (mol/l)	5.1×10^{-4}	1.2×10^{-2}	3.2×10^{-3}	4.9×10^{-2}

Table 3.1. Representative parameters for each base solution used for the bimolecular solutions preparations. They are presented by ascending order of concentration for each acid.

A first bimolecular solution-1 of TMA and BZA molecules was prepared from the two base solutions TMA-High and BZA-Low. The volume taken from each was calculated as follows. The number of TMA and BZA molecules in the solution-1 can be given as:

$$n_{TMA} = C_{TMA(f)} \times V_f \text{ and } n_{BZA} = C_{BZA(f)} \times V_f$$

Where $C_{TMA(f)} = \frac{C_{TMA(i)} \times V_{TMA}}{V_f}$, $C_{BZA(f)} = \frac{C_{BZA(i)} \times V_{BZA}}{V_f}$ are the concentrations of TMA and BZA in the bimolecular solution-1 and $V_f = V_{TMA} + V_{BZA}$ the total volume of the solution-1. $C_{TMA(i)}$, and $C_{BZA(i)}$, are the initial concentrations of the base solutions, and V_{TMA} and V_{BZA} are the taken volume from the initial solutions TMA-High and BZA-Low respectively.

Since the mass quantity is conserved: $C_{TMA(i)}V_{TMA} = C_{TMA(f)}V_f$, $C_{BZA(i)}V_{BZA} = C_{BZA(f)}V_f$, we can calculate the volume that should be taken from each acid solution for a stoichiometry ratio of about ~ 2.5:

$$\frac{n_{TMA}}{n_{BZA}} = \frac{C_{TMA(f)}}{C_{BZA(f)}} = 2.5$$

$$\frac{C_{TMA(i)}V_{TMA}}{C_{BZA(i)}V_{BZA}} = 2.5$$

$$V_{TMA} = 2.5 \times \frac{C_{BZA(i)}}{C_{TMA(i)}} V_{BZA}$$

Thus, solution-1 was prepared by combining 1.5 ml of BZA-Low and 1 ml of TMA-High solutions.

3.5 Bimolecular solution self-assembly by RT-STM

In this section, different bimolecular solutions were studied by varying the stoichiometry ratio between the two molecules. Table 3.2 shows the parameters of the different studied bimolecular solutions.

	Solution-1	Solution-2	Solution-3	Solution-4
Volume of TMA (ml)	1 (TMA-High)	0.5 (TMA-High)	0.2 (TMA-Low)	0.002 (TMA-Low)
Volume of BZA (ml)	1.5 (BZA-Low)	2.2 (BZA-Low)	2 (BZA-High)	2 (BZA-High)
Stoichiometry ratio	2.5	6.5×10^{-1}	1.0×10^{-3}	6.1×10^{-6}

Table 3.2. Table showing the parameters used for the preparation of the different bimolecular solutions.

We start by the study of the solution-1, with a stoichiometry ratio of 2.5 as estimated from Fig.3.14 and corresponding in principle to a domain size of 10 x 10 nm^2. The deposition of $5\mu l$ of this solution on HOPG surface is depicted in the STM image of Fig.3.15. An ordered structure was observed with a hexagonal arrangement of molecules. The unit cell parameters $(a = b = 17.5 \pm 1\,\text{Å}, \gamma = 60°)$ are similar to that observed in the literature for TMA honeycomb structure with two TMA molecules per unit cell. A structural model of the molecular geometry observed in STM image is shown in Fig.3.15b. The network is formed of a perfect arrangement of hydrogen bonds between carboxyl groups of TMA molecules and form sixfold rings. Remarkably, and in contrast to what was observed in Fig.3.8, here all TMA molecules are individually resolved.
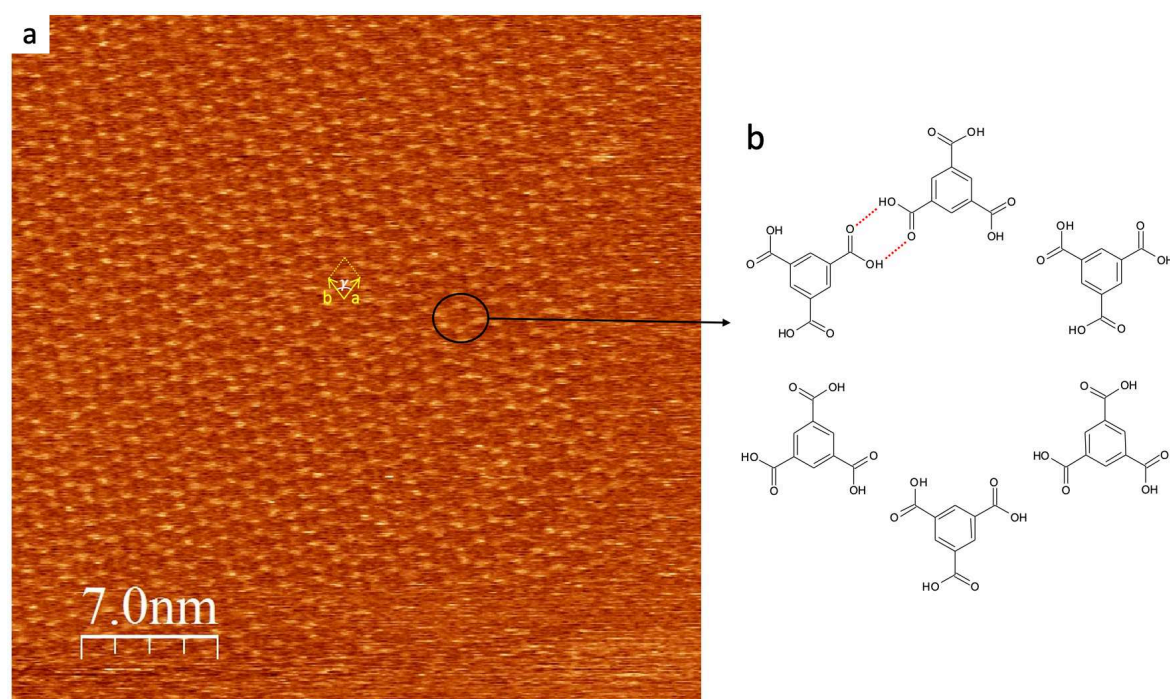
Figure 3.15. (a) STM images of the honeycomb structure formed after deposition the solution-1 on the HOPG surface at RT. The unit cell of the hexagonal lattice is indicated in yellow with $a = b = 17.5 \pm 1\,\text{Å}, \gamma = 60°$. (b) the structural model of the honeycomb network observed in (a). H-bonds are illustrated by red dashed lines. STM parameters: $I = 1.2\,\text{pA}, V = 368\,\text{mV}$.

For this latest solution with a stoichiometry ratio of 2.5, we observed only the honeycomb structure of the TMA molecules. No flower structure was found, in agreement with what was observed in the literature when using nonanoic acids as solvent (see Fig.3.1 and 3.2). Moreover, we did not observe any self-assembly of the BZA molecules presented in the solution nor any mixed TMA-BZA phase. Hence, the BZA molecules are not adsorbed on the surface, which corresponds to the case of an infinite TMA domain size. Thus, in the next step we reduced the

stoichiometry ratio between the two molecules in order to try to reduce the domain size and to favor BZA adsorption.

A second solution, solution-2 (Table 3.2) was prepared by decreasing the TMA/BZA ratio to 0.65. The deposition of 5µl of this second bimolecular solution on the HOPG surface leads to the formation of a 2D structure consisting of organized features with a periodic arrangement (Figure 3.16) with the nearest neighbor distance of 17.5 ± 1 Å. We could also attribute this structure to the honeycomb TMA structure also observed previously. Again, but now with a stoichiometry ratio of 0.65, no self-assembly between TMA and BZA molecules was observed, a network with only TMA molecules was obtained.
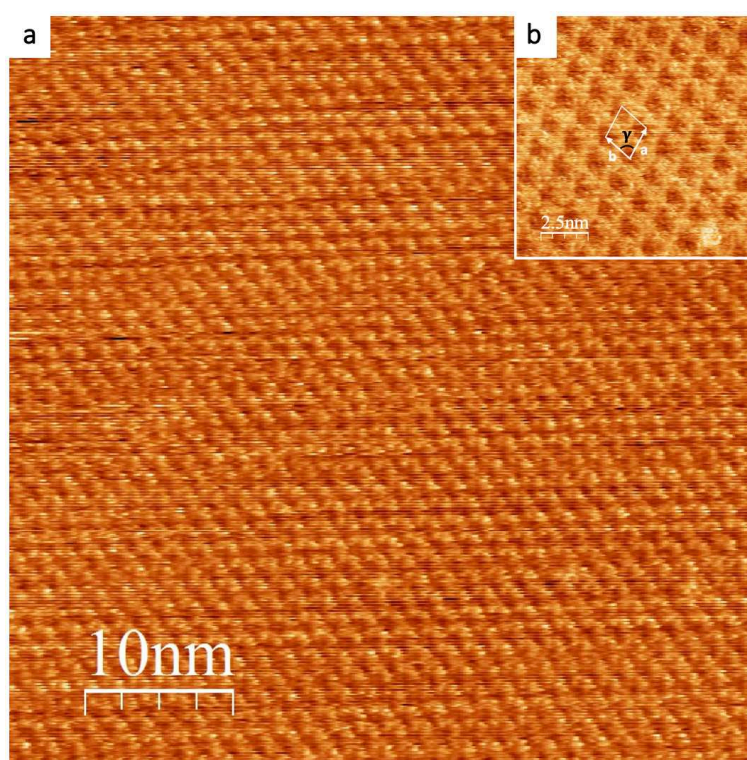
Figure 3.16 (a) STM images of solution-2 on HOPG surface (V=1.8 mV, I=55.8 pA). (b) STM image representing the hexagonal lattice with a = b = 1.75 nm.

We then decreased further the TMA/BZA stoichiometry ratio to 10^{-3} and 10^{-6} (solution-3 and 4 in Table 3.2). Different structures seen from solution-1 and 2 are observed by STM images in Figure 3.17a. The image is composed of an arrangement of parallel bright and dark rows. The distance between two equivalent bright rows is about $2.7 - 3$ nm (Fig.3.17b). According to the higher electron density of the aromatic core and based on the measured distances, the bright region may be attributed to the phenyl rings of molecules, while the darker region can be related to the alkoxy chains. A model of the observed structure is presented in

Fig.3.17c. Herein, BZA molecules arrange together by forming hydrogen bonds between carboxyl groups (red dashed line in Fig.3.17c) and the alkoxy chains are fully extended and arranged in parallel rows with a van der Waals interaction between them. The distance between two alkoxyl chains of two adjacent molecules is 7 ± 1 Å. Thus, this structure in in agreement to that observed in the literature for pure benzoic acid deposited on the HOPG surface[14].
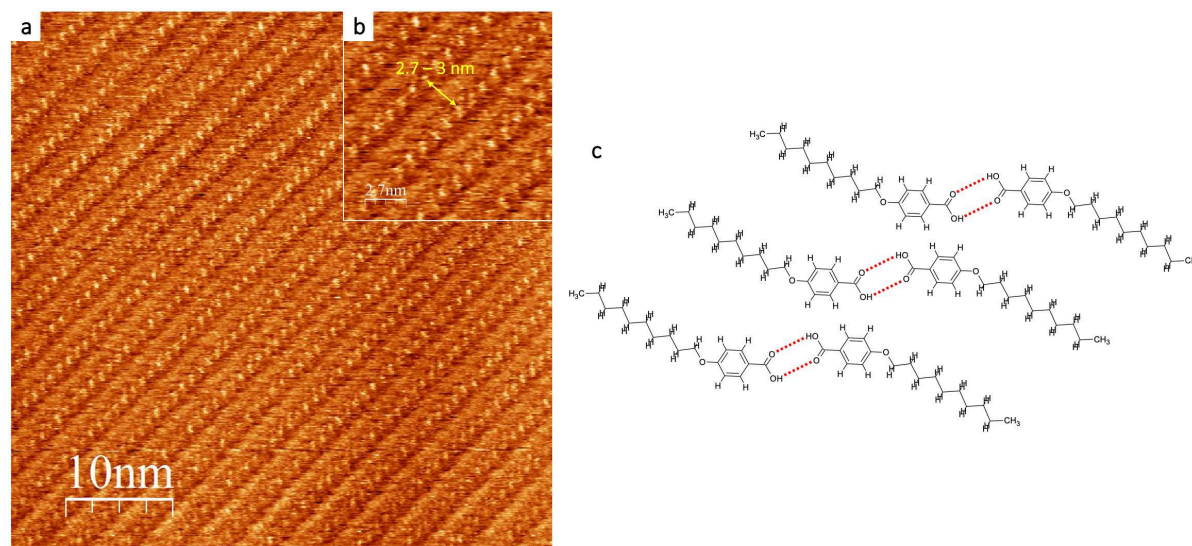
Figure 3.17. (a) STM images of solution-3 with a ratio of 1.0 x 10^{-3} between the two molecules on the HOPG surface. (b) Close-up STM image showing the distance between two dark regions (yellow arrow). (c) Structural model corresponding to the arrangement in (a). H-bonds are illustrated by red dashed lines. STM parameters: $I = 50$ pA, $V = 550$ mV.

Now, for these last solutions, no self-assembly of TMA molecules was observed, only structures of pure BZA molecules were founded. Based on our STM results, we can conclude that, if it exists, the ideal ratio between the two molecules (TMA and BZA) to form domains of finite size would be between 10^{-1} and 10^{-3}. It is possible that the formation of the domains is very sensitive to this stoichiometry ratio between the molecules and a fine tuning of the ratio could be necessary. Unfortunately, it was not been possible to explore in details this range of ratio in the framework of this thesis work due to a lack of available experimental time.

3.6 conclusions

Our work was inspired from a previous study to control the size of self-assembled domains by introducing a modulator precursor. To this aim, we have chosen the trimesic acid (TMA) and the benzoic acid (BZA) molecules previously studied at the liquid- HOPG interface. The 2D self-assembly process of the bimolecular solution of TMA and BZA on HOPG surface was

studied by using STM under ambient conditions. By varying the stoichiometry ratio between the two molecules we should in principle be able to directly control the domain size on the surface. We proposed an approximation model to estimate the desired stoichiometric ratio between the two molecule types in order to prepare the bimolecular solutions. We found that, for a ratio $^{n_{TMA}}/_{n_{BZA}}$ larger than 0.65, the honeycomb structure formed by only TMA molecules was solely observed. For a ratio smaller than 10^{-3}, the self-assembly between only BZA molecules was observed on the HOPG surface.

In our investigation, we started from the theoretically calculated stoichiometry ratio between TMA and BZA molecules. This value would have been correct if all molecules were adsorbed on the surface in a stoichiometric fashion. In fact, an equilibrium is achieved between the molecules dissolved in the liquid phase and those adsorbed at the solid interface. Such equilibrium does not need to be equivalent for the two molecular species, so the ratio of the molecules adsorbed on the surface certainly differs for that in the liquid phase. To overcome this effect, we have tried different stoichiometry ratios, but we were not able to observe anything more than the pure phase of TMA only or BZA only. It is possible that the formation of the domains is very sensitive to the stoichiometry ratio between the molecules and a fine tuning of the ratio could be necessary. In future work, a study of bimolecular solutions of these two precursors by varying the stoichiometry ratio between 10^{-3} and 0.65 may be explored. Moreover, different precursors may be used to control the size of the self-assembly domain formed on the surface. Preliminary experiments on HOPG were performed in the laboratory before this PhD work on a bimolecular solution of trimesic acid and benzoic acid without alkoxy chains. In this case extended domains of TMA only were observed and no self-assembly of benzoic acid, even in the limit of very low stoichiometry ratio. It is thus suggested that the presence of the alkoxy chain favors the adsorption of the BZA modulator molecules. To increase further this effect, a new benzoic acid precursor with two alkoxy chains like 4,5-dialkoxy benzoic acid may be envisioned.

For the next, different types of molecular precursors from TMA and BZA molecules may be used to create 2D self-assembled structure with finite size. For example, it could be based on the well-established system PTCDI and melamine[21] that we have described in chapter 1 (section 1.1.3). There the modulator molecule could be a monofunctionalized derivative of PTCDI, like e.g. perylene-3,4-dicarboximide. In such system, the dicarboximide group is bound to the melamine precursor through triple hydrogen bonds and the self-assembly process may be more robust than with carboxylic acids.

References of chapter 3

[1]   G. M. Whitesides, J. P. Mathias, and C. T. Seto, "Molecular Self-Assembly and Nanochemistry: a Chemical Strategy for the Synthesis of Nanostructures," *Science*, vol. 254, no. 5036, pp. 1312–1319, Nov. 1991, doi: 10.1126/science.1962191.

[2]   D. Philp and J. F. Stoddart, "Self-Assembly in Natural and Unnatural Systems," *Angew. Chem. Int. Ed. Engl.*, vol. 35, no. 11, pp. 1154–1196, Jun. 1996, doi: 10.1002/anie.199611541.

[3]   J.-M. Lehn, "Towards Complex Matter: Supramolecular Chemistry and Self-organization," *Eur. Rev.*, vol. 17, no. 2, pp. 263–280, May 2009, doi: 10.1017/S1062798709000805.

[4]   G. M. Whitesides and M. Boncheva, "Beyond molecules: Self-assembly of mesoscopic and macroscopic components," *Proc. Natl. Acad. Sci.*, vol. 99, no. 8, pp. 4769–4774, Apr. 2002, doi: 10.1073/pnas.082065899.

[5]   Gautam R. Desiraju, "Chemistry beyond the molecule," Nature, pp. 397–400, Jul. 26, 2001.

[6]   M. Lackinger, S. Griessl, T. Markert, F. Jamitzky, and W. M. Heckl, "Self-Assembly of Benzene−Dicarboxylic Acid Isomers at the Liquid Solid Interface: Steric Aspects of Hydrogen Bonding," *J. Phys. Chem. B*, vol. 108, no. 36, pp. 13652–13655, Sep. 2004, doi: 10.1021/jp048248o.

[7]   A. Dmitriev, N. Lin, J. Weckesser, J. V. Barth, and K. Kern, "Supramolecular Assemblies of Trimesic Acid on a Cu(100) Surface," *J. Phys. Chem. B*, vol. 106, no. 27, pp. 6907–6912, Jul. 2002, doi: 10.1021/jp014214u.

[8]   S. J. H. Griessl, M. Lackinger, F. Jamitzky, T. Markert, M. Hietschold, and W. M. Heckl, "Room-Temperature Scanning Tunneling Microscopy Manipulation of Single C$_{60}$ Molecules at the Liquid−Solid Interface: Playing Nanosoccer," *J. Phys. Chem. B*, vol. 108, no. 31, pp. 11556–11560, Aug. 2004, doi: 10.1021/jp049521p.

[9]   S. J. H. Griessl, M. Lackinger, F. Jamitzky, T. Markert, M. Hietschold, and W. M. Heckl, "Incorporation and Manipulation of Coronene in an Organic Template Structure," *Langmuir*, vol. 20, no. 21, pp. 9403–9407, Oct. 2004, doi: 10.1021/la049441c.

[10]   K. G. Nath *et al.*, "Rational Modulation of the Periodicity in Linear Hydrogen-Bonded Assemblies of Trimesic Acid on Surfaces," *J. Am. Chem. Soc.*, vol. 128, no. 13, pp. 4212–4213, Apr. 2006, doi: 10.1021/ja0602896.

[11]   D. C. Y. Nguyen, L. Smykalla, T. N. H. Nguyen, T. Rüffer, and M. Hietschold, "Deposition-Temperature- and Solvent-Dependent 2D Supramolecular Assemblies of Trimesic Acid at the Liquid–Graphite Interface Revealed by Scanning Tunneling Microscopy," *J. Phys. Chem. C*, vol. 120, no. 20, pp. 11027–11036, May 2016, doi: 10.1021/acs.jpcc.6b03409.

[12]   Stefan Griessl, Markus Lackinger, Michael Edelwirth, Michael Hietschold, Wolfgang M. Heckl, "Self-Assembled Two-Dimensional Molecular Host-Guest Architectures From Trimesic Acid."

[13]   M. Lackinger, S. Griessl, W. M. Heckl, M. Hietschold, and G. W. Flynn, "Self-Assembly of Trimesic Acid at the Liquid−Solid Interfacea Study of Solvent-Induced Polymorphism," *Langmuir*, vol. 21, no. 11, pp. 4984–4988, May 2005, doi: 10.1021/la0467640.

[14]   K. S. Mali, K. Lava, K. Binnemans, and S. De Feyter, "Hydrogen Bonding Versus van der

Waals Interactions: Competitive Influence of Noncovalent Interactions on 2D Self-Assembly at the Liquid-Solid Interface," *Chem. - Eur. J.*, vol. 16, no. 48, pp. 14447–14458, Dec. 2010, doi: 10.1002/chem.201001653.

[15]   J. A. Theobald, N. S. Oxtoby, M. A. Phillips, N. R. Champness, and P. H. Beton, "Controlling molecular deposition and layer structure with supramolecular surface assemblies," *Nature*, vol. 424, no. 6952, pp. 1029–1031, Aug. 2003, doi: 10.1038/nature01915.

[16]   K. Tahara, E. Ghijsens, M. Matsushita, P. Szabelski, S. De Feyter, and Y. Tobe, "Formation of a non-crystalline bimolecular porous network at a liquid/solid interface," *Chem. Commun.*, vol. 47, no. 41, p. 11459, 2011, doi: 10.1039/c1cc14362j.

[17]   C. Thalacker, A. Miura, S. De Feyter, F. C. De Schryver, and F. Würthner, "Hydrogen bond directed self-assembly of core-substituted naphthalene bisimides with melamines in solution and at the graphite interface," *Org Biomol Chem*, vol. 3, no. 3, pp. 414–422, 2005, doi: 10.1039/B414443K.

[18]   X. Bouju, C. Mattioli, G. Franc, A. Pujol, and A. Gourdon, "Bicomponent Supramolecular Architectures at the Vacuum–Solid Interface," *Chem. Rev.*, vol. 117, no. 3, pp. 1407–1444, Feb. 2017, doi: 10.1021/acs.chemrev.6b00389.

[19]   T. Tsuruoka, S. Furukawa, Y. Takashima, K. Yoshida, S. Isoda, and S. Kitagawa, "Nanoporous Nanorods Fabricated by Coordination Modulation and Oriented Attachment Growth," *Angew. Chem. Int. Ed.*, vol. 48, no. 26, pp. 4739–4743, Jun. 2009, doi: 10.1002/anie.200901177.

[20]   J. Adisoejoso, Y. Li, J. Liu, P. N. Liu, and N. Lin, "Two-Dimensional Metallo-supramolecular Polymerization: Toward Size-Controlled Multi-strand Polymers," *J. Am. Chem. Soc.*, vol. 134, no. 45, pp. 18526–18529, Nov. 2012, doi: 10.1021/ja308480x.

[21]   James A. Theobald, Neil S. Oxtoby, Michael A. Phillips, Neil R. Champness & Peter H. Beton, "Controlling molecular deposition and layer structure with supramolecular surface assemblies," Nature, pp. 1029–1031, 2003.

Chapter 4: On-surface synthesis of unsaturated hydrocarbon chains through C-S activation

In this chapter, on-surface synthesis approach is used to drive the homocoupling reaction of a simple dithiophenyl-functionalized precursor on Cu(111). The C-S activation reaction is initiated at low annealing temperature and yields unsaturated hydrocarbon chains interconnected in a fully conjugated reticulated network. High-resolution atomic force microscopy imaging reveals the opening of the thiophenyl rings and the presence of *trans-* and *cis*-oligoacetylene chains as well as pentalene units. The chemical transformations were studied by C 1s and S 2p core level photoemission spectroscopy and supported by theoretical calculations. At higher annealing temperature, additional cyclization reactions take place, leading to the formation of small graphene flakes.

4.1   Introduction

As described in chapter 1, a variety of chemical reactions have been explored in on-surface synthesis to create organic compounds by taking advantage of a solid surface acting as a confining template[1]–[6]. In particular, the C-C coupling currently represents the most widely used approach to build 1D molecular wires, nanoribbons and 2D covalent network. In this context, the C-S activation of a precursor based on thiophene unit has been investigated and represent an efficient mechanism to perform C-C coupling[7], [8]. On surfaces, using thiophene derivatives for C-S bond activation is receiving an increasing interest[9]–[11], particularly because it can initiate both *intra-* or *inter*-molecular reactions[11]. For instance, when the two mesomers of tetra-thieno-anthracene are deposited on Cu(111) a number of different reaction pathways can be triggered as a function of annealing temperature. Accordingly, different products are obtained (see Fig.4.1) which can either result from dehydrogenation (products II and III in Fig.4.1-1,2) or from desulfurization and consequent C-S activation. The latter yield either pentacene units (which eventually bind through MO bonds) by internal cyclization or intermolecular bonding (product V). Upon annealing above 150 °C, a disordered arrangement of oligomers is observed (Fig.4.1-e) which likely results from both desulfurization and dehydrogenation (structures V and III in Fig.4.1-2).
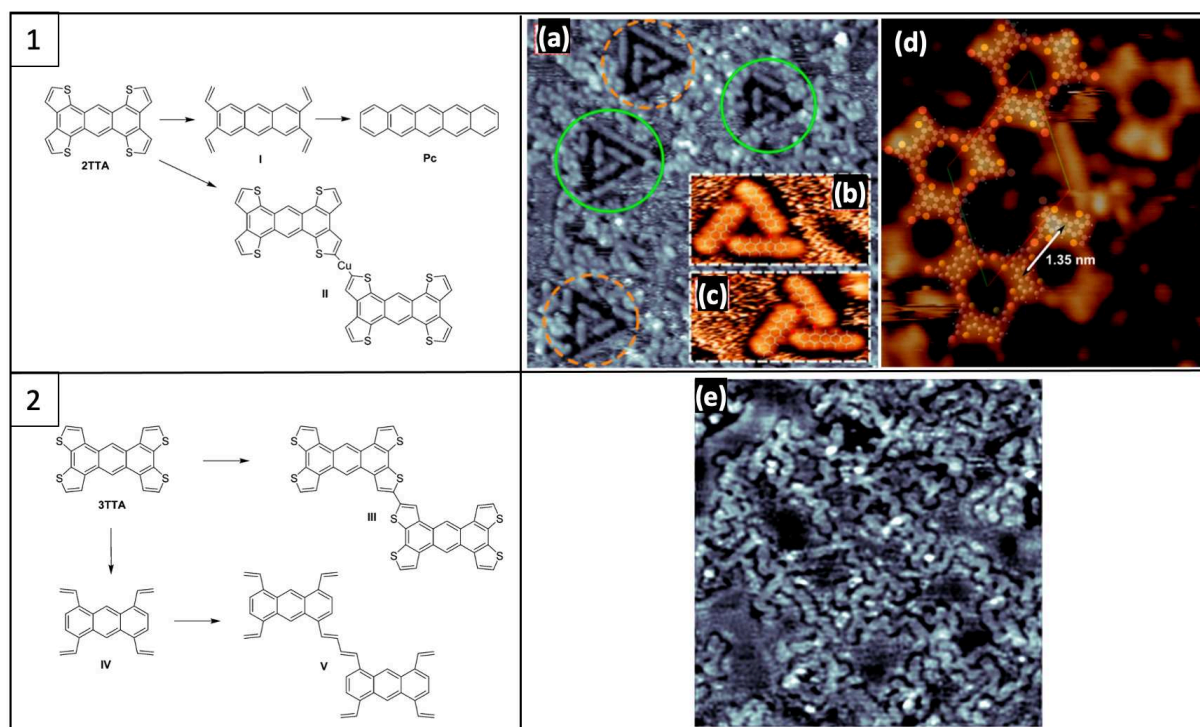
Figure 4.1. Left-hand panel: reaction pathways following desulfurization or dehydrogenation of the TTA isomers. (1) pentacene units are formed from 2TTA, after desulfurization whereas Cu adatom can coordinate with dehydrogenated units. (2) Two kind of C-C coupling can result from dehydrogenation (III) or desulfurization (v) of 3TTA. Right hand panel (observed products): according to the employed annealing temperature, 2TTA/Cu(111) transforms in (a) pentacene and (d) dehydrogenated 2TTA. Both bind through MO bonds in small aggregates. (e) Upon annealing to 150°C, 3TTA likely undergoes dehydrogenation and desulfurization, resulting in an extended but disordered network (e). Figures adapted from [11].

In order to further study the C-C coupling through the C-S activation approach from thiophene derivatives, we designed the precursor 1,4-di(thiophen-2-yl)benzene (DTB, Fig.4.3a)[12], [13] as a model system. Reducing the number of active sites per molecule is expected to help selectivity towards unbranched polymerization. Moreover, at variance with TTA, the thiophene unit in DTB is not fused with the core of the molecule but linked to it through a single C-C bond. This is expected to have two consequences: on one side, after desulfurization the resulting radical attachment can have different conformations that may result in multiple polymerization schemes (see Fig.4.2) (flexibility), on the other, the thiophene may pivot around the C-C axis favoring a suitable configuration of the S atom with respect to the surface, thus helping thiophene ring breaking and, in turn, allow for lower C-S activation temperature.

Moreover, this molecule was also chosen for the possibility of electropolymerization[14], [15] and because similar threefold precursors[16]–[19] have been reported to create materials with good conductivity or electrochromic properties.

The polymeric system obtained following the tentative schematics in Fig.4.2 is fully conjugated and composed mainly of oligoacetylene segments separated by benzene rings. Low-temperature atomic force microscopy (AFM) imaging using CO-terminated tips combined with photoemission spectroscopy and density functional theory (DFT) reveals the structure of the extended polymeric chains, with a mixture of *cis-* and *trans-* polyene as well as pentalene, which are globally aligned along the substrate high-symmetry directions. Our work thus positions C-S bond activation as an effective strategy in the on-surface synthesis approach, delivering compounds with high potential in molecular electronics applications under mild conditions.
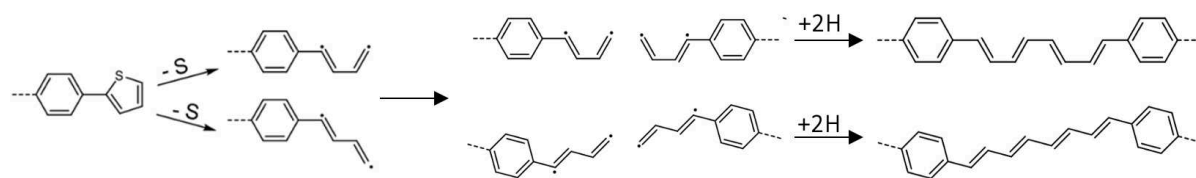
Figure 4.2. Schematic representation of the thiophene ring dissociation for the studied precursor (DTB) which leads to the formation of two oligoacetylene chain types after a desulfurization process.

4.2   Deposition of DTB on Cu(111) surface

DTB molecules were deposited on a Cu(111) surface kept at room temperature in a submonolayer regime. At room temperature the molecules are highly mobile and form a 2D gas phase. Upon cooling the substrate down to 4.8 K, the molecules become immobilized enabling the acquisition of stable scanning tunneling microscopy (STM) images (Fig.4.3d). DTB molecules exhibit very weak intermolecular interaction since no large self-assembly can be observed. Figure 4.3b shows an AFM image using a CO-terminated tip of an isolated molecule that confirms its chemical structure. The molecules remain intact upon sublimation with the benzene and thiophene rings lying almost flat on the surface[20]–[23].
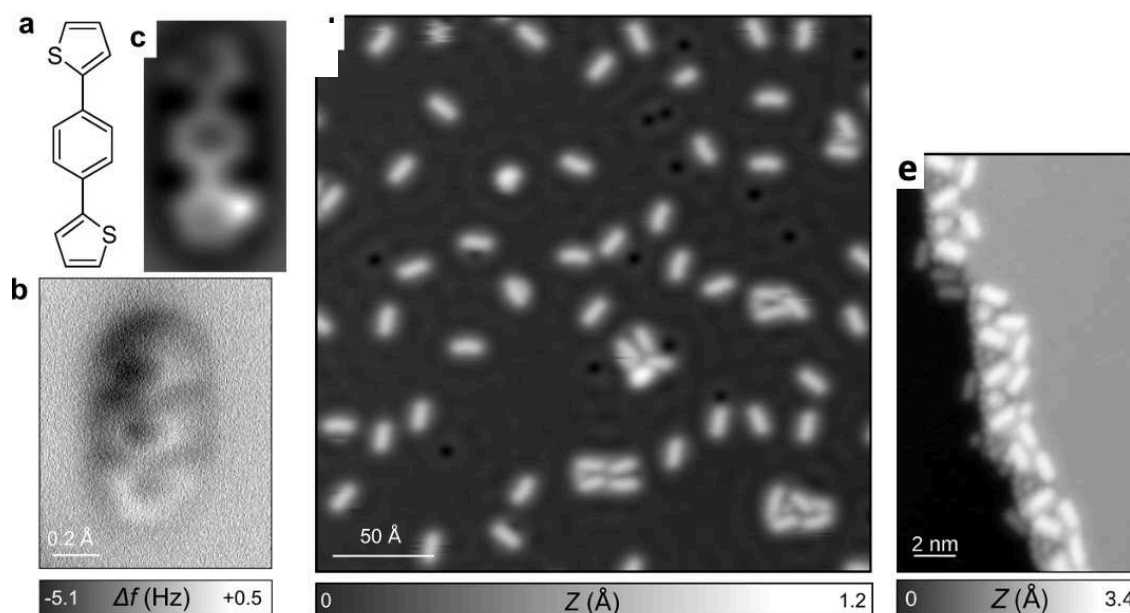
Figure 4.3.(a) 1,4-di(thiophen-2-yl)benzene (DTB) precursor. (b) High-resolution AFM image of a single DTB obtained with a CO-functionalized tip and (c) corresponding image simulation (DFT). (d) STM image of essentially isolated DTB molecules on Cu(111) acquired at 4.8 K. (e) STM topographic images acquired at 4.8 K after sublimation on the Cu(111) showing step edge decoration.

In order to address the precise molecular configuration upon adsorption, simulated AFM image using DFT coordinates of the relaxed DTB structure on Cu(111) is reported in Fig.4.3c. The thiophene rings are slightly tilted and appear elongated by AFM. The bright protrusion corresponding to the sulfur atom reproduces well the measured contrast. Several conformers coexist on the surface which differ according to the *syn-* or *anti-* orientation of the thiophene units with respect to the central phenyl (see Figure 4.4). Several configurations of the DTB molecule with S atoms either in contact with the Cu(111) surface or pointing towards the vacuum are all gathered within 20 meV adsorption energy range difference. This explains why they appear as stochastically distributed upon adsorption at RT.
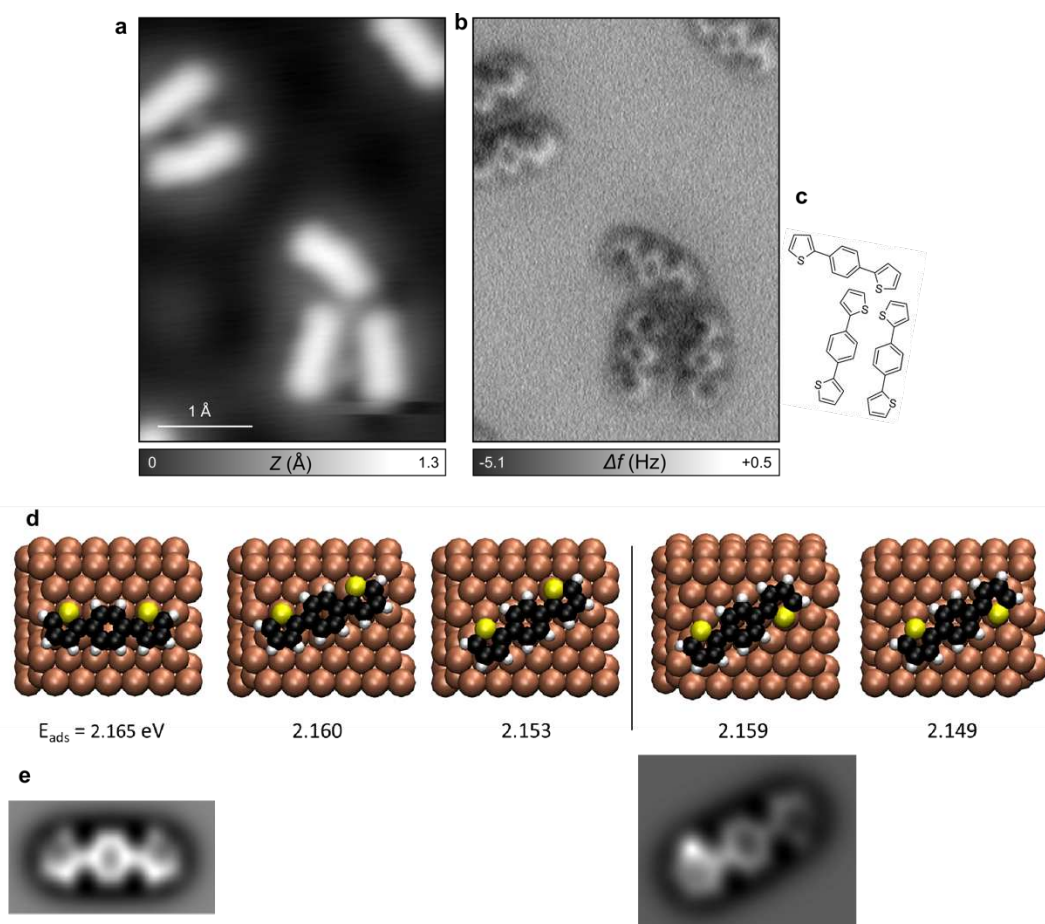
Figure 4.4. STM (a), corresponding AFM image with CO-terminated tip (b) and schematic model (c) of isolated DTB molecules adsorbed with different orientations of the *syn-* and *anti*-conformers. (d) Relaxed structures obtained from DFT calculations and (e) corresponding AFM image simulations.

4.3   Formation of polymeric chains after thermal annealing

An annealing temperature of 150°C was required to induce the full C-S activation and the opening of all thiophene rings. STM images acquired at room temperature (Figs.4.5a,b) show the formation of a polymeric network consisting of straight chains up to ~20 nm long and with a tendency to align with the $[1\bar{2}1]$ substrate directions. The chains are randomly interconnected, forming an extended 2D reticulated network. High-resolution AFM images confirmed that the chains consist of the original benzene rings of DTB interconnected by different configurations of oligoacetylene chains (Figs.4.5c,d). The chains and benzene rings are resolved with a homogeneous contrast, indicating a perfectly flat adsorption configuration and suggesting that the sulfur atoms were fully removed from the polymer. The contrast of the carbon chains resembles the *trans-* or *cis*-polyacetylene chains that were obtained on

Cu(110)[24] (see Fig.4.6 for a comparison) and has the periodicity (2.4 Å and 4.4 Å for the *trans*- and the *cis*-chains, respectively).
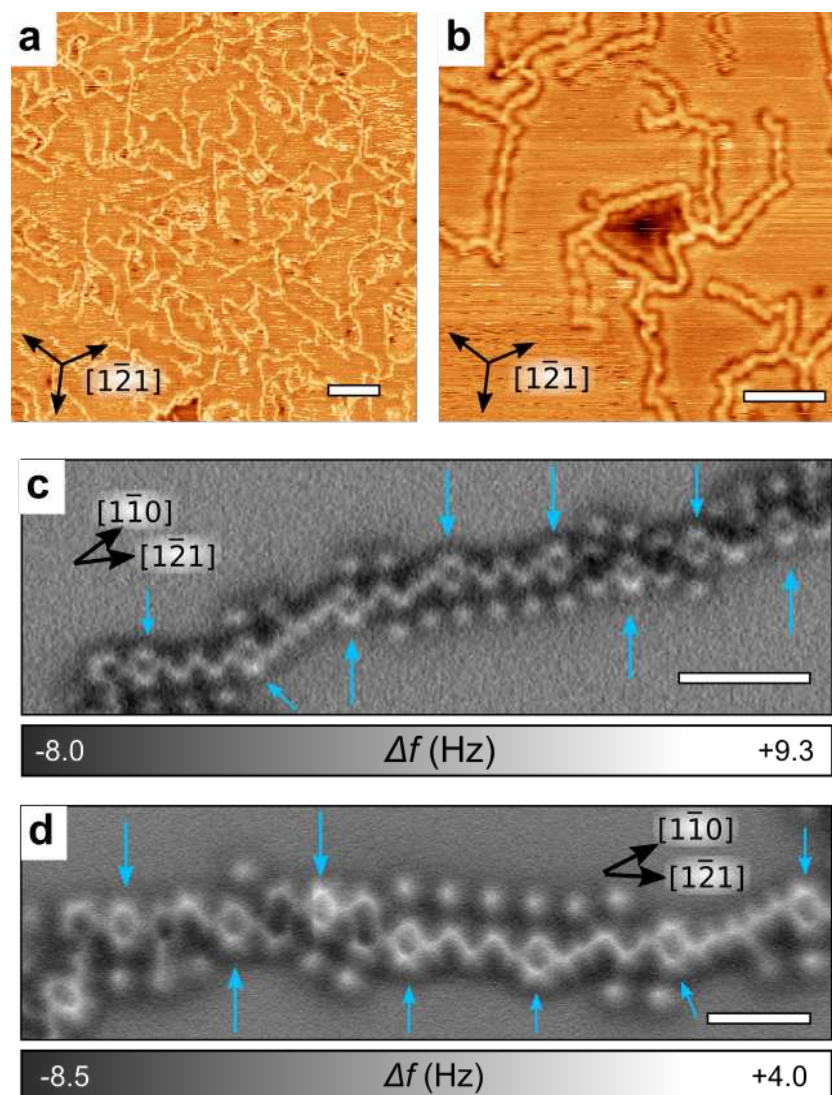
Figure 4.5. a,b) RT-STM images revealing the on-surface reaction of DTB on Cu(111) after annealing at 150 °C (a) or 200 °C (b). (c,d) High-resolution AFM images of the polymeric chains obtained after annealing at 130°C showing the preserved benzene rings (blue arrows) regularly distributed and linked by linear carbon chains. Scale bars: (a) 10 nm, (b) 4 nm, (c, d) 1 nm.
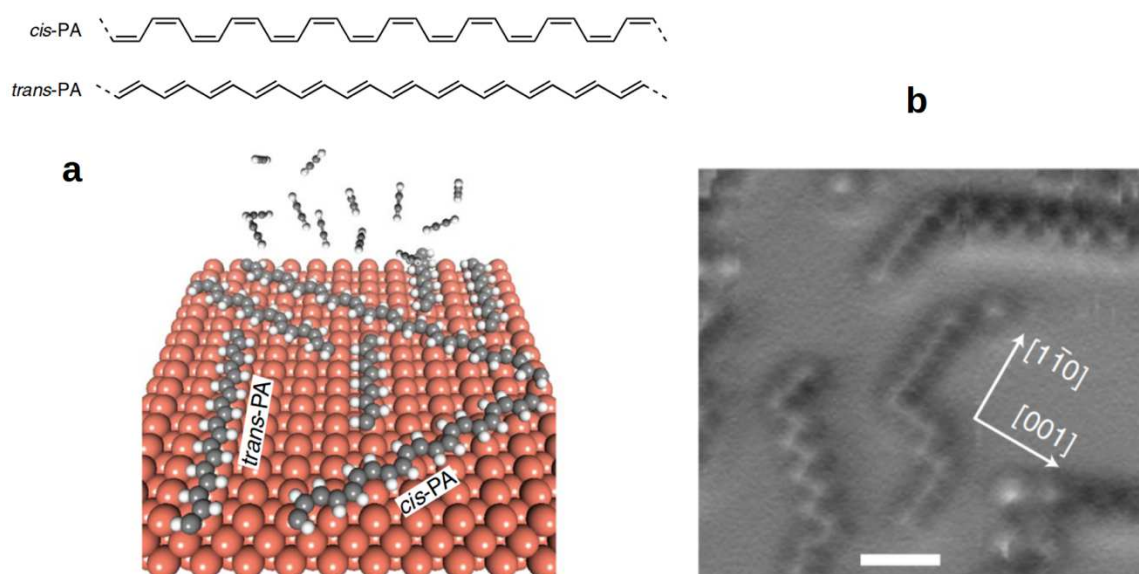
Figure 4.6. (a): Schematics of *cis* and *trans* polyacetylene chains (top) and the experimental protocol (bottom) for the on-surface synthesys. (b) AFM images of the two geometries as observed when acetylene is deposited on Cu(110) at RT and gently annealed at 100 °C. Figures reproduced from [24].

To investigate the tendency of the polymeric chains to orient along some surface high symmetry directions, DFT calculations were performed on model oligomers on Cu(111). Fig.4.7 shows that the most favorable orientation for the *trans*-chains is along the [1$\bar{1}$0]-direction (see 4.7-a). The *trans*-polyacetylene chains are in principle energetically more favorable than the *cis*-chains[24], but here the different stereoisomers appear to be locally stochastically distributed, which results in a main orientation of the polymeric chains along the average [1$\bar{2}$1]-directions (Fig.4.5).
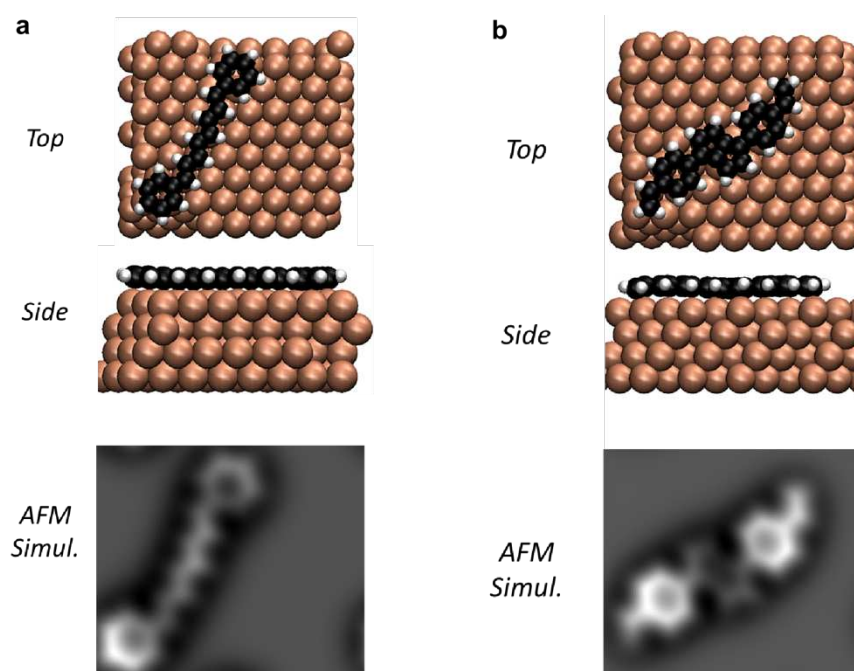
Figure 4.7. DFT Simulations. (a) Atomic structure of a relaxed diphenyl-*trans*-octatetraene model compound on Cu(111) showing its orientation along the [$1\bar{1}0$]-direction and corresponding AFM image simulation. (b) Atomic structure of a relaxed diphenylpentalene and corresponding AFM image simulation.

One important aspect in the design of the precursor is the activation temperature for the C-C coupling. As it will be showed below by XPS analysis, DTB starts polymerizing at temperatures well below 150 °C. Figure 4.8 shows the STM images of the polymeric chains obtained after annealing the sample at temperatures between 80 and 100°C. The AFM image acquired with a CO-terminated tip (Fig. 4.8) in the yellow rectangle highlighted shows that a partial reaction began at 80°C. The chains are not well ordered and unreacted thiophene end-groups are present.
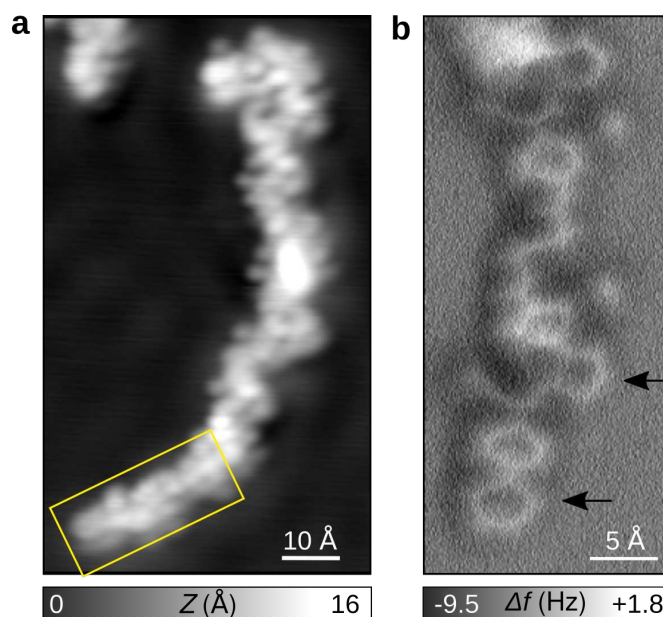
Figure 4.8. (a) STM image of the polymeric chains obtained after annealing the Cu(111) sample between 80-100°C. (b) AFM image acquired in the yellow rectangle highlighted in (a) with a CO-terminated tip. Unreacted thiophene end-groups are still present as shown by the dark arrows.

4.4   Investigation of on-surface coupling types using atomic force microscopy

Figure 4.9 shows the different reaction products that are formed locally, starting from the desulfurization of the thiophene units. In principle, the thiophene ring opening reaction creates bi-radical species, which couple predominantly at one radical site. The resulting polymeric radical chains are subsequently hydrogenated to produce unsaturated closed shell hydrocarbons (see below). Along with *cis*- and *trans*-oligoacetylene chains, pentalene units (Fig.4.9d) are also formed occasionally, with an occurrence lower than 20%. The darker contrast measured on these cyclic structures was well reproduced by DFT calculations (Fig.4.7b).
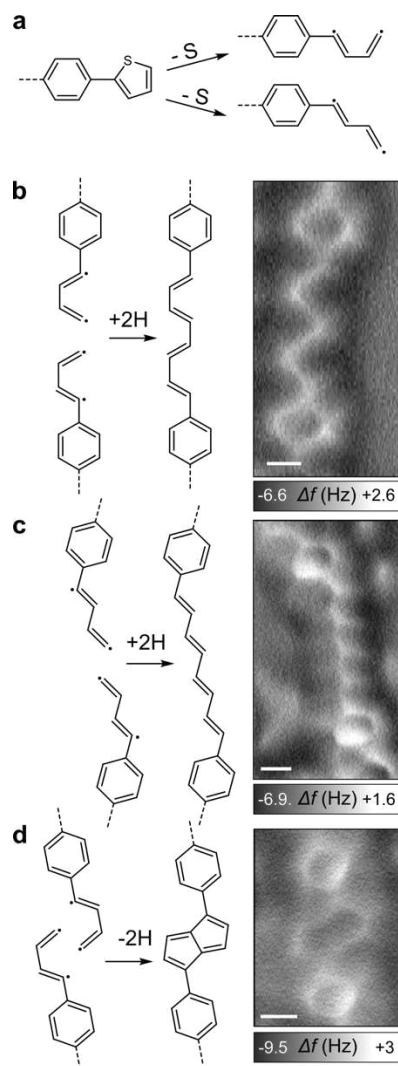
Figure 4.9. Schematic drawings of the different coupling schemes along with representative high-resolution AFM images. (a) Dissociation of the thiophene rings. Formation of (b) *cis*-oligoacetylene chains, (c) *trans*-oligoacetylene chains and (d) pentalene. Scale bars: 0.2 Å.

Besides the bifunctional coupling mechanism that creates linear chains, threefold crossing connections are also found. These are responsible for the reticulation of the polymeric network as observed at larger scales (Figs.4.5a,b). A high-resolution image of threefold connections is reproduced in Fig.4.10 along with suggestions of their chemical structure. These connections are obtained by coupling of the terminal carbon to the carbon radical closest to the benzene ring. Similar to the formation of pentalene, the creation of these threefold connections allows for a more advanced coupling reaction of the biradical species.
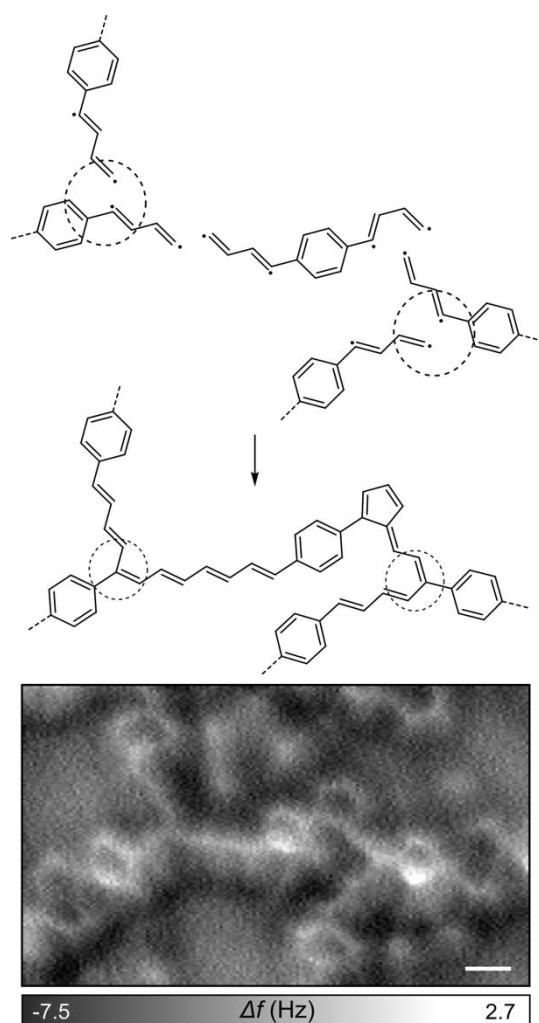
Figure 4.10. Schematic drawing of the suggested coupling schemes leading to the threefold crossings (dashed circles) along with the corresponding high-resolution AFM image. Scale bar: 2.5 Å.

As observed above, the reaction schemes proposed to account for the observed *cis-* and *trans-* oligoacetylene need the supply of two H atoms per bonding. The hydrogenation of radical products is a common process in on-surface synthesis for which the H supply may have different origins. The C-C coupling reaction leading to the formation of pentalene (Fig.4.9d) or chain interconnections (Fig.4.10) spontaneously releases hydrogen atoms that recombine with the carbon radicals[25]–[27], although probably in under-stoichiometric ratio. The residual hydrogen gas from the vacuum chamber could represent an additional hydrogen source, as it was similarly suggested for various other systems[28]–[33]. We also notice that the presence of a carbon radical is rather unlikely since it would lead to strong distortions inside the chains and to a substantial chemical shift[34] of the C 1s core level that are not compatible with the perfectly flat contrast of the structures observed in AFM images and XPS data. To illustrate the effect, in Fig.4.11 results from a DFT calculation are reported. A di-phenyl-oligoacetylene molecule

is first de-hydrogenated and then let relax on the Cu(111) surface. The free radicals have a natural tendency to sit in upright position on the copper surface[35], [36] and the nearby phenyl should twist out of plane, a behavior that is not observed experimentally. The chemical shift of the C radical with respect to C-H was estimated to be -1.1 eV toward low BE. This is not compatible with the measured spectral shape of Figs.4.12, giving further evidence that the chains have been hydrogenated. Finally, we never observed products in which the C-S bonds are replaced by C-H bonds without C-C coupling, thus suggesting that the hydrogenation takes place as the last reaction step. Interestingly, as it will be detailed below, no C-Cu bond was identified by XPS at this stage. While the complexation of radical species with adatoms is usually observed as an intermediate step in Ullmann-like coupling reactions[34], [37]–[39], in the present case, the C-C coupling followed by hydrogenation takes place without any observable organometallic intermediate. In addition to the carbon chains, small isolated dots (see Figs.4.5c,d) that we can assign as sulfur byproducts are observed in the vicinity of the polymeric chains. They are mostly aligned along the $[1\bar{2}1]$-directions and regularly positioned with an interspacing of 4.3 ± 0.1 Å thus compatible with an epitaxial relationship along this direction (for Cu(111), $a\sqrt{3} = 4.4$ Å).
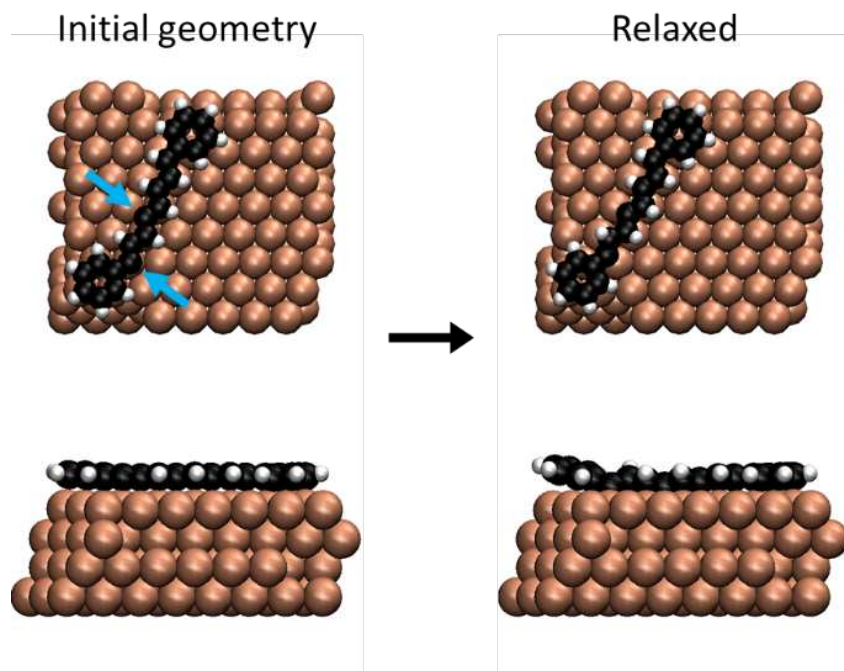
Figure 4.11. DFT simulations showing the relaxation of the radical sites (blue arrows) in diphenyl-*trans*-octatetraene and the induced twist, incompatible with the perfectly flat contrast of all structures observed experimentally.

4.5   Chemistry study of the system by the evolution of XPS core levels

To gain further insight into the chemistry at play in this system, we acquired temperature-dependent XPS spectra. The S 2p spectrum (Fig.4.12a) shows the evolution of the chemical state of S atoms during the polymerization process. The spectrum of a thick layer is used as fingerprint of the pristine molecule. It displays a strong component at a binding energy (BE) of 164.4 eV, in line with other thiophene derivatives on the same surface[37], [40]. Least-square fitting gives a full width at half maximum (FWHM) of 0.72 eV, essentially due to intermolecular π-stacking interactions. Two minor components are added to improve the fit which are likely due to different final state screening of surface (high BE) and interface (low BE) molecules.
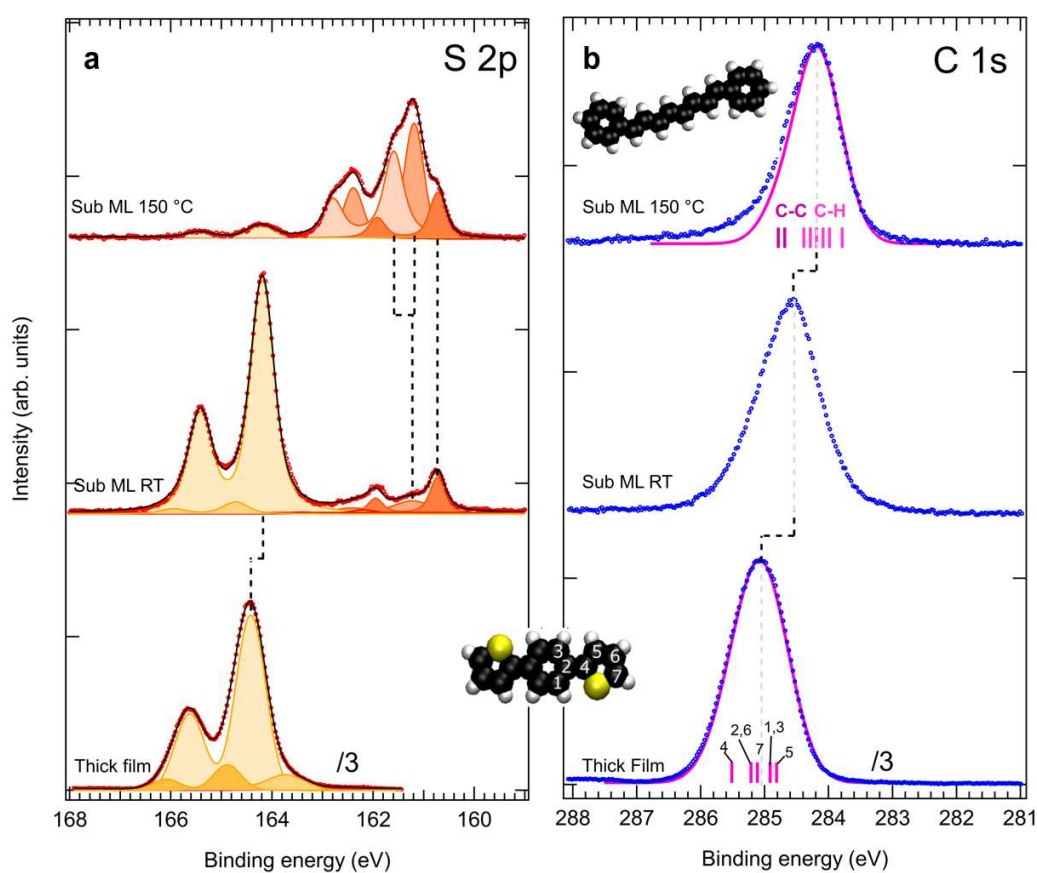
Figure 4.12. XPS data for DTB/Cu(111). Bottom spectra: a thick film deposited at RT. Upper spectra: sub-ML coverage deposited at RT and annealed at increasing temperatures. (a) S 2p core level (hν = 260 eV). The vertical dashed lines are intended to follow the evolution of the different components (peak fitting) as explained in the text. (b) C 1s core level (hν = 382 eV). Markers: experimental data. Magenta full lines: DFT simulated core levels. For the DTB (thick

film) the calculated core levels are numbered according to the inset molecular model. For the polyene chain (sub ML 150°C) the C-C and C-H eigenstates are colored differently.

When a submonolayer is deposited at room temperature, the DTB-derived peak is narrower (FWHM=0.55 eV), close to what is observed in the gas phase for other thiophene derivatives[41]. This is consistent with the 2D gas-phase observed by RT-STM and the consequent reduced intermolecular interaction. The observed shift to lower BE (by -0.24 eV) is characteristic of a reduced film thickness due to the enhanced screening from the metal substrate. An additional minor component at higher BE may be ascribed to a certain preferred adsorption site. At about 3 eV lower BE (between 160.5 and 162.5 eV) a new spectroscopic feature appears revealing atoms having left the molecule upon thiophene ring opening[37], [40]. A possible fragmentation of the thiophenes into thiolates (e.g. CHS) adsorbed on Cu(111) should give a BE of the $2p_{3/2}$ component around 162.0-162.5 eV[42]–[44], which is clearly not observed here. The positions and the line shape rather reveal the presence of atomic S coordinated with Cu[43], [45], [46].

When the temperature is increased to 150 °C, i.e. after polymerization, the spectral weight of DTB transfers almost completely into the low BE feature which now distinctively shows three atomic-S derived components at 161.6, 161.2 and 160.7 eV. The first two components were previously reported for sub-ML coverage of S/Cu(111)[45] and can be related to the formation of various S-Cu coordination structures in the vicinity of step edges. In fact, when adsorbed on Cu(111), the high affinity of S to Cu produces mass transport and step edge reconstruction leading to the formation of complex fourfold coordination sites[47]–[49]. The step edge regions shown in Fig.4.3e are clearly active sites for molecular adsorption. On the other hand, the lowest BE component at 160.7 eV was not observed in previous studies on atomic sulfur, thiols or thiolates adsorption on Cu(111)[37], [40], [42], [43], [45], [46]. We assign this component to the presence of lower-coordination S, i.e. terrace-supported, threefold-coordinated S. This feature can be traced back to the small protrusions observed beside the polymer chains in the AFM images (see Fig.4.5c,d). Such protrusions are smaller than the usual S-Cu complexes[47], [48] and are likely to be isolated S atoms restricted from diffusing by the interaction with the just-formed nearby polymers.

The C 1s spectrum (Fig.4.12b) reflects the presence of C atoms in different oxidation states within the DTB molecule and in the polymeric chains, as well as their interaction with the substrate. When possible, the C 1s spectrum was modeled by DFT calculations. As for the S 2p spectrum, the C 1s of the thick film is representative of the different C atoms in the pristine DTB molecule. The modeling (continuous pink line) using a DFT-calculated set of Gaussian

components (FWHM of 0.9 eV) represents a good fit for the measured spectrum. The small asymmetry observed at high BE can be attributed to the S-bonded C atom (labeled 4 in inset Fig.4.12b).

Differently to what is found for S 2p, when a submonolayer of DTB is deposited a visible broadening is observed for C 1s. Additionally, a larger shift of -0.48 eV towards lower BE is observed. This suggests that the molecule-substrate interaction occurs through C atoms (as compared with S atoms) that are found in a number of inequivalent sites with well-screened final states. Part of the broadening at the low-BE side can also be ascribed to the presence of a small fraction of molecules having started to react and lost their S atoms, as revealed by the corresponding S 2p spectrum.

Annealing the sub-ML from RT to 150 °C induces a progressive shift to low BE concurrent with the thiophene ring opening and S release (Fig.4.14). At the same time the spectrum narrows, testifying to a more homogeneous sample with well-defined atomic sites within the polymer chains. Its BE and line shape are very similar to those of other 2D polymer-derived spectra[24], [34], [50]–[52]. A simple modeling was performed by considering octatetraene chains terminated by two phenyl units adsorbed on the surface (inset in Fig.4.7a). This model reproduces the overall line shape with a pronounced asymmetry to high BE due to the presence of minority C's having three C-C bonds (the phenyl C's linking the oligoacetylene chains). We also tried modelling a possible effect of the molecule-substrate interaction in the simulated spectra. The inclusion of the Cu(111) surface does not affect the line shape as can be seen in Fig.4.13. Going back to Fig.4.7, compared to the simulated model, the real system includes more complex conformations (pentalene structure and threefold connection branches) with a larger C-C to C-H ratio that could be at the origin of the discrepancy in the high BE region. The C-C to C-H BE difference was previously detected in other on-surface polymerization studies involving aromatic compounds[34], [50], [52], [53], although sometimes with opposite shifts[51], [54], [55].
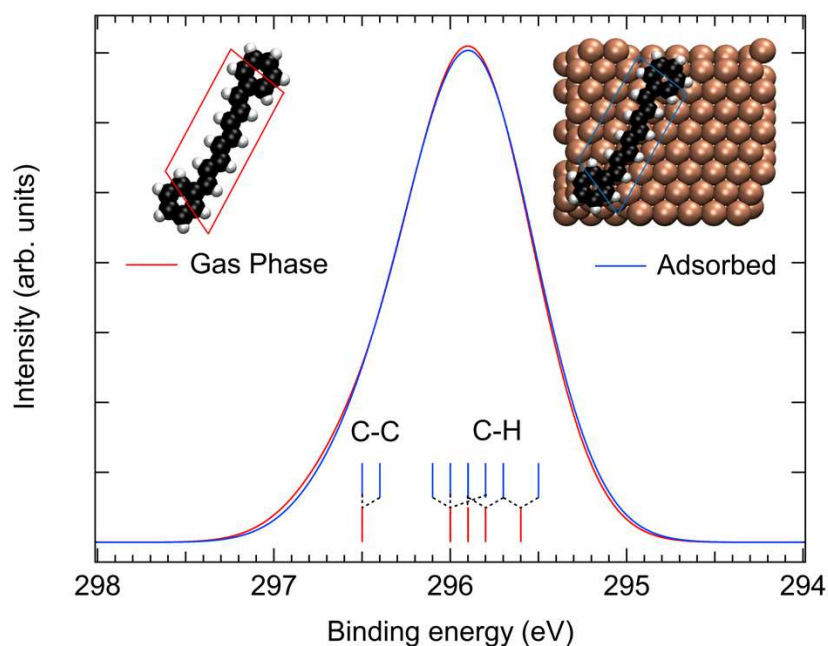
Figure 4.13. C 1s calculated spectra for the diphenyl-octatetraene molecule in gas phase and adsorbed on Cu(111).

Finally, the XPS data shows that the loss of carbon atoms upon annealing is limited to ~3%, in similar proportion as the loss of S (~2%), so we can conclude that most of the carbon and sulfur remain on the surface.

Temperature-programmed XPS

S2p and C1s temperature-programmed XPS of the submonolayer from RT to 150 °C were performed with an annealing rate of about 2.4 °C/min (Fig.4.14, central panel). Fig.4.14 shows also the high-resolution spectra at initial and final temperatures for the S 2p and C 1s. These results indicate that from about 40 °C, the thiophene S 2p component transforms into the three atomic sulfur doublets. At the same time, the C 1s shifts toward the BE corresponding to the polymeric chains. At around 120°C, the reaction is completed. These results show that the yield of the C-S activated reaction is very high and takes place in the range 50 to 120°C.
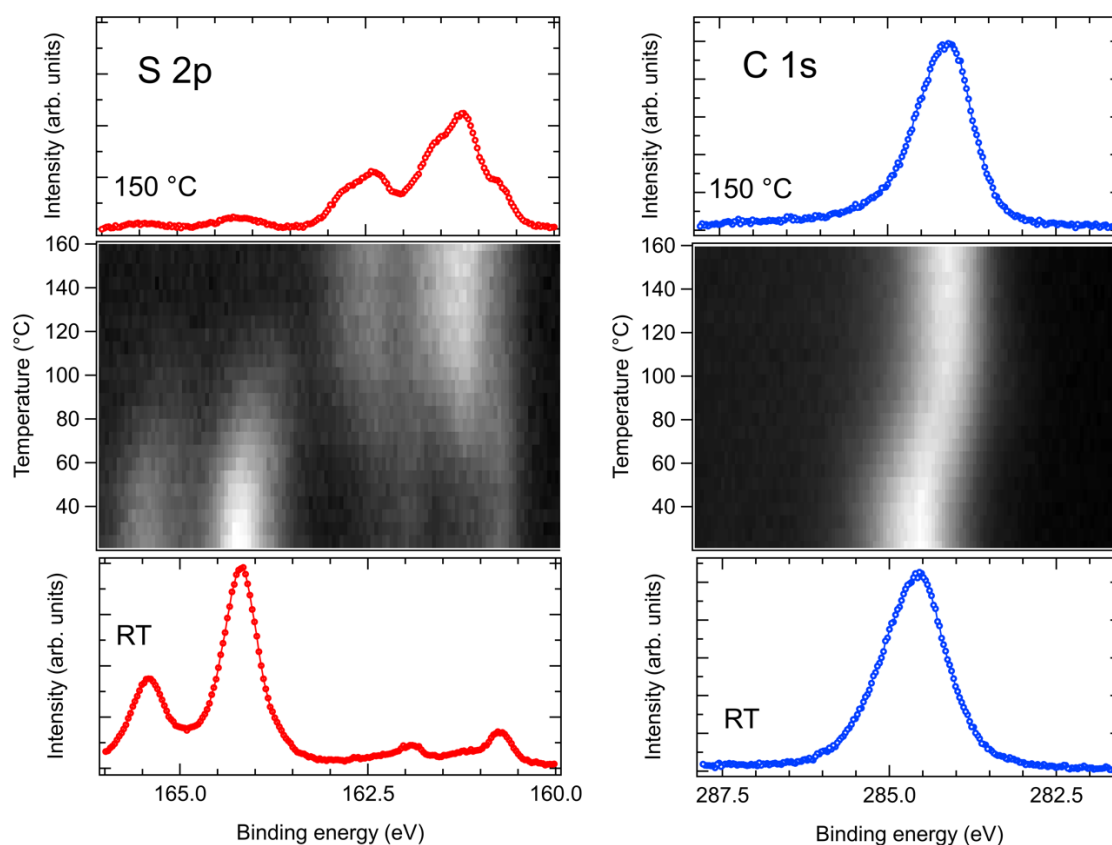
Figure 4.14. S 2p and C 1s temperature-programmed XPS (central panels) of a sub-ML DTB/Cu(111) from RT to 150 °C (annealing rate was 2.4 °C/min). Below and above are the high-resolution spectra at initial and final temperatures.

4.6 Morphology and electronic structure after annealing at high temperature

Further sample annealing up to 500 °C was performed in order to test the thermal stability of the polymeric chain. Figure 4.15a shows representative STM and AFM images of the system obtained after annealing at 300°C. We could not observe a transition to the more favorable *trans*-chain configuration[24], probably due to the strongly reduced mobility in this reticulated network. Similar to the case of polyacetylene chains[24], cyclization reactions take place and lead to the formation of narrow polyaromatic ribbons. Upon further annealing to 500°C the graphitization reaction is advanced further and small graphene flakes are formed on the surface (Figs.4.15, 4.16). Similar amorphous phases obtained from massive dehydrogenative coupling have been observed for various systems after high temperature annealing of covalent networks on noble metal surfaces[39], [56]–[60]. Indeed graphene formation can take place on a copper surface at sufficiently high temperature from virtually any carbon source[61], [62].
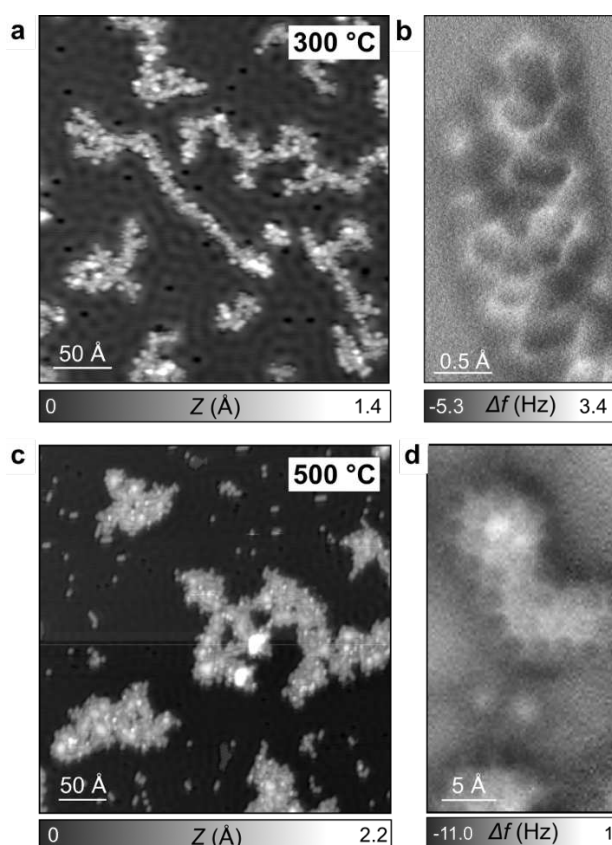
Figure 4.15. STM (a,c) and AFM images (b,d) of DTB/Cu(111) after annealing at 300°C (a,b) and 500°C (c,d).

The cyclization reaction process is visible also in the C 1s spectra. In Fig.4.16 (right panel) spectra taken after annealing at increasing temperatures are shown. Up to 200 °C the spectrum is unchanged with respect to the linear polymer but, from 225 °C onwards, a gradual narrowing occurs (see the intensity reduction between 285 and 286 eV), indicating an overall rearrangement towards a more homogeneous C site population. Above 300 °C, the narrowing is accompanied by the emergence and growth of a typical low BE component at 283.2 eV, previously found also in nanographene patches[34], [39] and coming from defective or Cu-coordinated C atoms at the edge of polycyclic ribbons and flakes[37], [63]–[65]. This low BE component does not appear at 150 °C, thus excluding the possibility of having free or Cu-bonded C radicals in the polymeric chains (see Figs.4.11 and 4.12).
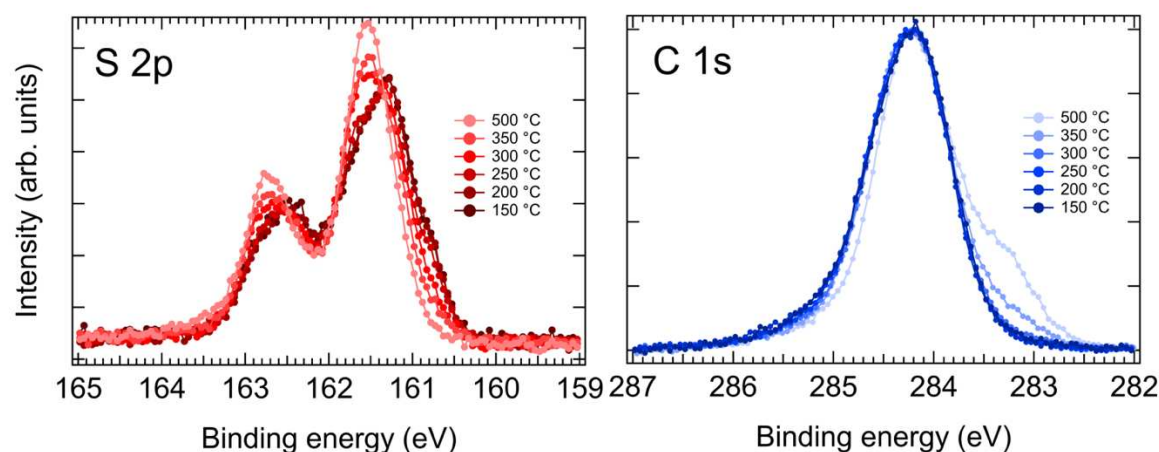
Figure 4.16. S 2p and C 1s core levels of the polymerized DTB as a function of increasing annealing temperature from 150 °C to 500 °C. To facilitate the comparison, the C 1s spectra of samples annealed at 350 °C and 500 °C were shifted to higher BE (by 0.03 and 0.08 eV, respectively) to match the BE of the peak maxima at 150 °C.

Significant changes are observed at high temperature also in the S 2p spectra. The interaction between isolated atomic S and the chains gradually decreases as seen by reduction of the low BE S 2p component (Fig.4.16). At 325 °C it has completely disappeared to the benefit of the two high-coordination components that eventually merge into a single component at 161.45 eV, representative of copper sulfides formed at high temperatures[43], [46], [66].

4.7   Conclusions and perspectives

We presented the formation of a fully conjugated polymeric network from simple thiophene-functionalized precursors. The C-S activation at 120°C annealing temperature initiates the formation of carbon radicals that couple to form oligoacetylene chains or pentalene units linking the original benzene rings. Although the coupling reaction is not selective towards *cis*- or *trans*-stereoisomers, the mainly linear chains maintain an overall [1$\bar{2}$1]-orientation along the high symmetry directions of the Cu(111) surface. An alternate reaction mechanism occasionally takes place that leads to the creation of threefold interconnections and the overall formation of a reticulated network. Upon further annealing, additional cyclodehydrogenation reactions occur, leading finally to the formation of small graphene flakes up to a temperature of 500°C.

Our study demonstrates that the strong reactivity of copper toward sulfur-containing species can be exploited to steer an on-surface homocoupling reaction and to create extended polyene chains at low activation temperature. Unfused thiophene precursors offer simpler synthesis and more diverse coupling chemistry than fused precursors[11], as they form diradical butadiene moieties instead of ethylene monoradicals. For the synthetic approach in general, C-S activation could be complementary to Ullmann-type coupling as it provides access to antiaromatic and nonbenzenoid structures, such as the pentalene minor product we obtained. However, the precise reaction mechanism still needs to be elucidated, in particular with regard to the role of the atomic sulfur, that is known to affect the bonding of hydrocarbons on Cu(111)[67]. Compared to Ullmann-like coupling of halogenated molecules[34], [37]–[39], no organometallic intermediate was detected, which suggests that the desulfurization step is rate-limiting with respect to both the C-C coupling and the hydrogenation reactions.

In future work, different strategies may be explored to improve the order and density of the polymeric network. Preliminary experiments on Cu(110) (Fig.4.17) showed that the strong anisotropy of this surface did not noticeably steer the alignment of the chains, but alternate solutions like e.g. the use of vicinal surfaces[68], co-adsorbed oxygen[69] or hydrogen[70], or supramolecular templating[71] may still deliver interesting results.

Thiophene groups are sometimes used as constitutive groups in on-surface synthesis on various metal surfaces[37], [66], [72]–[75]. In view of our results showing a relatively low activation temperature of the thiophene ring opening reaction, it is certainly necessary to confirm the integrity of these monomers. Conversely, solutions to preserve the integrity of sulfur in on-surface polymerization reactions include providing an out-of-plane structure of the precursors like in diamantanethiol[76], or following other strategies that have proved successful to maintain specific functions even on reactive surfaces[77], [78].
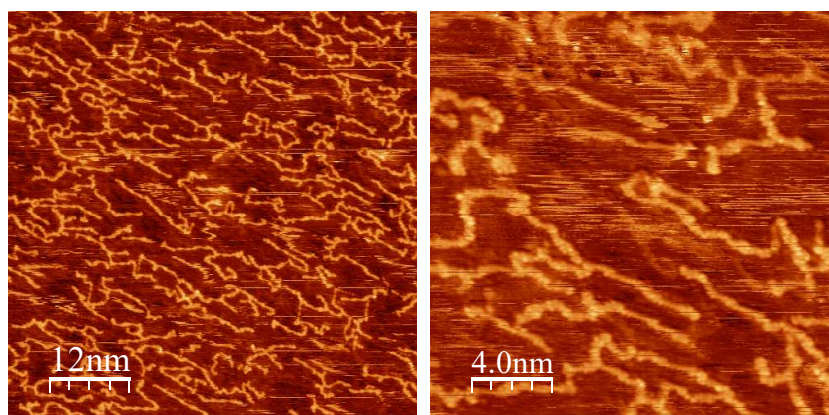

Figure 4.17. RT-STM images showing the polymer formed on the Cu(110) surface after annealing at 200°C. The alignment of the chains is not particularly improved as compared to the Cu(111) case.

References of chapter 4

[1]   S. Clair and D. G. de Oteyza, "Controlling a Chemical Coupling Reaction on a Surface: Tools and Strategies for On-Surface Synthesis," *Chem. Rev.*, vol. 119, no. 7, pp. 4717–4776, Apr. 2019, doi: 10.1021/acs.chemrev.8b00601.

[2]   S. Clair, M. Abel, and L. Porte, "Growth of boronic acid based two-dimensional covalent networks on a metal surface under ultrahigh vacuum," *Chem Commun*, vol. 50, no. 68, pp. 9627–9635, 2014, doi: 10.1039/C4CC02678K.

[3]   L. Grill, M. Dyer, L. Lafferentz, M. Persson, M. V. Peters, and S. Hecht, "Nano-architectures by covalent assembly of molecular building blocks," *Nat. Nanotechnol.*, vol. 2, no. 11, pp. 687–691, Nov. 2007, doi: 10.1038/nnano.2007.346.

[4]   F. Palmino, C. Loppacher, and F. Chérioux, "Photochemistry Highlights on On-Surface Synthesis," *ChemPhysChem*, vol. 20, no. 18, pp. 2271–2280, Sep. 2019, doi: 10.1002/cphc.201900312.

[5]   D. P. Goronzy *et al.*, "Supramolecular Assemblies on Surfaces: Nanopatterning, Functionality, and Reactivity," *ACS Nano*, vol. 12, no. 8, pp. 7445–7481, Aug. 2018, doi: 10.1021/acsnano.8b03513.

[6]   D. Cui, D. F. Perepichka, J. M. MacLeod, and F. Rosei, "Surface-confined single-layer covalent organic frameworks: design, synthesis and application," *Chem. Soc. Rev.*, vol. 49, no. 7, pp. 2020–2038, 2020, doi: 10.1039/C9CS00456D.

[7]   L. Wang, W. He, and Z. Yu, "Transition-metal mediated carbon–sulfur bond activation and transformations," *Chem Soc Rev*, vol. 42, no. 2, pp. 599–621, 2013, doi: 10.1039/C2CS35323G.

[8]   J. Li, H. Huang, W. Liang, Q. Gao, and Z. Duan, "Catalytic C–H and C–S Bond Activation of Thiophenes," *Org. Lett.*, vol. 15, no. 2, pp. 282–285, Jan. 2013, doi: 10.1021/ol303136x.

[9]   B. Borca *et al.*, "Electric-Field-Driven Direct Desulfurization," *ACS Nano*, vol. 11, no. 5, pp. 4703–4709, May 2017, doi: 10.1021/acsnano.7b00612.

[10]   D. R. Huntley, D. R. Mullins, and M. P. Wingeier, "Desulfurization of Thiophenic Compounds by Ni(111): Adsorption and Reactions of Thiophene, 3-Methylthiophene, and 2,5-Dimethylthiophene," *J. Phys. Chem.*, vol. 100, no. 50, pp. 19620–19627, Jan. 1996, doi: 10.1021/jp962825u.

[11]   L. E. Dinca *et al.*, "Tailoring the Reaction Path in the On-Surface Chemistry of Thienoacenes," *J. Phys. Chem. C*, vol. 119, no. 39, pp. 22432–22438, Oct. 2015, doi: 10.1021/acs.jpcc.5b05418.

[12]   K. Tamao, S. Kodama, I. Nakajima, M. Kumada, A. Minato, and K. Suzuki, "Nickel-phosphine complex-catalyzed Grignard coupling—II," *Tetrahedron*, vol. 38, no. 22, pp. 3347–3354, Jan. 1982, doi: 10.1016/0040-4020(82)80117-8.

[13]   M. Yang, Q. Zhang, P. Wu, H. Ye, and X. Liu, "Influence of the introduction of phenylene units into the polymer backbone on bandgap of conjugated poly(heteroarylene methines)," *Polymer*, vol. 46, no. 16, pp. 6266–6273, Jul. 2005, doi: 10.1016/j.polymer.2005.05.054.

[14]   R. Danieli, P. Ostoja, M. Tiecco, R. Zamboni, and C. Taliani, "Poly[1,4-di-(2-thienyl)benzene]: a new conducting polymer," *J. Chem. Soc. Chem. Commun.*, no. 19, p. 1473, 1986, doi: 10.1039/c39860001473.

[15]   L. Xu, J. Zhao, C. Cui, R. Liu, J. Liu, and H. Wang, "Electrosynthesis and characterization of

an electrochromic material from poly(1,4-bis(2-thienyl)-benzene) and its application in electrochromic devices," *Electrochimica Acta*, vol. 56, no. 7, pp. 2815–2822, Feb. 2011, doi: 10.1016/j.electacta.2010.12.062.

[16]   K. R. Idzik, R. Beckert, S. Golba, P. Ledwon, and M. Lapkowski, "Synthesis by Stille cross-coupling procedure and electrochemical properties of C3-symmetric oligoarylobenzenes," *Tetrahedron Lett.*, vol. 51, no. 18, pp. 2396–2399, May 2010, doi: 10.1016/j.tetlet.2010.02.051.

[17]   T. Nakae *et al.*, "Benzo[*b*]trithiophene Polymer Network Prepared by Electrochemical Polymerization with a Combination of Thermal Conversion," *Chem. Lett.*, vol. 41, no. 2, pp. 140–141, Feb. 2012, doi: 10.1246/cl.2012.140.

[18]   C. Gu *et al.*, "π-Conjugated Microporous Polymer Films: Designed Synthesis, Conducting Properties, and Photoenergy Conversions," *Angew. Chem.*, vol. 127, no. 46, pp. 13798–13802, Nov. 2015, doi: 10.1002/ange.201506570.

[19]   P. Ledwon *et al.*, "Doping behaviour of electrochemically generated model bithiophene meta-substituted star shaped oligomer," *Mater. Chem. Phys.*, vol. 147, no. 1–2, pp. 254–260, Sep. 2014, doi: 10.1016/j.matchemphys.2014.04.037.

[20]   T. Kakudate, S. Tsukamoto, O. Kubo, M. Nakaya, and T. Nakayama, "Electronic Structures of Quaterthiophene and Septithiophene on Cu(111): Spatial Distribution of Adsorption-Induced States Studied by STM and DFT Calculation," *J. Phys. Chem. C*, vol. 120, no. 12, pp. 6681–6688, Mar. 2016, doi: 10.1021/acs.jpcc.6b00566.

[21]   W. Malone, J. Matos, and A. Kara, "Adsorption of thiophene on transition metal surfaces with the inclusion of van der Waals effects," *Surf. Sci.*, vol. 669, pp. 121–129, Mar. 2018, doi: 10.1016/j.susc.2017.11.013.

[22]   N. Richardson and J. Campuzano, "The adsorption of thiophene on a Cu(111) surface," *Vacuum*, vol. 31, no. 10–12, pp. 449–451, Oct. 1981, doi: 10.1016/0042-207X(81)90032-4.

[23]   P. K. Milligan, B. Murphy, D. Lennon, B. C. C. Cowie, and M. Kadodwala, "A Complete Structural Study of the Coverage Dependence of the Bonding of Thiophene on Cu(111)," *J. Phys. Chem. B*, vol. 105, no. 1, pp. 140–148, Jan. 2001, doi: 10.1021/jp002186u.

[24]   Shiyong Wang, Qiang Sun, Oliver Gröning, Roland Widmer, Carlo A. Pignedoli, Liangliang Cai, Xin Yu, Bingkai Yuan, Can Li, Huanxin Ju, Junfa Zhu, Pascal Ruffieux, Roman Fasel & Wei Xu, "On-surface synthesis and characterization of individual polyacetylene chains," Nature Chemistry View all journals Search Login, pp. 11, pages 924-930 (2019), Sep. 02, 2019.

[25]   C. Wäckerlin *et al.*, "On-Surface Hydrogenation of Buckybowls: From Curved Aromatic Molecules to Planar Non-Kekulé Aromatic Hydrocarbons," *ACS Nano*, vol. 14, no. 12, pp. 16735–16742, Dec. 2020, doi: 10.1021/acsnano.0c04488.

[26]   J. Castro-Esteban, F. Albrecht, S. Fatayer, D. Pérez, L. Gross, and D. Peña, "An on-surface Diels–Alder reaction," *Angew. Chem. Int. Ed.*, vol. 60, no. 50, pp. 26346–26350, Dec. 2021, doi: 10.1002/anie.202110311.

[27]   C. Ma *et al.*, "On-surface cyclodehydrogenation reaction pathway determined by selective

molecular deuterations," *Chem. Sci.*, vol. 12, no. 47, pp. 15637–15644, 2021, doi: 10.1039/D1SC04908A.

[28]   M. E. Cañas-Ventura *et al.*, "Coexistence of one- and two-dimensional supramolecular assemblies of terephthalic acid on Pd(111) due to self-limiting deprotonation," *J. Chem. Phys.*, vol. 125, no. 18, p. 184710, Nov. 2006, doi: 10.1063/1.2364478.

[29]   J. I. Urgel *et al.*, "Overcoming Steric Hindrance in Aryl-Aryl Homocoupling via On-Surface Copolymerization," *ChemPhysChem*, vol. 20, no. 18, pp. 2360–2366, Sep. 2019, doi: 10.1002/cphc.201900283.

[30]   A. Sánchez-Grande *et al.*, "Unravelling the Open-Shell Character of Peripentacene on Au(111)," *J. Phys. Chem. Lett.*, vol. 12, no. 1, pp. 330–336, Jan. 2021, doi: 10.1021/acs.jpclett.0c02518.

[31]   B. Cirera *et al.*, "On-Surface Synthesis of Gold Porphyrin Derivatives via a Cascade of Chemical Interactions: Planarization, Self-Metalation, and Intermolecular Coupling," *Chem. Mater.*, vol. 31, no. 9, pp. 3248–3256, May 2019, doi: 10.1021/acs.chemmater.9b00125.

[32]   S. Kawai *et al.*, "Competing Annulene and Radialene Structures in a Single Anti-Aromatic Molecule Studied by High-Resolution Atomic Force Microscopy," *ACS Nano*, vol. 11, no. 8, pp. 8122–8130, Aug. 2017, doi: 10.1021/acsnano.7b02973.

[33]   C. Zhang, E. Kazuma, and Y. Kim, "Atomic-Scale Visualization of the Stepwise Metal-Mediated Dehalogenative Cycloaddition Reaction Pathways: Competition between Radicals and Organometallic Intermediates," *Angew. Chem.*, vol. 131, no. 49, pp. 17900–17908, Dec. 2019, doi: 10.1002/ange.201909111.

[34]   K. A. Simonov *et al.*, "Effect of Substrate Chemistry on the Bottom-Up Fabrication of Graphene Nanoribbons: Combined Core-Level Spectroscopy and STM Study," *J. Phys. Chem. C*, vol. 118, no. 23, pp. 12532–12540, Jun. 2014, doi: 10.1021/jp502215m.

[35]   J Björk1, "Reaction mechanisms for on-surface synthesis of covalent nanostructures," Phys.: Condens. Matter 28 083002, Feb. 02, 2016.

[36]   Q. Du, W. Pu, Z. Sun, and P. Yu, "On-Surface Synthesis of All-cis Standing Phenanthrene Polymers upon Selective C–H Bond Activation," *J. Phys. Chem. Lett.*, vol. 11, no. 13, pp. 5022–5028, Jul. 2020, doi: 10.1021/acs.jpclett.0c01349.

[37]   R. Gutzler *et al.*, "Ullmann-type coupling of brominated tetrathienoanthracene on copper and silver," *Nanoscale*, vol. 6, no. 5, pp. 2660–2668, 2014, doi: 10.1039/C3NR05710K.

[38]   Q. Sun, L. Cai, H. Ma, C. Yuan, and W. Xu, "The stereoselective synthesis of dienes through dehalogenative homocoupling of terminal alkenyl bromides on Cu(110)," *Chem. Commun.*, vol. 52, no. 35, pp. 6009–6012, 2016, doi: 10.1039/C6CC01059H.

[39]   L. Ferrighi *et al.*, "Control of the Intermolecular Coupling of Dibromotetracene on Cu(110) by the Sequential Activation of C   Br and C   H Bonds," *Chem. - Eur. J.*, vol. 21, no. 15, pp. 5826–5835, Apr. 2015, doi: 10.1002/chem.201405817.

[40]   G. Galeotti *et al.*, "Surface-mediated assembly, polymerization and degradation of thiophene-based monomers," *Chem. Sci.*, vol. 10, no. 19, pp. 5167–5175, 2019, doi: 10.1039/C8SC05267K.

[41]   T. Zhang *et al.*, "Lone-Pair Delocalization Effects within Electron Donor Molecules: The Case of Triphenylamine and Its Thiophene-Analog," *J. Phys. Chem. C*, vol. 122, no. 31, pp. 17706–17717, Aug. 2018, doi: 10.1021/acs.jpcc.8b06475.

[42]   J. Jia, A. Giglia, M. Flores, O. Grizzi, L. Pasquali, and V. A. Esaulov, "1,4-Benzenedimethanethiol Interaction with Au(110), Ag(111), Cu(100), and Cu(111) Surfaces: Self-Assembly and Dissociation Processes," *J. Phys. Chem. C*, vol. 118, no. 46, pp. 26866–26876, Nov. 2014, doi: 10.1021/jp509184t.

[43]   T. Sirtl *et al.*, "From Benzenetrithiolate Self-Assembly to Copper Sulfide Adlayers on Cu(111): Temperature-Induced Irreversible and Reversible Phase Transitions," *J. Phys. Chem. C*, vol. 118, no. 7, pp. 3590–3598, Feb. 2014, doi: 10.1021/jp411084k.

[44]   X. Meng *et al.*, "Cover Feature: Tunable Thiolate Coordination Networks on Metal Surfaces (ChemNanoMat 10/2020)," *ChemNanoMat*, vol. 6, no. 10, pp. 1418–1418, Oct. 2020, doi: 10.1002/cnma.202000287.

[45]   E. Wahlström, I. Ekvall, H. Olin, S.-Å. Lindgren, and L. Walldén, "Observation of ordered structures for S/Cu(111) at low temperature and coverage," *Phys. Rev. B*, vol. 60, no. 15, pp. 10699–10702, Oct. 1999, doi: 10.1103/PhysRevB.60.10699.

[46]   J. Jia, A. Bendounan, K. Chaouchi, and V. A. Esaulov, "Sulfur Interaction with Cu(100) and Cu(111) Surfaces: A Photoemission Study," *J. Phys. Chem. C*, vol. 118, no. 42, pp. 24583–24590, Oct. 2014, doi: 10.1021/jp5078517.

[47]   H. Walen *et al.*, "Cu 2 S 3 complex on Cu(111) as a candidate for mass transport enhancement," *Phys. Rev. B*, vol. 91, no. 4, p. 045426, Jan. 2015, doi: 10.1103/PhysRevB.91.045426.

[48]   H. Walen *et al.*, "Reconstruction of steps on the Cu(111) surface induced by sulfur," *J. Chem. Phys.*, vol. 142, no. 19, p. 194711, May 2015, doi: 10.1063/1.4921258.

[49]   D.-J. Liu, P. M. Spurgeon, J. Lee, T. L. Windus, P. A. Thiel, and J. W. Evans, "Sulfur adsorption on coinage metal(100) surfaces: propensity for metal–sulfur complex formation relative to (111) surfaces," *Phys. Chem. Chem. Phys.*, vol. 21, no. 48, pp. 26483–26491, 2019, doi: 10.1039/C9CP03449H.

[50]   C. Moreno *et al.*, "Critical Role of Phenyl Substitution and Catalytic Substrate in the Surface-Assisted Polymerization of Dibromobianthracene Derivatives," *Chem. Mater.*, vol. 31, no. 2, pp. 331–341, Jan. 2019, doi: 10.1021/acs.chemmater.8b03094.

[51]   I. Píš *et al.*, "Surface-Confined Polymerization of Halogenated Polyacenes: The Case of Dibromotetracene on Ag(110)," *J. Phys. Chem. C*, vol. 120, no. 9, pp. 4909–4918, Mar. 2016, doi: 10.1021/acs.jpcc.5b12047.

[52]   M. Panighel *et al.*, "Stabilizing Edge Fluorination in Graphene Nanoribbons," *ACS Nano*, vol. 14, no. 9, pp. 11120–11129, Sep. 2020, doi: 10.1021/acsnano.0c01837.

[53]   B. Cirera *et al.*, "On-surface synthesis of organocopper metallacycles through activation of inner diacetylene moieties," *Chem. Sci.*, vol. 12, no. 38, pp. 12806–12811, 2021, doi: 10.1039/D1SC03703J.

[54]   Q. Fan *et al.*, "Biphenylene network: A nonbenzenoid carbon allotrope," *Science*, vol. 372, no.

6544, pp. 852–856, May 2021, doi: 10.1126/science.abg4509.

[55]   S.-A. Savu *et al.*, "Nanoscale assembly, morphology and screening effects in nanorods of newly synthesized substituted pentacenes," *RSC Adv.*, vol. 2, no. 12, p. 5112, 2012, doi: 10.1039/c2ra20168b.

[56]   A. Rabia *et al.*, "Structural, Electronic, and Vibrational Properties of a Two-Dimensional Graphdiyne-like Carbon Nanonetwork Synthesized on Au(111): Implications for the Engineering of sp-sp^2 Carbon Nanostructures," *ACS Appl. Nano Mater.*, vol. 3, no. 12, pp. 12178–12187, Dec. 2020, doi: 10.1021/acsanm.0c02665.

[57]   F. Sedona *et al.*, "On-surface synthesis of extended linear graphyne molecular wires by protecting the alkynyl group," *Phys. Chem. Chem. Phys.*, vol. 22, no. 21, pp. 12180–12186, 2020, doi: 10.1039/D0CP01634A.

[58]   M. Lischka *et al.*, "Remote functionalization in surface-assisted dehalogenation by conformational mechanics: organometallic self-assembly of 3,3′,5,5′-tetrabromo-2,2′,4,4′,6,6′-hexafluorobiphenyl on Ag(111)," *Nanoscale*, vol. 10, no. 25, pp. 12035–12044, 2018, doi: 10.1039/C8NR01987H.

[59]   J. Huang, H. Jia, T. Wang, L. Feng, P. Du, and J. Zhu, "Kinetic Control over Morphology of Nanoporous Graphene on Surface," *ChemPhysChem*, vol. 20, no. 18, pp. 2327–2332, Sep. 2019, doi: 10.1002/cphc.201900349.

[60]   M. Smerieri *et al.*, "Synthesis of corrugated C-based nanostructures by Br-corannulene oligomerization," *Phys. Chem. Chem. Phys.*, vol. 20, no. 41, pp. 26161–26172, 2018, doi: 10.1039/C8CP04791J.

[61]   G. Ruan, Z. Sun, Z. Peng, and J. M. Tour, "Growth of Graphene from Food, Insects, and Waste," *ACS Nano*, vol. 5, no. 9, pp. 7601–7607, Sep. 2011, doi: 10.1021/nn202625c.

[62]   J. Zhang, L. Lin, K. Jia, L. Sun, H. Peng, and Z. Liu, "Controlled Growth of Single-Crystal Graphene Films," *Adv. Mater.*, vol. 32, no. 1, p. 1903266, Jan. 2020, doi: 10.1002/adma.201903266.

[63]   G. Galeotti *et al.*, "An unexpected organometallic intermediate in surface-confined Ullmann coupling," *Nanoscale*, vol. 11, no. 16, pp. 7682–7689, 2019, doi: 10.1039/C9NR00672A.

[64]   M. Di Giovannantonio *et al.*, "Insight into Organometallic Intermediate and Its Evolution to Covalent Bonding in Surface-Confined Ullmann Polymerization," *ACS Nano*, vol. 7, no. 9, pp. 8190–8198, Sep. 2013, doi: 10.1021/nn4035684.

[65]   G. Galeotti *et al.*, "The role of halogens in on-surface Ullmann polymerization," *Faraday Discuss.*, vol. 204, pp. 453–469, 2017, doi: 10.1039/C7FD00099E.

[66]   I. Di Bernardo, P. Hines, M. Abyazisani, N. Motta, J. MacLeod, and J. Lipton-Duffin, "On-surface synthesis of polyethylenedioxythiophene," *Chem. Commun.*, vol. 54, no. 30, pp. 3723–3726, 2018, doi: 10.1039/C8CC01465E.

[67]   G. B. D. Rousseau, N. Bovet, and M. Kadodwala, "Sulfur the Archetypal Catalyst Poison? The Sulfur-Induced Promotion of the Bonding of Unsaturated Hydrocarbons on Cu(111)," *J. Phys. Chem. B*, vol. 110, no. 43, pp. 21857–21864, Nov. 2006, doi: 10.1021/jp0638742.

[68]   N. Merino-Díez *et al.*, "Switching from Reactant to Substrate Engineering in the Selective

Synthesis of Graphene Nanoribbons," *J. Phys. Chem. Lett.*, vol. 9, no. 10, pp. 2510–2517, May 2018, doi: 10.1021/acs.jpclett.8b00796.

[69]   Penghui Ji, Oliver MacLean, Gianluca Galeotti, Dominik Dettmann, Giulia Berti, Kewei Sun, Haiming Zhang, Federico Rosei & Lifeng Chi, "Oxygen-promoted synthesis of armchair graphene nanoribbons on Cu(111)," Science China Chemistry volume, Mar. 01, 2021.

[70]   C. Sánchez-Sánchez *et al.*, "On-Surface Hydrogen-Induced Covalent Coupling of Polycyclic Aromatic Hydrocarbons via a Superhydrogenated Intermediate," *J. Am. Chem. Soc.*, vol. 141, no. 8, pp. 3550–3557, Feb. 2019, doi: 10.1021/jacs.8b12239.

[71]   Meizhuang Liu, Mengxi Liu, Limin She, Zeqi Zha, Jinliang Pan, Shichao Li, Tao Li, Yangyong He, Zeying Cai, Jiaobing Wang, Yue Zheng, Xiaohui Qiu & Dingyong Zhong, "Graphene-like nanoribbons periodically embedded with four- and eight-membered rings," Nature Communications volume, Mar. 31, 2017.

[72]   J. A. Lipton-Duffin *et al.*, "Step-by-step growth of epitaxially aligned polythiophene by surface-confined reaction," *Proc. Natl. Acad. Sci.*, vol. 107, no. 25, pp. 11200–11204, Jun. 2010, doi: 10.1073/pnas.1000726107.

[73]   J. Lu *et al.*, "On-Surface Synthesis and Characterization of Polythiophene Chains," *J. Phys. Chem. C*, vol. 124, no. 1, pp. 764–768, Jan. 2020, doi: 10.1021/acs.jpcc.9b10106.

[74]   L. Liu *et al.*, "Conformation modification of terthiophene during the on-surface synthesis of pure polythiophene," *Nanoscale*, vol. 12, no. 35, pp. 18096–18105, 2020, doi: 10.1039/D0NR04529B.

[75]   G. Reecht *et al.*, "Oligothiophene Nanorings as Electron Resonators for Whispering Gallery Modes," *Phys. Rev. Lett.*, vol. 110, no. 5, p. 056802, Jan. 2013, doi: 10.1103/PhysRevLett.110.056802.

[76]   K. Feng, E. Solel, P. R. Schreiner, H. Fuchs, and H.-Y. Gao, "Diamantanethiols on Metal Surfaces: Spatial Configurations, Bond Dissociations, and Polymerization," *J. Phys. Chem. Lett.*, vol. 12, no. 13, pp. 3468–3475, Apr. 2021, doi: 10.1021/acs.jpclett.1c00387.

[77]   S. Kawai *et al.*, "Three-dimensional graphene nanoribbons as a framework for molecular assembly and local probe chemistry," *Sci. Adv.*, vol. 6, no. 9, p. eaay8913, Feb. 2020, doi: 10.1126/sciadv.aay8913.

[78]   L. Sosa-Vargas, E. Kim, and A.-J. Attias, "Beyond 'decorative' 2D supramolecular self-assembly: strategies towards functional surfaces for nanotechnology," *Mater. Horiz.*, vol. 4, no. 4, pp. 570–583, 2017, doi: 10.1039/C7MH00127D.

Chapter 5: On-surface homocoupling reactivity of a chiral bifunctional bromoindanone molecule on Cu(111)

On-surface synthesis has provided exciting concepts for the building of covalently bonded molecular nanostructures as well as the exploration of new synthetic pathways alternative to chemical synthesis in solution. The surface-supported reaction of precursor molecules can result in the formation of 2D molecular networks as well as novel 0D molecular structures. In this chapter, we investigate in ultrahigh vacuum by low-temperature scanning tunneling microscopy the adsorption of the chiral molecule (*R*)-6-bromo-3-phenyl-2,3-dihydro-1*H*-inden-1-one (BrPhINDO) on the Cu(111) surface. Annealing an as-deposited layer of molecules allows to activate two kinds of homocoupling reactions, the Ullmann-like coupling and the Knoevenagel reaction, resulting in the formation of various low-dimensional structures. By studying their prochirality and comparing with the products obtained with the enantiomer precursor, we demonstrate adsorption-induced chiral inversion generating partial racemization.

5.1   Introduction

As described in chapter 1, on-surface chemistry is a recent research field with great potential for the bottom-up production of specific nanostructures[1]–[8]. Thermal annealing, UV excitation, or tunneling electrons inside an STM junction can all be used to initiate on-surface synthesis reactions. Pioneering studies described, e.g., the formation of a covalent bond between two iodobenzene molecules[9], the thermally activated synthesis of an oligomer of porphyrins[10], or the formation of extended graphene nanoribbons[11]. In this approach, the molecular building blocks are deposited on a well-defined metal surface in (sub)monolayer regime and the homocoupling reaction is activated by thermal annealing. The metallic substrates used, such as copper, silver and gold single crystals, provide usually an important catalytic activity and take a fundamental role into the reaction mechanism. Over the years, several reaction mechanisms for the covalent coupling of molecular building blocks have been extensively studied, among them the Ullmann-[10]–[14], the Glaser-[15]–[17] or the Knoevenagel-type[18]–[20] reactions. In particular, molecular building blocks based on indanone are interesting because they can form covalent networks upon high temperature annealing. For instance, the s-indacene-1,3,5,7(2H,6H)-tetrone (INDO$_4$) molecule[21], [22] (see Fig.5.2a) is a symmetrical precursor with several O and H peripheral atoms which make it a highly versatile structure in terms of self-assembly[23], [24] and reactivity[20], [25]. N. Kalashnyk et al. showed that INDO$_4$

molecules undergo oxidative coupling and Knoevenagel reactions through the indanedione groups.

Playing with the substate symmetry and temperature allowed to trigger preferentially one of the two reactions and large domains of oriented oligomers could be created on Ag(110) (Fig.5.1-a). On the other hand, the repartition of the 4 O atoms in D_{2h} high symmetry allows a variety of different coupling configurations, which can be a source of disorder precluding the formation of extended 2D covalent networks[20]. Moreover, several ketone functions are rapidly isolated, thus blocking the extension of the polymer network (see Fig.5.2a). This can be seen on the Ag(111) surface, where bifurcations and elbows of the 1D polymer are observed after annealing at a temperature of 240°C due to Knoevenagel and trimerization reactions (Fig.5.1d). As expected, the resulting polymers are short and poorly ordered.
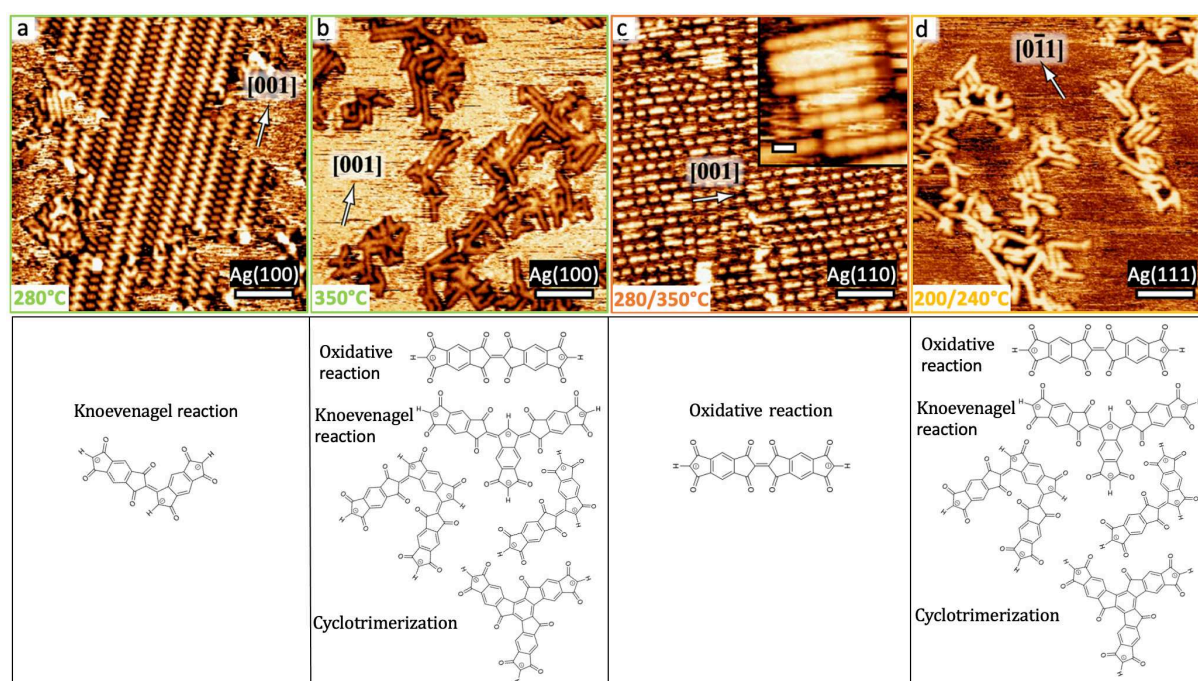
Figure 5.1. STM images of the polymeric structures and the corresponding molecular models obtained after annealing on Ag(100) (a, b), Ag(110) (c), and Ag(111) (d). Scale bars: (a-d) 6nm; inset of c: 1nm. Figures adapted from [20].

In order to improve the growth control of 2D networks based on indene derivatives, a strategy was developed in which the ketones number was reduced and the monomers arrangement on the surface controlled by forcing their adsorption orientation. The chiral (3*R*,7*R*)-3,7-dimethyl-2,3,6,7-tetrahydro-*s*-indacene-1,5-dione is thus envisaged in Fig.5.2b. Its out of plane methyl groups are intended to force the adsorption only with one side of the molecular place. If an enantiomerically pure sample is employed, a Knoevenagel-type

trimerization can repeat indefinitely, developing polymer with chiral character. On the other hand, if a racemic mixture is employed (Fig.5.2c), the polymerization will be impeded, likely resulting in ordered structures.
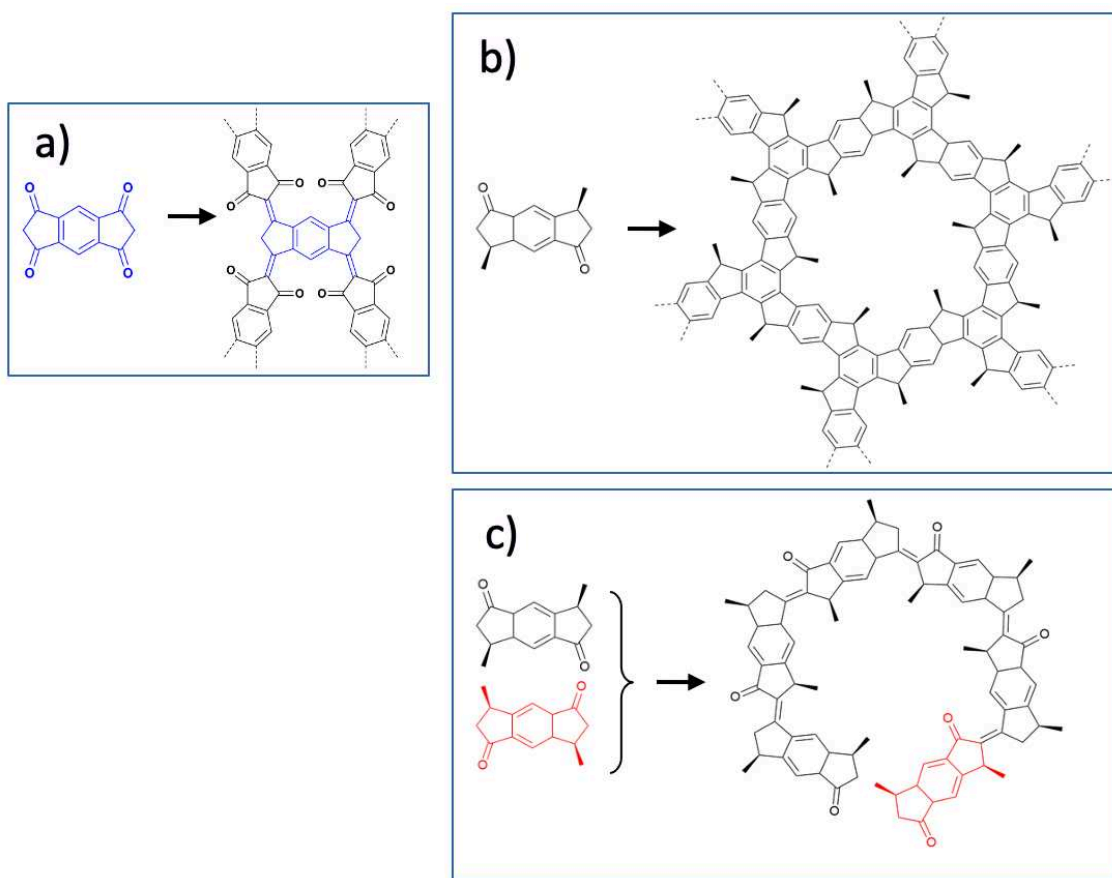
Figure 5.2. Molecular structure of the expected reaction schemes of (a) s-indacene-1,3,5,7(*2H,6H*)-tetrone (INDO$_4$), (b) (3*R*,7*R*)-3,7-dimethyl-2,3,6,7-tetrahydro-*s*-indacene-1,5-dione and (c) racemic mixture of (b) and (3*S*,7*S*)-3,7-dimethyl-2,3,6,7-tetrahydro-s-indacene-1,5-dione.

Unfortunately, in preliminary studies for the RR-Me2-INDO$_2$ adsorption on Ag(111) no ordered motifs could be observed, we thus moved to a further strategy consisting in diversifying the nature of the active sites. In fact, in previous works it was shown that the introduction of a bifunctionality in the molecular precursor producing an adequate sequential reactivity can improve the growth process in on-surface polymerization[4], [26]–[28]. We have thus designed the molecular precursor (*R*)-6-bromo-3-phenyl-2,3-dihydro-1*H*-inden-1-one (BrPhINDO, Fig.5.3) as a model system. It is composed of a 1-indanone backbone substituted with a bromine atom at the 6-position and a phenyl group at the 3-position.
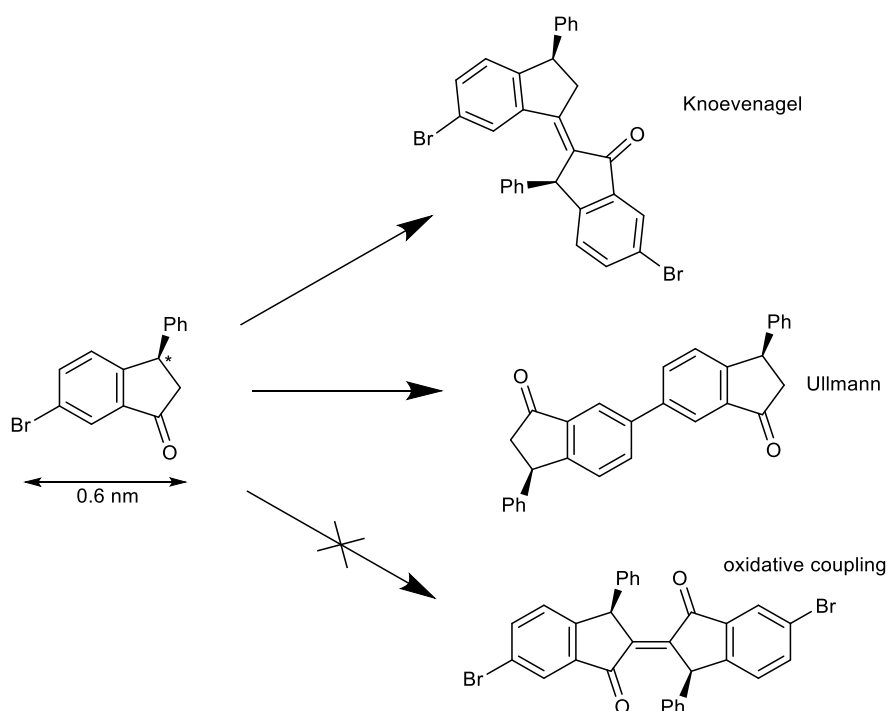
Figure 5.3. Molecular structure of (R)-6-bromo-3-phenyl-2,3-dihydro-1H-inden-1-one (BrPhINDO) and expected homocoupling reaction schemes. The oxidative coupling[25] was not observed on Cu(111).

This chiral molecule is expected to adsorb with the indanone backbone preferentially on one side due to the strong interaction of the carbonyl group with the metal surface and the presence of the bulky phenyl group on the asymmetric carbon[29]. As detailed above for INDO4, different intermolecular couplings such as Ullmann-like, Knoevenagel or oxidative couplings can take place with these molecular tectons, (see Fig.5.3). The subject of this chapter is to study the development of the diverse couplings that may originate from the concomitant presence of a bromine but also of the indane-1,3-dione moiety in the case of BrPhINDO. The Cu(111) surface was chosen as reaction template due to its hexagonal symmetry and its high reactivity[30] with respect to other coinage metals, in particular towards halogenated precursors[4], [14], [31]. The formation of the different reaction products was studied by low-temperature scanning tunneling microscopy (LT-STM) in combination with core-level photoemission spectroscopy (XPS).

5.2   Chemical synthesis of BrPhINDO

In order to study the chirality of a molecule based on indanone after deposition on Cu(111) surface, the molecule was synthesized by introducing a phenyl group that could produce a better arrangement of molecules. It was also synthesized with a bromine atom in the position 6 since

this position can provide different types of arrangement on the metal surface. The synthesis of BrPhINDO was performed by our collaborators C.Pigot and F.Dumur at ICR laboratory at Aix-Marseille University (detailed in Appendix). The indane nucleus is complex to derivate. To solve this problem, several solutions have been proposed in the literature, mostly involving diverse pre-functionalizations of the substrate, followed by an intramolecular cyclization, providing the indane core[32], [33]. The nature of these reactions is diverse but, in our case, this classical strategy was abandoned (Fig.5.4a). Indeed, the ring closure occurred only on the previously introduced phenyl group due to the presence of the bromine on the cycle (Fig.5.4b). Based on the work of Zheng et al.[34], we first performed an oxidation of 6-bromo-2,3-dihydro-1*H*-inden-1-one by mean of a radical bromination followed by an elimination reaction. This intermediate, i.e. 6-bromo-1*H*-inden-1-one, could be obtained in 45% yield (see details in Fig.5.4c).

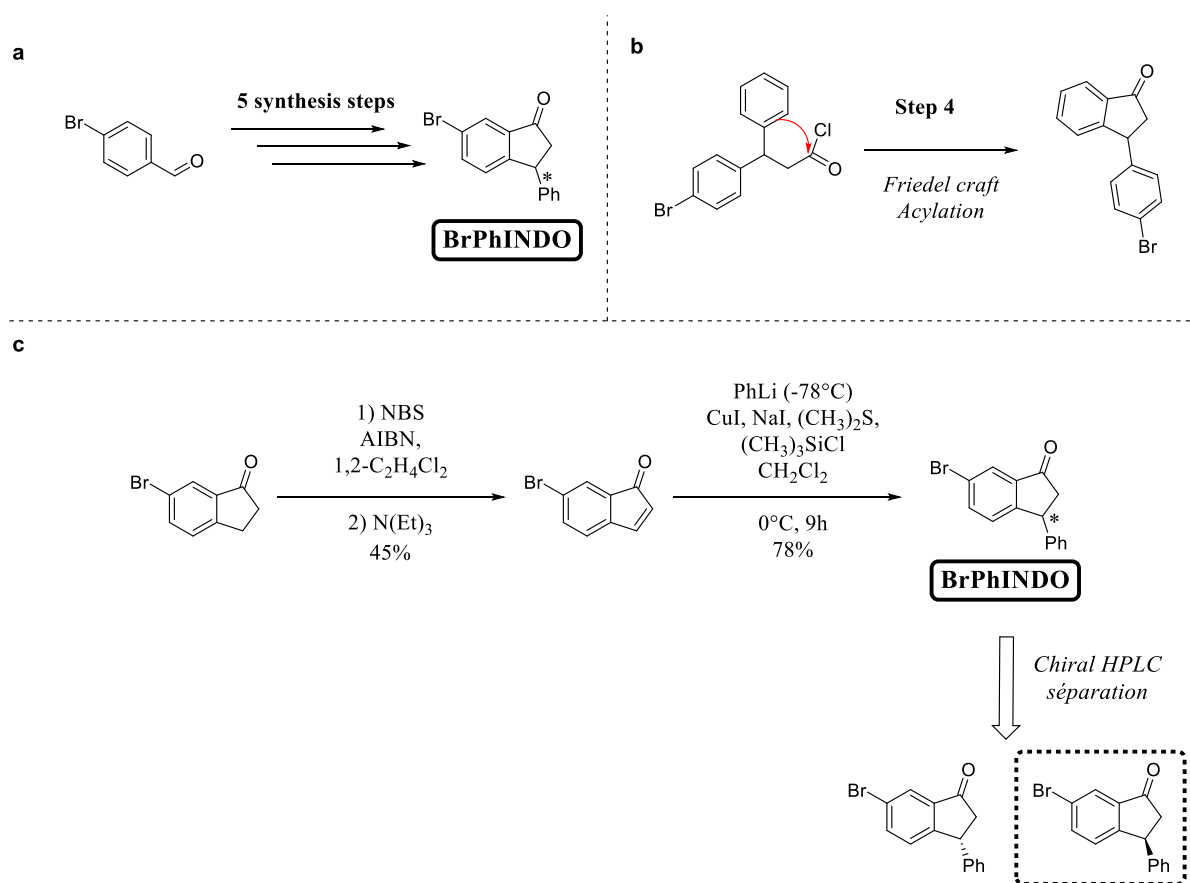**Figure 5.4.** Synthesis strategy of BrPhINDO molecules.

Compared to the original procedure, 6-bromo-1*H*-inden-1-one was prepared with one major change, i.e. the solvent used for the reaction. Indeed, CCl_4 was substituted by 1,2-dichloroethane due to its lower toxicity and its easier availability. Afterwards, the phenyl group was introduced through a 1,4-addition with a cuprate, formed with PhLi, providing BrPhINDO

with 78% yield. In addition, it is the first example of such reaction performed on the inden-1-one core, allowing to obtain our final product in only two steps. Finally, a semi-preparative chiral HPLC separation was performed to obtain enantiomerically pure BrPhINDO, where both enantiomers were used during the study (detailed in the thesis of C.Pigot[35]).

5.3 Deposition of BrPhINDO on Cu(111) surface

In a first part, we consider the *R*-stereoisomer of the chiral BrPhINDO precursor. The room-temperature deposition in submonolayer regime resulted in several different features rendering difficult to single out the intermolecular interactions possibly at play. A deposition close to one monolayer on the substrate kept at 100°C was then performed, resulting in a much more homogeneous phase (Fig.5.5a). Subsequently, annealing at increasing temperatures was performed to activate different intermolecular interactions (Fig.5.5b-d). In the as-deposited sample, two main features were observed, both ascribable to supramolecular arrangements of a common building block. The most abundant motif consists of molecular chains (type-1, pink rectangle in Fig.5.5a) about 7-10 nm long and 2.6 nm wide in which the repeating units arrange in coupled parallel rows with an average period of 0.25 nm. At the end of these rows or in between them, a less abundant structure, sometimes fused within, is present: a molecular ring made of three sub-units, presenting a C_3 symmetry (green circle in Fig.5.5a), called α structure in the following. The building block in the chains and in the α structures is imaged as an oval feature of size 0.9 nm×0.7 nm, close to the indane backbone size of the BrPhINDO molecule. No contrast asymmetry is detected in each sub-unit (Fig.5.6a), suggesting that the phenyl ring may have left the molecule or is not involved in the imaging contrast due to its out-of-plane orientation. A combination of metal-ligand coordination and hydrogen bonding can be envisaged as the driving force for the formation of these structures, especially considering the ability of such halogenated molecules to debrominate[36], [37] that is also confirmed by the XPS analysis below. Nevertheless, the details of this non-covalent bonding are out of the scope of this study and will not be discussed further.
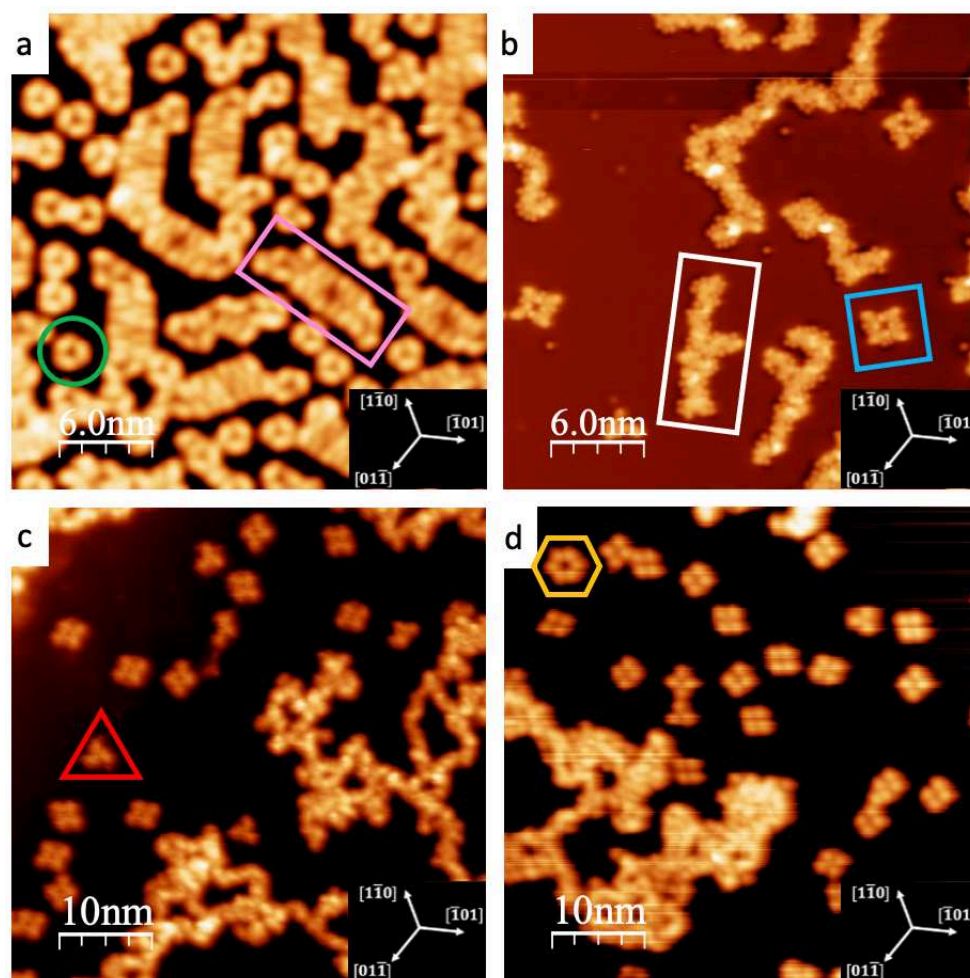
Figure 5.5. LT-STM images obtained after deposition of *R*-BrPhINDO molecule on hot Cu (111) surface (T_{Cu} = 100 °C) (a) and after annealing at 200 °C (b), 300 °C (c), and 400 °C (d). The different features are highlighted by colored frames: green circle for α structure, pink rectangle for type-1 chains, blue square for γ structure, white rectangle for type-2 chains, red triangle for β structure and yellow hexagon for δ structure.

5.4   Formation of intermolecular covalent coupling after thermal annealing

An annealing at increasing temperatures was performed to activate intermolecular covalent bonding and the results were analyzed by STM. Upon annealing at 200 °C, the coverage is reduced by more than 50 % due to substantial desorption. The precursor diffusion is then increased, facilitating intermolecular coupling and resulting in two main outcomes: elongated type-2 chains (white rectangle in Fig.5.5b) and isolated well-defined γ structures displaying C_2 symmetry (highlighted by a blue square in Fig.5.5b). By annealing at higher temperatures (Fig.5.5c-d), the type-2 chains evolve in longer and intertwined structures whereas new isolated features appear sparsely next to the - now more abundant - γ forms: features with C_3 symmetry,

named β (red triangle in Fig.5.5c), and hexagonal features with C_3 symmetry (see below), named δ (yellow hexagon in Fig.5.5d). Interestingly, all well-defined products obtained upon annealing above 100 °C display a defined chirality, as it will be discussed later. Concerning the type-2 chains, they are partially cross-linked and are about 8-24 nm long and 1-3 nm wide, in line with typical sizes for covalent polymerization of similar systems based on small aromatic precursors[30], [38]–[41]. The presence of 1D extended chains testifies that both active sites designed for covalent coupling are activated at this temperature, together with possible co-operating metal-organic bonds. Nevertheless, due to their intricate and stochastic structure, the chain analysis does not allow a clear assignment of precursor evolution upon coupling. We then turn to the description of the isolated products γ, β and δ which, given their high temperature stability can be classified as covalent structures.

5.5   Model structures for reaction products

Based on the LT-STM results and the expected reactivity of the precursor, we can suggest structural models for the products γ, β and δ. The precursor presents three sites likely to be activated on a surface, namely the Br, O and CH_2 sites able to promote the formation of covalent bonds through Ullmann, Knoevenagel and oxidative condensation reactions, respectively (see reaction schemes in Fig.5.3). The STM images of the three covalent features and the corresponding structural models are presented in Fig.5.6. Feature γ is composed of two "L"-shaped subunits. The best fit in size and shape for each of these subunits is realized by considering four monomers corresponding to two Ullmann-coupled dimers linked through a Knoevenagel reaction. The two subunits can then bind through hydrogen bonding (H-bonds) in a head to tail fashion conferring a chiral C_2 symmetry character to the structure. The less abundant β structure is made up of smaller branches and is then not likely to derive from the γ feature. In fact, when low coverage samples are explored, the β feature is found already for annealing at 200 °C, thus enlarging its actual stability range. The best fit to the STM images of the β product is obtained by considering three Ullmann-coupled dimers, assembled by H-bonds cand with a chiral C_3 symmetry. The β structures tend to disappear at higher annealing temperatures (see below), possibly by forming higher level products such as γ and δ. The feature δ appears at 300 °C and grows as a function of the annealing temperature, suggesting a progression in the reaction pathway. In fact, feature δ is composed of a close macro-ring obtained through alternating Ullmann and Knoevenagel couplings (Fig.5.6h). The small stress induced by the deformation due to the presence of 5-membered rings in this hexagonal macro-ring is probably overcome by the energy gain in the formation of the fully covalent structure.

It is interesting to note that in all the above models, the inclusion of oxidative couplings that could have occurred through the CH$_2$ groups (see Fig.5.3) did not give satisfactory agreements to the STM and can thus be ruled out from the processes leading to the observed products.

Temperature stability range	100 °C	200 °C − 300°C	200 °C − 400°C	300 °C − 400°C
STM image	a α 1.2nm	b β 1.2nm	c γ 1.2nm	d δ 1.2nm
Molecular models	e	f	g	h
Superimposed models	i α	j β	k γ	l δ
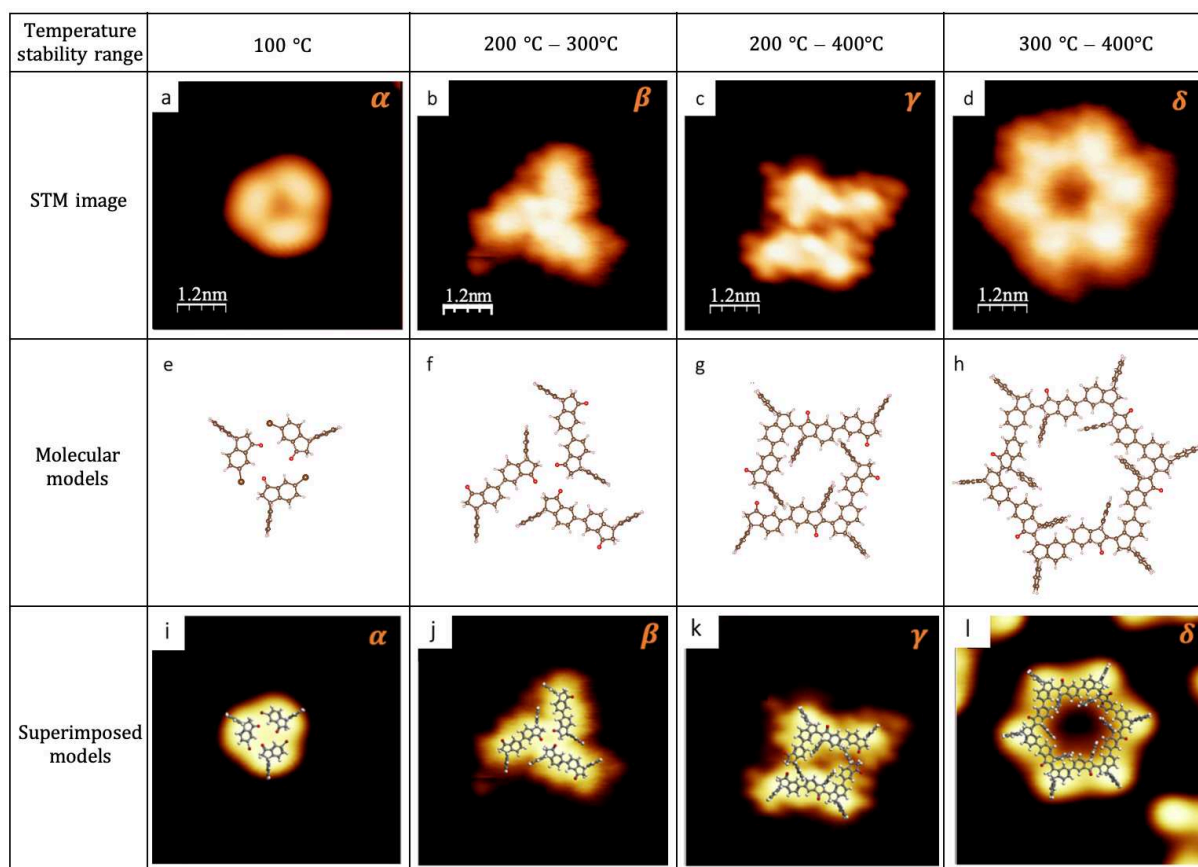
Figure 5.6. STM images (a-d) and corresponding models (e-h) of all observed isolated structures as a function of their stability range of temperature on the Cu(111) surface. STM images with superimposed models of the different structures (i-l).

5.6   Chemistry study of the system by XPS measurements

As a support to the above models, additional XPS measurements were performed in a separate UHV system in PIIM laboratory with the non-monochromatized Al Kα line (hν = 1486.6 eV) of an X-ray tube from PREVAC. The measurements being performed *ex-situ,* instead of trying to exactly reproduce the samples described above, we studied the evolution of a monolayer deposited at RT and sequentially annealed at increasing temperatures. Fig.5.7 displays the XPS spectra of C 1s, O 1s and Br 3p core levels. All spectra display a single peak (a spin-orbit doublet for Br 3p) with an asymmetric line shape, representative of multiple atomic sites. The resolution in XPS measurements, determined from the full width at half-maximum of Cu 3d core levels recorded on the clean surface, was 0.9 eV. This may come either from the

presence of different chemical environments within each molecule (as it is the case for the C 1s) or from different interactions with the substrate or between the molecules. In any case, given the inhomogeneous distribution of the different compounds in the present system, a deconvolution in multiple components to extract information about the molecular structures or intermolecular bonding is not relevant. The analysis will then focus on the main line binding energy (BE) position as well as the intensity ratios between the peaks.
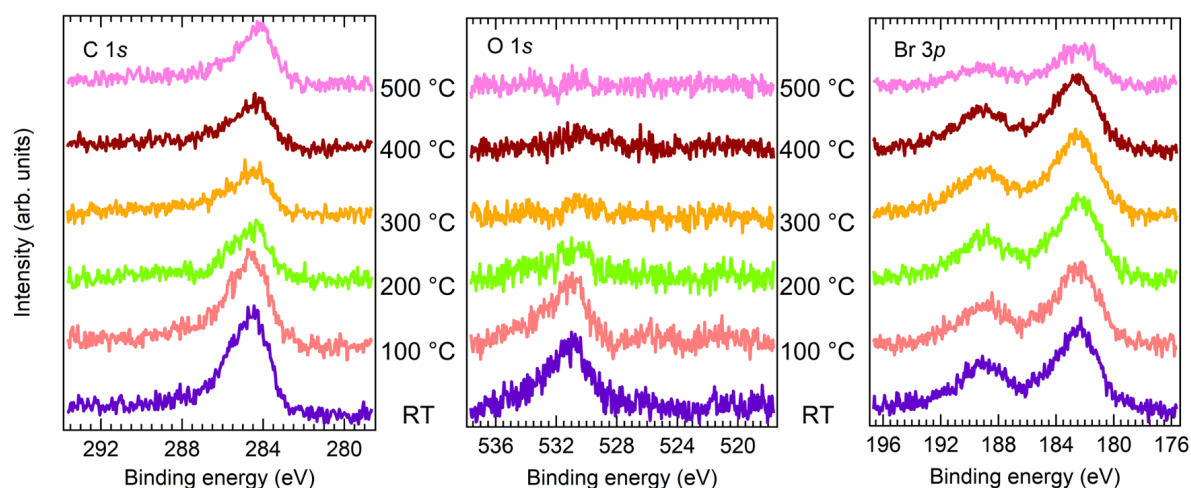

Figure 5.7. XPS data for BrPhINDO on Cu(111): C 1s (a), O 1s (b) and Br 3p (c) core levels as a function of the annealing temperature.

The Ullmann coupling reaction is very common when brominated precursors are adsorbed on coinage metal surfaces. In this reaction, as a first step, the debromination should occur and then, after a possible intermediate step in which C-metal adatom bonds are temporary formed, the as-created radical can induce C-C coupling. On Cu(111) the debromination is expected to occur as soon as the precursors are adsorbed, even at RT[40], [42]. This is confirmed by the present XPS data since the Br 3p spectrum does not change as a function of temperature up to 500 °C, when Br starts desorbing. Accordingly, its BE is 182.5 eV, representative of Br adatoms on Cu surfaces as found for similar systems[42], [43]. Unfortunately, the energy resolution does not allow to conclude on the presence of the C-Cu intermediate state which would manifest as a shoulder to the low BE side of the main C 1s peak[36]. With the aim of understanding the reactional mechanisms occurring on the surface, we computed the stoichiometric ratio between the carbon and the bromine atoms. Before the Ullmann and Knoevenagel covalent reactions set in, the stoichiometric ratio between the different chemical species composing the molecule should be reflected in the intensities of the respective core levels. For an intact BrPhINDO molecule, the expected C:Br ratio is 15 (see Fig.5.3), while it should be 9 for a molecule having lost its phenyl

functionalization. Upon adsorption at RT as well as after annealing at 100 °C the measured C:Br ratio is about 14, in line with a pristine precursor. As can be seen in Fig. 5.7, for 200 °C annealing temperature the C 1s intensity is sensibly reduced and the C:Br ratio decreased. Unfortunately, it is not possible to conclusively address this effect to a potential loss of phenyl functionalization, as mentioned above. Indeed, while the Br adatoms remained adsorbed up to 500°C, part of this reduction can be attributed to the desorption of debrominated molecules, as also observed in STM. For higher annealing temperatures the C 1s peak intensity stabilizes. This supports the picture in which the thermally activated reaction forms more stable compounds with no further loss of material upon annealing, in-line with the formation of covalently bonded superstructures. The thermal desorption should also affect the O 1s and indeed a net drop in peak intensity is observed at 200 °C. Here, the presence of substrate-related Auger peaks in this energy region prevents from a reliable measurement of the actual stoichiometry ratios of O with regard to C and Br. Interestingly, at variance with what is observed for C 1s, the O 1s exhibits a continuous decrease as the temperature increases. This behavior can be correlated with the progression of the Knoevenagel reaction with temperature, leading to the observed growth of the γ and δ populations and indicating that the Knoevenagel reaction is thermally activated as it has been already observed elsewhere[20].

5.7   Prochirality study of the reaction products

As observed above, all the isolated features resulting from the thermally activated covalent couplings of the *R*-BrPhINDO precursor show a defined prochirality on the surface. Prochirality is here defined as the loss of symmetry induced by the planar adsorption, i.e. on which side the molecule is lying on the surface. In BrPhINDO, the phenyl function is bonded to a carbon atom with sp^3 hybridization. Its out-of-plane configuration with respect to the indanone backbone is meant to guide the prochiral adsorption configuration of the molecule and, in turn, to determine the prochiral character of the reaction products. In the model structures of Fig.5.6, the indanone plane is lying flat on the surface and the phenyl group is pointing outwards, thus providing a defined prochiral symmetry of the structures in agreement with the STM images shown here. In fact, we also observed a substantial number of structures presenting the opposite prochirality, with an abundance of 15 to 30 % (see Fig.5.9). To account for such prochirality inversion, two distinct mechanisms can be proposed (see Fig.5.8).
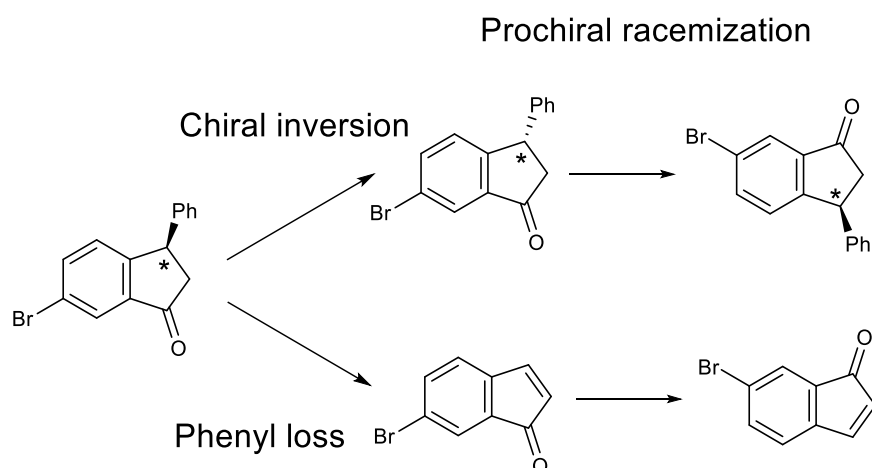
Figure 5.8. Prochiral racemization of the structures observed due to chiral inversion of the asymmetric carbon or phenyl loss.

A loss of the phenyl group upon adsorption would remove the intrinsic chirality of the precursor and the two prochiral adsorption configurations can be achieved by flipping of the adsorption side. On the other hand, a chiral inversion of the asymmetric carbon could occur leading to an inversion of the more favorable adsorption side of the indanone moiety. Similar internal modifications of the precursor such as spontaneous conformational changes were previously reported[44]–[47]. The present isomerization rather goes through a configuration inversion involving bond breaking and radical exchange. Whichever the origin of the prochirality inversion, the larger abundance of the original chirality in the reaction products suggests a relatively high energy barrier for the process. XPS data indicate that, at RT and after annealing at 100 °C, there is no degradation of the molecule other than the Br loss, thus indicating that the phenyl functions are still attached to the molecules deposited at that temperature. In any case, it is suggested that the chiral inversion is taking place within individual precursors, before any homocoupling reaction occurs, because the enantiomeric asymmetry is preserved even at high annealing temperature.

Figure 5.9. STM images showing the two prochiralities and their relative abundance observed for the β, γ and δ-structures obtained after deposition of the molecule *R*-BrPhINDO on Cu(111).

In order to verify this chiral asymmetry, the other enantiomer of the same molecule (*S*-BrPhINDO) was deposited on the Cu(111) surface and studied in similar conditions (Figure 5.10). In this case also, the two prochirality forms of all the structures (β, γ, δ) are observed. As expected, the distribution of these two prochirality forms on the surface is reversed, thus confirming the partial racemic inversion that is taking place on the Cu(111) surface.
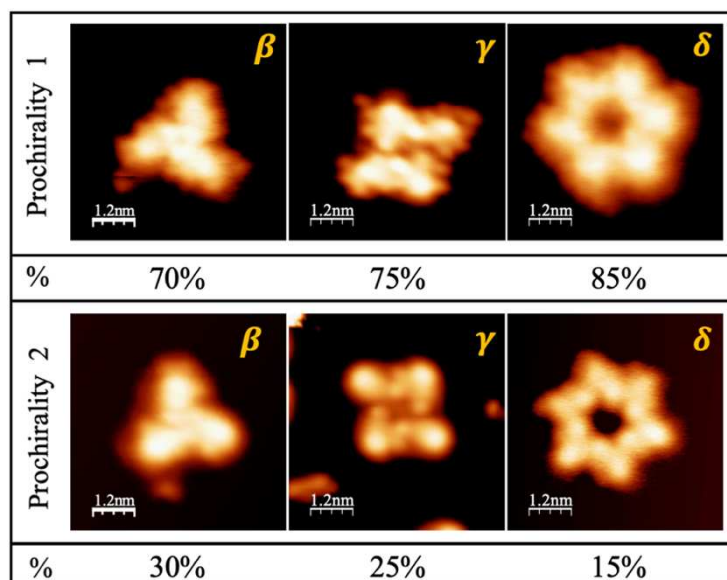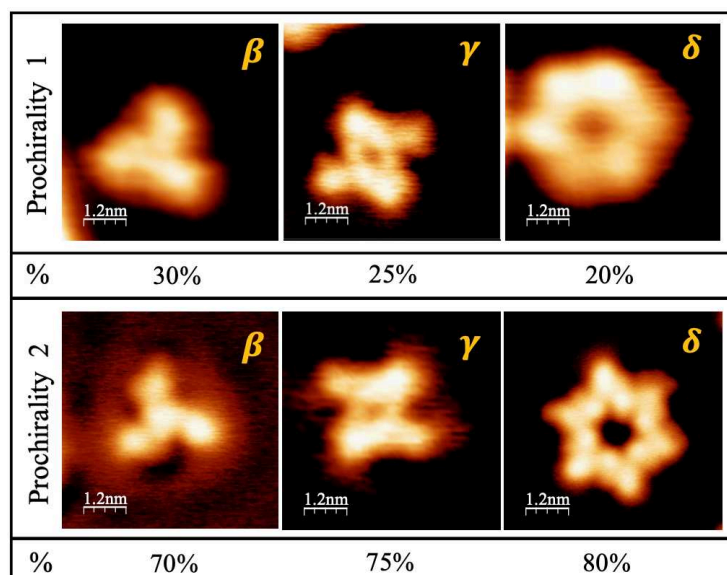

Figure 5.10. STM images showing the two prochiralities and their relative abundance observed for the β, γ and δ-structures obtained after deposition of the molecule *S*-BrPhINDO on Cu(111).

5.8   Conclusions

In summary, by employing a new precursor with multiple reaction sites, namely (*R*)-6-bromo-3-phenyl-2,3-dihydro-1*H*-inden-1-one (BrPhINDO), different reaction products were synthesized on Cu(111) as a function of the annealing temperature. H-bonded C_3 threefold assemblies of Ullmann-coupled dimers were singled out as the smallest reacted entities. Knoevenagel reactions between these dimers resulted in the formation of tetramers coupled twofold to form larger C_2 structures. Finally, three tetramers further couple through Knoevenagel reactions to produce large C_3 hexagons. All structures present a defined prochirality with an asymmetric enantiomeric distribution due to the occurrence of chiral inversion for a fraction of the precursors (partial racemization). The latter is imputed to a phenyl loss or to a chiral switch upon adsorption.

In future work, different strategies may be explored to control the chirality of the precursors and the formation of a 2D networks. We propose to change the size and the nature of the functional group (phenyl) by another that may be better in term of chirality stabilization. For this, the same molecule was synthesized with methyl (Me), butyl (Bu), and tert-butyl (t-Bu). The methyl group would serve as a reference, the addition of a butyl chain allows to keep a certain lability, and the tert-butyl group brings a high steric perturbation between the molecules. Unfortunately, it was not been possible to explore these new molecules in the framework of this thesis work due to a lack of available experimental time. Another strategy can be applied to form 2D networks with these molecules by changing the halogen group, the bromine, in the molecule by another one less reactive such as Chlorine (Cl). This strategy allows first the formation of a Knoevenagel reaction through the indanedione groups and then the formation of extended network by Ullmann coupling through the halogen atom.

References of chapter 5

[1]   A. Sweetman, N. R. Champness, and A. Saywell, "On-surface chemical reactions characterised by ultra-high resolution scanning probe microscopy," *Chem. Soc. Rev.*, vol. 49, no. 13, pp. 4189–4202, 2020, doi: 10.1039/D0CS00166J.

[2]   L. Grill and S. Hecht, "Covalent on-surface polymerization," *Nat. Chem.*, vol. 12, no. 2, pp. 115–130, Feb. 2020, doi: 10.1038/s41557-019-0392-9.

[3]   F. Palmino, C. Loppacher, and F. Chérioux, "Photochemistry Highlights on On-Surface Synthesis," *ChemPhysChem*, vol. 20, no. 18, pp. 2271–2280, Sep. 2019, doi: 10.1002/cphc.201900312.

[4]   S. Clair and D. G. de Oteyza, "Controlling a Chemical Coupling Reaction on a Surface: Tools and Strategies for On-Surface Synthesis," *Chem. Rev.*, vol. 119, no. 7, pp. 4717–4776, Apr. 2019, doi: 10.1021/acs.chemrev.8b00601.

[5]   P. A. Held, H. Fuchs, and A. Studer, "Covalent-Bond Formation via On-Surface Chemistry," *Chem. Eur. J.*, vol. 23, no. 25, pp. 5874–5892, May 2017, doi: 10.1002/chem.201604047.

[6]   M. Lackinger, "On-surface polymerization - a versatile synthetic route to two-dimensional polymers: On-surface polymerization," *Polym. Int.*, vol. 64, no. 9, pp. 1073–1078, Sep. 2015, doi: 10.1002/pi.4943.

[7]   J. Méndez, M. F. López, and J. A. Martín-Gago, "On-surface synthesis of cyclic organic molecules," *Chem. Soc. Rev.*, vol. 40, no. 9, p. 4578, 2011, doi: 10.1039/c0cs00161a.

[8]   Q. Fan, J. M. Gottfried, and J. Zhu, "Surface-Catalyzed C–C Covalent Coupling Strategies toward the Synthesis of Low-Dimensional Carbon-Based Nanostructures," *Acc. Chem. Res.*, vol. 48, no. 8, pp. 2484–2494, Aug. 2015, doi: 10.1021/acs.accounts.5b00168.

[9]   S.-W. Hla, L. Bartels, G. Meyer, and K.-H. Rieder, "Inducing All Steps of a Chemical Reaction with the Scanning Tunneling Microscope Tip: Towards Single Molecule Engineering," *Phys. Rev. Lett.*, vol. 85, no. 13, pp. 2777–2780, Sep. 2000, doi: 10.1103/PhysRevLett.85.2777.

[10]   L. Grill, M. Dyer, L. Lafferentz, M. Persson, M. V. Peters, and S. Hecht, "Nano-architectures by covalent assembly of molecular building blocks," *Nature Nanotech*, vol. 2, no. 11, pp. 687–691, Nov. 2007, doi: 10.1038/nnano.2007.346.

[11]   J. Cai *et al.*, "Atomically precise bottom-up fabrication of graphene nanoribbons," *Nature*, vol. 466, no. 7305, pp. 470–473, Jul. 2010, doi: 10.1038/nature09211.

[12]   J. A. Lipton-Duffin, O. Ivasenko, D. F. Perepichka, and F. Rosei, "Synthesis of Polyphenylene Molecular Wires by Surface-Confined Polymerization," *Small*, vol. 5, no. 5, pp. 592–597, Mar. 2009, doi: 10.1002/smll.200801943.

[13]   M. Bieri *et al.*, "Porous graphenes: two-dimensional polymer synthesis with atomic precision," *Chem. Commun.*, no. 45, p. 6919, 2009, doi: 10.1039/b915190g.

[14]   M. Lackinger, "Surface-assisted Ullmann coupling," *Chem. Commun.*, vol. 53, no. 56, pp. 7872–7885, 2017, doi: 10.1039/C7CC03402D.

[15]   Y.-Q. Zhang *et al.*, "Homo-coupling of terminal alkynes on a noble metal surface," *Nat Commun*, vol. 3, no. 1, p. 1286, Jan. 2012, doi: 10.1038/ncomms2291.

[16]   H.-Y. Gao, H. Wagner, D. Zhong, J.-H. Franke, A. Studer, and H. Fuchs, "Glaser Coupling at Metal Surfaces," *Angew. Chem. Int. Ed.*, vol. 52, no. 14, pp. 4024–4028, Apr. 2013, doi: 10.1002/anie.201208597.

[17]   A. Saywell, A. S. Browning, P. Rahe, H. L. Anderson, and P. H. Beton, "Organisation and ordering of 1D porphyrin polymers synthesised by on-surface Glaser coupling," *Chem. Commun.*, vol. 52, no. 68, pp. 10342–10345, 2016, doi: 10.1039/C6CC03758E.

[18]   K. H. Au-Yeung *et al.*, "On-Surface Formation of Cyano-Vinylene Linked Chains by Knoevenagel Condensation," *Chem. Eur. J.*, vol. 27, no. 69, pp. 17336–17340, Dec. 2021, doi: 10.1002/chem.202103094.

[19]   Y. Geng, H. Dai, S. Chang, F. Hu, Q. Zeng, and C. Wang, "Formation of C≡C Bond via Knoevenagel Reaction between Aromatic Aldehyde and Barbituric Acid at Liquid/HOPG and Vapor/HOPG Interfaces," *ACS Appl. Mater. Interfaces*, vol. 7, no. 8, pp. 4659–4666, Mar. 2015, doi: 10.1021/am508068m.

[20]   N. Kalashnyk *et al.*, "The Orientation of Silver Surfaces Drives the Reactivity and the Selectivity in Homo-Coupling Reactions," *ChemPhysChem*, vol. 19, no. 15, pp. 1802–1808, Aug. 2018, doi: 10.1002/cphc.201800406.

[21]   P. Krief, J. Y. Becker, A. Ellern, V. Khodorkovsky, O. Neilands (the late), and L. Shapiro, "*s* -Indacene-1,3,5,7(2 *H* ,6 *H*)-tetraone (' *Janus* dione') and 1,3-Dioxo-5,6-indanedicarboxylic Acid: Old and New 1,3-Indandione Derivatives," *Synthesis*, vol. 2004, no. 15, pp. 2509–2512, 2004, doi: 10.1055/s-2004-831184.

[22]   R. S. Sprick, A. Thomas, and U. Scherf, "Acid catalyzed synthesis of carbonyl-functionalized microporous ladder polymers with high surface area," *Polym. Chem.*, vol. 1, no. 3, p. 283, 2010, doi: 10.1039/b9py00375d.

[23]   N. Kalashnyk and S. Clair, "Self-Accommodating Honeycomb Networks from Supramolecular Self-Assembly of *s* -Indacene-tetrone on Silver Surfaces," *Langmuir*, vol. 38, no. 3, pp. 1067–1071, Jan. 2022, doi: 10.1021/acs.langmuir.1c02640.

[24]   N. Kalashnyk, F. Dumur, D. Gigmes, and S. Clair, "Molecular adaptation in supramolecular self-assembly: brickwall-type phases of indacene-tetrone on silver surfaces," *Chem. Commun.*, vol. 54, no. 61, pp. 8510–8513, 2018, doi: 10.1039/C8CC04883E.

[25]   N. Kalashnyk *et al.*, "On-surface synthesis of aligned functional nanoribbons monitored by scanning tunnelling microscopy and vibrational spectroscopy," *Nat Commun*, vol. 8, no. 1, p. 14735, Apr. 2017, doi: 10.1038/ncomms14735.

[26]   L. Lafferentz, V. Eberhardt, C. Dri, C. Africh, G. Comelli, F. Esch, S. Hecht & L. Grill, "Controlling on-surface polymerization by hierarchical and substrate-directed growth," nature chemistry, pp. 215–220, Jan. 15, 2012.

[27]   T. Faury, S. Clair, M. Abel, F. Dumur, D. Gigmes, and L. Porte, "Sequential Linking To Control Growth of a Surface Covalent Organic Framework," *J. Phys. Chem. C*, vol. 116, no. 7, pp. 4819–4823, Feb. 2012, doi: 10.1021/jp300417g.

[28]   C. Pigot and F. Dumur, "Recent Advances of Hierarchical and Sequential Growth of Macromolecular Organic Structures on Surface," *Materials*, vol. 12, no. 4, p. 662, Feb. 2019, doi: 10.3390/ma12040662.

[29]   M. M. Knudsen *et al.*, "Controlling Chiral Organization of Molecular Rods on Au(111) by Molecular Design," *J. Am. Chem. Soc.*, vol. 133, no. 13, pp. 4896–4905, Apr. 2011, doi: 10.1021/ja110052n.

[30]   L. Giovanelli *et al.*, "On-Surface Synthesis of Unsaturated Hydrocarbon Chains through C−S Activation," *Chemistry A European J*, vol. 28, no. 47, Aug. 2022, doi: 10.1002/chem.202200809.

[31]   L. Dong, P. N. Liu, and N. Lin, "Surface-Activated Coupling Reactions Confined on a Surface," *Acc. Chem. Res.*, vol. 48, no. 10, pp. 2765–2774, Oct. 2015, doi: 10.1021/acs.accounts.5b00160.

[32]   B. Gabriele, R. Mancuso, and L. Veltri, "Recent Advances in the Synthesis of Indanes and Indenes," *Chem. Eur. J.*, vol. 22, no. 15, pp. 5056–5094, Apr. 2016, doi: 10.1002/chem.201503933.

[33]   C. Borie, L. Ackermann, and M. Nechab, "Enantioselective syntheses of indanes: from organocatalysis to C–H functionalization," *Chem. Soc. Rev.*, vol. 45, no. 5, pp. 1368–1386, 2016, doi: 10.1039/C5CS00622H.

[34]   S. Zheng, H. Tan, X. Zhang, C. Yu, and Z. Shen, "Synthesis of benzo[c]fluorenone through a one-pot cascade reaction using inden-1-one derivatives," *Tetrahedron Letters*, vol. 55, no. 5, pp. 975–978, Jan. 2014, doi: 10.1016/j.tetlet.2013.11.081.

[35]   Corentin Pigot, "Dérivés d'indanes: de la chimie sur surface à la synthèse de composés push-pull aux multiples applications," Aix-Marseille Université, 2021.

[36]   M. Di Giovannantonio *et al.*, "Insight into Organometallic Intermediate and Its Evolution to Covalent Bonding in Surface-Confined Ullmann Polymerization," *ACS Nano*, vol. 7, no. 9, pp. 8190–8198, Sep. 2013, doi: 10.1021/nn4035684.

[37]   J. Björk, F. Hanke, and S. Stafström, "Mechanisms of Halogen-Based Covalent Self-Assembly on Metal Surfaces," *J. Am. Chem. Soc.*, vol. 135, no. 15, pp. 5768–5775, Apr. 2013, doi: 10.1021/ja400304b.

[38]   F. Sedona *et al.*, "On-surface synthesis of extended linear graphyne molecular wires by protecting the alkynyl group," *Phys. Chem. Chem. Phys.*, vol. 22, no. 21, pp. 12180–12186, 2020, doi: 10.1039/D0CP01634A.

[39]   M. Smerieri *et al.*, "Synthesis of corrugated C-based nanostructures by Br-corannulene oligomerization," *Phys. Chem. Chem. Phys.*, vol. 20, no. 41, pp. 26161–26172, 2018, doi: 10.1039/C8CP04791J.

[40]   G. Galeotti *et al.*, "Surface-mediated assembly, polymerization and degradation of thiophene-based monomers," *Chem. Sci.*, vol. 10, no. 19, pp. 5167–5175, 2019, doi: 10.1039/C8SC05267K.

[41]   P. S. Deimel *et al.*, "Bisphenol A and Diethylstilbestrol on Cu(111): On-Surface Polymerization Initiated by Hydroxy-Directed *Ortho* C–H Bond Activation," *J. Phys. Chem. C*, vol. 123, no. 2, pp. 1354–1361, Jan. 2019, doi: 10.1021/acs.jpcc.8b11047.

[42]   M. Chen *et al.*, "Combined Photoemission and Scanning Tunneling Microscopy Study of the

Surface-Assisted Ullmann Coupling Reaction," *J. Phys. Chem. C*, vol. 118, no. 13, pp. 6820–6830, Apr. 2014, doi: 10.1021/jp4121468.

[43]   M. Abyazisani, J. M. MacLeod, and J. Lipton-Duffin, "Cleaning up after the Party: Removing the Byproducts of On-Surface Ullmann Coupling," *ACS Nano*, vol. 13, no. 8, pp. 9270–9278, Aug. 2019, doi: 10.1021/acsnano.9b03812.

[44]   A. Nuermaimaiti *et al.*, "Chiral Induction with Chiral Conformational Switches in the Limit of Low 'Sergeants to Soldiers' Ratio," *ACS Nano*, vol. 8, no. 8, pp. 8074–8081, Aug. 2014, doi: 10.1021/nn502097h.

[45]   S. Weigelt *et al.*, "Chiral switching by spontaneous conformational change in adsorbed organic molecules," *Nature Mater*, vol. 5, no. 2, pp. 112–117, Feb. 2006, doi: 10.1038/nmat1558.

[46]   G. Goubert, Y. Dong, M. N. Groves, J.-C. Lemay, B. Hammer, and P. H. McBreen, "Monitoring interconversion between stereochemical states in single chirality-transfer complexes on a platinum surface," *Nature Chem*, vol. 9, no. 6, pp. 531–536, Jun. 2017, doi: 10.1038/nchem.2753.

[47]   M. Ammon, T. Sander, and S. Maier, "On-Surface Synthesis of Porous Carbon Nanoribbons from Polymer Chains," *J. Am. Chem. Soc.*, vol. 139, no. 37, pp. 12976–12984, Sep. 2017, doi: 10.1021/jacs.7b04783.

Conclusion

The scope of this thesis was the engineering and the control of new strategies for the formation of organic nanostructures on surface and the study of their properties. The creation of the nanostructures is based on the concepts of supramolecular self-assembly and on-surface synthesis through the elaboration of respectively on noncovalent and covalent intermolecular interactions. Until now, numerous studies were performed to show that all these reactions can be controlled and manipulated at the nano-scale by different factors and parameters. For example, the consideration of the well-defined geometry structure of the solid surface used as well as the molecular design and the thermal annealing can drastically affect the reaction path and the desired end-products. All these reactions based on self-assembly processes and on-surface synthesis concepts were investigated and controlled with novel strategies in the framework of this thesis.

In the first stage of my work, we explored the control of the self-assembled domains by introducing a modulator molecule in addition to the main organic linker. In previous studies, it was shown that this strategy is a good way to control the size of self-assembled domains. To this aim, we have chosen the trimesic acid (TMA) molecules as the linker and the benzoic acid (BZA) molecules as the modulator. TMA and BZA belong to the family of aromatic molecules that possess carboxyl functionalities which are frequently studied on graphite surface. The self-assembled structure at the liquid-HOPG interface of a mixed solution of these two acids was investigated by RT-STM. The control of the domain size on the surface can be directly obtained by varying the stoichiometry ratio between the two molecules. For this, we proposed an approximation model to estimate the desired stoichiometric ratio. We started from the theoretically calculated ratio between TMA and BZA but no intermolecular interaction between the two molecules was observed. This is due to the nonequivalent equilibrium achieved between the molecules dissolved in the liquid phase and those adsorbed at the solid interface. Then, different stoichiometry ratios of bimolecular solutions were studied. All obtained results showed the pure phases of TMA only or BZA only. Therefore, the formation of the domain may be very sensitive to the stoichiometry ratio between the molecules and a fine tuning of the ratio could be necessary. Unfortunately, it has not been possible to do this fine study in the framework of this thesis due to the lack of available experimental time.

In the second stage of this thesis, we investigated the formation of covalently bonded nanostructures on a metal surface. By now, the reported examples of on-surface reactions based on covalent bonds are investigated by STM/AFM under UHV conditions and at ambient

conditions at the liquid-solid interface. XPS technique is also used to study these types of reactions. Our objective was to explore novel strategies to control the formation of organic nanostructures by on-surface synthesis. The first was to explore new chemistry types based on an original activation reaction and the second was the study of the influence of a particular bifunctionnality and symmetry of the molecular precursor on the growth of nanostructures. For these investigations, we used two different molecules: DTB molecule, bearing thiophene group, for thermally-induced new activation reaction leading to the formation of covalently bonded self-assembled network and BrPhINDO molecules, bearing bifunctional groups, for the study of the influence of the chirality on the formed structure. Both molecules are deposited onto clean Cu(111) surface by sublimation under UHV conditions.

DTB molecules is a new thiophene-functionalized precursor. The deposition of DTB on Cu(111) surface kept at room temperature in a submonomayer regime was studied under UHV conditions by LT-STM, nc-AFM, XPS and DFT analysis techniques. After deposition of DTB, no self-assembly of the molecules was observed reflecting the very weak intermolecular interactions. An annealing temperature of 120°C leads to the formation of a fully conjugated polymeric network composed mainly of oligoacetylene segments separated by benzene rings. Such relatively low temperature allows a new type of activation, the C-S activation reaction, which initiates the formation of carbon radicals. These latter are coupled to form the oligoacetylene chains or pentalene units linking the original benzene rings. The coupling reaction is not selective towards *cis-* or *trans-* stereoisomers and the chains are mainly aligned with the high symmetry directions of the Cu(111) surface. DTB presents another reaction mechanism leading to the creation of threefold interconnections and the overall formation of a reticulated network. Finally, the formation of small graphene flakes occur after cyclodehydrogenation reactions upon further annealing up to a temperature of 500°C. Therefore, we demonstrated that the strong reactivity of copper toward sulfur-containing species can be exploited to steer an on-surface homocoupling reaction and to create extended polyene chains at low activation temperature.

BrPhINDO molecule is a new precursor with multiple reaction sites. In previous studies it was shown that the introduction of a bifunctionality in the molecular precursor producing an adequate sequential reactivity can improve the growth process in on-surface polymerization. BrPhINDO is composed of indanone backbone substituted with a bromine at the 6-position and a phenyl group at the 3-position. The deposition of this chiral molecule on the Cu(111) surface

was investigated under UHV by LT-STM. Different reaction products are observed as a function of the annealing temperature. The presence of the halogen atoms leads to the formation of Ullmann coupling reactions between the molecules after debromination on copper surface while the ketone group allows the formation of Knoevenagel reactions. Different structures formed by these two reactions are observed on the surface with a defined prochirality. The smallest reacted entities are an H-bonded C_3 threefold assemblies of Ullmann coupled dimers. A larger C_2 structure is present, formed of tetramers coupled twofold by Knoevenagel reactions between three dimers. Finally, larger C_3 hexagonal structures are formed from three coupled tetramers through Knoevenagel reactions. An asymmetric enantiomeric distribution of the prochirality is observed due to the occurrence of chiral inversion for a fraction of the precursors. As mentioned before, this is imputed to a phenyl loss or to a chiral switch upon adsorption.

Appendix of chapter 4

A 4.1. Chemical synthesis of 1,4-di(thiophen-2-yl)benzene

Tetrakis(triphenylphosphine)palladium (0) (0.46 g, 0.744 mmol, M = 1155.56 g.mol^{-1}) was added to a mixture of 1,4-dibromobenzene (1.44 g, 6.11 mmol, M = 235.90 g.mol^{-1}), 2-thiopheneboronic acid (1.62 g, 12.66 mmol, M = 127.96 g.mol^{-1}), toluene (54 mL), ethanol 26 mL) and an aqueous potassium carbonate solution (2 M, 6.91 g in 25 mL water, 26 mL) under vigorous stirring. The mixture was stirred at 80 °C for 48 h under a nitrogen atmosphere. After cooling to room temperature, the reaction mixture was poured into water and extracted with ethyl acetate. The organic layer was washed with brine several times, and the solvent was then evaporated. Addition of DCM followed by pentane precipitated a white solid which was filtered off. The residue was purified by column chromatography (SiO2, pentane/DCM: 1/1 and pure DCM) and isolated as a white solid (1.15 g, 78% yield). ^{1}H NMR, see Fig. S11 (250 MHz, CDCl$_3$) δ 7.63 (s, 4H), 7.32 (dd, J = 11.9, 3.9 Hz, 4H), 7.14 – 7.05 (m, 2H); ^{13}C NMR, see Fig. S12 (63 MHz, CDCl$_3$) δ 143.87, 140.28, 133.45, 128.08, 126.27, 124.88, 123.07, 77.50, 76.99, 76.49; HRMS (ESI MS) m/z: theor: 242.0224 found: 242.0224 (M$^+$ detected).

A 4.2 Theoretical modeling

Theoretical calculations were performed with the Vienna *Ab initio* Simulation Package (VASP)[1], [2] using the Perdew-Burke-Ernzerhof[3] generalized-gradient approximation (PBE-GGA) for the exchange-correlation potential, the projector augmented wave (PAW) method[4], [5], and a plane-wave cutoff of 450 eV. The zero-damping DFT-D3 method of Grimme[6] was used for the van der Waals (vdW) correction of the potential energy, and calculations were performed at the gamma *k*-point. Geometry optimizations for the AFM simulations were performed with an (8×8) orthogonal Cu(111) slab constructed using a lattice constant of 0.363 nm and a 1.8 nm vacuum layer, with four atomic layers and the positions of atoms in the bottom two layers fixed (supercell dimensions: 2.05620 nm × 17.8073 nm × 24.2958 nm). Calculations for DTB on Cu(111) used a smaller (6×6) orthogonal slab with the same lattice constant, five atomic layers (bottom two fixed), and a 1.6 nm vacuum layer. The geometries were optimized until the force on each atom was below 0.02 eV/Å. Images of the calculated structures were generated using the VMD software[7]. The AFM image simulation was performed using the Probe Particle model[8], [9] for a CO-terminated tip with a charge of 0.05 e, lateral bending stiffness of 0.5 N/m and a particle-tip bond stiffness of 20.0 N/m. The simulated XPS spectra are the result of the

convolution of several Gaussians centered at the calculated core level positions (vertical ticks). A negative global shift was applied to the calculated energies to match the maxima of the experimental spectra.

References of Appendix

[1]   G. Kresse and J. Hafner, "*Ab initio* molecular dynamics for liquid metals," *Phys. Rev. B*, vol. 47, no. 1, pp. 558–561, Jan. 1993, doi: 10.1103/PhysRevB.47.558.

[2]   Kresse, G.; Furthmuller, J., "Efficient iterative schemes for ab initio total-energy calculations using a plane-wave basis set," Phys.Rev.B, pp. 11169–11186, 1996.

[3]   J. P. Perdew, M. Ernzerhof, and K. Burke, "Rationale for mixing exact exchange with density functional approximations," *J. Chem. Phys.*, vol. 105, no. 22, pp. 9982–9985, Dec. 1996, doi: 10.1063/1.472933.

[4]   P. E. Blöchl, "Projector augmented-wave method," *Phys. Rev. B*, vol. 50, no. 24, pp. 17953–17979, Dec. 1994, doi: 10.1103/PhysRevB.50.17953.

[5]   G. Kresse and D. Joubert, "From ultrasoft pseudopotentials to the projector augmented-wave method," *Phys. Rev. B*, vol. 59, no. 3, pp. 1758–1775, Jan. 1999, doi: 10.1103/PhysRevB.59.1758.

[6]   S. Grimme, J. Antony, S. Ehrlich, and H. Krieg, "A consistent and accurate *ab initio* parametrization of density functional dispersion correction (DFT-D) for the 94 elements H-Pu," *J. Chem. Phys.*, vol. 132, no. 15, p. 154104, Apr. 2010, doi: 10.1063/1.3382344.

[7]   W. Humphrey, A. Dalke, and K. Schulten, "VMD: Visual molecular dynamics," *J. Mol. Graph.*, vol. 14, no. 1, pp. 33–38, Feb. 1996, doi: 10.1016/0263-7855(96)00018-5.

[8]   P. Hapala, G. Kichin, C. Wagner, F. S. Tautz, R. Temirov, and P. Jelínek, "Mechanism of high-resolution STM/AFM imaging with functionalized tips," *Phys. Rev. B*, vol. 90, no. 8, p. 085421, Aug. 2014, doi: 10.1103/PhysRevB.90.085421.

[9]   P. Hapala, R. Temirov, F. S. Tautz, and P. Jelínek, "Origin of High-Resolution IETS-STM Images of Organic Molecules with Functionalized Tips," *Phys. Rev. Lett.*, vol. 113, no. 22, p. 226101, Nov. 2014, doi: 10.1103/PhysRevLett.113.226101.

Appendix of chapter 5

A 5.1. Chemical synthesis of (*R*)-6-bromo-3-phenyl-2,3-dihydro-1*H*-inden-1-one (BrPhINDO)

- Synthesis of 6-bromo-1*H*-inden-1-one:

N-bromosuccinimide (NBS) (2.7 g, 1.1 eq.) and azobisisobutyronitrile (AIBN) (30 mg, 0.01 eq.) were added to a 1,2-dichloroethane solution (60 mL) of 6-bromo-2,3-dihydro-1*H*-inden-1-one (3 g, 1 eq., 14.2 mmol). The resulting mixture was stirred at reflux temperature for 2.5 h, then cooled and filtered through Celite, washed with CH_2Cl_2 and evaporated. The filtrate was cooled to 0 °C and treated with triethylamine (0.6 mL, 6.0 mmol) overnight, then concentrated in vacuo. The crude product was chromatographed (1 : 9~1 : 4 EtOAc/pentane, flash with acetone) and afforded the 6-bromo-1*H*-inden-1-one as a brown solid (m = 1.2 g, 45% yield).

¹H NMR (300 MHz, CDCl₃) δ: 7.55 (dd, *J* = 6.0, 0.9 Hz, 1H), 7.41 (dd, *J* = 7.6, 1.6 Hz, 1H), 7.30 (d, *J* = 7.6 Hz, 1H), 7.23 (d, *J* = 1.6 Hz, 1H), 5.95 (d, *J* = 6.0 Hz, 1H).

- Synthesis of 6-bromo-3-phenyl-2,3-dihydro-1*H*-inden-1-one (BrPhINDO):

A solution composed of copper iodide (3.1 g, 2.7 eq.), sodium iodide (4.5 g, 5 eq.), dimethylsulfide (3.6 mL, 8 eq.) in DCM (50 mL) was cooled to -78°C. Then, phenyl lithium (7.92 mL, 1.9 M in dibuthylether, 2.5 eq.) was added followed by chlorotrimethylsilane (0.63 mL, 5 eq.) and the solution was stirred at -78°C for 20 min. Then, the 6-bromo-1H-inden-1-one (1.2 g, 6 mmol, 1eq.), dissolved in DCM (50 mL), was added and the reaction mixture was allowed to warm to 0°C. The solution was stirred at this temperature for 9 hours and finally at room temperature. The mixture was quenched with half saturated ammonium chloride (20 mL) and then filtered. Afterwards, the crude was extracted with DCM (3 x 25 mL), washed with sodium thiosulfate, dried over magnesium sulfate and the solvent removed under reduced pressure. The residue was purified by column chromatography (SiO_2) using DCM as the eluent. The product was isolated as a yellow oil (1.3 g, 4.7 mmol, 78 % yield).

¹H NMR (300 MHz, CDCl₃) δ: 7.93 (s, 1H), 7.66 (dd, *J* = 8.2, 1.8 Hz, 1H), 7.31 (dd, *J* = 13.4, 5.9 Hz, 3H), 7.13 (dd, *J* = 15.2, 7.6 Hz, 3H), 4.52 (dd, *J* = 7.9, 3.8 Hz, 1H), 3.25 (dd, *J* = 19.4, 8.1 Hz, 1H), 2.71 (dd, *J* = 19.4, 3.8 Hz, 1H).

- Fits with literature data: Ref. [39]
- Semi-preparative Chiral HPLC

DAD1 D, Sig=230,4 Ref=off
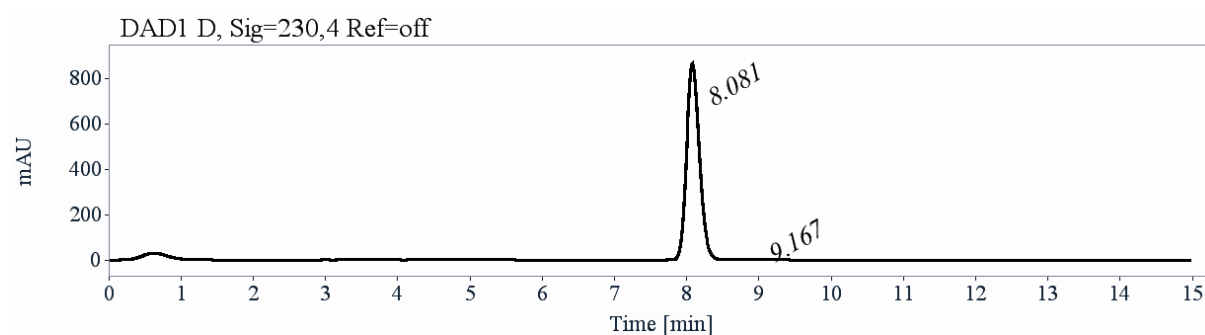
- Sample preparation: About 175 mg of compound 4-Br-INDO-Ph are dissolved in 7 mL of a mixture of hexane / isopropanol / ethanol / dichloromethane (46/12/28/14).

- Chromatographic conditions: Chiralpak IG (250 x 10 mm), hexane/isopropanol (80/20) as mobile phase, flow-rate = 5 mL/min, UV detection at 254 nm.

- Injections (stacked): 70 times 100 mL, every 9.4 minutes.